NASA CR 152377

ANALYTICAL DESIGN AND EVALUATION OF AN ACTIVE CONTROL SYSTEM FOR HELICOPTER VIBRATION REDUCTION AND GUST RESPONSE ALLEVIATION

By R. B. Taylor, P. E. Zwicke, P. Gold and W. Miao

July, 1980

(NASA-CR-152377) ANALYTICAL DESIGN AND EVALUATION OF AN ACTIVE CONTROL SYSTEM FOR HELICOPTER VIBRATION REDUCTION AND GUST RESPONSE ALLEVIATION (United Technologies Research Center) 165 p HC A08/MF A01 G3/08

N80-28369

Uncias 26014

Prepared under Contract No. NAS2-10121 by

United Technologies Research Center
East Hartford, Connecticut
and
Sikorsky Aircraft
Stratford, Connecticut

for

AMES RESEARCH CENTER
NATIONAL AERONAUTICS AND SPACE ADMINISTRATION

ACKNOWLEDGEMENT

The authors wish to thank J. Molusis for the selection of some of the control algorithms, F. Farrar for development of the controller design, and K. Dauphinas, S. Cassarino and R. Sopher for their assistance in coding the analysis and running the many computer cases. Their contributions to this effort are gratefully acknowledged.

TABLE OF CONTENTS

TABLE OF CONTENTS - CONTINUED

LIST OF FIGURES

LIST OF FIGURES CONTINUED

LIST OF FIGURES CONTINUED

LIST OF FIGURES CONTINUED

LIST OF FIGURES CONTINUED

LIST OF TABLES

SECTION 1

SUMMARY

An analytical study has been conducted to define the basic configuration of an active control system for helicopter vibration and gust response alleviation. The study culminated in a control system design which has two separate systems: narrow band loop for vibration reduction and wider band loop for gust response alleviation. The narrow band vibration loop utilizes the standard swashplate control configuration to input higher harmonics of blade cyclic pitch once every rotor revolution. The controller for the vibration loop is based on adaptive optimal control theory and is designed to adapt to any flight condition including maneuvers and transients. The prime characteristic of the vibration control system is its real-time capability. Advanced control techniques utilizing a real-time identifier are coupled with a transfer matrix approach representing the rotorcraft so that the transfer matrix is completely updated once every rotor revolution and commands higher harmonic blade cyclic pitch input. This enhancement of the transfer matrix approach provides the capability to handle all flight conditions including maneuvers and transients without gain scheduling and also without having to open the loop and perturbate the system to determine the transfer matrix.

The gust alleviation control system studied consists of optimal sampled-data feedback gains together with an optimal one-step-ahead prediction. A sampled-data approach facilitates implementation of the control law in an onboard digital computer. The prediction permits the estimation of the gust disturbance which can then be used to minimize the gust effects on the helicopter. To simplify the control system, a sub-optimal system, using a few feedback paths, was also studied and developed. A significant reduction in the gust response has been achieved with this sub-optimal system.

Theoretical results are presented for a non-linear four-bladed single rotor helicopter which demonstrate the effectiveness of the active control system. For the narrow band vibration control loop, 4/rev fuselage vibration reductions on the order of 80-90 percent are achieved with the active controller for airspeeds up to 150 kn. The amplitude of higher harmonic pitch required to achieve this level of vibration reductions is on the order of one degree at 3, 4, and 5 per rev. For the wide band gust response alleviation loop, a 70 percent alleviation is achieved while augmenting the basic aircraft stability.

The studies have shown that rotor blade loads may or may not be increased significantly by HHC inputs. The potential for control inputs that do not increase loads has been shown. However the designer should be alert to the possibility for significantly increased loads due to two mechanisms: 1) nonoptimum rotating to fixed system hub load vectoral cancellation and 2) by resonant amplification of higher blade modes through interharmonic coupling.

SECTION 2

INTRODUCTION

In order to achieve full potential in the coming generation of helicopters, significant reductions in the vibration and gust response levels must be accomplished. The vibration and gust response of a helicopter affects not only ride quality but also maintenance costs. Commericial passenger acceptance will largely depend upon perception of low vibration and gust response during the ride, and the feasibility of commercial utilization of the helicopter is directly impacted by the maintenance costs attributed to the vibrating environment.

Many advances in the reduction of vibration have been accomplished and are operational on the current generation of helicopters. Some notable methods are: fuselage and rotor blade tuning, transmission isolation devices, hub-mounted, blade-mounted and fuselage-mounted vibration absorbers. Another method that could be extremely effective for both vibration and gust response alleviation is the use of active feedback control. A promising application of active control is for vibration reduction with the use of higher harmonic cyclic pitch. Much theoretical and experimental work has been done in this area, References 1 through 9, and also in the related areas of jet flaps and servo flaps, References 10 through 17. The basis for all this work is the beneficial change in rotor blade harmonic airloads caused by the higher harmonic control inputs so that a net reduction results in forces and moments transmitted to the rotor hub. The overall conclusion of these experimental and analytical studies is that higher harmonic control in its many forms of implementation in different rotor types can be used to achieve substantial reduction in helicopter vibration.

One important observation of the experimental and theoretical work done to date is that most of the work has been addressed to vibration reduction with open loop higher harmonic control. Only two studies, (References 3 and 10), deal explicitly with a closed loop system. This is not surprising since it follows the normal course of events in the development of a concept. But this observation does highlight the present status of higher harmonic control as being proven feasible experimentally with the next step being determination of the feasibility of implementing the concept on a helicotper by closed loop control.

More experimental and theoretical work has been done in the area of gust alleviation by feedback control, References 18 through 23, and the present level of sophistication has probably been set by the use of linear optimal control theory and Kalman filtering in Reference 23. The overall conclusion reached from the work documented in these references is that gust alleviation with active control is promising. However there are presently no active gust alleviation control systems on production heli-

copters, so in this sense the status of the gust alleviation active control concept is about the same as the active vibration control concept.

The next logical step is to define a control system configuration to realize the expected gains in vibration and gust response alleviation. The primary objective of this analytical study is to define the basic configuration of an active control system, to evaluate its effectiveness for vibration and gust response alleviation, and to establish the feasibility of the concept.

SECTION 3

APPROACH FOR ACTIVE VIBRATION AND GUST ALLEVIATION CONTROL

The approach used for formulating an active vibration and gust alleviation controller is fundamentally based upon the need to avoid compromising the capability of a vibration control configuration by forcing the same concept to also alleviate gusts, or vice versa. There is no over-riding requirement to have the same sensors, actuators, or controllers perform for both vibration and gust alleviation. The simplicity in the total system gained by a compromising approach could be negated by loss in effectiveness. This can be stated because of the fundamental differences between vibration and gusts on helicopters. These differences are profound so that clear advantages and disadvantages can be seen for a particular advanced control concept when applied to either vibration or gust alleviation control. Following are three areas in which there are large differences between vibration and gust characteristics.

THE HARMONIC NATURE OF VIBRATION - A marked difference between vibration and gust is that vibration is harmonic whereas gust characteristics are not. The input-output relationships for vibration are fundamentally periodic and a transfer matrix approach is naturally suited to this type of system. The gust problem is random in nature with no primary input-output frequency and best treated statistically.

THE MINIMUM GAIN SCHEDULING REQUIREMENTS FOR GUST ALLEVIATION - Analytic investigation for CH-53 has shown (Reference 19) that the gain scheduling requirements for gust alleviation are minimal and therefore the linear quadratic optimal control concept is well suited for gust control. On the other hand, experimental results (Reference 2, 4) have shown that gain scheduling requirements for vibration control can be expected to be more complex, even if the flight envelope is restricted to steady state flight conditions. Therefore the use of gain scheduling for vibration can possibly become quite complex. When the total helicopter envelope is considered, some type of adaptive control could be more suited for vibration to simplify the control system.

FREQUENCY BANDWIDTHS OF GUST AND VIBRATION ARE SEPARATED - The frequency bandwidth of vibration is very closely tied to the number of rotor blades. For a 4-bladed rotor the frequencies of interest are discrete harmonics at 3, 4, 5 per rev and 7, 8, 9 per rev frequencies in rotating frame. Compared to this, the frequency bandwidth of gust forcing is generally considered to be 0 up to 1 per rev for conventional helicopters with 200 m/s to 230 m/s tip speeds. The distinction is probably most pronounced in the hardware aspects of implementation. The best solution to both the vibration and gust alleviation control problems is to design each system so that it is best suited to its own characteristics and bandwidth requirements and then compare the two systems and look for areas of commonality. This

is the approach used in the design and evaluation of the active vibration and gust alleviation control system.

Figure 3.1 shows that the active control system has been separated into two separate systems; a vibration loop whose sensors, actuators and controllers are designed specifically for active vibration control; and a gust alleviation loop whose sensors, actuators and controllers are designed specifically for gust alleviation control.

The vibration control system is termed the Real Time Self Adaptive (RTSA) control system. The system will use the standard swashplate actuator configuration for control inputs. The swashplate will be oscillated at 4 per rev to provide 3, 4, 5 per rev control inputs to the individual rotor blades for a four-bladed rotor to control 4 per rev vibration. Higher harmonic control inputs of 7, 8, 9 per rev can also be input to control 8 per rev vibration in the same manner. However, the scope of this study is limited to addressing 4 per rev vibration on a four-bladed rotor. The vibration control system is based upon the transfer matrix approach that has been extensively validated in the last twenty years, e.g., References 13 through 16. The prime characteristic of the RTSA control system is its real time capability. Advanced control techniques utilizing a real time identifier discussed in Section 4.3.2 are compatible with the transfer matrix approach so that the transfer matrix will be completely updated and command higher harmonic controls input every rotor revolution.

This enhancement of the transfer matrix approach provides the capability to handle all flight conditions (steady state, maneuvers, transients) without gain scheduling and also without having to open the loop and perturbate the system to determine the transfer matrix. For the system proposed, the closed loop control inputs are the excitations required for determination of the transfer matrix. Other important characteristics of this system are:

a) the use of fixed system sensors

b) adaptability for reduction of vibration that emanates from many sources (not just the main rotor)

c) independence from analytical calculations when implemented in flight test or production aircraft

The gust alleviation control system is an application of linear quadratic optimal control theory to provide control inputs to the standard swashplate/actuator control configuration. This approach is favored because it has a sound theoretical basis (References 19 and 23) and therefore presents a minimum risk approach. Linear quadratic Gaussian optimal control techniques are used to transform sensor measurements into state estimates for control optimization, along the same lines as discussed in Reference 23.

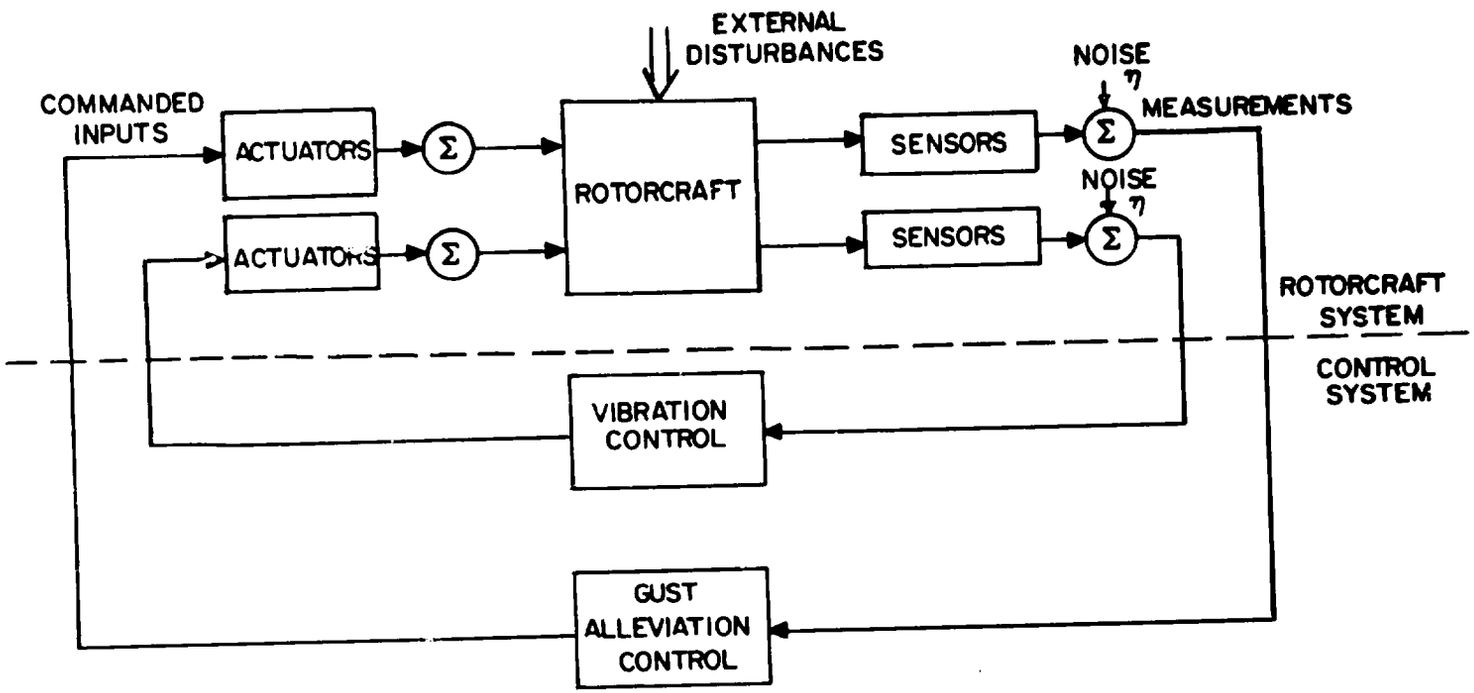

Figure 3.1 Active Vibration and Gust Alleviation Control Approach.

The application of two separate control techniques, real time transfer matrix for vibration and linear quadratic optimal control techniques for gusts represents the best solution to the total problem because the best solution is found for each individual problem rather than a single compromising complex solution for both vibration and gust alleviation. Guidelines of minimum risk and simplicity are followed to maximize the probability of success for vibration and gust alleviation control.

SECTION 4

VIBRATION CONTROL

The vibration control approach consists of three distinct components: (1) a method for mechanically implementing higher harmonic blade pitch; (2) an active controller to calculate and then command the required higher harmonic pitch; and (3) a system of sensors to provide inputs to the active controller. Together these three components form a closed-loop control system which will minimize vibration of the helicopter fuselage. Each of these systems will be discussed separately.

4.1 Mechanical Implementation

The vibration control approach uses higher harmonic blade root cyclic pitch which modifies the blade airloads to minimize harmonic blade forcing. The higher harmonic blade pitch is mechanically input through the standard helicopter swashplate configuration. By harmonically oscillating the primary servos (actuators) that support the fixed swashplate, harmonic blade pitch motions are induced by the blade pitch links following the motion of the rotating swashplate.

In order for all the rotor blades to have the same harmonic pitch amplitude and phasing, there is a limitation on the frequency of swashplate oscillation in the fixed system. The simple rule to follow to ensure that all blades on an N-bladed rotor are performing the same harmonic pitch oscillations as they travel around the azimuth is that the harmonic frequency of oscillation of the swashplate must be N or some integer multiple of N. For example, on a four-bladed rotor, the frequency of swashplate oscillation must be 4/rev or some integer multiple of 4. In the present study, 4/rev swashplate oscillation was used on a four-bladed rotor to create 3, 4, and 5/rev harmonic blade pitch in the rotating system. The 4/rev blade pitch results from symmetric oscillation of the swashplate and the 3 and 5/rev blade pitch results from cyclic oscillation of the swashplate (still at 4/rev) about two orthogonal axes. Reference 26 provides a thorough discussion of the transfer of control inputs from fixed to rotating systems. In summary, the higher harmonic cyclic pitch concept was implemented on the four-bladed helicopter model by oscillating the stationary swashplate at 4/rev in collective and cyclic motions to create blade cyclic pitch at 3, 4, and 5/rev. Implementing higher harmonic cyclic pitch in this manner provides maximum utilization of the present swashplate control system so that only minor modifications to the present control configuration will be required for implementation. Obviously the actuators that support the swashplate will have new requirements for frequency response, rate, and stroke. This is discussed in Section 6.

4.2 Sensors

The purpose of the sensors is to provide information to the active controller so that it can calculate and then command required higher harmonic

control inputs. The sensors can be thought of as measuring meaningful outputs of the helicopter as it responds to higher harmonic control inputs. The sensors in the present vibration control approach are linear accelerometers. The accelerometers sense vibration and are placed throughout the aircraft wherever vibration minimization is desired. The accelerometers are located only in the fixed system (not on the rotor or on any component in the rotating system). Sensors in the rotating system are avoided because a slip ring or an expensive telemetry package is required to transmit data to the fixed system. Also, it has been found and will be discussed in Section 4.5 that hub vibration can be minimized by placing accelerometers in the fixed system as close to the hub as possible. Another important reason for using fixed system sensors is to accomodate the possibility of compensating for vibration caused by excitation sources other than the main rotor (e.g. empennage response to main rotor wake impingement). The only real need for a sensor in the rotating system would be to minimize or restrict blade fatigue stresses while minimizing vibration. However, even this use of rotating system sensors can be avoided on a production version of the active control system by the use of a state estimator. The state estimator is actually an optional component of the active vibration controller, and will be discussed more fully later.

In summary, the sensors used in the vibration control approach are all linear accelerometers that measure vibration throughout the aircraft. Since the vibration is sensed in the fixed system, the output is predominantly 4/rev for a four-bladed rotor with some 8 and 12/rev content. In the present study, sensors were placed in the cockpit, in the nose of the helicopter, in the cabin and close to the hub in the fixed system as shown in Table 4.1.

TABLE 4.1 LOCATION OF ACCELEROMETER SENSORS

Cockpit	
Pilot - STA (205)	Vertical Lateral Longitudinal
Copilot - STA (205)	Vertical
Cabin - STA (320)	Vertical
Nose - STA (165)	Vertical
Hub (Fixed System)	Vertical Lateral Longitudinal Pitch Roll Yaw

Note: Angular accelerations are obtained by combining signals from appropriately placed linear accelerometers.

4.3 Active Controller

The controller used in the vibration control approach for achieving minimum vibration is an explicit adaptive controller and is termed the Real-Time-Self-Adaptive (RTSA) controller. The controller consists of three interrelated algorithms: (1) a real-time minimum variance controller for vibration minimization; (2) a real-time identification algorithm for identifying and tracking the transfer matrix relating input higher harmonic cyclic pitch to output vibration; and (3) a harmonic analyzer for obtaining real-time harmonic components of measured vibration.

There are three fundamental characteristics that (when combined to work as a total control algorithm) distinguish this controller from all others proposed to date for helicopter vibration control:

(1) The approach is based upon a well validated fact that there exists a transfer matrix between vibrations and higher harmonic cyclic pitch. The transfer matrix (here-after called the T-matrix) develops a static linear relationship between harmonics of vibration (4/rev for a four-bladed rotor) and harmonics of blade cyclic pitch (3, 4, and 5/rev for a four-bladed rotor).

(2) The transfer matrix (T-matrix) is identified on-line and is tracked by a real-time identification and tracking algorithm. This means that no previous theoretical calculations or experimental results are required to establish the T-matrix. This also means that any changes in the T-matrix due to nonlinearity or transient conditions such as a maneuver will automatically be identified in real-time.

(3) Higher harmonic control inputs are updated on the order of every rotor revolution on a full-scale rotor system. This ability to update very quickly makes it possible for the identification and tracking algorithm to track during a time-varying situation such as a manuever or a transient so that the update in the T-matrix is close in time to the actual change. The quick update in higher harmonic control inputs also facilitates the use of the linear T-matrix approach to the nonlinear helicopter-aerodynamic environment problem by linearizing over a small range of control angle input.

With these three fundamental characteristics the time-varying nonlinear helicopter vibration problem has been transformed into a near real-time static linear problem with a simple solution. A diagram of the RTSA controller is shown in Figure 4.1. The controller consists of three primary interrelated algorithms. Each of the three algorithms will be discussed subsequently.

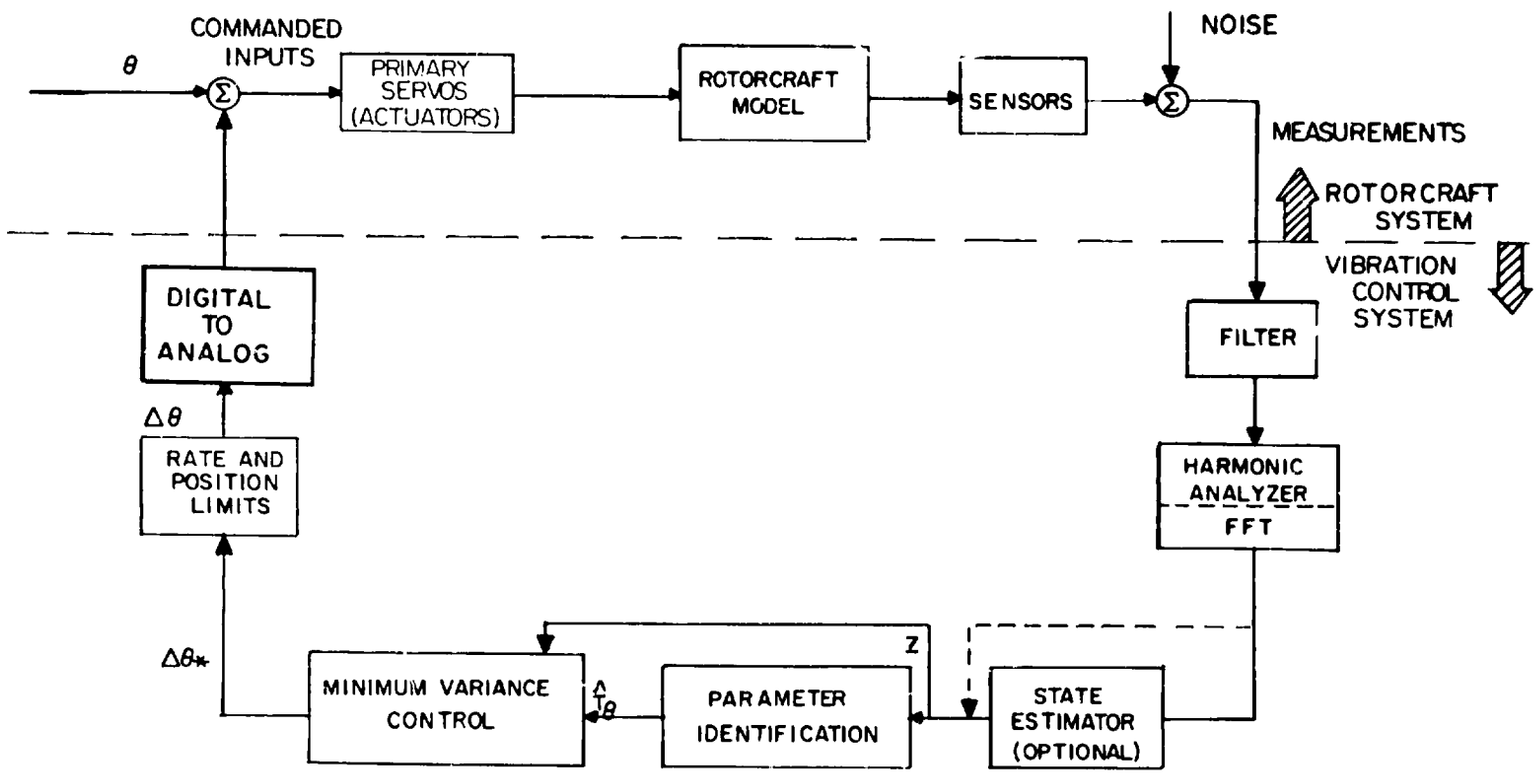

Figure 4.1 Real Time Self Adaptive (RTSA) Controller for Vibration Minimization.

4.3.1 Minimum Variance Control Algorithm

A minimum variance control gain adjustment algorithm is shown which provides a real-time solution to minimize a weighted mean square sum of harmonic vibration and control inputs. A minimum variance controller is one which minimizes the expected value of the mean square. The expected value is used to account for the stochastic nature of the problem due to random noise on the signal.

The minimum variance controller is obtained by minimization of the criteria:

$$J = E\left\{ Z_{i+1}^T W_z Z_{i+1} + \Delta\theta_i^T W_\theta \Delta\theta_i \right\} \qquad (4.1)$$

where

J is the performance index (a scalar)

Z is a (nx1) vector of harmonic coefficeints of vibration for the (i+1)th rotor rev

W_Z is the (nxn) vibration weighting matrix (diagonal)

$\Delta\theta_i$ is the (mx1) delta higher harmonic control input vector for the ith rotor rev

W_θ is the (mxm) control input weighting matrix

Superscript T denotes transpose

$E\{\ \}$ denotes expected value

Subscript i or i+1 denotes the i or i+1 rotor revolution

The performance index J includes not only the measured harmonics of vibration but also the higher harmonic control angle inputs. Therefore each element of vibration or control angle input can be individually weighted to make it more or less important than the other elements.

The transfer matrix relationship between inputs and outputs is

$$Z_{i+1} = T_\theta \Delta\theta_i + Z_i \qquad (4.2)$$

Where T_θ is the nxm transfer matrix (T-matrix) relating input higher harmonic control angles ($\Delta\theta_i$) to output harmonic vibration (Z_i and Z_{i+1}). The control angle is expressed in terms of an incremental update so that the total higher harmonic control angles are the sum of the $\Delta\theta$ inputs for all rotor revolutions up to the ith revolution. Expressing the control inputs in terms of a delta facilitates linearization of the elements of the T-matrix about the control vector point for the previous rotor revo-

lution and over a range of $\Delta\theta$. This can be important for controller stability and effectiveness if the T-matrix is highly nonlinear. This method is contrasted with expressing the control angle in terms of an absolute number θ so that the T-matrix are linearized about a zero higher harmonic control input.

The minimum variance control is obtained by taking the partial derivative of J with respect to $\Delta\theta$ and setting it equal to zero.

$$\partial J/_{\partial \Delta\theta_i} = 0 \tag{4.3}$$

The resulting solution for the minimum variance controller is:

$$\Delta\theta^*_i = -(T_\theta{}^T W_z T_\theta + W_\theta)^{-1} T_\theta{}^T W_z Z_i \tag{4.4}$$

Where the superscript * denotes the optimal higher harmonic input for minimum variance. An important consideration in the minimum variance controller is that the optimum controller is a closed form expression. That is, once the weighting matrices have been selected and the transfer matrix determined, substitution of these values into Eq. (4.4) results in an immediate control signal which is optimum in the sense of minimum variances. The closed form solution is a direct result of the linearity between the input and output transfer relationship. If Eq. (4.2) were formulated to include nonlinear terms, then this closed form solution would not exist and an iterative technique would be required. Such an approach is unfavorable because the real-time capability required for transients and maneuvers is lost due to computation time.

The nonlinear variation of the T-matrix is accounted for in the RTSA controller by treating the T-matrix as a time-varying matrix which changes throughout each flight condition. By performing real-time identification and tracking of the T-matrix the nonlinearity is accounted for and yet the minimum variance controller of Eq. (4.4) remains linear.

4.3.2 Real-Time T-matrix Identification and Tracking Algorithm

Successful identification of the T-matrix is important for good vibration reduction since the minimum variance controller discussed in the previous section depends explicitly on the identified T-matrix. The method used for deriving the real-time identification algorithm parallels the approach taken in Ref. 27 and is based on the fact that least squares is analogous to a Kalman filter and, therefore, all the well-known Kalman filter algorithms apply. The Kalman filter formulation for the identification problem is obtained by noting that Eq. (4.2) can be rewritten as:

$$\begin{Bmatrix} Z_1 \\ Z_2 \\ \vdots \\ Z_j \end{Bmatrix}_{i+1} = \begin{bmatrix} \Delta\theta^T T_{\theta 1}^T + Z_1 \\ \Delta\theta^T T_{\theta 2}^T + Z_2 \\ \vdots \\ \Delta\theta^T T_{\theta j}^T + Z_j \end{bmatrix}_i \qquad (4.5)$$

where $T_{\theta j}^T$ is the jth column of $T\theta^T$

A state vector (X) can then be defined for each row of the T-matrix. The rows in Eq. (4.5) then become

$$Z_{j\ i+1} = H_i X_{ji} + \eta \qquad (4.6)$$

where $$X_{ji} = \begin{bmatrix} T_{\theta j}^T \\ \hline Z_{ji} \end{bmatrix}$$

$$H = \left[\ \Delta\theta^T \mid 1\ \right]$$

η is zero mean white Gaussian measurement noise

The state vector (X) with dimensions ((m+1)x1) represents a row in the T-matrix and can be represented as a varying quantity to be tracked by:

$$X_{j\ i+1} = X_{ji} + W_{ji} \qquad j = 1 \text{ to } N \qquad (4.7)$$

where W_{ji} is a discrete white random sequence and j denotes the jth row of the vibration vector Z.

The quantity W_{ji} can be considered the forcing vector for changes in state (X). Equation (4.7) implies that the state vector (the jth row of the nxm T-matrix) at time sequence i+1 equals its value at time sequence i plus a random change. This random change conveys to the mathematical formulation that the elements of the T-matrix vary with flight condition. Equations (4.6) and (4.7) present a well-defined problem, and the Kalman filter solution provides a real-time identification and tracking of the T-matrix. The Kalman filter solution as taken from Reference 27, Chapter 12, is:

$$\hat{X}_{j\ i+1} = \hat{X}_{ji} + K_i(Z_{ji} - H_i\hat{X}_{ji}) \qquad (4.8)$$

$$K_i = P_i H^T R_i^{-1} \qquad (4.9)$$

$$P_i = P_{i-1} + Q_i \qquad (4.10)$$

$$P_{i+1} = P_i - P_i H_i^T (H_i P_i H_i^T + R_i)^{-1} H_i P_i \qquad (4.11)$$

where K_i is the Kalman gain ((m+1)X1) vector

P_i is the (m+1)x(n+1) covariance matrix of the error in the estimate $\hat{X}_j$

$\hat{X}_{ji}$ is the state vector representing the jth row of the T-matrix

Q_i is the (m+1)x(m+1) covariance matrix of W

R_i is the (1x1) covariance of noise n

And the superscript Λ denotes estimated value

The covariance of noise R can be made a scaler constant or vary between updates, depending upon the variability of noise to signal ratio or other factors influencing vibration measurement accuracy. One method of varying R from update to update is shown below:

$$R_{i+1} = R_i \frac{Ji}{J_{i-1}} \qquad R_{low} \leq R_{i+1} \leq R_{high} \qquad (4.12)$$

where J is the vibration performance index as defined in Equation (4.1).

The matrix P is the covariance of the state X and is therefore a measure of confidence in the estimate of the state X. If the estimate of X is good, then the elements of the estimated T matrix will be close to the elements of the actual T matrix and P will be small. Conversely, if the estimate of X is poor, P will then be calculated to be large. The matrix Q is the covariance of the discrete white random noise sequence. The value of Q is not calculated like P but instead is assigned. The magnitude of its elements should be set in direct proportion to the variability of the actual T matrix from update to update. If the actual T matrix varies widely and rapidly then the elements of Q should be large.

Note Equation (4.8) is a model of the system defined by Equation (4.7) with a correction term that is proportional to the difference between the measured vibration (Z_i) and the predicted vibration ($H_i X_i$) with higher harmonic control. The Kalman gain vector K_i is a ratio of the confidence in the predicted T-matrix to the confidence in the accuracy of the vibration measurements. This can be seen by inspection of Equation (4.9) which shows P_i, the covariance of the state, X_i, in the numerator and R_i, the covariance of the noise on the measurement, in the denominator. When R_i is large (or conversely P_i small) to reflect more confidence in the estimate of the T-matrix than in the measurements, the state vector (X_i) will change proportionately less even though there will be a difference between measured vibrations (Z_i) and predicted vibrations ($H_i X_i$).

This also demonstrates that the important parameter for Q and R is the ratio of Q to R rather than the individual magnitudes. For if the calculated T matrix is a good estimate of the actual T-matrix, then P will

be essentially equal to Q, Equation (4.10), and the Kalman gain will be directly proportional to the ratio of Q to R, Equation (4.9). Actually Q and R must be judiciously selected to match the system. For wind tunnel or flight test implementation, the selection process should combine some knowledge of the system (is T linear and how does it vary, are the measurements noisy) with some trial and error combination of Q and R to optimize their relative magnitudes. In this study, R has been varied between .001 and 1 with an initialized value of .1. Q has been made a constant diagonal matrix with all diagonal elements equal to .001. Also the P matrix has been initialized to 10 on the diagonal for the zeroth rotor rev.

An important characteristic of the identification and tracking algorithm contained in Equations (4.8) - (4.11) is that computation of the updated estimate of the elements of the T-matrix involves only the current vibration measurement and error covariance. Therefore, the procedure can be carried out recursively with information from only the present rev, (i+1)th, and the previous rev, ith. The importance of this characteristic is that implementation can easily be carried out in real time. Also, this capability helps satisfy the requirement for effective identification and tracking of the T-matrix during transients and maneuvers.

The harmonic analyzer used to provide vibration measurement information to both the minimum variance controller and the parameter identifier is discussed in the next section.

4.3.3 Harmonic Analyzer

As previously mentioned in Section 4.2, the sensors used to supply information to the controller are all accelerometers located in the fixed system. Therefore, for a four-bladed rotor, the vibration measurements are predominately 4/rev with some 8/rev and 12/rev in a steady state flight condition, provided all four blades are executing the same motions. The active vibration control system takes advantage of the periodic nature of vibration and seeks to minimize the 4/rev fuselage motions. The purpose of the harmonic analyzer is to transform the sensor measurements of acceleration into digitized 4/rev harmonic coefficients. To accomplish this, a fast Fourier transform (FFT) approach is used to operate on the sensor analog signal. The particular FFT used is taken from the International Mathematics and Statistical Library and the basis for the algorithm can be found in Reference 28. The FFT used refers to this theoretical investigation only and is not necessarily the best for other applications. In fact for full scale implementation, some method other than an FFT may be more attractive. The proposed use of an FFT to obtain the harmonic components of vibration is intended only to be a starting point for preliminary discussions on hardware definition and implementation.

An optional part of the harmonic analyzer is a high pass-low pass filter. Although this filter was not used in the analytical simulation, it is recommended for use on a flight worthy control system. The filter operates on the analog sensor measurements to remove harmonic content above or

below 4/rev from the signal. This will increase the accuracy of the FFT for small record lengths, and more will be said in this regard later. Depending upon the filter design, it is possible that some signal attenuation and phase lag might be introduced. However, since the desired signal is at a discrete frequency (4/rev); this can be accounted for directly by signal amplification and phase lead corrections in the controller algorithms after the FFT has digitized the signal.

Additional functions performed by the controller shown in Figure 4.1 are limiting of $\Delta\theta$ and digital to analog (D/A) conversion of the actuator signals. The $\Delta\theta$ limiter serves to keep the amplitude of higher harmonic control input at each update within the capability of the actuators. For example, if the higher harmonic control is updated with the first quarter of every rotor revolution, which is about 60 milliseconds for a full scale rotor system, and the actuators are physically limited to a .1 degree change in that time span; then the actuator command signal is limited to .1 deg so that the actuator is always working within its capability. The same type of limiting applied to the total amplitude of higher harmonic control required to ensure that the actuators are not commanded beyond their maximum stroke capability.

After the limiting operation is complete the D/A conversion of the actuator signals is performed and the analog electrical signals are sent to the swashplate servos to oscillate the swashplate for higher harmonic control inputs.

4.4 Vibration Control System Implementation

To implement the vibration controller on a helicopter, the controller must be integrated into the system so that it can receive information (vibration measurements) from the helicopter and then send updated information to the helicopter (the actuators) to mechanically implement higher harmonic control. This section describes how the controller is integrated into the standard helicopter control system and the complete sequence of events that occur from the initial sensor measurement of vibration to the input of higher harmonic control. The computational requirements for implementation of the controller algorithms are also discussed.

A variety of methods exist by which higher harmonic cyclic pitch can be input to the rotor blades. Four options are discussed in Section 6. For purposes of this section of the report, it is assumed that the input is electrical and made directly to the primary servos which support the non-rotating swashplate; these servos having been modified to accept electrical inputs.

4.4.1 Controller Integration

A schematic of one of the configurations for the vibration control system integrated with the helicopter is shown in Figure 4.2. With the ex-

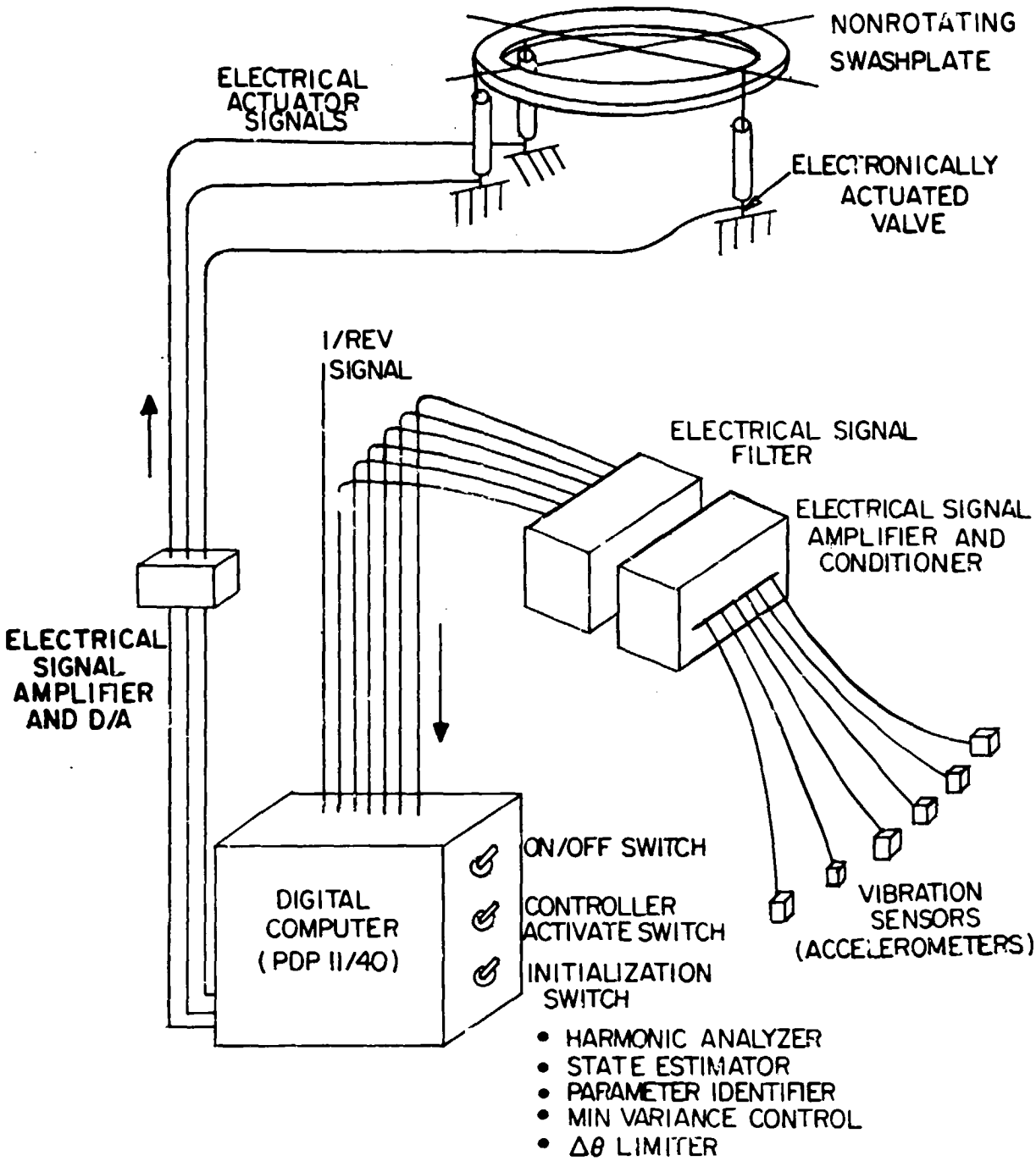

Figure 4.2 Schematic of Vibration Control System Integrated with the Helicopter.

ception of the electrical signal amplifiers and the electrical signal filter, D/A conversion and the 1/rev counter, the entire vibration controller can be programmed onto a digital computer. The PDP 11/40 computer is shown in the figure only to indicate the physical size of computational capability required and not to indicate the computer preference. Computational requirements are discussed in a later section, so it is sufficient to say at this point that a flightworthy PDP 11/40 requires only one shelf of a standard electrical storage unit and weighs less than 50 pounds. For a production version of the vibration controller, it would be worthwhile to make a special computer that is hardwired to perform only the vibration controller functions. This would result in a faster, lighter, more compact computer/controller.

An important features of the computer/controller shown in Figure 4.2 is that there are only three switches available to the pilot to activate the vibration controller. There is an on/off switch to energize the system, a switch to activate the controller and also an initialization switch to set the higher harmonic control angles to zero and also to initialize the vibration controller. Since the vibration controller operates recursively, that is, it needs information from the present rotor revolution plus information from the past revolution, the initialization function satisfies the past revolution information requirement when the controller is turned on. The initialization process consists of zeroing the $\Delta\theta$ vector, and defining Q, R and the P matrix in the identification algorithms and the initial T-matrix for the zeroth rotor rev. For full scale implementation, the initial T-matrix will probably be the vibration sensitivities to higher harmonic control inputs in hover, based on open loop flight test results. However the T-matrix need not be so well defined, since the controller will identify and track it automatically. The only criterion for defining the initial T-matrix is that it maintain controller stability and not generate vibration when the controller is activated. Once the computer/controller is turned on and initialized, there are no other functions required of the pilot. There are no gain switches, weighting switches or override switches because the controller does not depend upon gain scheduling, flight speed or maneuvering rates or any parameter other than the vibrations measured by the sensors.

Except for the initialization of the controller to get it started, the controller is completely independent of theoretical predictions of helicopter response or flight test measured helicopter response to higher harmonic control. No such information is stored in the computer and the controller is completely on its own to identify and track the helicopter response to higher harmonic control and then compute and command the required control angles. Once the controller is turned on and initialized, which will presumably be in hover at the start of flight, the controller performs its calculation and update functions once every rotor revolution throughout the whole flight including all maneuvers and transients. The sequence of events that occur within a typical rotor revolution with the controller activated is shown in Figure 4.3.

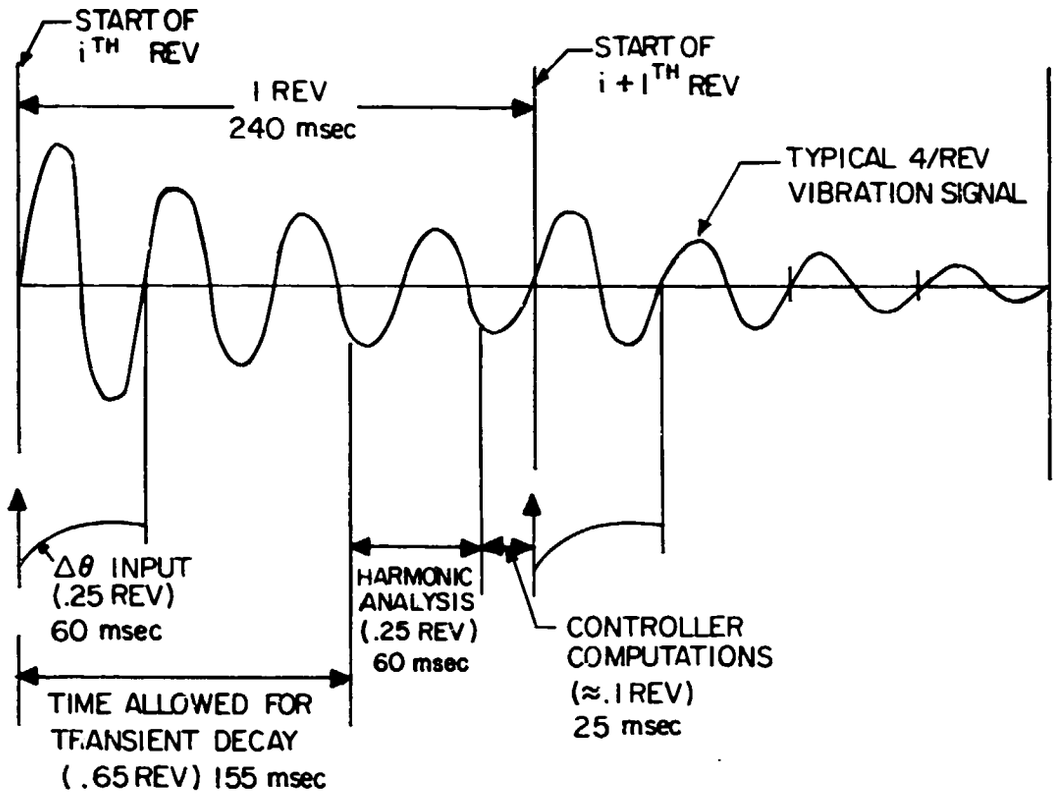

Figure 4.3 Sequence of Events Occurring in Vibration Control System for One Rotor Revolution.

The commanded $\Delta\theta$ higher harmonic control input for the its rotor revolution is shown being input at the start of the revolution. Actually the sequence can be started at any point in time during a rotor revolution, but for explanatory purposes it is shown being input when a particular reference rotor blade is at zero degrees azimuth. The actuator response is described as a "softened" step input that lasts no more than 1/4 rev. The characteristic of the $\Delta\theta$ update depends largely upon the actuator dynamic response characteristics to a nearly step change in the 4/rev electrical voltage that controls the actuator valve. It suffices to say that the actuator will be required to complete the commanded $\Delta\theta$ input within 1/4 rev. During the time that the $\Delta\theta$ is being updated there will be a transient vibration response of the helicopter due to the transient change in rotor higher harmonic airloads as affected by the $\Delta\theta$ update. The transient vibration response is certainly dependent upon the shape and amplitude of the $\Delta\theta$ update and Figure 4.3 shows that about .65 rev (155 msec) is allowed to pass from the start of the $\Delta\theta$ update before the harmonic analyzer in the vibration controller is activated. This time block is essentially "dead" time in which the controller must wait, but it is very important to the performance of the controller. If the harmonic analysis is performed earlier, the FFT algorithm will be operating on a largely transient signal and therefore pass inaccurate information to the parameter identifier and minimum variance control algorithms. The result will be an inaccurately identified T-matrix with a resultant reduction in controller performance since the commanded $\Delta\theta$ inputs will then be in error.

The time that must pass before the harmonic analysis is performed is certainly arbitrary. The more time allowed for transient decay the better for controller performance, but this may not be true in flight maneuvers where the vibration is changing rapidly. For such a case, it is desirable to update the higher harmonic control as quick as possible to track any maneuver induced transient changes in the T-matrix and also to minimize the lag time between optimum and input higher harmonic control. The .65 rev time allowed for transient decay shown in Figure 4.3 is based upon a theoretically predicted typical transient vibration response to a step input of higher harmonic control. Figure 4.4 shows the transient 4/rev response of two fixed system hub components to a step input of .1 degree each of 3/rev, 4/rev and 5/rev cyclic pitch. The predictions are from the G-400 aeroelastic simulation of the helicopter used for the controller studies. (The G-400 analysis is described in detail in Reference 29 and will be discussed briefly in Section 4.5.1.) A harmonic analysis of the vibration components was performed 4 times for each rotor revolution. The data points show the results of the harmonic analysis performed at the end of each rotor quadrant, and the solid line at rev 4 shows the new steady state level of vibration. After waiting for three quarters of a rotor revolution and performing a harmonic analysis on the vibration time history in the last rotor quadrant, the predicted 4/rev content is 107 percent of the new steady state value, or 7 percent in error. The earlier the harmonic analysis is performed the larger the error in the 4/rev content.

Certainly these results depend upon the nature of the $\Delta\theta$ input, the initial vibration level and the sensitivity of the particular vibration com-

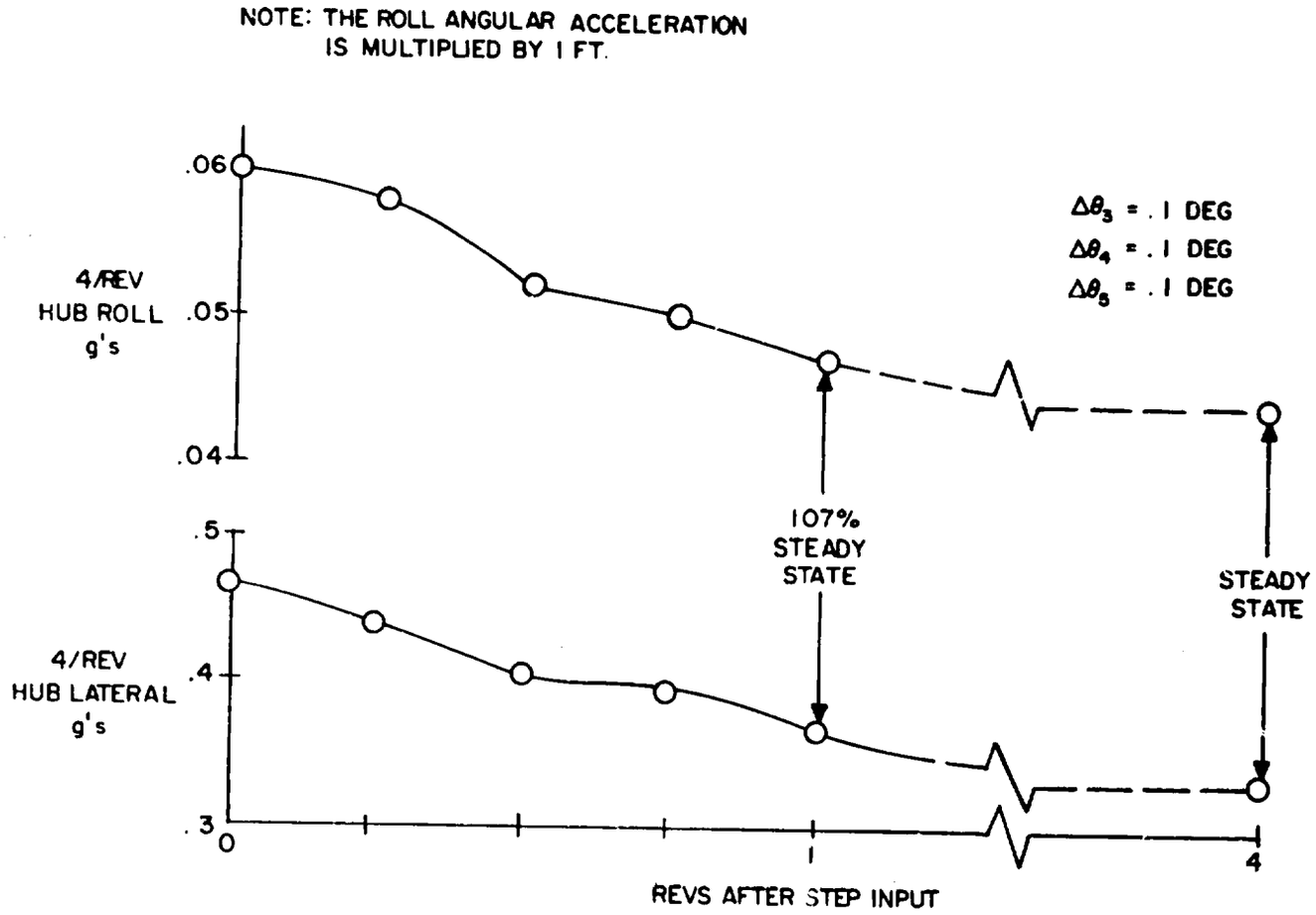

Figure 4.4 Predicted Typical Transient Vibration Response to Step Input of Higher Harmonic Control.

ponents to higher harmonic control. But they do underline the importance of the transient vibration response to $\Delta\theta$ inputs. For the present study it was decided that the .65 rev lapse time after the start of the update was sufficient for a 1 rev update. The impact of waiting longer between updates to further minimize the transient effect will be discussed in a later section.

Referring to Figure 4.3, after waiting .65 rev to allow for transient decay, the filtered analog signal from each vibration component is read into the harmonic analyzer for the next 1/4 rev (60 msec). Since the signal is filtered to allow only 4/rev content to pass through, only a quarter rev is required to complete one cycle of vibration. Filtering the signal before performing the FFT seems like duplicated effort and it would be if the impact of record length on the time between updates were not a concern. However, because of the desire to update once every rotor rev for effective vibration alleviation in maneuvers and transients, the record length must be limited to a quarter rev while at the same time the number of data samples are limited. This impacts detrimentally on resolution and also induces aliasing distortion. If the signal is band pass filtered for 4/rev then aliasing of high frequencies into 4/rev will not be a problem and high resolution can be obtained with a smaller record length. The time required for the FFT to analyze six components is less than 1 msec and is not shown in Figure 4.3. There are many schemes for further decreasing the time allotted for harmonic analysis; e.g., reading the analog signal over only half a vibration cycle (1/8 rev) and completing the 1/4 rev sine wave with the negative of that read or reading the analog signal for only a quarter of a vibration cycle (1/16 rev) and mathematically constructing the complete sine wave from that measurement. For the present study it was deemed sufficient to formulate the controller with a quarter rev devoted to the harmonic analyzer and let further sophistication follow.

After the harmonic analyzer has performed its function and the amplitude and phase of each vibration component has been calculated, a total of 215 msec has elapsed. The next 25 msec are devoted to controller computations for parameter identification and minimum variance control calculations for the next $\Delta\theta$ update. It is important to note that the time allotted to the controller for computations is the smallest by at least a factor of two compared to the time slotted for the other functions that occur during one rotor revolution and this is based upon an off-the-shelf general purpose computer (PDP 11/40). The next section discusses in detail the computational requirements for the vibration controller.

4.4.2 Controller Computational Requirements

Figure 4.1 showed that seven separate computational functions must be performed by the vibration controller from the time it receives the electrical signals from the sensors to the time it sends the commanded electrical signals to the swashplate actuators. With each computation there is associated a certain block of dedicated computer time and the length of computer time required is a function of the digital computer being used and also a function of the number of parameters being considered.

For this study of the computational requirements, a total of nine parameters have been considered: six vibration signals at 4/rev, and 3 higher harmonic control inputs (3, 4, and 5 per rev). Since all of the parameters are harmonic and have cosine and sine values, the vibration vector previously defined by Z for six vibration sensors has the dimension of (12x1) and the higher harmonic control vector previously defined as $\Delta\theta$ has the dimensions of (6x1). Using these dimensions for the parameters involved, the computational requirements for the vibration controller were calculated and are summarized in Table 4.2. The DEC PDP 11/40 processor was used for the time calculations primarily to demonstrate the level of sophistication required of the off-the-shelf computer to implement the vibration controller on a full scale helicopter. The number of additions and multiplications required for each function performed by the controller were calculated and the associated computation times were calculated. To be conservative, all of the functions were assumed to be performed in series so that any advantage of parallel calculations was neglected.

Results show that about 24 milliseconds are required to complete all the computations. This corresponds to about .1 of a rotor rev for full scale rotors operating in the 198 m/s to 228.6 m/s (650-750 fps) tip speed range.

In summary, these computation time results show that by using a readily available off-the-shelf computer the vibration controller can be implemented and a full scale rotor system with six vibration pickups and operate within the one rev update time, as previously outlined in Figure 4.3. With the use of microprocessors and parallel computations the total computation time can be significantly lowered if desired to accommodate even more vibration pickups.

4.5 Controller Computer Simulation

The previous sections outlined the vibration controller, discussed its separate components, and also explained how the controller could be implemented on a full scale helicopter. This section discusses the simulation of the controller coupled with a helicopter to optimize and then evaluate the performance of the controller. The controller simulation was performed on a digital computer by linking an existing nonlinear aeroelastic simulation of a helicopter with a computer subroutine that performed all of the functions of the vibration controller as outlined in the previous sections. The nonlinear aeroelastic computer analysis used to represent the vibrating helicopter, and the computer subroutine that performed all of the vibration controller functions are discussed below.

4.5.1 Nonlinear Aeroelastic Helicopter Simulation

The nonlinear aeroelastic analysis used to simulate the helicopter is the G400 analysis, documented in Reference 29. Improvements to the analysis have been made since the publication of the reference, however the reference can still be used for a detailed basic description of the analysis.

Table 4.2 Computational Requirements for Vibration Controller

$Z\ (12 \times 1),\ \theta\ (6 \times 1)$

SUBROUTINE	NUMBER OF ADDITIONS	NUMBER OF MULTIPLICATIONS	COMPUTATION TIME* (msec)	
			ADDITIONS	MULTIPLICATIONS
HARMONIC ANALYZER	--	--	< .01	< .01
STATE ESTIMATOR	--	--	--	--
PARAMETER IDENTIFICATION	294	315	0.78	3.33
MINIMUM VARIANCE CONTROL	1164	1532	3.11	16.18
LIMITER	12	27	0.03	0.29
TOTAL	1470	1874	3.92	19.80

TOTAL COMPUTATION TIME -- 23.72 msec (≈0.1 rev)

* DEC PDP 11/40 PROCESSOR

TIME INCLUDES SOURCE ADDRESS TIME, DESTINATION ADDRESS TIME, EXECUTE/FETCH TIME

This computer analysis performs a time history solution of the differential equations of rotor blade motions. The nonlinear equations of motion are solved by using a Galerkin procedure wherein the normal "uncoupled mode" shapes and spanwise derivatives of blade pitch angle and nonlinear twist are appropriately combined to describe the coupled blade deflections in response to the fully coupled inertial and aerodynamic load distributions. The rotor is coupled to the fuselage at the hub by six fuselage degrees of freedom. The six fuselage modes can be either rigid body modes, or flexible modes. Flexible motion at any point in the fuselage is achieved by multiplying the modal hub deflections by a linear transformation matrix to the point of interest in the fuselage. The flexible fuselage mode option was used for this study and the particular modes used will be discussed later. Salient features of the G-400 aeroelastic analysis are listed below:

- transient time history capability
- uncoupled modes
- fully coupled inertia and aerodynamic loads
- Galerkin type modal solution
- articulated or hingeless rotor types
- individual blade motions
- aerodynamics

  nonlinear
  constant or variable inflow

- flexible fuselage (6 degrees of freedom)

The most important features of the G-400 analysis with respect to its use for the vibration controller study are the time history solution method and the flexible fuselage modes. The time history solution format allowed the simulation of how the controller would actually be implemented on a full scale helicopter. In the simulation, at the end of every rotor rev the controller subroutine is entered and new higher harmonic control angles are calculated. The new control angles are then input at the start of the next rev in the G-400 solution. In actual implementation the controller calculations would be done in the last 25 msec (.1 rev) and the updated control angles would be input at the start of the next rotor revolution. The time history solution also allows close simulation of a transient or maneuver so that the controller can be evaluated under these conditions. The use of flexible fuselage modes allowed close simulation of how the actual sensors would work on a full scale implementation. In the simulation, time history of accelerations at six selected points in the fuselage are passed to the controller subroutine for the last quarter of every rotor revolution just as it would be done in full scale implementation. In this manner the importance of sensor location or combination of sensors can be accurately evaluated.

The articulated rotor helicopter that was modeled in the G-400 analysis is the BLACK HAWK (UH-60A) with some modifications. The modifications are in the description of the main rotor and were made to simplify the rotor system to minimize any effect that rotor system pecularities might have on

higher harmonic control performance. The rotor modifications are as follows: (a) rotor blade tip sweep was removed and blade chord is constant at the tip, (b) the nonlinear twist was replaced with equivalent linear twist, (c) the blade chordwise center of gravity, shear center, and neutral axis were placed on the quarter chord.

The resulting simulation of the modified BLACK HAWK used in the G-400 analysis will hereafter be termed the baseline helicopter. Results presented later will show the effect of parametric variations from the baseline in controller performance. The pertinent characteristics of the baseline helicopter are shown in the following table.

Design Gross Weight	7620 kg (16800 lb)
Rotor System	
Type - Articulated	
No. of Blades	4
Radius	8.169 m (26.8 ft)
Chord (nominal)	0.527 m (20.75 in)
Twist	-16 deg
Tip Speed	221 m/s (725 fps)

The G-400 analysis uses uncoupled modes to represent the baseline helicopter rotor system. The analysis uses four blade flatwise modes, two edgewise modes and one torsion mode to simulate the rotor blade dynamics. The natural frequencies of these blade modes are tabulated below.

Mode	Frequency, $\frac{\omega}{\Omega}$
Flat 1	1.01
2	2.85
3	5.11
4	8.01
Edge 1	.28
2	4.80
Torsion 1 (including control system flexibility)	4.22

Six flexible fuselage modes are used in the G-400 analysis to represent the fuselage of the baseline helicopter. These modes (which are defined from shake test data) were chosen for the proximity of their natural frequencies to the prime excitation frequency of 4/rev. These modes are listed below.

Frequency (Hz)	Mode Description
11.6	Second Lateral
12.1	Tail Vertical
13.8	Transmission Vertical/Pitch
14.3	Transmission Roll
15.3	Second Vertical
17.4	Transmission Pitch

All of these modes are fully coupled and the mode descriptions are only indicative of the primary characteristic motions. The corresponding generalized masses and the modal vectors at the main rotor hub are shown in Table 4.3. Note that the hub modal vectors are represented in terms of the 6 degrees of freedom of hub motion (3 displacements and 3 rotations). The generalized coordinates of the fuselage modes can then be calculated by

$$Z_{HUB} = \phi_{HUB}\, q \qquad (4.13)$$

$$q = \phi_{HUB}^{-1}\, Z_{HUB} \qquad (4.14)$$

where Z_{HUB} is the (6x1) vector of hub motions

ϕ_{HUB} is the (6x6) hub modal matrix

q is the (6x1) vector of modal coordinates.

In addition to the main rotor hub, six additional locations were selected throughout the fuselage for vibration measurements by the sensors. The fuselage modal vectors for each of these locations are shown in Table 4.4. Note that after the hub motions have been calculated by G-400 and the modal coordinates have been calculated by Equation 4.14, the 4/rev motions at the sensor locations can be calculated by

$$Z_{Sensors} = \phi_{Sensors}\, q \qquad (4.15)$$

Table 4.3 Modal Fuselage Representation of Baseline Helicopter at Hub

Mode No.	Freq. Hz	Generalized Mass kg $\frac{lb\text{-}s^2}{in}$	x	y	z	Modal Vector at Hub					
						θ_x		θ_y		θ_z	
						rad/m	(rad/in)	rad/m	(rad/in)	rad/m	(rad/in)
1	11.6	2.36 (1.941)	.05	-.065	.022	-.049	(-.001244)	-.0186	(-.000473)	-.236	(-.006)
2	12.1	2.43 (2)	.24	-.15	.022	-.049	(-.001244)	-.0186	(-.000473)	-.236	(-.006)
3	13.8	3.34 (2.747)	-.402	.15	-.11	-.315	(-.008)	-.126	(-.0032)	-.0173	(-.00044)
4	14.3	2.76 (2.268)	.001	.54	-.001	.478	(.01214)	.0031	(.00008)	.0157	(.0004)
5	15.3	6.24 (5.13)	1.	.001	-.31	.5126	(.01320)	-.2126	(-.0054)	.006	(.00015)
6	17.4	5.78 (4.75)	.7	.52	.125	-.0027	(-.00007)	.91	(.0231)	.006	(.00015)

Table 4.4 Modal Fuselage Representation of Baseline Helicopter at Sensor Locations

Mode No.	Freq. Hz.	Fuselage Modal Vector					
		Pilot Longitudinal	Pilot Lateral	Pilot Vertical	Copilot Vertical	Nose Vertical	Cabin Vertical
1	11.6	.001	-.05	-.01	-.015	.03	-.02
2	12.1	-.05	-.02	.04	.04	-.3	-.04
3	13.8	.066	-.08	.2	.2	.45	-.10
4	14.3	.001	-.035	-.08	.08	.001	.001
5	15.3	-.03	-.019	.325	.36	1.1	-.5
6	17.4	-.035	-.03	-.2	-.04	.1	-.6

where $Z_{Sensors}$ is the (6x1) vector of 4/rev motions at the sensors

$\phi_{Sensors}$ is the (6x6) sensor modal matrix

q is the previously defined modal coordinate vector.

This result is essentially a linear transformation between motion at the hub and motion at any point in the fuselage.

4.5.2 Vibration Controller Subroutine

This section describes the computer simulation of the vibration controller outlined in Section 4.3. The vibration controller was formulated into an independent subroutine named CONTRL which is linked to the G-400 aeroelastic simulation of the baseline helicopter. The subroutine CONTRL performs all the functions of a full scale production controller and also interacts with the G-400 helicopter simulation in much the same manner that a production controller would interact with a production helicopter. Figure 4.5 shows a schematic of subroutine CONTRL including the interface with the G-400 analysis.

During the time history solution process in G-400, the time integration step is normally set to an equivalent 2.5 degrees of rotor azimuth. At the end of the 360 degree azimuth calculation, the subroutine CONTRL is called by the G-400 main program and the vibration controller is entered. By means of a matrix in the subroutine argument, the time varying fuselage accelerations for the last quarter rev (270 to 360 degrees azimuth) as computed by G400 are passed to the controller to simulate analog sensor signals. This step initiates the vibration controller functions which are simulated by additional subroutines in CONTRL. The subroutine INPUT stores the fuselage accelerations received from G-400. If this is the first rotor rev after the controller is activated, the subroutine INIT initializes all of the required processing parameters. This includes the initial T-matrix and nulling of the higher harmonic control vector. Then the subroutine HARMON is entered which performs the harmonic analysis (FFT) on the fuselage accelerations stored on subroutine INPUT. The output of subroutine HARMON is a vibration vector, Z, with dimension of (12x1). These are the cosine and sine components of the 4/rev vibrations as calculated by the harmonic analyzer from the last quarter rev data for the six vibration sensors.

At this point there is a variation from the format of a production controller. An additional subroutine termed NOISE is entered to add discrete 4/rev noise to each of the calculated 4/rev vibrations if desired. The purpose of this subroutine is to test the tolerance and performance of the vibration controller in the presence of signal noise. The noise is input in terms of noise to signal ratio based on a normal distribution and the level of this noise can be varied by a single input to the controller subroutine. The particular noise model used is taken from the International Mathematics and Statistical Library.

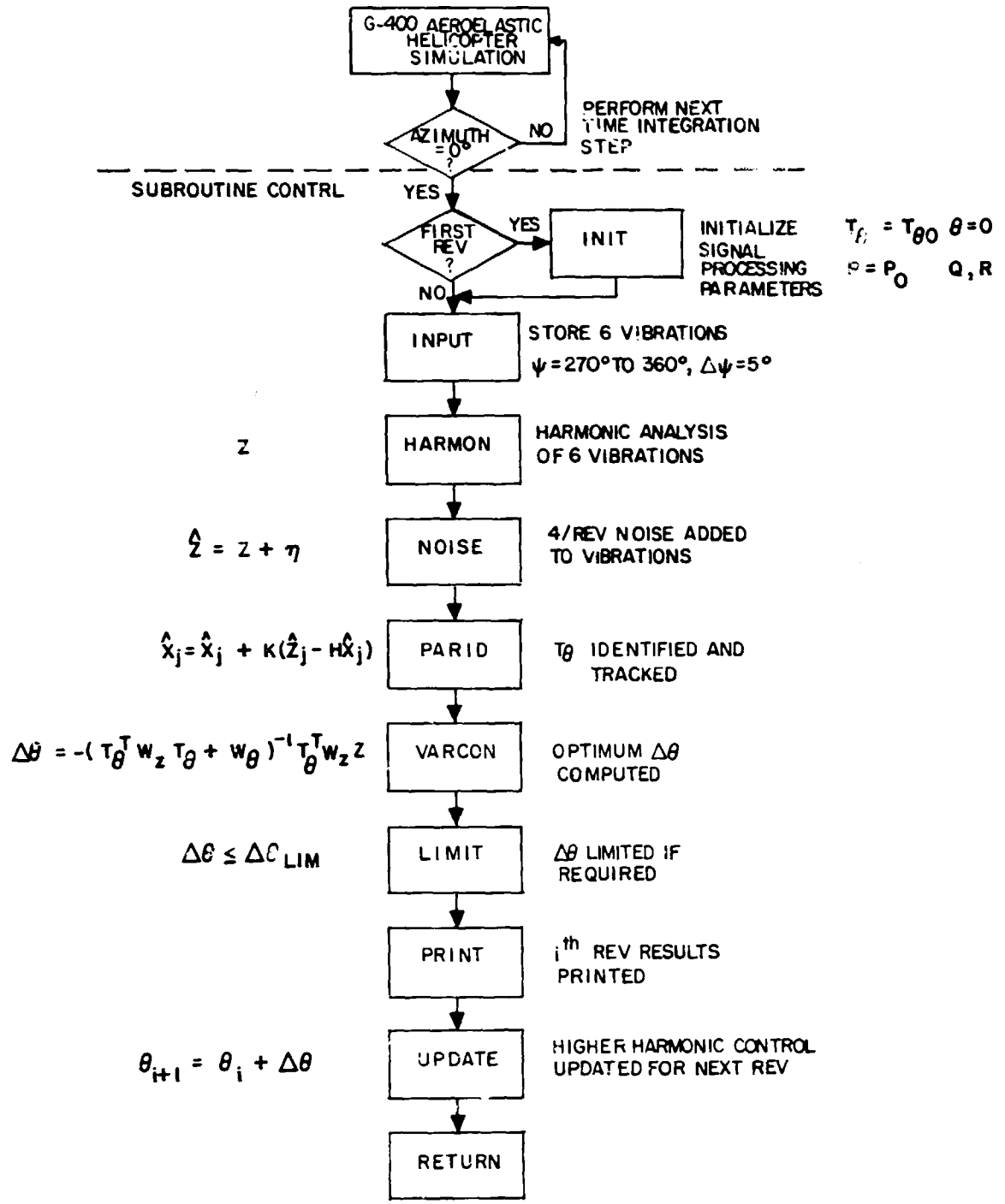

Figure 4.5 Flow Diagram of Controller Subroutine.

After noise has been added to the 4/rev vibrations, the subroutine PARID is entered. The subroutine performs all of the functions of the parameter identifier and tracker discussed previously in Section 4.3. The primary purpose of this subroutine is to identify and track the T-matrix which relates fuselage vibration response to higher harmonic control inputs. The T-matrix is required by the minimum variance control algorithms, and once it has been computed by PARID it is passed to the subroutine VARCON which performs the minimum variance control calculations. The end product of VARCON is a computed optimum $\Delta\theta$ to update the higher harmonic control vector.

Before the higher harmonic control vector is updated, the calculated $\Delta\theta$ from VARCON is passed into subroutine LIMIT. This subroutine performs the same functions that the limiter would perform on a production controller. If the calculated optimum $\Delta\theta$ is larger than that allowed due to actuator hardware limitations or other reasons, the $\Delta\theta$ is limited to the prescribed amplitude, but the phase of the higher harmonic control vector is unchanged. For example if a .1 degree limit is placed on each control update due to actuator response limitations, the $\Delta\theta$ signal to be sent to the actuators will not exceed the value even though the optimum input may have required larger value. At this point in subroutine CONTRL, the $\Delta\theta$ needed for the next rev update has been calculated and the results for the present rotor rev are printed in subroutine PRINT. The new higher harmonic control vector for the next rotor rev is calculated in subroutine UPDATE by adding the computed $\Delta\theta$ to the total θ from the previous rev. Having completed all of its functions the subroutine CONTRL then passes the new θ vector back to G-400 and the analysis continues its time history solution with the updated higher harmonic control.

4.6 Theoretical Results

Analysis, optimization and evaluation of the vibration controller were performed by operating the G-400 helicopter simulation with the vibration controller subroutine CONTRL linked as discussed in the previous section. The theoretical study consists of two parts. The first part of the study deals with the characteristics of the controller for a high speed baseline helicopter flight condition. The second part of the study is a parametric evaluation of how well the controller performs for different flight conditions and different rotor configurations.

4.6.1 Controller Analysis and Optimization at High Speed

A 150 kn baseline helicopter flight condition was selected as the point for studying how the controller operates in a nonlinear simulation. Many different controller configurations were tested at the 150 kn condition to evaluate the controller and then optimize its configuration for the second part of the theoretical study in which many parametric variations in aircraft and flight conditions are made. These theoretical studies resulted in a baseline controller configuration which showed the best

overall performance. The characteristics of the baseline controller configuration are listed in the following table.

Sensors	Weightings
pilot vertical	1.0
pilot lateral	1.0
pilot longitudinal	1.0
copilot vertical	1.0
nose vertical	.01
cabin vertical	1.0
Time between updates	One rotor revolution
$\Delta\theta$ between updated	Not more than .1 degree at 3, 4, 5 per rev
Control weights	3, 4, 5 per rev equally weighted

Six vibration sensors were used to demonstrate a broad, rather than a local, vibration reduction. The nose vertical sensor is practically unweighted for reasons to be discussed later. The time between updates is set at one rotor revolution to demonstrate fast update capability for a transient or maneuver and the maximum $\Delta\theta$ between updates is limited to .1 degree. The performance of this baseline controller for the 150 kn condition is discussed below.

Vibration Reduction - Figure 4.6 shows the G-400 helicopter simulation results with the baseline controller operating in closed loop. The figure shows G-400 time histories of vibration and higher harmonic control amplitude after the controller is turned on at the fourth revolution. The vibration performance index J (sum of the squares of all of the weighted vibrations) is shown along with one typical component of vibration (pilot vertical) and one typical component of higher harmonic cyclic pitch (3/rev). The vibration performance index J is a good overall indicater of controller performance since it includes all of the sensed vibrations. Figure 4.6 shows that after the controller is activated at rev 4, the performance index (J) immediately starts to decrease and by rev 12 the value of J is 10% of its initial value (equivalent to 30% of initial RMS value). The elapsed time from the time the controller was turned on at rev 4 to rev 12 is about 2 seconds. After rev 12, J continues to decrease and by rev 40 the value is 1 percent of the baseline value at rev 4. The pilot vertical vibration also decreases abruptly after rev 4 and, 2 seconds later, at rev 12 its amplitude is 15 percent of the baseline level. By rev 40, the pilot vertical vibration is .04g compared to the baseline .87g. The change in 3/rev cyclic with time after the controller is activated shows a gradual increase in amplitude with perturbations from rev to rev. The initial rate of 3/rev cyclic pitch update is about .06 degrees per rev and it is over this range that the greatest reduction in vibrations occur. By rev 12 the 3/rev pitch has

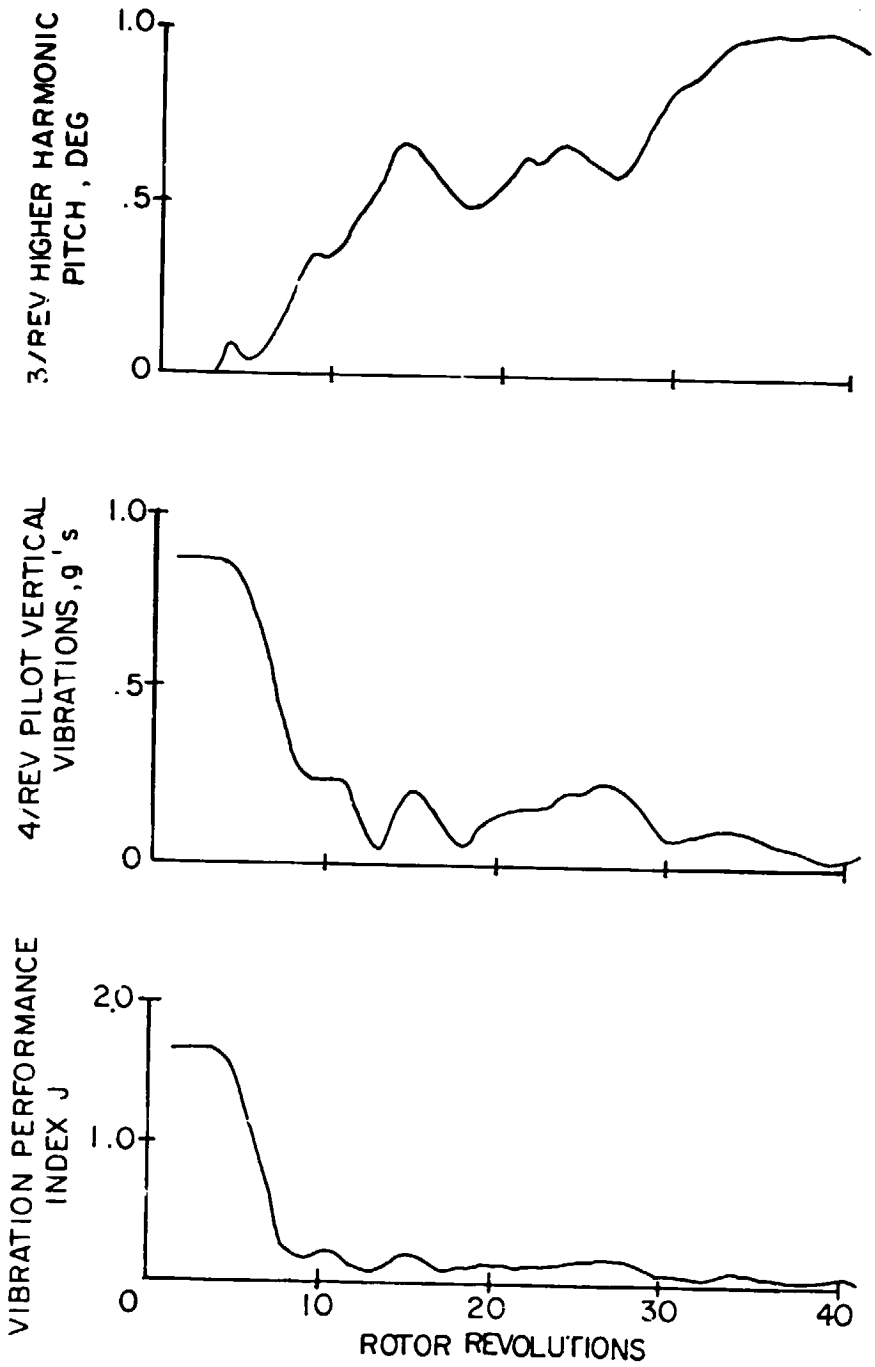

Figure 4.6 Time History of Vibration Controller at 150 Knots.

reached half of its final value and the vibrations have been reduced by about 75 percent. By rev 34 the 3 per rev cyclic pitch has settled to an amplitude of about one degree.

The last point to be made about the transient results in Fig. 4.6 is that the controller would normally be activated in hover and not at 150 kn so that the vibration controller would not have to change the higher harmonic control by a degree in such a short time to reach the optimal input. The fact that the vibration performance index J is reduced by 90 percent in 2 seconds after the controller is activated indicates that the controller should have good transient and maneuver vibration performance.

The change in the individual vibration components are shown in Fig. 4.7. In this figure a comparison is made between the 4/rev vibration levels at rev 4 without higher harmonic control and at rev 40 with the controller activated. The fuselage vibrations at the six sensor locations along with the fixed system hub vibrations are shown. All of the fuselage vibrations have decreased substantially except for the nose vertical vibration which has doubled in amplitude. Since the nose vertical vibration is practically unweighted in the performance index this increase is not unexpected. It is possible to reduce the nose vibrations and the implications of this will be discussed more fully later. The components with the largest reductions are the pilot, copilot and cabin vertical vibrations. All these components have been reduced by more than 90 percent with higher harmonic control. The remaining two components (pilot lateral and longitudinal) both have reductions greater than 50 percent. Two important points should be made concerning these results. First, the vibration reductions are in all three directions, not just vertical. In addition to reductions in the lateral and longitudinal directions, the pilot and copilot vertical vibrations contain a substantial roll component. So it can be said that the effect of higher harmonic control is not directionally sensitive but rather that the benefits of higher harmonic control can be realized in all three axes. The second point to be made is that all of the cabin and cockpit vibrations are less than .1g and therefore the resultant vibration levels conform to the latest military vibration specifications. Although the results are theoretical, the important point is that the vibration controller has reduced rather large vibrations to acceptable levels in the crew inhabited areas without the use of any other kind of vibration device such as vibration absorbers or transmission isolation. It is reasonable to expect that such delta changes on a flight helicopter can also be realized.

Also shown in Fig. 4.7 are the fixed system hub vibrations. The three angular vibrations have been multiplied by 0.305m (1 foot) so that all six hub vibrations are presented in the form of g's. All six hub vibrations have been substantially reduced with the vibration controller even though the sensor measurements for the vibration controller are the six fuselage accelerations. This indicates that the vibration reductions with higher harmonic control are primarily due to reduced forcing at the rotor hub rather than a vectoral cancellation of the fuselage modal contributions to vibrations.

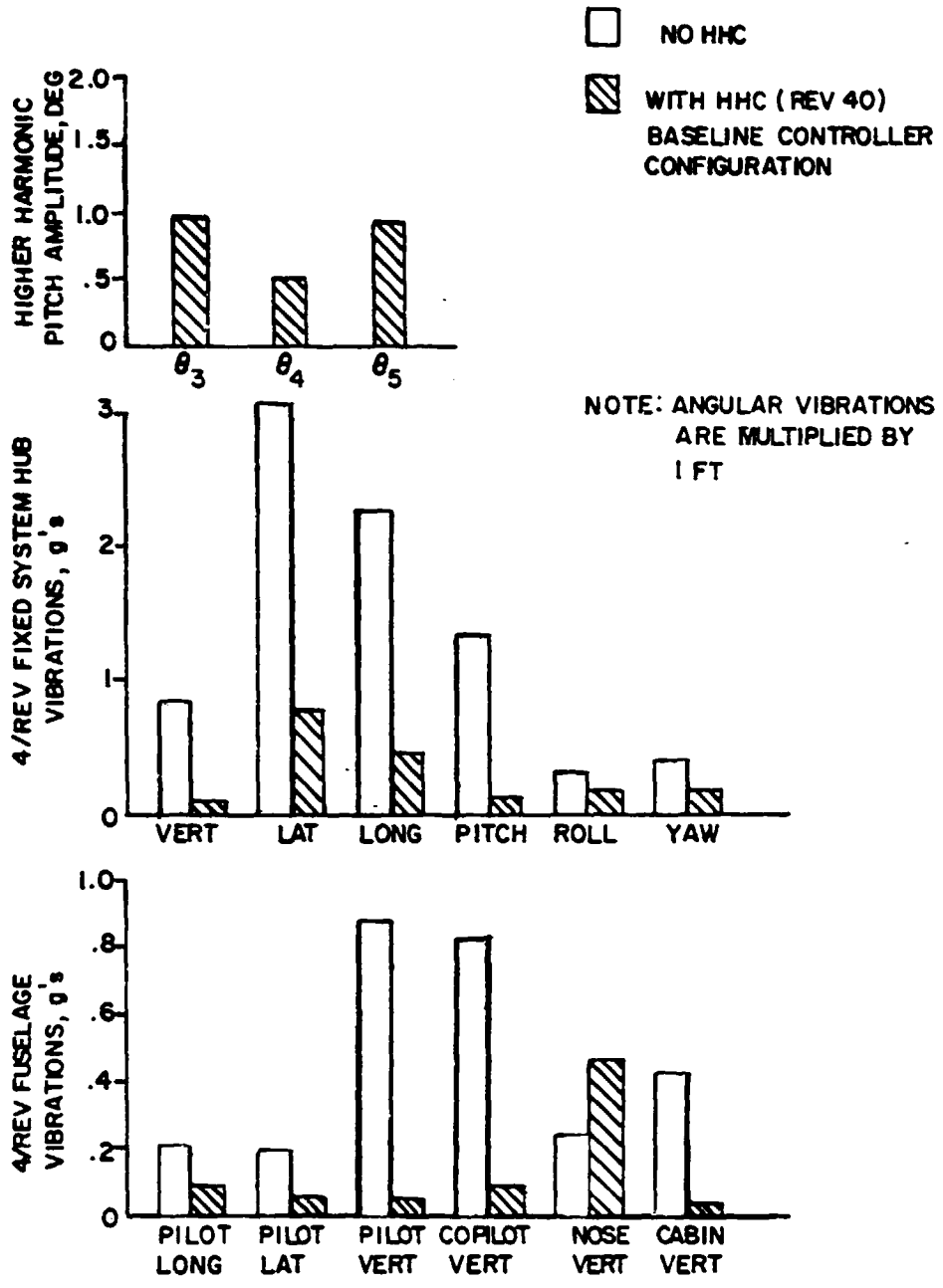

Figure 4.7 Effect of Active Vibration Control on Vibrations at 150 Knots.

The amplitudes of higher harmonic control required to achieve the vibration reductions are also shown in Fig. 4.7. All three cyclic pitch amplitudes are less than 1 degree. Since high speed flight is a high vibration condition it is reasonable to assume that the amount of higher harmonic control required for vibration reductions throughout the flight envelope is on the order of one degree.

Nonlinearity of Transfer Matrix - One of the primary concerns addressed during the formulation of the controller configuration is the possible nonlinear sensitivity of fuselage vibrations to higher harmonic control inputs. The nonlinearity could occur during maneuvers or transients, during changes in airspeed in accelerated flight or just with higher harmonic control amplitude for a steady flight condition. The presence and severity of such nonlinearities is fundamentally important to the stability and effectiveness of the controller configuration because the controller is founded on the static linear transfer matrix approach. If the helicopter vibratory response to control inputs is nonlinear, then the controller algorithms must be appropriately adjusted.

The nonlinearity of the predicted 150 kn T-matrix with control input amplitude is evident in Figure 4.8. The 4/rev pilot vertical vibration response (amplitude and phase) is shown as a function of 3/rev cyclic input as determined from open loop perturbation at 150 kn. The 3/rev cyclic amplitude is perturbated at .5, 1.0, and 1.5 degrees about the zero point and the phase of the cyclic input is swept through 360 degrees. A linear response would be represented by a circular or elliptical pattern with straight line axes for constant phase input. Figure 4.9 also shows the 4/rev pilot vertical vibration response to 3/rev cyclic except that now the 3/rev perturbation is performed with 1 degree of 5/rev input fixed. These results show even more severe nonlinearity than the previous results in Figure 4.8; the pilot vertical response has folded back on itself with increased amplitude of control input so that the input-output relationship is double valued. Also note that the overall shape of the deformed elliptical response is changed significantly from Figure 4.8 to 4.9. In Figure 4.8 the deformed elliptical response developed counterclockwise with input phase; in Figure 4.9 the deformed elliptical response developed clockwise. This shows that the T-matrix elements are not only nonlinear with input amplitude but also vary nonlinearly with and are dependent upon the total control input vector; e.g., the sensitivity of vibration to 3/rev input changes with 5/rev input, etc. These results indicate that singly perturbating open loop and then inverting the T-matrix so developed to calculate the solution will not work because the T-matrix changes significantly with the amplitude, phase and mix of 3, 4, and 5 per rev inputs.

To investigate this point, a closed loop simulation was performed with G400. The controller was configured with the initial T-matrix for the zeroth rev set equal to the transfer matrix obtained from a .5 degree open loop perturbation. Also, the Kalman gain in the identification algorithms was made very small by making R, the noise covariance, large. With this configuration the T-matrix was allowed to change very slowly through identification so that, in effect, the controller was always operating with the input T-matrix for the zeroth rev. The time variation of the vibration performance

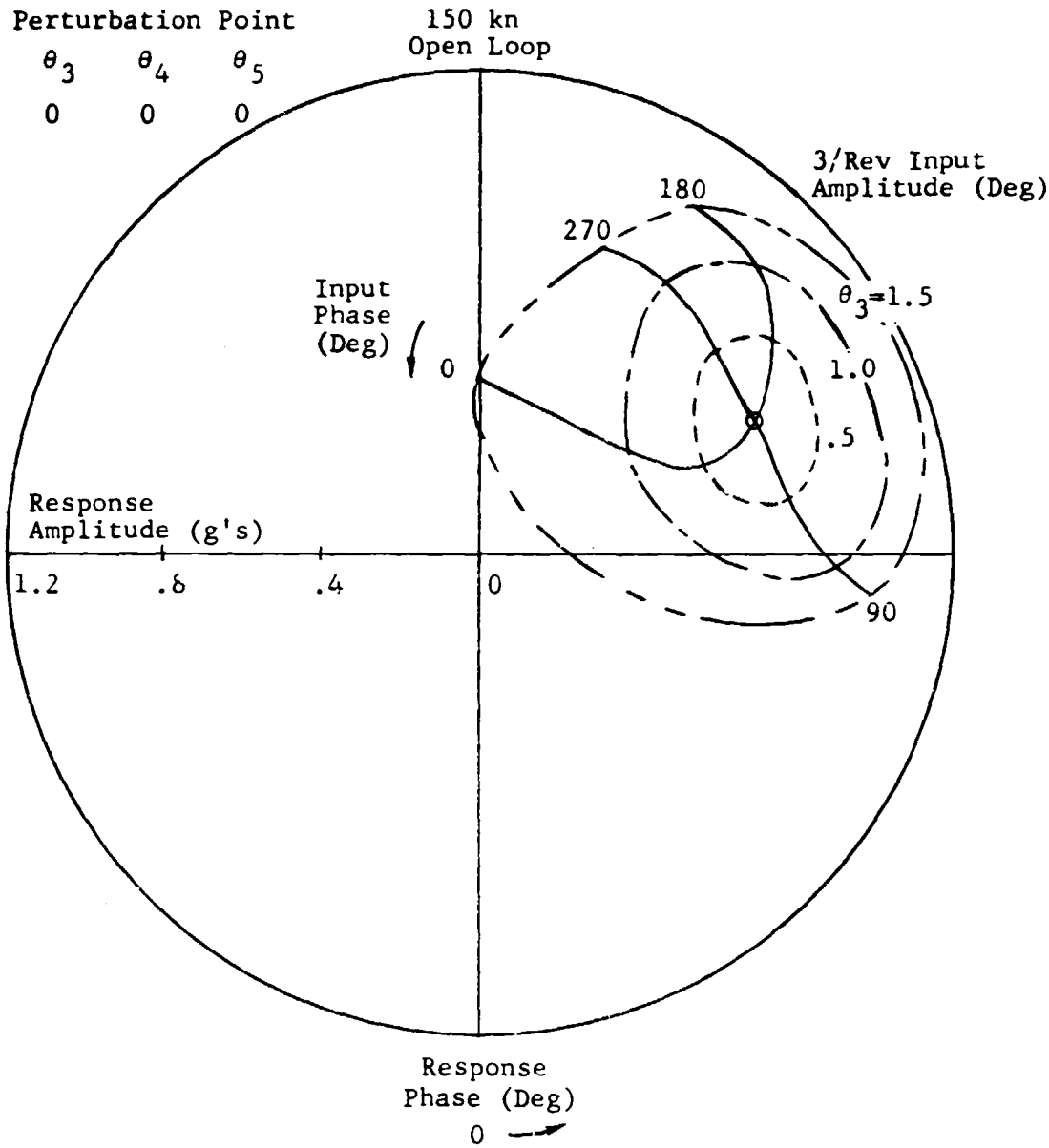

Figure 4.8 Amplitude and Phase Relationship Between 4/Rev Pilot Vertical Vibration and 3/Rev HHC Perturbation About Zero HHC Point.

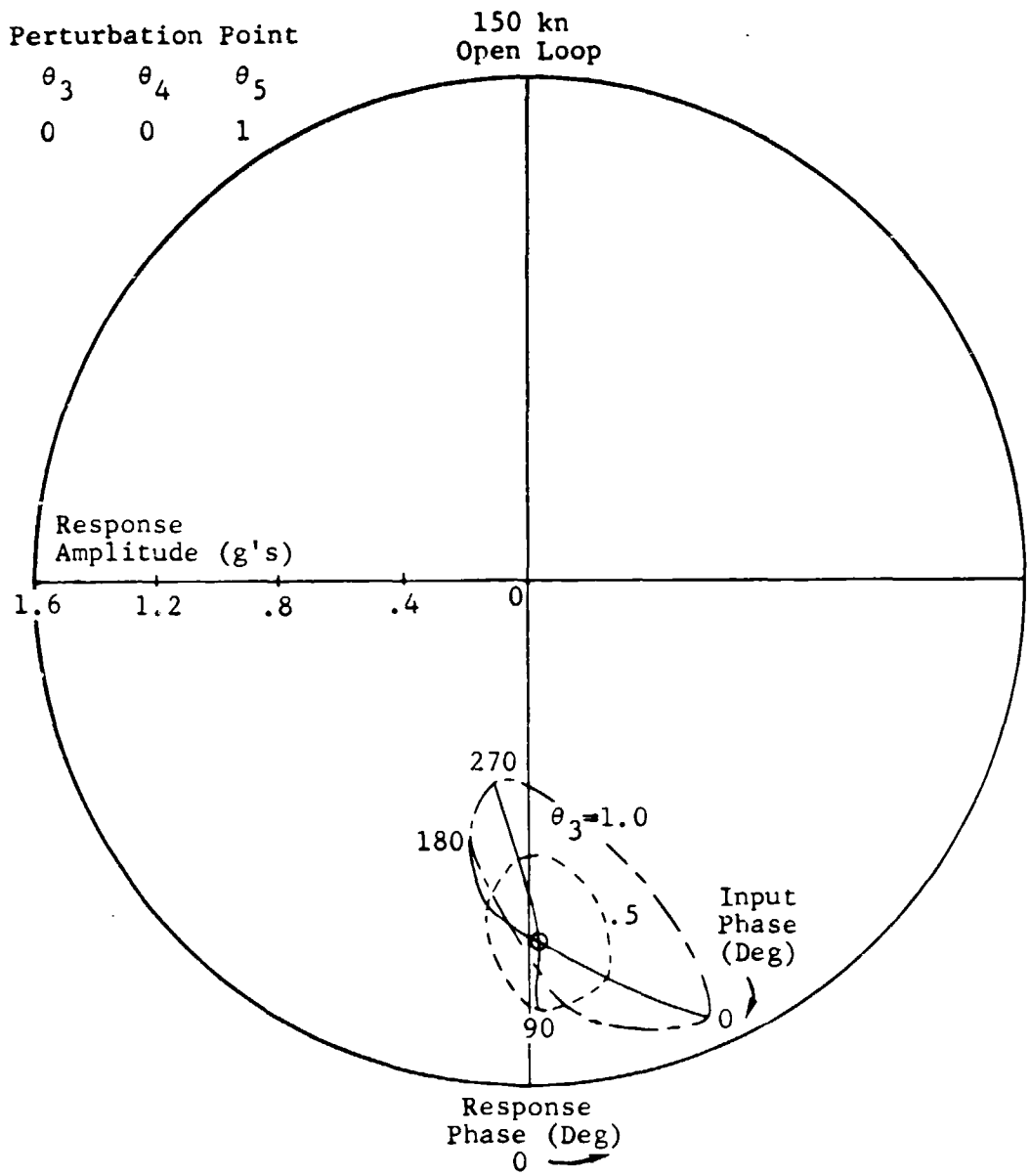

Figure 4.9 Amplitude and Phase Relationship Between 4/Rev Pilot Vertical Vibration and 3/rev HHC Perturbation about 1^0 of 5/Rev.

index for this case is shown in Figure 4.10. After only a few rotor revs after the controller is initiated at rev 4, the controller is amplifying instead of alleviating vibration. In fact, the controller appears to be unstable and is producing vibration levels that are oscillating between good attenuation and four times amplification. The level of higher harmonic control input steadily increases so that by rev 40 the amplitudes of the HHC are on the order of 2 degrees. It is clear that the T-matrix varies nonlinearly and that the T-matrix determined from open loop perturbation is an inadequate estimate of the actual nonlinear T-matrix. If the transfer matrix approach is applied to operate in a closed loop under such severe nonlinear conditions, then real time identification and tracking of the T-matrix is a fundamental requirement. It also becomes quite important to increment the $\Delta\theta$ input and determine the limit of the increment based upon the severity of the nonlinearity. Tuning of the controller (P, Q, R, weightings) will also be required.

Another measure of the nonlinearity is shown in Figure 4.11. This figure compares the T-matrices generated from open loop perturbation and that identified by the controller in closed loop for the same flight condition. The closed loop identified T-matrix is for rev 40 for the results shown in Figure 4.6. Nearly every element of the identified T-matrix changes from the open loop T-matrix results. Figure 4.12 graphically shows the extent of the changes for the pilot vertical vibration. The elements of the T-matrices in Figure 4.11 are plotted in polar form in Figure 4.12 for the pilot vertical vibration. These results show significant differences in both amplitude and phase of the sensitivities, and underline the need for on-line identification and tracking.

In summary, the theoretical results for the 150 kn case have shown that the T-matrix varies nonlinearly not only with control input amplitude but also with the mix of higher harmonic inputs. This emphasizes the need for real time identification and tracking of the T-matrix in situations where rapid changes in control amplitude and/or phase may be required, such as in a transient or maneuver. It is also clear that a scheme for identification and tracking of a nonlinear system will be needed just to reach the optimum solution for a steady state flight condition. This scheme would entail the tailoring of the identification algorithm with a $\Delta\theta$ limiter and the time between updates along with the covariances Q and R so that the nonlinear problem can be effectively solved piecewise with a linear solution. More investigation should be performed into the observed theoretical nonlinearities to determine the source and understand the mechanisms involved.

Rotor Blade Stresses - Another area of interest that could be affected by higher harmonic control is cyclic rotor blade stresses. Since higher harmonic cyclic pitch affects the rotor blade airloads, it is reasonable to assume that some changes in blade stresses would accompany changes in

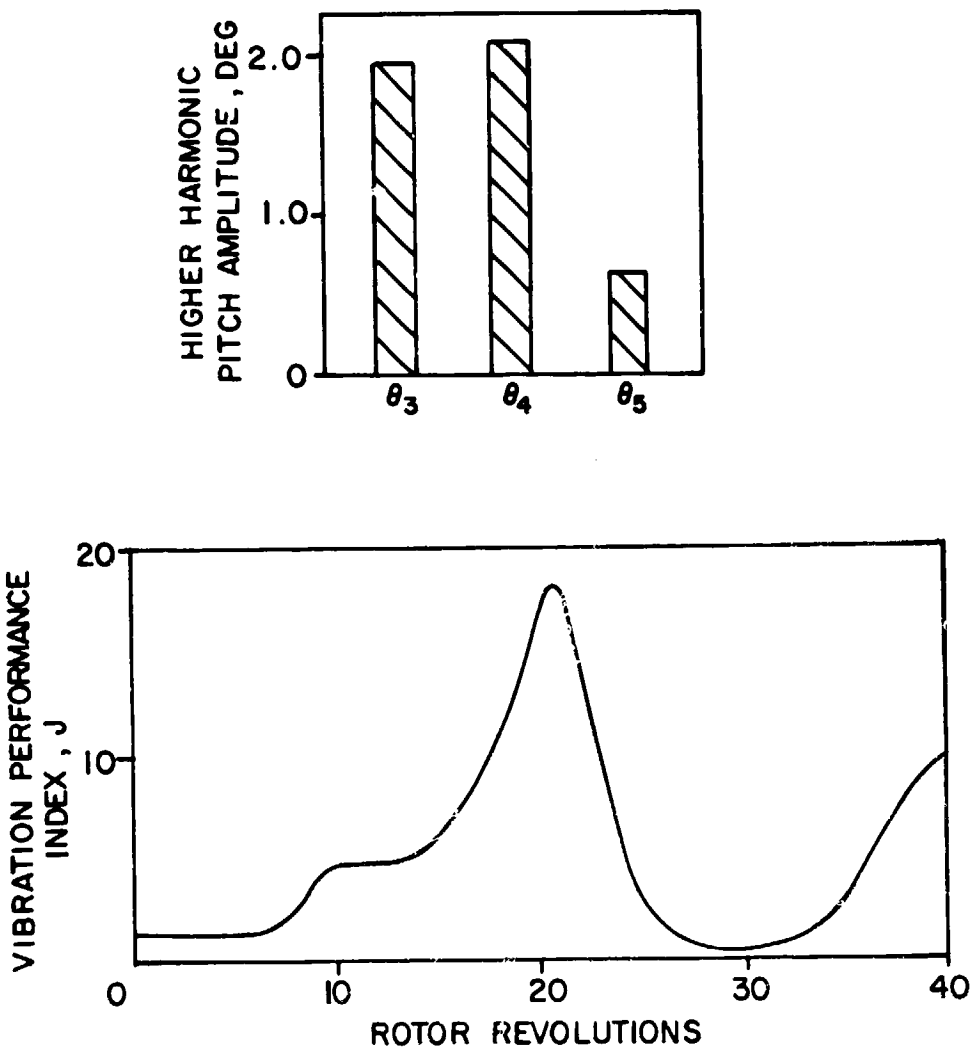

Figure 4.10 Performance of Active Vibration Controller.

			θ_{3C}	θ_{3S}	θ_{4C}	θ_{4S}	θ_{5C}	θ_{5S}
Pilot	Long	C	-.055	-.080	.696	.030	-.166	.451
		S	.050	-.010	-.212	.328	-.211	.027
Pilot	Lat	C	.032	-.029	-.453	.246	-.453	-.049
		S	.019	.058	-.211	.063	-.083	-.460
Pilot	Vert	C	.162	-.174	-.132	-1.062	-.857	-1.392
		S	.246	.327	.565	-1.575	2.158	1.038
Copilot	Vert	C	.130	-.122	-.074	-1.537	-.562	-1.058
		S	.331	.328	.776	-1.589	2.305	1.610
Nose	Vert	C	.224	-.620	6.300	-1.951	-1.814	.245
		S	.985	.470	.642	-1.089	1.640	1.567
Cabin	Vert	C	-.174	.049	-.687	.876	-.008	.822
		S	-.234	-.132	-.840	1.085	-.983	-.767

(a) Open-Loop Perturbation

			θ_{3C}	θ_{3S}	θ_{4C}	θ_{4S}	θ_{5C}	θ_{5S}
Pilot	Long	C	-.177	.097	-.225	.003	.200	.434
		S	-.036	-.388	-.268	.110	.088	-.219
Pilot	Lat	C	.114	-.224	-.375	.012	.365	-.058
		S	-.080	-.178	-.166	.092	-.079	-.426
Pilot	Vert	C	.293	.487	-.661	-.521	.330	-.629
		S	.727	.003	.778	-.164	-.217	.668
Copilot	Vert	C	.048	.776	-.618	-.492	.304	-.199
		S	.603	.362	1.154	-.038	-.176	1.175
Nose	Vert	C	-.173	1.400	-1.023	-.930	.001	.986
		S	2.239	.084	.394	-.349	-.027	.255
Cabin	Vert	C	-.353	-.371	-.220	.448	.577	.520
		S	-1.028	-1.021	-.771	.519	.167	-.860

(b) Closed-Loop Identification

Figure 4.11 Transfer Matrix at 150 Kn.

150 kn

	θ_3	θ_4	θ_5
Open loop perturbation -----	0	0	0
Closed loop identified ———	.95	.5	.92

g's per degree

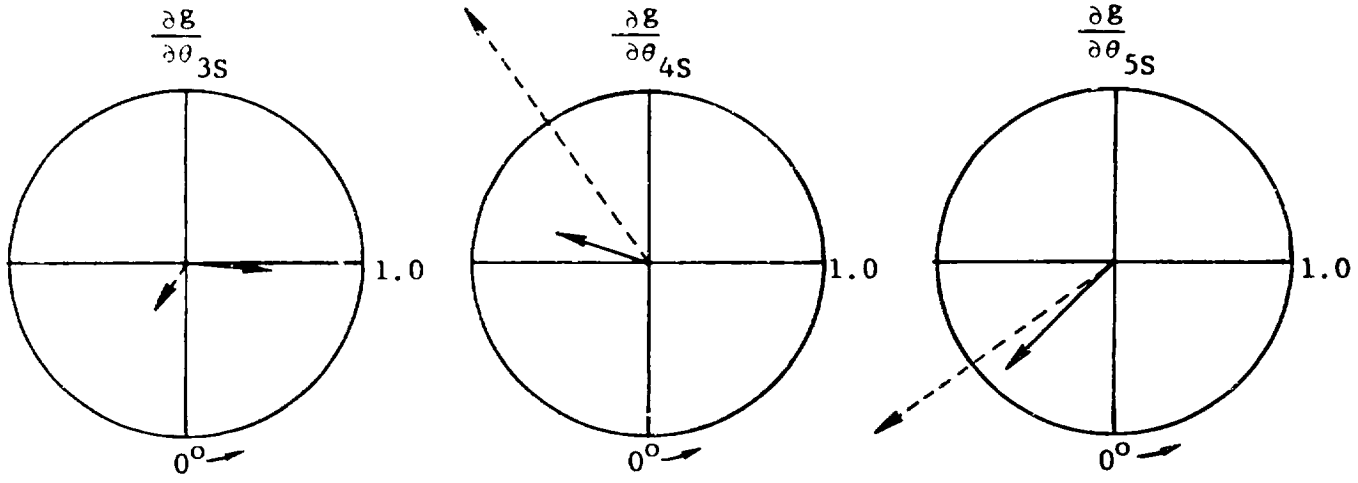

Figure 4.12 Change in Sensitivity of Pilot Vertical Vibration to HHC Input.

vibrations. Figure 4.13 shows that blade stresses do change to varying degrees with higher harmonic control. This figure shows the peak to peak blade bending moments and torsional moments along the rotor blade for the baseline condition, compared to those at rev 40 with optimum higher harmonic control. There is an increase in both bending and torsional moments with higher harmonic control. The inboard flatwise moments increase by about 35 percent, the edgewise moments increase only slightly (5 percent) near midspan and the torsional moments increase by about 20 percent at the blade root. Figure 4.14 breaks down the peak to peak moments shown into harmonics at key stations along the rotor blade span to reveal the source of the increased blade stresses.

The flatwise moment increases with higher harmonic control have 1, 2, 7 and 8 per rev content, while the 3, 4, and 5 per rev content are either reduced or unchanged. This indicates that the direct effect of higher harmonic control on blade moments (N/rev cyclic pitch affecting N/rev blade moments) is small but the indirect effect of harmonic coupling can be important. By linear aerodynamics, it is possible to create 1 and 2 per rev airloads with 3 and 4 per rev cyclic pitch as a function of advance ratio (μ). It is suggested that this interharmonic coupling is the source of the increased flatwise moments. The importance of the coupling is a function of advance ratio and also a function of the phasing of 3 and 4 per rev cyclic pitch. It would seem to be just as possible to have a net decrease in 1 and 2 per rev airloading and also no net change, depending upon the phases of all of the airloads. The edgewise moment increases are at 1, 4, 6, 7 and 8 per rev. The 1/rev increases is most likely due to an associated increase in 1/rev drag. However, 4/rev edgewise moment increase is not so easily explained since the 4/rev flatwise moment decreased with higher harmonic control, and this indicates a net decrease in 4/rev airloads. Equally important for the edgewise moments is the decrease in the 5/rev component. The large 5/rev reduction compensates for the other harmonic increases and may be the reason for the relatively small increase in edgewise peak to peak moments shown previously.

The harmonic content of the torsional moments shown in Fig. 4.14 reveals that increased peak to peak moments with higher harmonic control are due to increases in the 4 and 5 per rev contributions. This is not surprising since the blade torsion frequency is near 4/rev and oscillating the blade at frequencies near 4/rev provides strong inertial forcing. However, the 1/rev content dominates the torsion peak to peak moment so the large increase in 4 and 5 per rev content is not felt nearly as strong on a peak to peak stress basis. In summary, higher harmonic control affects rotor blade cyclic moments to varying degrees, and interharmonic coupling is the probable source of the increased bending moments. Both bending moments and torsion moments increase but the edgewise and torsion moment increases are relatively small and can probably be tolerated. The area of largest increase is inboard flatwise moments due to increased 1, 2, 7 and 8 per rev content. The increase is about 35 percent and it is likely that this level of increase is significant from a blade life point of view. The questions of increased

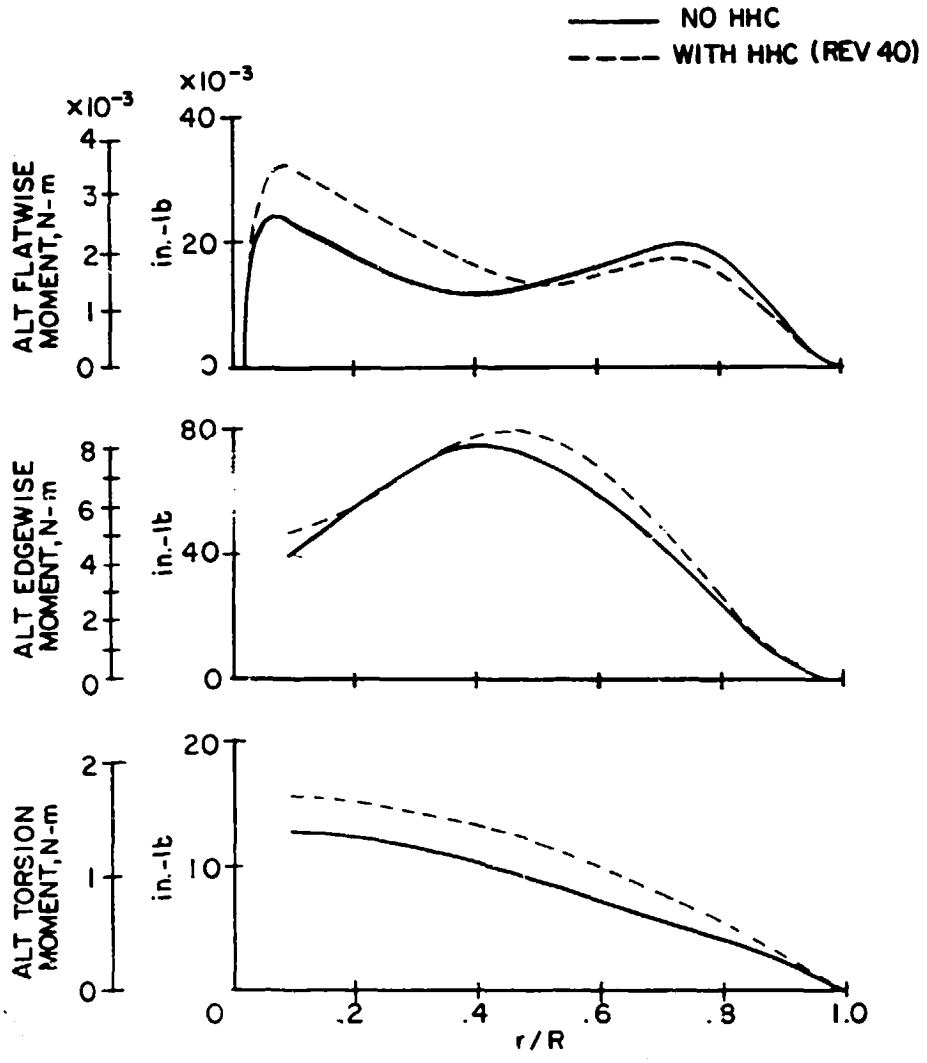

Figure 4.13 Effect of Active Vibration Control on Rotor Blade Vibratory Moments at 150 Knots.

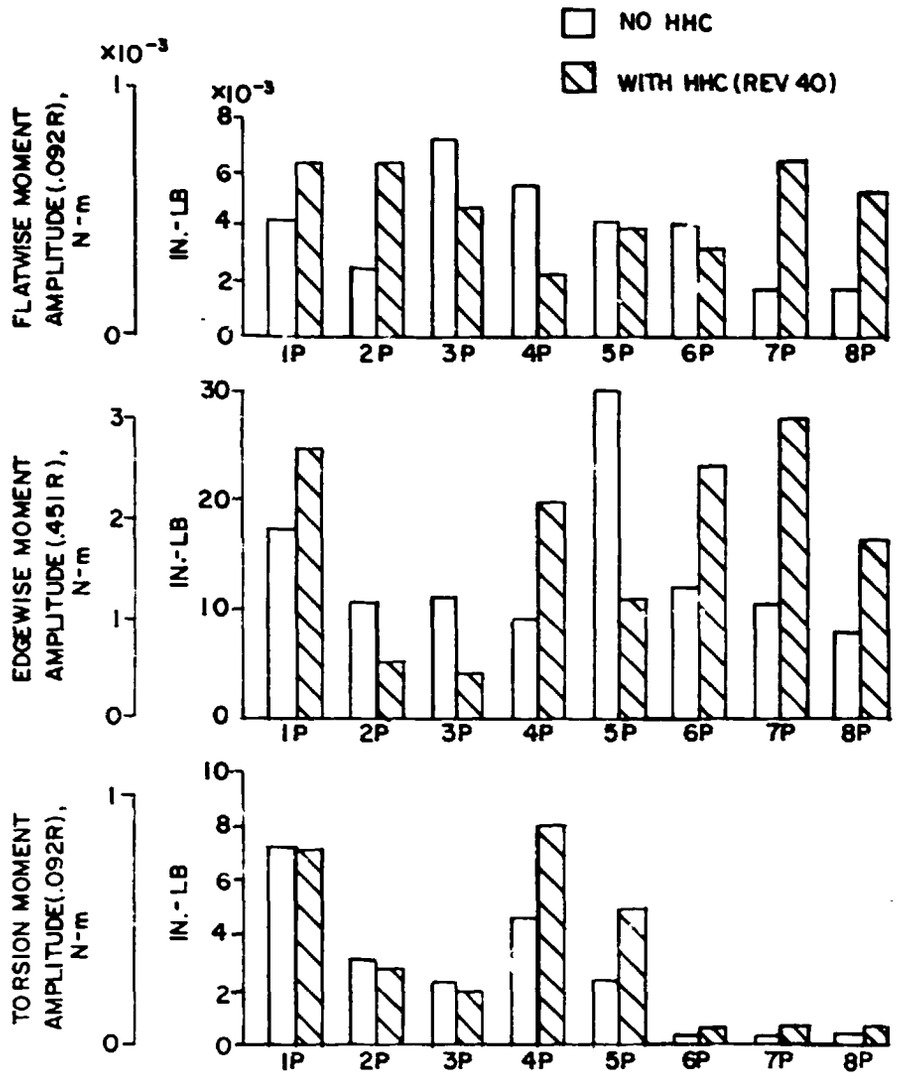

Figure 4.14 Change in Rotor Blade Harmonic Moments with Active Vibration Control at 150 Knots.

blade stresses and control loads are only germaine if one wants to incorporate higher harmonic control into an existing production helicopter with minimum change to the rotor and control system. For a new aircraft, or significant model change, increases in loads such as indicated by this study could easily be accomodated in the basic design (redesign). For a flight program to demonstrate the higher harmonic control concept accepting reduced component lives or restricting the flight envelope are appropriate procedures for insuring safety. An alternate approach to accepting higher blade stresses is to include them in the performance criteria J, having computed them with a state estimator. This approach was not pursued during the present study however.

Rotor Performance - In addition to vibration and rotor loads, another area of interest that could be affected by higher harmonic control is rotor performance. It is desirable not to pay a direct power penalty for higher harmonic control and this question is addressed in Fig. 4.15. Key rotor performance and trim parameters are shown for the baseline compared to that for optimum higher harmonic control. Higher harmonic control causes a 3 percent increase in rotor thrust. In the G-400 simulation, with the vibration controller linked to the rotor, the rotor cannot be retrimmed for thrust after the controller is activated so any increase in thrust must be accepted. In actual flight, any impact of higher harmonic control or rotor thrust would be accounted for by the pilot's adjustment of collective pitch. The increase in thrust is accompanied by a 5% increase in torque and a 1% increase in propulsive force. The equivalent L/D is decreased by 5% with HHC. This is within the accuracy of the performance analysis which assumes both constant inflow and steady aerodynamics. Hydraulic power required to oscillate the swashplate actuators is not included in this performance estimate.

Effect of Vibration Sensor Weightings - An important aspect of the vibration controller configuration is the selection of locations for vibration measurements and the weighting of relative importance of one vibration measurement to the other vibration measurements. As previously discussed, the locations of the sensors were chosen to provide a broad vibration reduction throughout the fuselage. Using the six sensor locations, different combinations of sensor weightings were tried with the vibration controller to evaluate the effect of sensor weightings.

The G-400 simulation with controller was run with the different weighting combinations in the same manner as previously described. The controller was activated at rev 4 and the time simulation continued for a total of 40 revs. Results of the effects of sensor weightings are shown in Fig. 4.16. Four different combinations of sensor weightings were tried and the vibration results for each weighting configuration are compared in the figure with the baseline vibration with no higher harmonic control. At the top of Fig. 4.16 the results for the baseline controller configuration (nose unweighted) previously shown in Fig. 4.7 are presented again for comparison purposes. Below the baseline configuration results are the equal weighting

	BASELINE	HHC	% NET CHANGE
THRUST	71 919 N (16 168 lb)	74 072 N (16 652 lb)	+3%
TORQUE	53 013 N-m (39 115 ft-lb)	55 730 N-m (41 104 ft-lb)	+5%
PROPULSIVE FORCE	8 283 N (1862 lb)	8 389 N (1886 lb)	+1%
EQUIVALENT L/D	6.46	6.65	-5%

BASELINE: 150 kn LEVEL FLIGHT

Figure 4.15 Effect of Higher Harmonic Control on Rotor Performance.

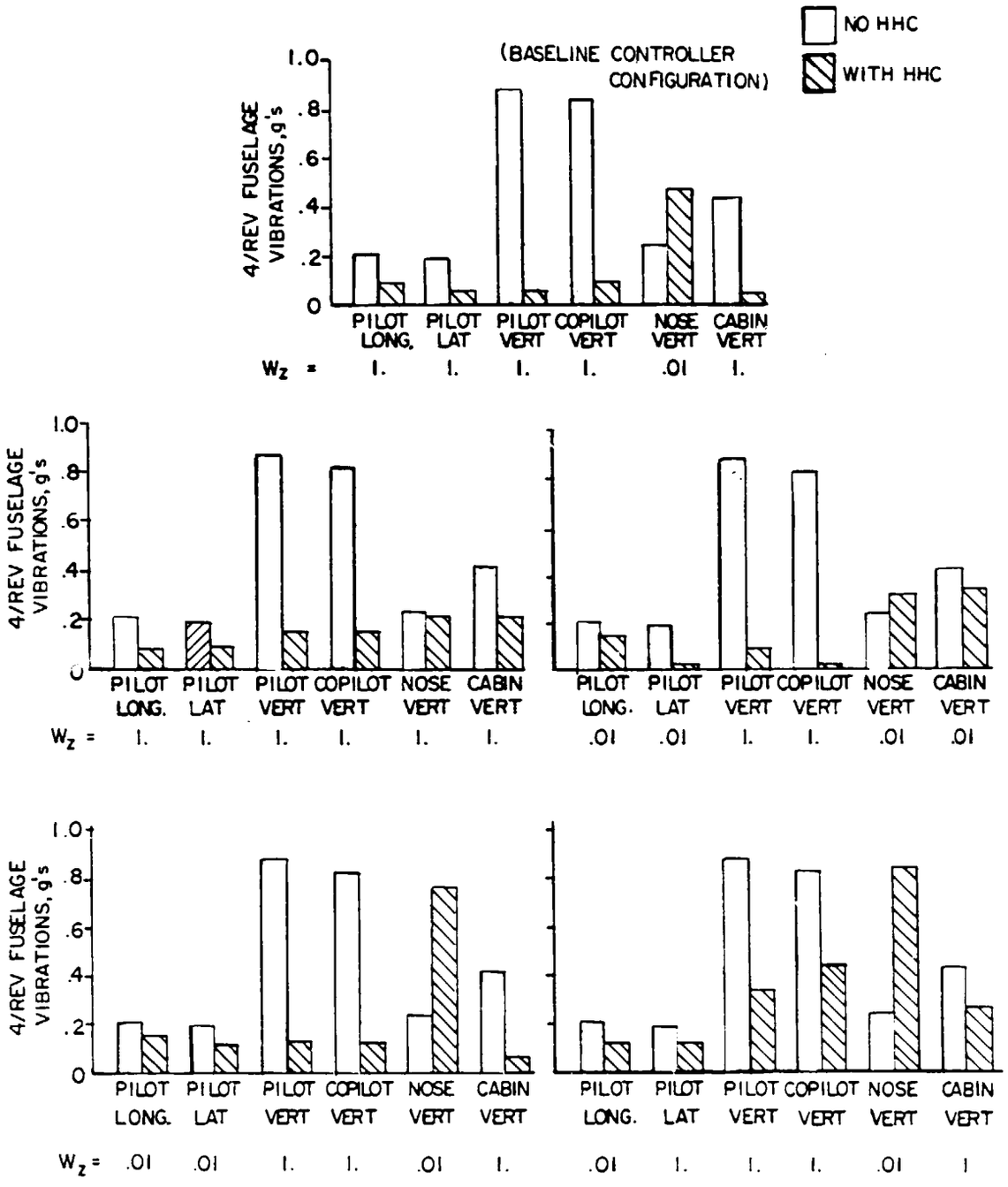

Figure 4.16 Effect of Vibration Sensor Weightings on Active Controller Performance at 150 Knots.

case results in which all sensor measurements are equally weighted. These results compare well with the baseline controller configuration results and are even better for the nose vertical vibration which shows nearly no change for the equal weighting case. However, all three vertical vibration components are slightly larger than the baseline controller configuration case with the unweighted nose sensor. Therefore increasing the importance of the nose vibration sacrifices vibration reductions possible elsewhere in the fuselage. A possible explanation for this is that fuselage modal vectoral cancellation is just as easily accomplished at the nose as a reduction in modal excitation because the nose is the antinode for many important fuselage modes.

However, modal vectoral cancellation at the nose does not guarantee reductions elsewhere because individual modal excitations have not been reduced. Therefore at other points in the fuselage where only one or two modes dominate, the vibration is not greatly reduced. It is for this reason that the baseline controller configuration has an unweighted nose sensor. Since nose of a helicopter is normally used to house avionics, which typically are designed to withstand vibrations as high as 2g, it is prudent to let the nose vibration increase moderately as a result of reduced vibration in crew inhabited areas rather than let it influence the vibration in the crew inhabited areas.

The next weighting configuration shown in Fig. 4.16 is for equally weighted pilot and copilot vertical with the other four sensors unweighted. This configuration showed surprisingly broad vibration reduction for such a simple weighting configuration. Compared to the baseline controller configuration results, the biggest variation is a larger cabin vibration with little variation from the case with no higher harmonic control. The next weighting configuration has equally weighted pilot, copilot and cabin vertical with the other three components unweighted. This case is essentially an attempt to improve upon the previous case by increasing the importance of cabin vertical vibrations. These results show that weighting the cabin equally with the pilot and copilot definitely benefits cabin vibration with only a small increase in cockpit vibration. The net overall reductions with higher harmonic control are impressive except for the unweighted nose vibration which has more than doubled. The last weighting configuration shown in Fig. 4.16 is an attempt to improve on the previous case of equally weighted pilot, copilot and cabin vertical vibrations. In addition to weighting these vibrations, pilot lateral was also equally weighted so that only pilot longitudinal and nose vertical were unweighted. The results show good reductions from the baseline condition without higher harmonic control, but compared to the previous case, the vibration controller performance have significantly diminished. Most notable are the pilot, copilot and cabin vertical vibrations which have tripled from the previous weighting case, while the pilot lateral vibration is essentially unchanged. The reason for this adverse effect of weighting pilot lateral vibration is unclear, however a possible answer could be that the controller has reached a local solution to the nonlinear system and is satisfied with the result because the performance index has decreased to a local minimum. For the other two cases shown in which the pilot lateral

vibration was weighted, the pilot longitudinal vibration was also weighted and the results for all cockpit vibrations are very good. It seems that equally weighting pilot lateral and longitudinal vibrations (whether large or small) is desirable to avoid this problem. In summary, Fig. 4.16 shows that different weighting combinations have a definite effect on vibration reductions and the best weighting configuration has equal weightings on all six vibrations except for the nose vertical vibration which is unweighted.

These results indicate that the vibration weighting for any specific HHC application will require some flight development in order to achieve the best overall vibration reduction. It is unlikely that apriori weighting can be enforced principally because of the interdependence of vibration and rotor loads.

Effect of Hub Sensors - Another important aspect of sensor location and sensor weightings is the possible use of remote sensors to achieve vibration reductions in the cockpit and cabin. Specifically, what is implied here is the use of hub vibration sensors in the fixed system to account for hub motions in all six degrees of freedom. The rationale for this approach is that if the rotor hub excitations are decreased with higher harmonic control so that hub vibrations decrease, then vibration reductions throughout the fuselage can also be expected. The remote sensor approach was tried in the G-400 simulation by using the 6 hub sensors (fixed system) outlined in Table 4.1 to drive the vibration controller. All six hub sensors were equally weighted and the procedure followed in the simulation is the same as that previously described. In the G-400 time history solution for the 150 kn condition, the controller was activated at rev 4 and the G-400 simulation was continued for 40 revs. Results for the remote hub sensors are shown in Fig. 4.17. The time variation of the vibration performance index (J), a typical cockpit vibration (pilot vertical), and a typical control angle (3/rev) are shown. In this case the performance index is composed of the equally weighted hub vibrations instead of the fuselage vibrations. Results show that, after the controller is activated at rev 4, there is an abrupt steady descrease in J. By rev 14, which is 10 revs or 2.5 second after the controller was activated at rev 4, the performance index has been reduced by 99 percent. There is virtually no change in J from rev 14 to rev 40.

The pilot vertical vibration also shows an abrupt decrease after the controller is activated, but the final vibration level is higher than for the baseline controller configuration case shown in Fig. 4.6 in which the sensors were located on the fuselage. This suggests that the selected hub vibration weighting is not at an optimum for minimum cockpit and cabin vibration. Since hub vibration and cockpit and cabin vibration are linearly dependent, a hub vibration weighting vector can be generated which will reproduce, exactly, the vibration reduction achieved with the optimized fuselage vibration weighting vector. A fundamantal potential shortcoming of the hub vibration sensors is that minimum performance index J may not produce minimum cockpit and cabin vibration.

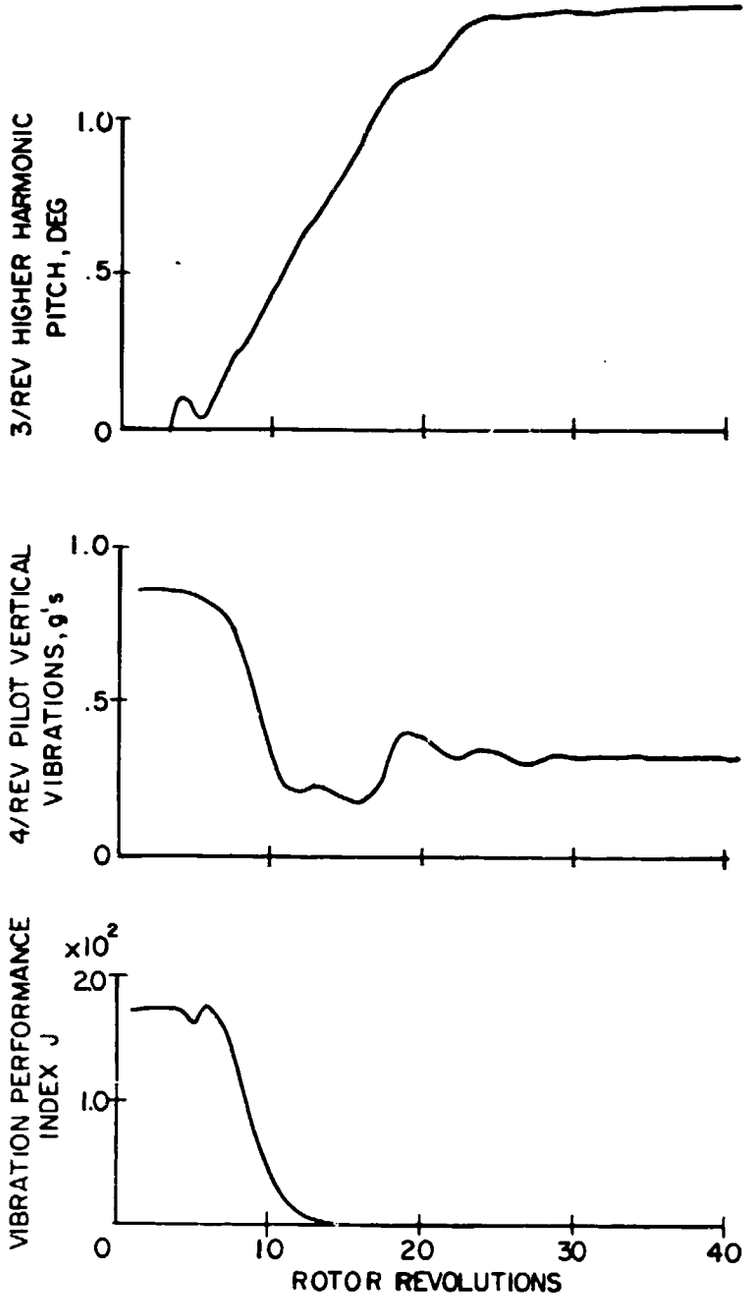

Figure 4.17 Time History of Vibration Controller Performance with Hub Sensors at 150 Knots.

The time variation of 3/rev cyclic pitch input is slightly steeper and smoother than that shown in Fig. 4.6 for the local sensor case and the final amplitude of 3/rev pitch is also substantially higher. This indicates variations in higher harmonic control angle vectors between remote and local sensor solutions. Figure 4.18 compares the hub and fuselage vibrations for the case of remote hub and local fuselage sensors. The local fuselage sensor results are reproduced from Fig. 4.7 for the baseline controller configuration. Refering to the hub vibrations, there is little difference between remote and local sensor results. However, the fuselage vibrations show a significant reduction in controller performance with the use of remote hub sensors. The fuselage vibrations with hub sensors still show large reductions compared to the baseline case with no higher harmonic control, but the reductions are definitely less than those for the local sensor case for the four vertical vibration components. There are two possible explanations for this result. First, the remote hub sensor case did not reduce the hub vertical vibration as much as the local fuselage sensor case (69 percent versus 88 percent) so more fuselage vertical excitation is present. Second, there is probably substantial vectoral modal cancellation occurring for the fuselage vibration sensors so that the phasing as well as the magnitude of the hub excitations is important. Thinking in terms of a transfer matrix between hub and fuselage vibrations, this logic would indicate a fully populated matrix as opposed to an essentially diagonal transfer matrix with dominance between prime directions, e.g., lateral hub motion causing lateral cockpit motion.

In summary, these results indicate the remote (hub) vibration sensors, while mathematically equivalent, are probably not a viable alternative to the use of local sensors at the points of interest. The weighting of the remote sensors and the performance index would have to produce minimum vibration in the areas of interest. Applied thusly, the weighting and performance index will serve to take best advantage of response cancellation by generating optimum phasing of rotor vibratory loads. However, the use of hub sensors can be potentially useful when used in conjunction with local vibration sensors in the fuselage. Since the response of the helicopter to higher harmonic control inputs is nonlinear there is a greater possibility of reaching the optimum solution rather than a local solution if both the amplitude and the phase of the fuselage modal response are controlled. This might be accomplished by including both hub and fuselage sensors (appropriately weighted) in the performance index. The hub sensors work to reduce the amplitude of the fuselage excitation without regard to phase, and the fuselage sensors work to reduce the fuselage response by vectoral cancellation with emphasis primarily on phase. This approach could potentially lead to a vectoral cancellation of small numbers as opposed to a vectoral cancellation of large numbers (fuselage sensors) or uncontrolled response to minimized forcing (hub sensors). If both hub sensors and local fuselage sensors are included in the performance index, this type of control can be implemented and could result in lower hub and fuselage vibrations.

Effect of Time Between Updates - An important parameter in the controller configuration is the time between higher harmonic control updates. A quick update time is advantageous for transient or maneuver conditions.

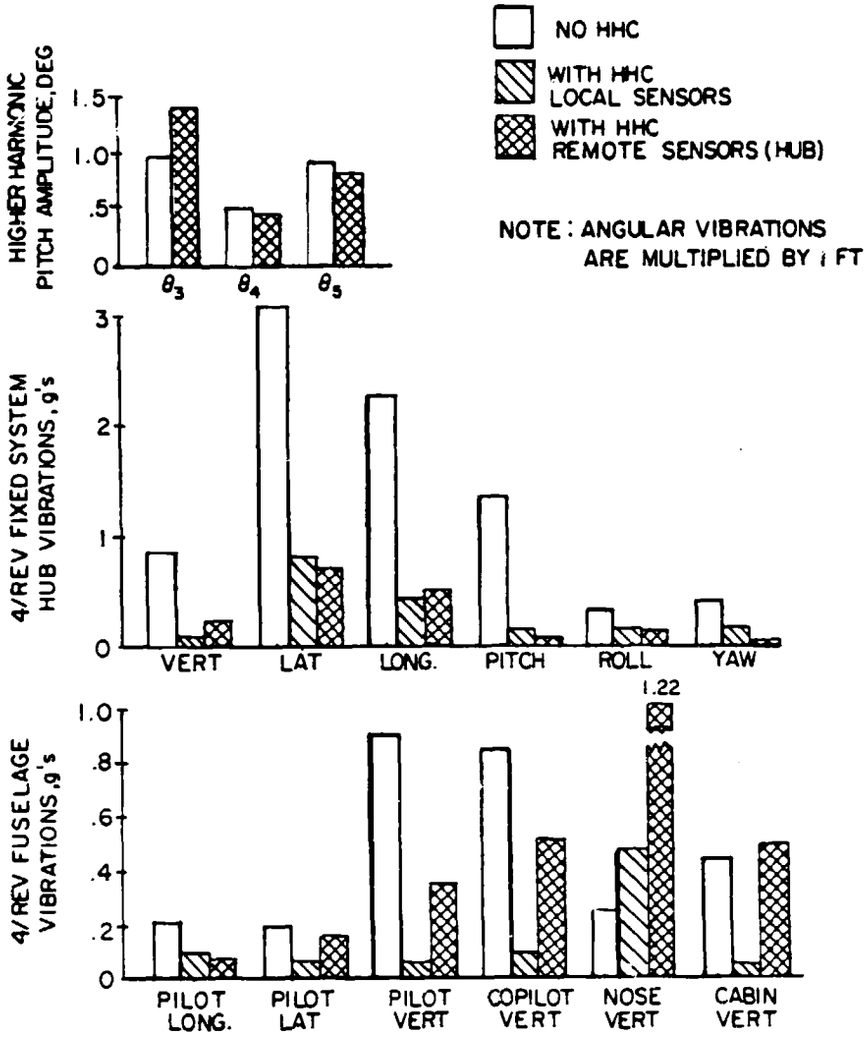

Figure 4.18 Comparison of Vibration Results for Hub Sensors and for Local Fuselage Sensors at 150 Knots.

But if the control angle updates are performed too quickly so that the vibrations are still in a transient response from the previous control input, the controller performance will be compromised due to errors in the sensor measurements. The baseline controller configuration has set the time between updates to one rotor rev. This update time is considered to be the shortest reasonable update time based upon the estimated transient vibrations for a .1 degree higher harmonic control input. To determine whether a one rotor rev update time compromises controller performance, a G-400 simulation was performed with an update time of two rotor revs. For this configuration, the harmonic analyzer in the vibration controller used the sensor measurements from the last quarter rev of the second rotor revolution. This increased the time allowed for vibration transient decay by a factor of 2.5 (1.65 revs versus .65 revs) over that allowed for the one rev update configuration. The results for the two rev update time controller configuration are shown in Fig. 4.19. The vibration performance index, pilot vertical vibration and 3/rev cyclic pitch are shown as a function of time. Comparing these results to those shown in Fig. 4.6 for the one rev update time, the most notable difference is the smoothness of the 3/rev cyclic pitch input for the 2-rev-update configuration. The slope of the 3/rev input is nearly constant while the slope in Fig. 4.6 shows perturbations. The perturbations for the quicker update indicates that the time allowed for transient decay does affect the controller calculations of higher harmonic control. However, the 3/rev pitch converges to the same value. More importantly, the pilot vertical vibration and the performance index for the 2-rev-update look similar to that for the one-rev-update in Fig. 4.6. In fact after 40 revs, pilot vertical vibration and the performance index for the one-rev-update configurations are lower than for the two-rev-update configuration. However, over the 40 rev time period, the two-rev-update controller configuration has updated only half as much as the one-rev-update configuration. Therefore a more meaningful comparison of the two configurations is to evaluate controller performance as a function of the number of updates after the controller is activated.

This comparison is shown in Fig. 4.20. Even when evaluated on this basis the one-rev-update controller configuration results compares well to the two-rev-update configuration results. As previously mentioned, 3/rev cyclic converges more smoothly and with fewer updates, and the pilot vertical vibration seems to be converging more smoothly for the 2-rev-update configuration. However, the overall performance of the vibration controller as indicated by the vibration performance index is nearly the same for both controller configurations. This indicates that although there are some specific effects of transient vibrations and time between updates, the overall performance of the controller is not compromised by using a one-rev-update time. Figure 4.21 shows a comparison of hub and fuselage vibrations for the one-and two-rev-update configurations after 40 revs. Both hub vibration and fuselage vibrations show that the one-rev-update configuration has overall lower vibrations than the two-rev-update configuration, whereas the opposite would be expected since the vibration transient effects on the measurement harmonic analysis would be minimized with longer time between updates. This result is partially

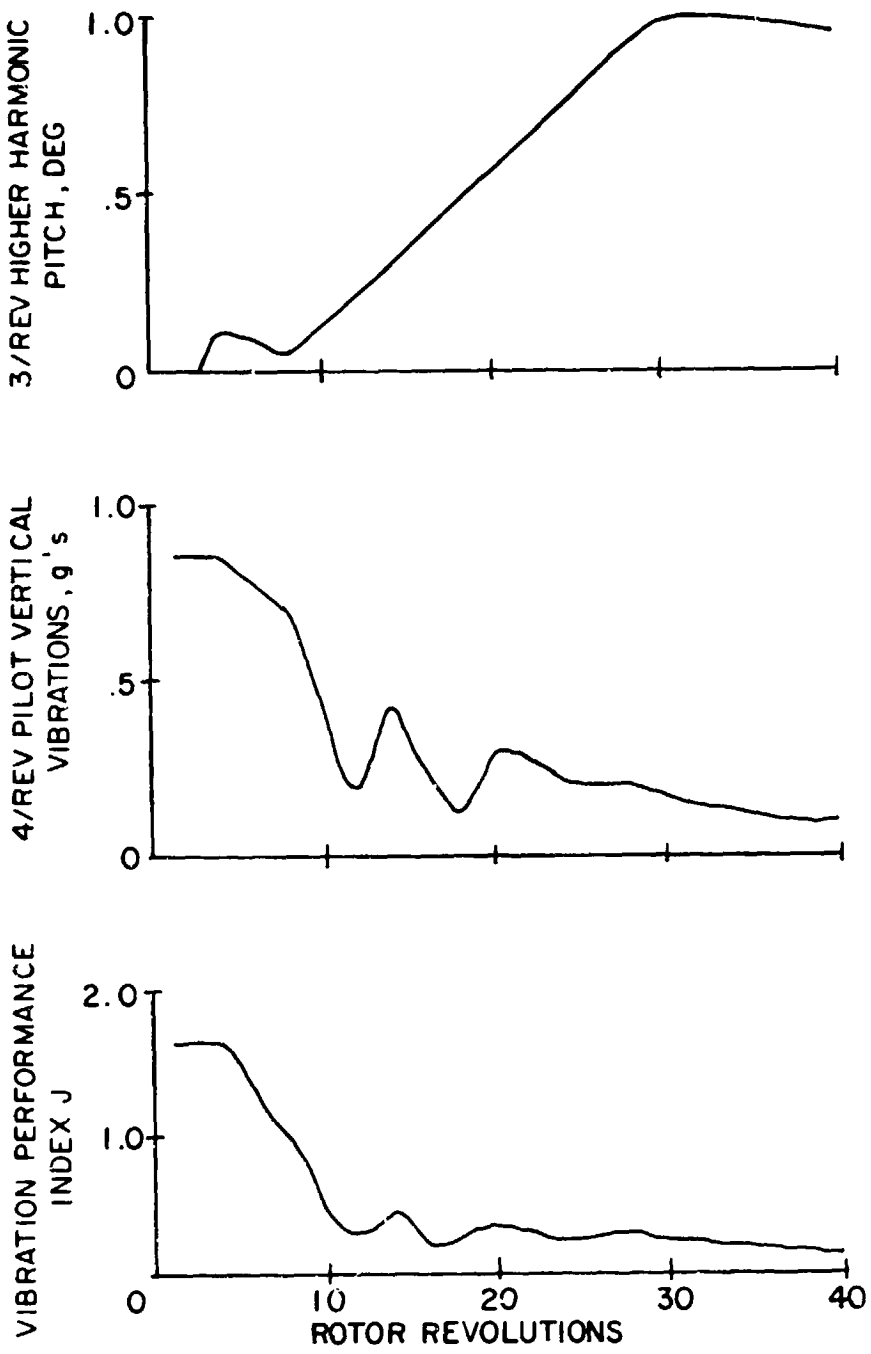

Figure 4.19 Time History of Vibration Controller Performance with Two Revs Between Control Updates at 150 Knots.

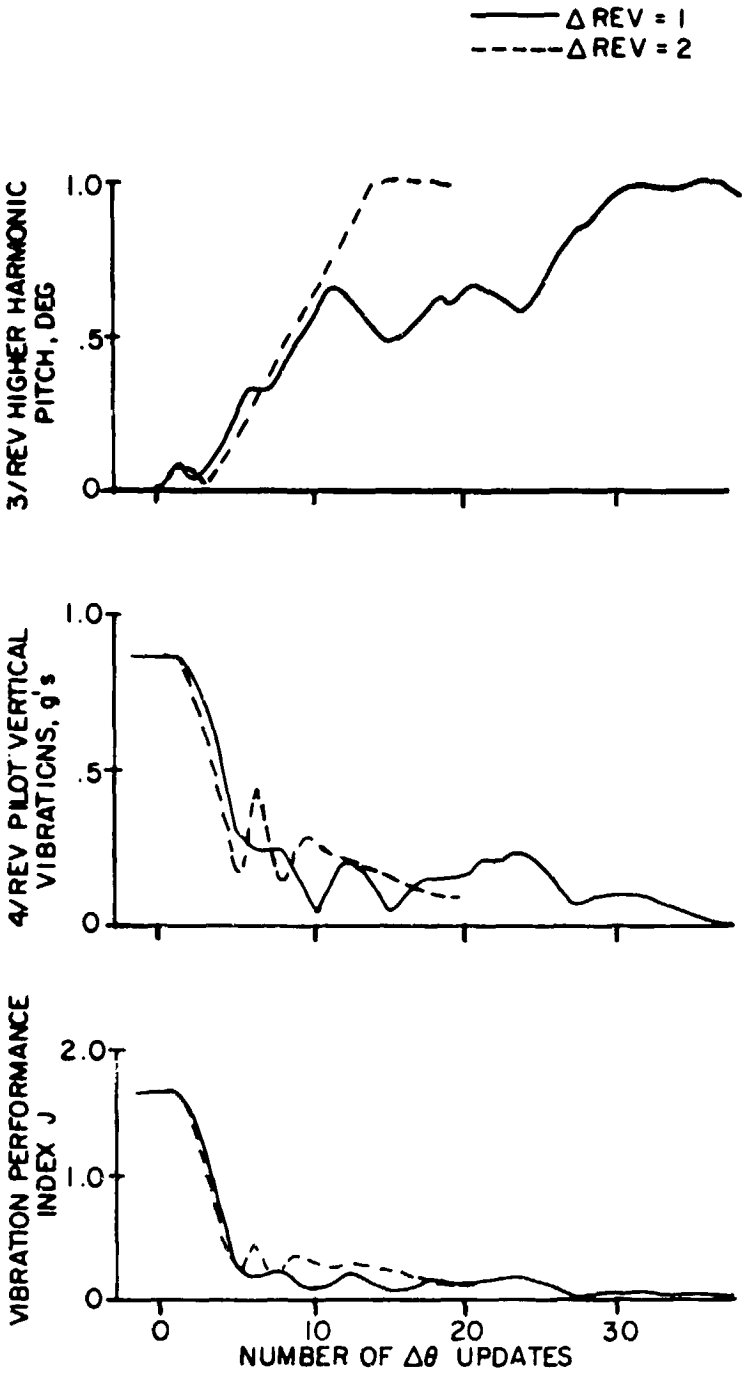

Figure 4.20 Comparison of Controller Performance for One and Two Revs Between Control Updates at 150 Knots.

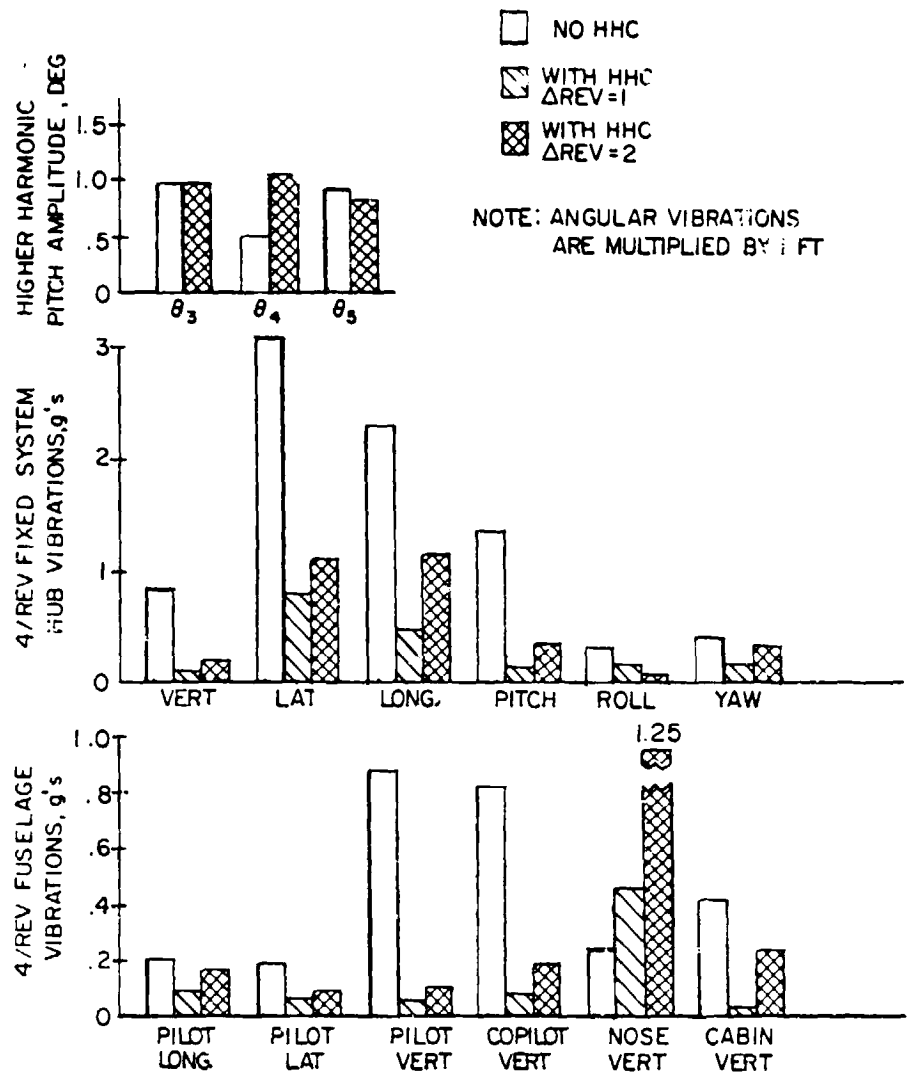

Figure 4.21 Comparison of Vibration Results for One and Two Revs Between Control Updates at 150 Knots.

due to half as many updates being performed for the 2-rev-update configuration; but the important point is that the controller configuration with a one-rev-update time can tolerate errors in the harmonic analysis due to transient vibration response to control inputs and converges quickly to an effective controller solution.

Effect of Limited $\Delta\theta$ Between Updates - An important aspect of the controller configuration is the $\Delta\theta$ limiter. As previously discussed in Section 4.3, one reason for limiting the change in higher harmonic control at each update is to stay within the potential hardware limitations of the swashplate actuators. It is also intuitively obvious that the magnitude of a vibratory transient response is proportional to the magnitude of the $\Delta\theta$ change so the accuracy of the harmonic analysis of the measurements could also be affected. Another possible impact of $\Delta\theta$ is related to the nonlinearity of the relationship between vibrations and HHC amplitudes. Since the controller is linearizing this relationship over the perturbation range of $\Delta\theta$ for each rev, it could be necessary to limit $\Delta\theta$ updates to provide a better linear estimate, depending upon the severity of the nonlinearity.

To address the effect of limited $\Delta\theta$ between updates, the controller configuration was modified to allow a maximum of 0.2 degree for $\Delta\theta$ between updates, compared to the baseline configuration value of 0.1 degree. The G-400 simulation results are shown in Figure 4.22. The vibration performance index has the characteristic abrupt decrease after the controller is activated at rev 4, and by rev 20 J has been reduced by about 90 percent. This result for J compares well to the result shown in Figure 4.6 for $\Delta\theta$ limit of 0.1 degree. However there are large differences in the time history higher harmonic control inputs. Comparing the 3/rev higher harmonic pitch results in Figures 4.6 and 4.22 the 0.2 degree $\Delta\theta$ limiter allows the desired amplitude (about 1 degree) to be reached more quickly than the 0.1 degree $\Delta\theta$ limiter but after rev 20 there are significant excursions in the 3/rev input for the 0.2 degree $\Delta\theta$ limiter case. The 5/rev input in Figure 4.22 also shows significant excursions with time. This result indicates controller sensitivity to the magnitude of the $\Delta\theta$ limiter during a transient which could affect controller performance during a maneuver.

It is believed that these excursions in control inputs are due to the controller attempting to further imporve its performance after rev 20 while the sensitivities of the vibrations to control inputs are decreasing nonlinearly. The decreased sensitivity is demonstrated by the small change in J after rev 30 with large changes in control inputs, compared to large reductions in J after rev 4 with comparable control inputs. The nonlinearity causes changes in the T-matrix that require identification and tracking, but this can be adequately accounted for if the $\Delta\theta$ limiter is appropriately chosen and the controller identification algorithms are sensitized by R and Q in Equations (4.9) through (4.12) for such nonlinear changes. In other words, depending upon the severity of the nonlinearity, it takes a judicious selection of $\Delta\theta_{LIM}$ to set the maximum range of linearization plus a selection

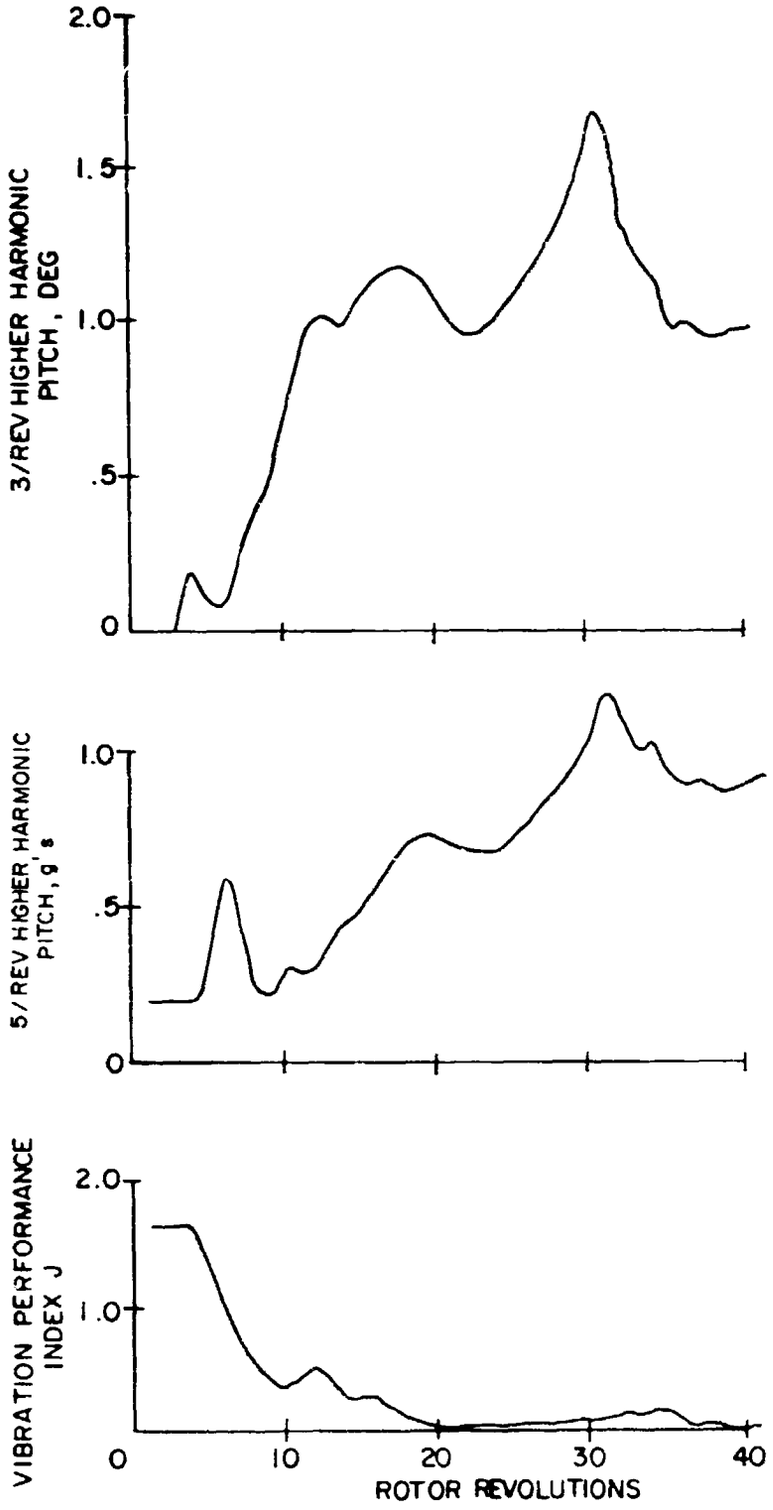

Figure 4.22 Time History of Vibration Controller Performance for $\Delta\theta$ Limiter of 0.2 Degree at 150 Knots.

of Q and R to attenuate or amplify the Kalman gain in the identification algorithms for proper T-matrix tracking because the controller will perform only as good as it tracks and identifies the T-matrix. At first glance it might seem that small $\Delta\theta_{LIM}$ and high Kalman gain authority are desirable for nonlinear situations. But high Kalman gain to allow for quick tracking could cause controller skittishness or instability because of amplified T-matrix errors, and small $\Delta\theta_{LIM}$ restricts vibration reduction capability in transients and maneuvers where high rates of control input may be required. Figure 4.22 shows the controller is stable for a .2 degree $\Delta\theta$ limiter, however the controller configuration on a full scale implementation will probably be specifically tailored to provide adequate vibration performance for the nonlinear system and also acceptable performance for transients and maneuvers. Figure 4.23 compares the level of vibration for the hub and fuselage components at rev 40 for the 0.1 degree and 0.2 degree $\Delta\theta$ limiter cases. Both hub and fuselage vibrations are nearly the same after 40 revs and the higher harmonic control angles required are about the same.

In summary, the convergent solution of the vibration controller is unaffected by the magnitude of the $\Delta\theta$ limiter up to 0.2 degrees, but there is a significant effect on the transient response of the controller after it is activated. It seems that the 0.1 degree $\Delta\theta$ limit is better than 0.2 degree for smoothing the vibration controller transient response. The suspected source of the controller sensitively to $\Delta\theta$ is the nonlinearity of the vibration response to control inputs. This area should be investigated more thoroughly to understand the phenomena involved since it affects controller performance, stability and can impact on the controller configuration.

Effect of Signal Noise - An important consideration in the development and evaluation of the vibration controller is performance in the presence of signal noise. Certainly there will be noise on the accelerameter measurements, and this noise will affect the quality of the harmonic analysis of the vibrations. The impact of this will be erroneous identification of the T-matrix and ultimately non-optimal higher harmonic control inputs. For large values of noise to signal ratio, even the stability of the controller is in question because the controller performance and stability is highly dependent on the identification of the T-matrix. To evaluate the tolerance of the vibration controller to signal noise, varying levels of noise were added to the vibration measurements in the G-400 simulation to purposely introduce errors in the controller parameter identification and tracking algorithms. The noise was input as random (Gaussian) discrete 4/rev noise in terms of noise to signal ratio. The noise was added to each of the vibrations after the harmonic analysis.

Signal noise is usually considered white noise but the high pass-low pass filter previously discussed in Section 4.3 should remove all frequencies of noise except at 4/rev. Therefore the definition of noise to signal ratio used here is more stringent than the normal definition in that the noise level amplitude is at 4/rev instead of the combined amplitudes of all noise frequencies.

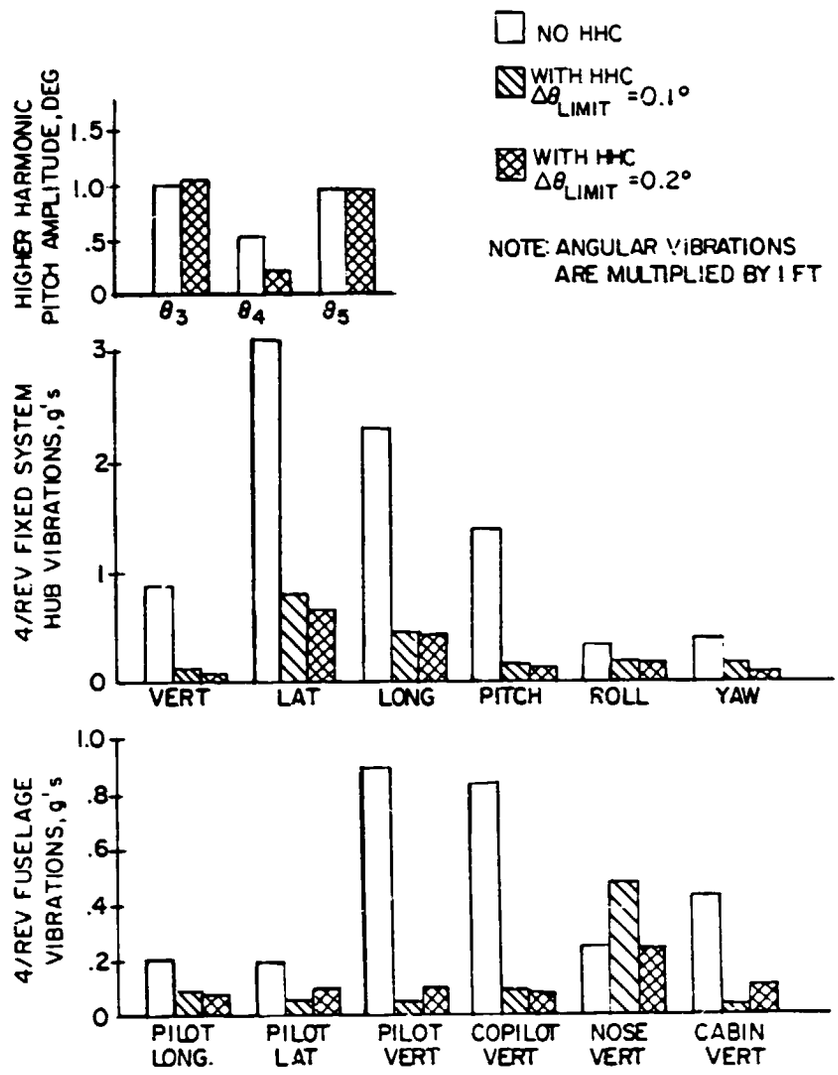

Figure 4.23 Comparison of Vibration Results for 0.1 and 0.2 Degree $\Delta\theta$ Limiter at 150 Knots.

To simulate the noisy signals, the G-400 simulation was run as previously described with the controller activated at rev 4. Five different levels of noise to signal ratio were input and the results are shown in Fig. 4.24. The time variation of the vibration performance index is shown for the 5 cases and can be compared to the baseline controller results for no noise on the signal. As the noise level increases there are increasingly more perturbations in J with time although for noise levels up to 15 percent the performance index has smoothly converged. When the noise level is increased to 20 percent, the controller performance has seriously deteriorated; in fact, the vibration levels are increased with the controller over the baseline level at rev 4, and the stability of the controller is in question. It can be concluded from these results that the vibration controller is tolerant of noise levels up to 15 percent of the signal amplitude. This result is important for two reasons. First, the controller behaved smoothly with 15 percent noise for large vibration levels (rev 5 to 10) when it was initially activated. This is significant for T-matrix identification and tracking because the level of random vibration for 15 percent noise is equivalent to that controlled by .15 degrees of higher harmonic control (about 1 degree is required for the baseline case to reach the optimum as in Figure 4.7). But the control update has been restricted to .1 degree per rev by the $\Delta\theta$ limiter so that the random vibration levels due to noise are larger than the vibration control authority from rev to rev. Even under these conditions the controller demonstrated the capability to identify and track the T-matrix to reach the optimum solution. Second, accelerameter noise is on the order of 1% to 2% noise to signal ratio for properly shielded cables so the demonstrated theoretical noise tolerance is for a noise level well above that to be expected from the actual hardware.

Figure 4.25 shows how the 15 percent noise level affected the individual vibration components at the hub and also in the fuselage at rev 40. The results with noise are compared to the baseline controller results with no signal noise. Refering to the hub vibration results, there is nearly no difference between the no noise and 15 percent noise cases. This is also true for the fuselage vibrations except for the unweighted nose vertical vibration which has increased by .35g for the 15 percent noise case. In summary the vibration controller shows good tolerance to noise levels up to 15 percent and no problems due to signal noise can be anticipated for actual hardware implementation.

4.6.2 Parametric Studies

The previous section investigated the characteristics of the vibration controller at a representative 150 kn high speed flight condition. The controller has been optimized based on those results. The performance of the controller is further evaluated in this section at several operating conditions including variations in airspeed, rotor speed and gross weight. The generality of the controller in terms of its applicability to various helicopters with different disc loading, blade loading, structural dynamics (i.e. airframe and blade natural frequencies) and rotor types is also explored.

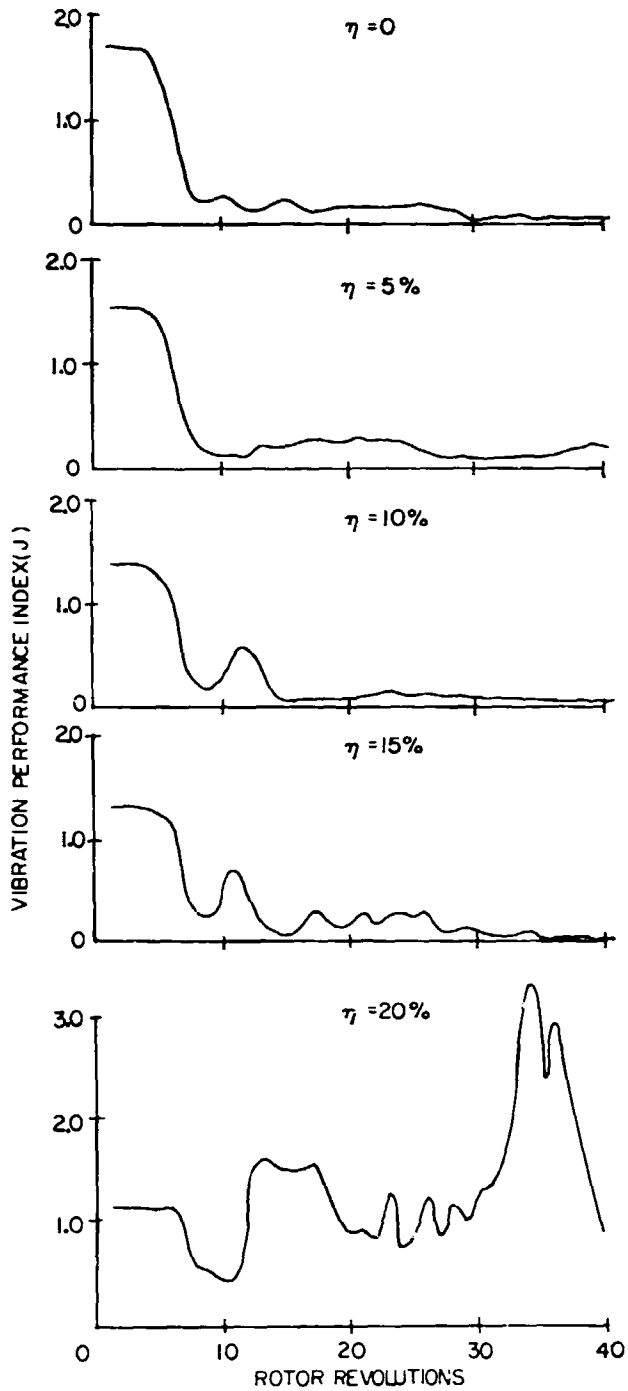

Figure 4.24 Effect of Signal Noise on Vibration Controller Performance at 150 Knots.

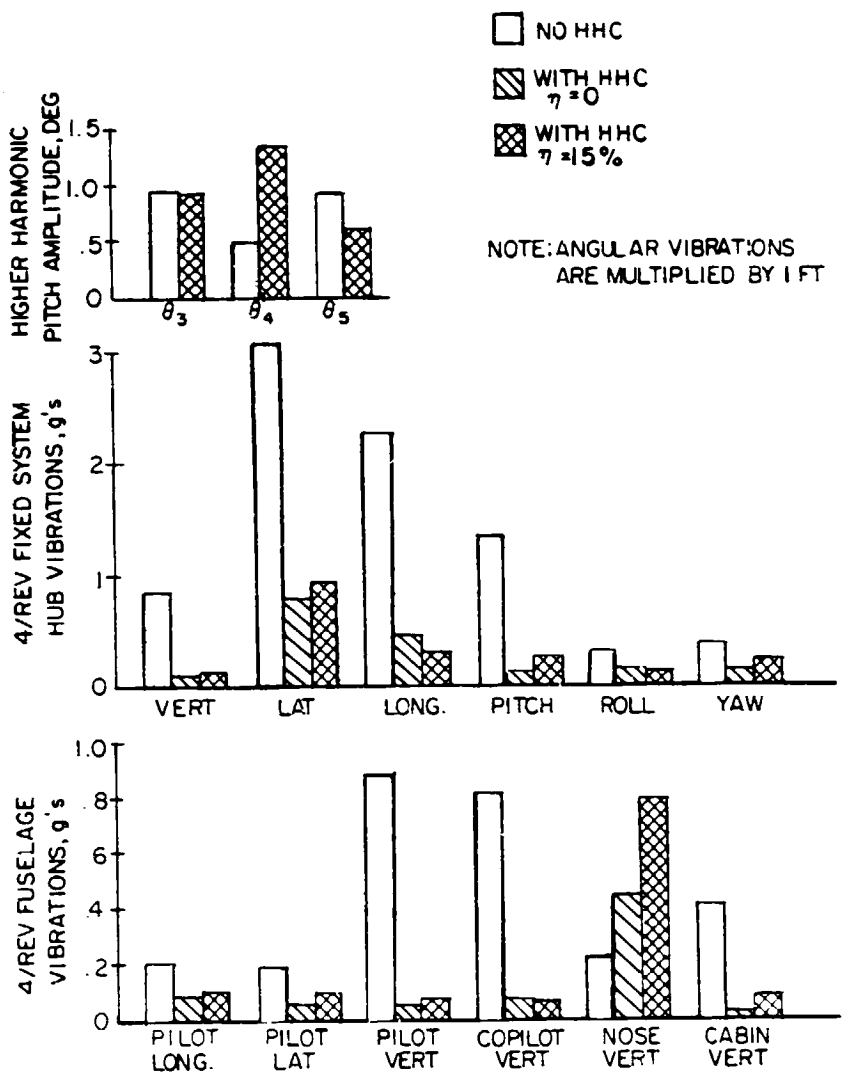

Figure 4.25 Comparison of Vibration Results for Zero and Fifteen Percent Noise on Measurements at 150 Knots.

A summary of the sixteen conditions analyzed is presented in Table 4.5. Case 1 is the baseline 150 kn condition that has been explored thoroughly in Section 4.6.1. Cases 2, 3 and 4 are the airspeed variation from 120 kn through transition, 30 kn, to hover. Constant inflow has been used for cases 1 and 2 to simplify the calculation. Variable inflow is used for transition and hover cases since at these conditions variable inflow is expected to be the major source of higher harmonic airloads. To check the effect of variable inflow on the baseline case, case 5 is presented. In these applications, the variable inflow is calculated just for the initial trim condition and is not updated with control changes. Cases 6 and 7 are for maximum and minimum gross weights, respectively, both at 150 kn. Variation in tip speed is examined in case 8. Blade loading and disc loading variations are examined in terms of blade chord and radius changes, cases 9 and 10. Case 11 examines the effect of the blade natural frequencies, with the flatwise mode frequency changed from less than 3/rev to 3.5/rev to alter the phase of blade dynamic response to the 3/rev airloads, while at the same time, the torsional mode frequency is moved to exactly 3/rev for possible load amplification at input higher harmonic control frequency. Case 12 examines the airframe dynamic response effect by arbitrary moving an airframe mode frequency closer to 4/rev such that the amplification factor is doubled. Cases 13 through 16 are an airspeed sweep for a hingeless rotor BLACK HAWK. A more detailed definition of the hingeless rotor system can be found in Section 5.1. Since the prime source of vibration for a hingeless rotor is the hub moment, a departure from the hub inplane forces of the articulated rotor system, this is a stringent test of the applicability of the vibration controller which is designed by using an articulated rotor as a baseline.

To test the adaptability of the vibration controller, the initial T-matrix used for all the cases shown in Table 4.5 is the same as that for the 150 kn baseline case. It will be shown that the controller exhibits excellent adaptability resulting in good vibration reduction for all the cases.

The results of the parametric studies are presented in Figures 4.26 through 4.40. Each figure is made up of three parts. The first part (a) presents the 4/rev fuselage vibrations at the six sensor locations with and without the controller, the 4/rev hub vibrations in three translational and three rotational directions and the 3/rev, 4/rev and 5/rev higher harmonic pitch controls required of the controller. The second part (b) shows the radial variation of the blade vibratory (one-half peak-to-peak) flatwise, edgewise, and torsional bending moments with and without the controller. The third part illustrates the harmonic components of the vibratory root flatwise moment, the peak edgewise moment and the root torsional moment with and without the controller. The root flatwise and torsional moments are defined at 9% radius for the articulated rotor cases (number 1 through 12 in Table 4.5) and at 11% radius for the hingeless rotor cases (number 13 through 16). The peak edgewise bending moment occurs between 24 and 53% radius for the articulated rotor and at the blade root or 11% radius for the hingeless rotor.

Effect of Forward Speed - The effect of forward speed variations on the performance of the higher harmonic controller can be seen from a comparison

Table 4.5 Aircraft Flight Conditions and Rotor Configurations

Case No.	V kn	Gross Weight kg	(lb)	Inflow N.D.	Rotor Type	Parametric Variations
1	150	7484.3	(16500)	Constant	Articulated	Baseline
2	120	7484.3	(16500)	Constant	Articulated	Velocity
3	30	7484.3	(16500)	Variable	Articulated	Velocity
4	0	7484.3	(16500)	Variable	Articulated	Velocity
5	150	7484.3	(16500)	Variable	Articulated	Inflow
6	150	9185.2	(20250)	Constant	Articulated	Max. Gross Weight (123%)
7	150	5987.4	(13200)	Constant	Articulated	Min. Gross Weight (80%)
8	150	7484.3	(16500)	Constant	Articulated	110% Rotor Speed
9	150	7484.3	(16500)	Constant	Articulated	90% Rotor Chord
10	150	7484.3	(16500)	Constant	Articulated	90% Rotor Radius
11	150	7484.3	(16500)	Constant	Articulated	Blade Frequencies
12	150	7484.3	(16500)	Constant	Articulated	Fuselage Frequency
13	150	7484.3	(16500)	Constant	Hingeless	Rotor Type
14	120	7484.3	(16500)	Constant	Hingeless	Rotor Type & Velocity
15	30	7484.3	(16500)	Variable	Hingeless	Rotor Type & Velocity
16	0	7484.3	(16500)	Variable	Hingeless	Rotor Type & Velocity

of the baseline 150 kn configuration (discussed in Section 4.6.1, Figures 4.7, 4.13 and 4.14) with the results at 120 kn, 30 kn and in hover shown in Figures 4.26, 4.27, and 4.28 respectively. Variable inflow is utilized for the 30 kn and hover conditions in an attempt to model more accurately the inflow field experienced by the rotor. The intersection of the blade tip vortices with the following rotor blade is more pronounced as forward speed is reduced. It is seen that the controller is very effective in reducing both hub and fuselage vibrations at different forward speeds. At 120 knots, about ½ degree of higher harmonic pitch controls at 3/rev, 4/rev and 5/rev are required for vibration reduction. The controller requirements are less stringent as forward speed is decreased due to the corresponding decrease in the magnitude of the higher harmonic blade loads which are transmitted to the rotor hub. The important fact that is emphasized again is that the initial transfer matrix between vibrations and higher harmonic pitch developed for the baseline configuration at 150 kn has been used as the initial T-matirx for all the cases presented in this section. Although the final T-matrices as identified by the controller at different forward speeds are quite different, the controller is able to identify them correctly using the common initial T-matrix. For an example, Table 4.6 lists the final T-matrix identified by the controller for the 120-knot case. This transfer matrix is quite different from that for the baseline case shown in Figure 4.11. Thus, it is shown that the vibration controller is quite adaptive in its application at different forward speeds. Fuselage vibrations at the five weighted sensor locations are all below .1g in the speed range from hover to 150 knots. The rotor hub vibrations are all below .8g at 150 kn and .3g at lower forward speeds.

The effect of the vibration controller on the blade bending moments has already been discussed in Section 4.6.1. As forward speed is lowered, the increases in blade bending moments associated with application of the controller are reduced. In hover, however, the presence of higher harmonic pitch controls results in small blade vibratory moments which are made up mostly of 4/rev and 5/rev harmonics, as seen from Figure 4.28(c).

In summary, the results from the airspeed parametric study show that: (1) with the controller optimized at 150 kn, excellent vibration reduction is achieved at lower airspeeds where the vibratory rotor hub loads are lower, (2) the controller operation is satisfactory at conditions where vibration reduction is not required (hover), (3) only modest increases in rotor blade loads occur due to higher harmonic control over the airspeed range from hover to 150 kn and (4) the maximum higher harmonic control inputs occur at the most highly loaded condition, 150 kn.

Effect of Variable Inflow - The vibration controller performance was investigated for the baseline rotor configuration using variable inflow. The analytical results using variable inflow are shown in Figure 4.29. The reductions in the hub and fuselage vibrations obtained with the controller, while substantial, are not as great as those predicted for the baseline case with constant inflow from Figure 4.7. The weighted fuselage vibrations are all below .2g. One important difference between the two inflow conditions

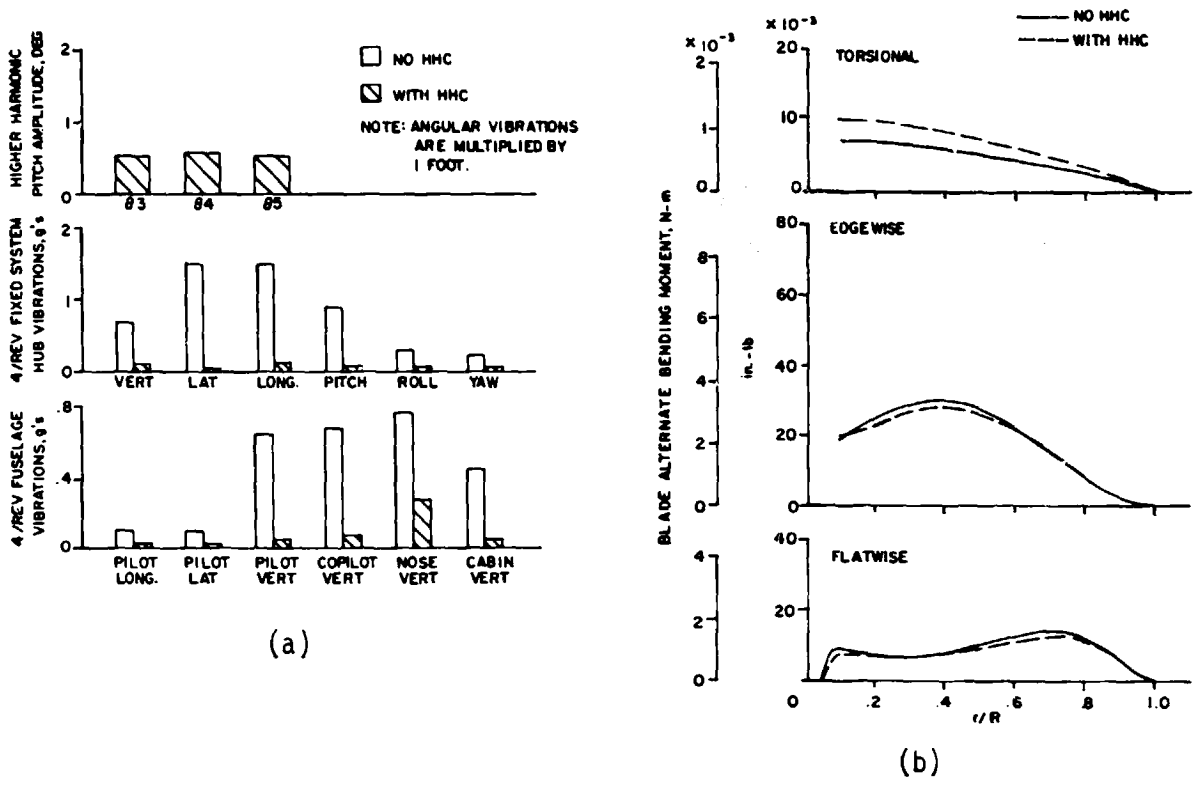

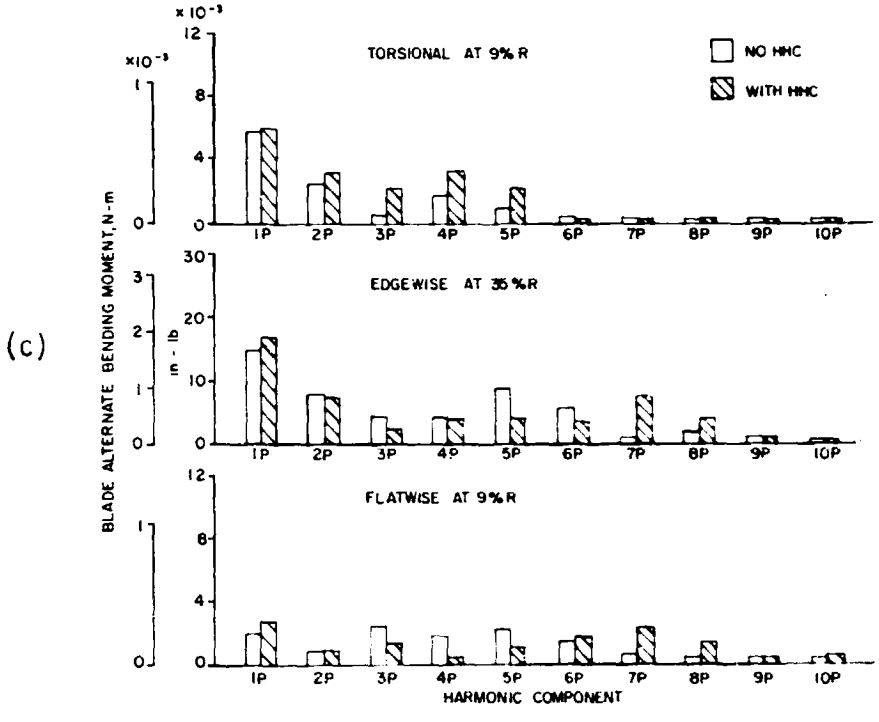

Figure 4.26 Case 2, Normal Gross Weight, 120 Kn.

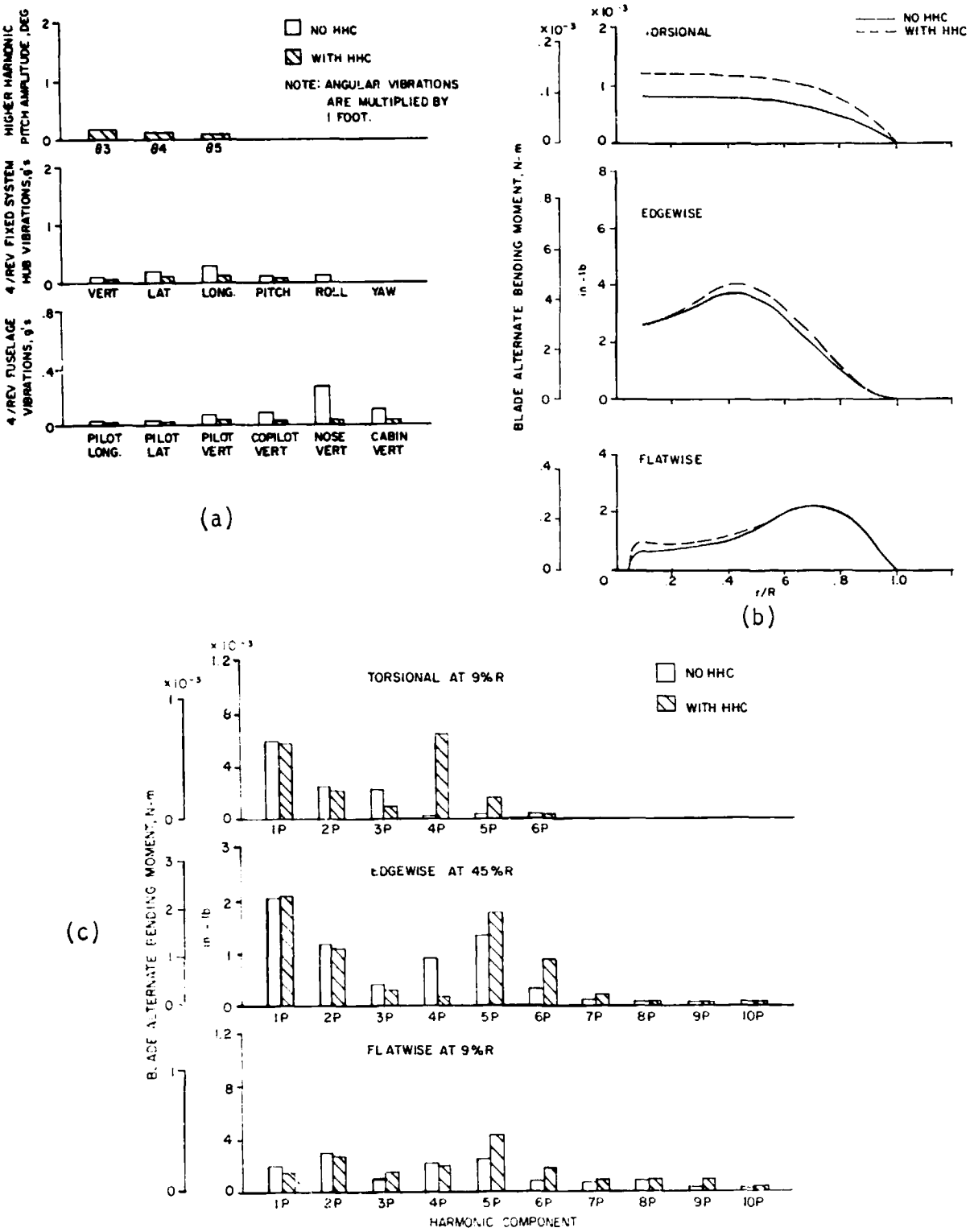

Figure 4.27 Case 3, Normal Gross Weight, 30 Kn.

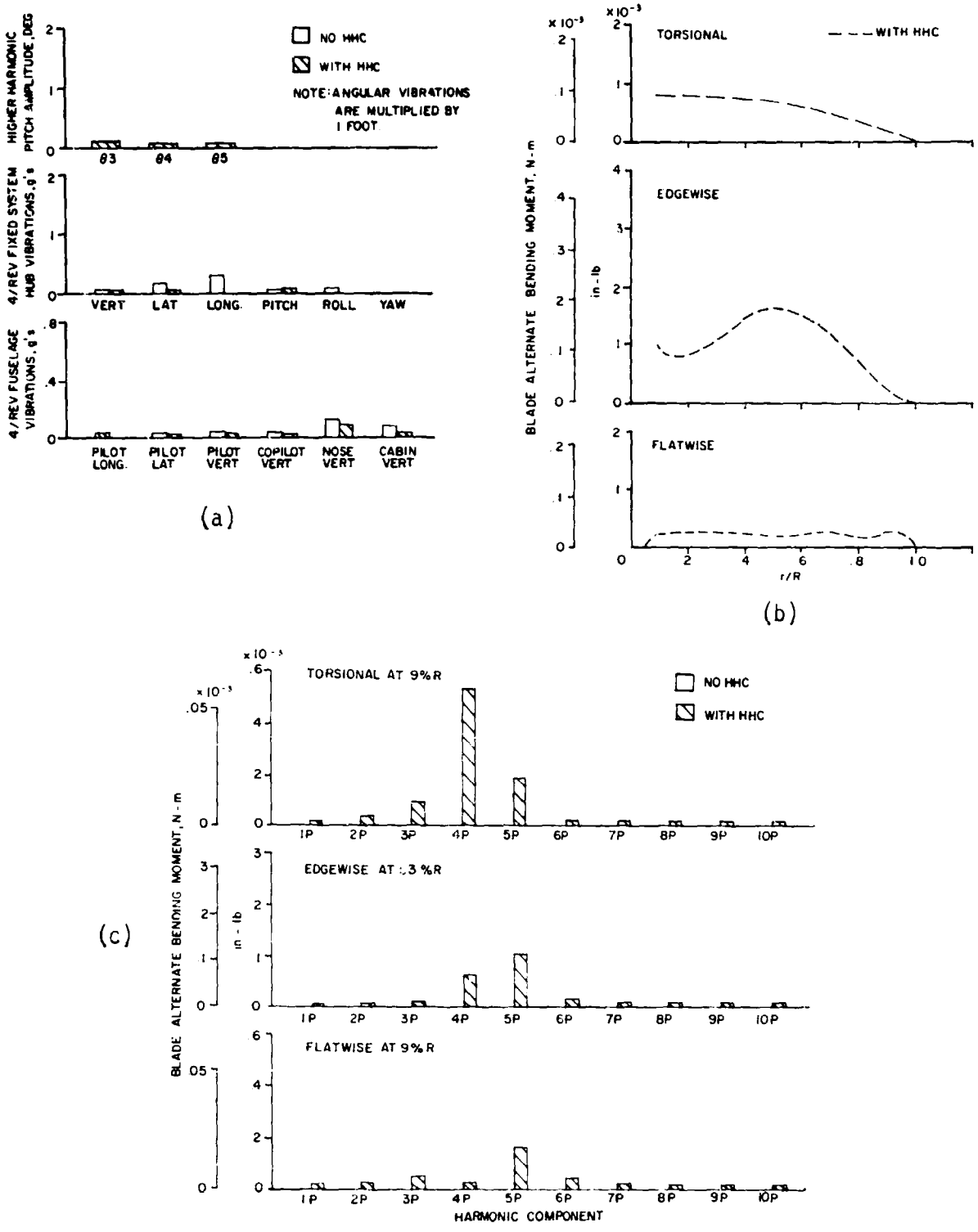

Figure 4.28 Case 4, Normal Gross Weight, Hover.

TABLE 4.6 TRANSFER MATRIX AT 120 KN - CLOSED LOOP IDENTIFICATION

			θ_{3C}	θ_{3S}	θ_{4C}	θ_{4S}	θ_{5C}	θ_{5S}
Pilot	Long	C	.111	.476	-.201	-.004	.838	.444
		S	-.397	-.573	-.646	-.245	-.573	.293
Pilot	Lat	C	.398	-.036	.216	.814	1.711	-.688
		S	-.010	-.202	-.176	-.085	-.216	-.085
Pilot	Vert	C	1.917	2.336	-.045	-.070	3.531	-.749
		S	-.049	1.123	-1.097	-1.509	-.287	2.365
Copilot	Vert	C	2.086	2.565	.322	-.060	3.933	-1.132
		S	-.649	.935	-.807	-1.795	-1.736	2.746
Nose	Vert	C	3.416	4.828	.724	-.289	7.117	-.423
		S	-.493	.711	-3.857	-3.065	-2.595	4.934
Cabin	Vert	C	-.836	-.836	-.603	.489	.060	.670
		S	-.420	-1.610	.464	1.136	.606	-1.950

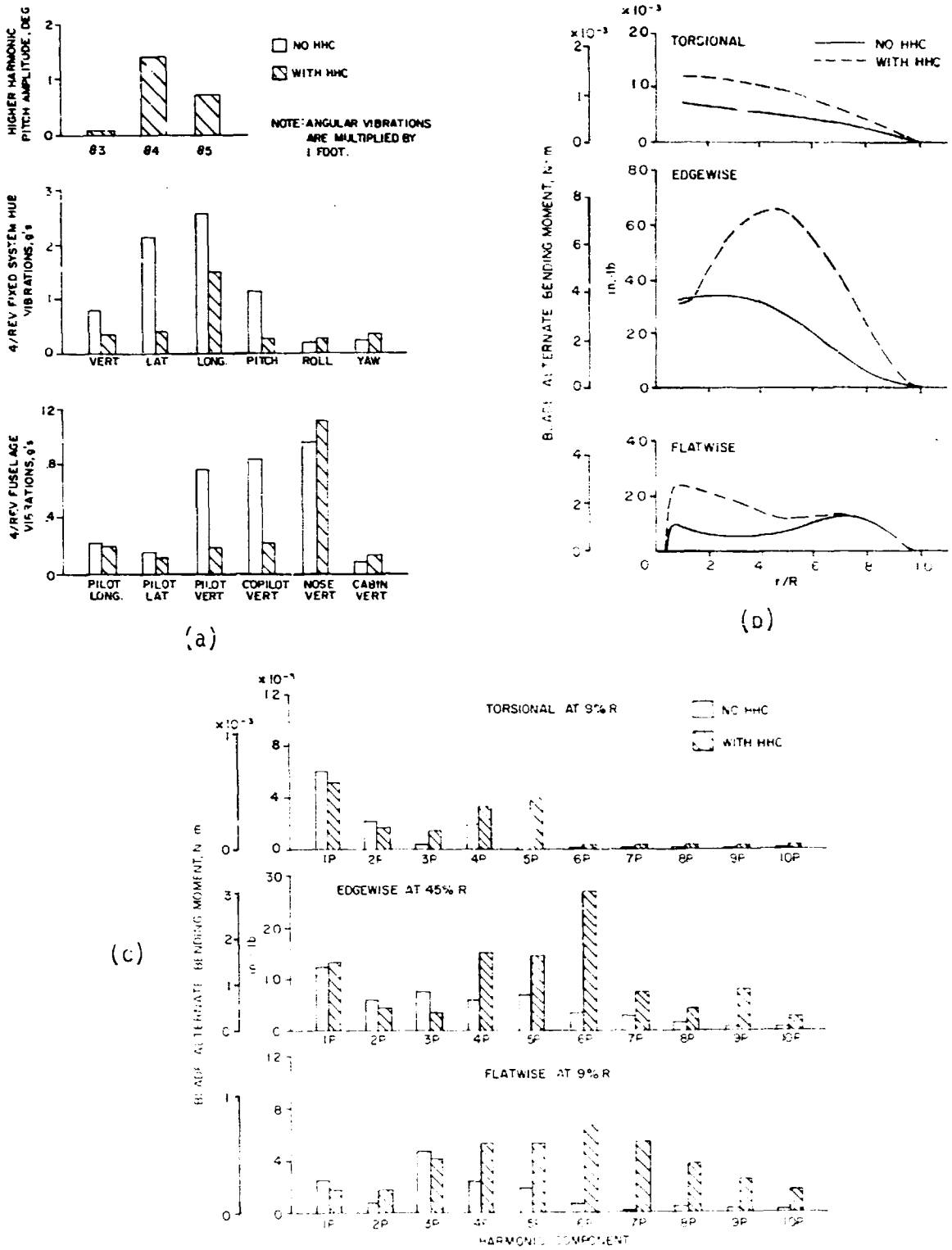

Figure 4.29 Case 5, Baseline With Variable Inflow.

is the amount of higher harmonic pitch necessary for optimum controller performance: the variable inflow model requires about one degree less 3/rev cyclic pitch with a corresponding increase in 4/rev cyclic pitch.

For the analytical model incorporating variable inflow substantial increases in blade vibratory edgewise and flatwise bending moments accompany the higher harmonic control inputs, Figure 4.29(b). These increases in blade moments are caused primarily by 6, 7 and 8/rev responses, Figure 4.29(c), which are the result of interharmonic coupling. Interharmonic coupling is the mechanism by which airloads are generated at harmonic frequencies greater than the HHC input frequencies. These airloads result from the product of the 3, 4 and 5/rev HHC pitch motions and 1, 2 and 3/rev velocities. The validity of the higher harmonic responses represents an area for further study. The aerodynamic model certainly must be scrutinized as well as the structural model of the blade.

These predictions of substantially higher blade loads appear on the surface to contradict model test results reported in Reference 1. The model tests however did not include 5/rev HHC inputs and the higher blade bending modes (from 3rd flatwise up) are in excess of 8/rev. These two factors minimize both the magnitude of the excitation and the responsiveness of the blade. If, however, these higher harmonic blade loads are found to be real, they will certainly be a significant design factor for either the rotor or the controller or both.

There are several other important points suggested by the results of this case. First, the weighting of the fuselage vibration is probably not an optimum for the particular combination of hub loads associated with this analytical model. Just as several combinations of weightings had to be explored to find the optimum for the baseline configuration, so it should be expected that lower fuselage vibration could be achieved here with a modification in weighting. Second, force vectoral cancellation is the probable mechanism responsible for the reduction in hub vibration. Force vectoral cancellation occurs when the magnitude and phase of the rotating 3/rev and 5/rev hub loads are adjusted to minimize the 4/rev nonrotating system loads. It is not necessary that the magnitudes of either the 3/rev or 5/rev loads be reduced, only that they be phased properly. It is quite possible that the 3/rev and 5/rev loads will actually be increased by the HHC inputs. For this case it appears that the rotating 5/rev load has been increased and the 3/rev load left unchanged to produce a decrease in the resolved (fixed system) 4/rev longitudinal and lateral loads. This obviously can not be considered a generally acceptable procedure and implies that weighted rotating system loads may be a required contribution to the performance index to keep blade loads within limits. A third observation from the results of this case is that favorable fuselage response vectoral cancellation from the rotor hub to the cockpit and cabin has played a role in reducing vibration. This mechanism is reflected by the presence of low fuselage vibration and higher hub vibration. Finally, it is possible for this case, that a local nonlinear minimum (of the performance index) has been reached rather than a true minimum.

Effect of Gross Weight - The effectiveness of the higher harmonic controller in reducing aircraft vibrations was investigated as a function of aircraft gross weight. The results are presented in Figure 4.30 for maximum gross weight, an increase of 23 percent over the baseline, and in Figure 4.31 for minimum gross weight, a decrease of 20 percent. These results can be compared to the baseline gross weight results in Figures 4.7, 4.13 and 4.14. It is seen that higher levels of vibration occur in both the rotor hub and the fuselage sensor locations with an increase in gross weight; this is a direct result of the increase in hub loads corresponding to a greater rotor disc loading. The controller is effective in reducing both hub and fuselage vibrations at all gross weights. The fuselage vibrations are all below .07 for the low gross weight, .10 for the baseline gross weight and below .30 for the high gross weight. A similar trend is evident for the hub vibrations. The higher harmonic pitch controls required for all three gross weights are well within one degree.

A comparison of the blade vibratory moments at different gross weights show that the increases in moments due to the vibration controller are lower as gross weight is increased. The peak edgewise moment and the root flatwise moment are actually lowered with the controller activated at the highest gross weight. The increases in blade moments at minimum gross weight are caused by 6/rev and 7/rev responses due to interharmonic coupling.

The conclusions from the gross weight parametric study in many ways mirror the conclusions from Case No. 5 (baseline with variable inflow). Interharmonic coupling is evident in the results. Force vectoral cancellation has clearly played a significant role in minimizing fuselage vibration. In Case No. 6 (maximum GW) cancellation of 3, 4 and 5/rev rotating loads to reduce 4/rev stationary system loads is implied since the blade root loads at these harmonics are not substantially reduced. Response vectoral cancellation from the hub to the fuselage sensor location is also suggested by the relatively high hub vibration levels. Because of the high hub vibration levels and the modest higher harmonic control inputs it is also suspected that a nonlinear local solution has been reached by the conroller rather than a true minimum. One final observation is offered at this point. For all conditions which represent reduced vibratory loading (i.e. lower airspeed & GW) compared to the baseline condition at which the controller was optimized, the fuselage vibration reductions have been better than the baseline. For all conditions which are more severe (variable inflow, higher GW), the vibration reductions have been worse than the baseline. If this generalization holds, than the controller need only be optimized for one (appropriately severe) design condition to insure satisfactory performance for the helicopter flight envelope.

Effect of Rotor Speed - The rotor speed of the baseline aircraft configuration was increased by 10 percent to evaluate its effect on the higher harmonic controller performance. The results, which are shown in Figure 4.32, indicate that the controller is slightly more effective at the overspeed condition. It reduces the vibration levels of the rotor hub and of the fuselage sensor locations including the nose vertical. The higher

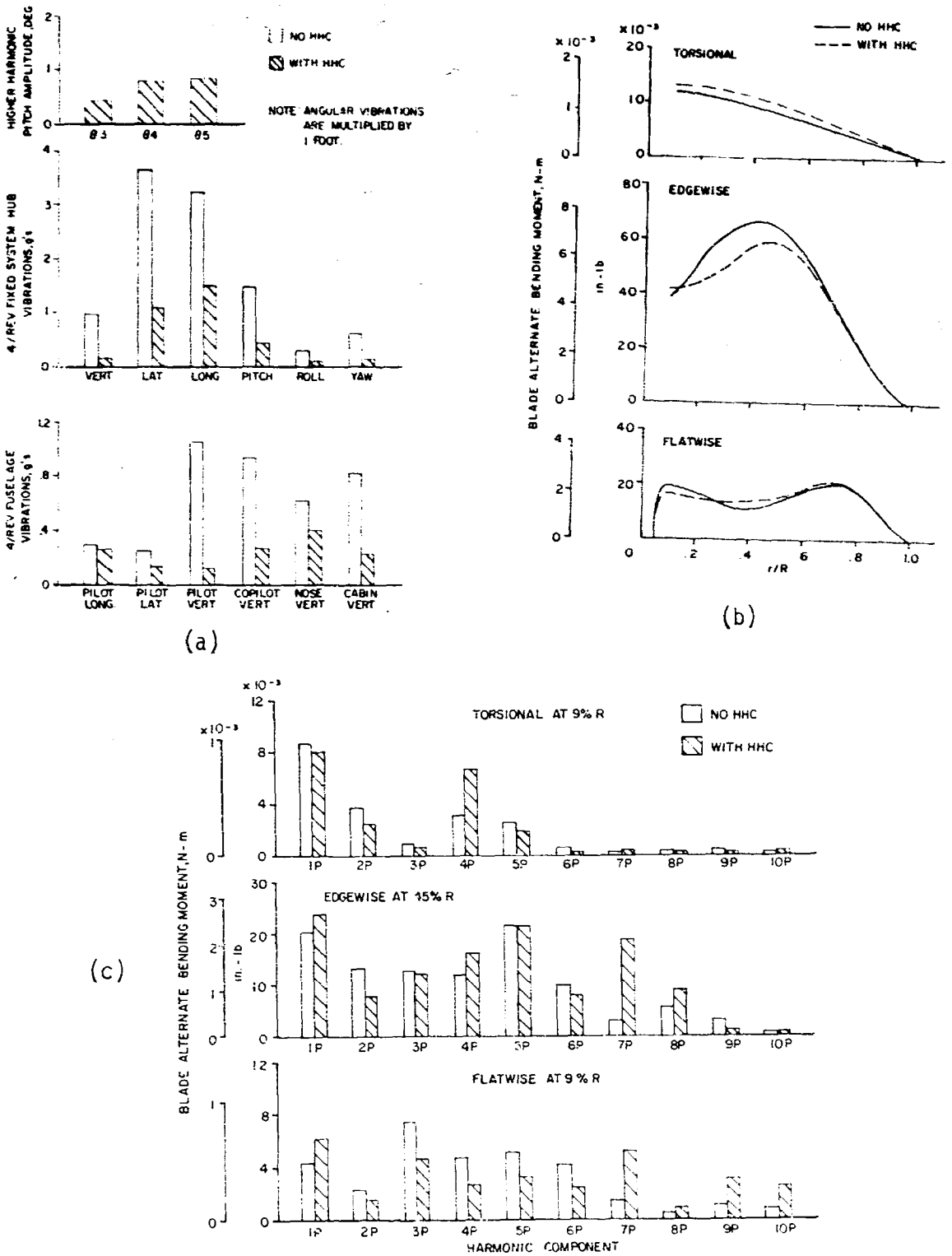

Figure 4.30 Case 6, Max Gross Weight, 150 Kn.

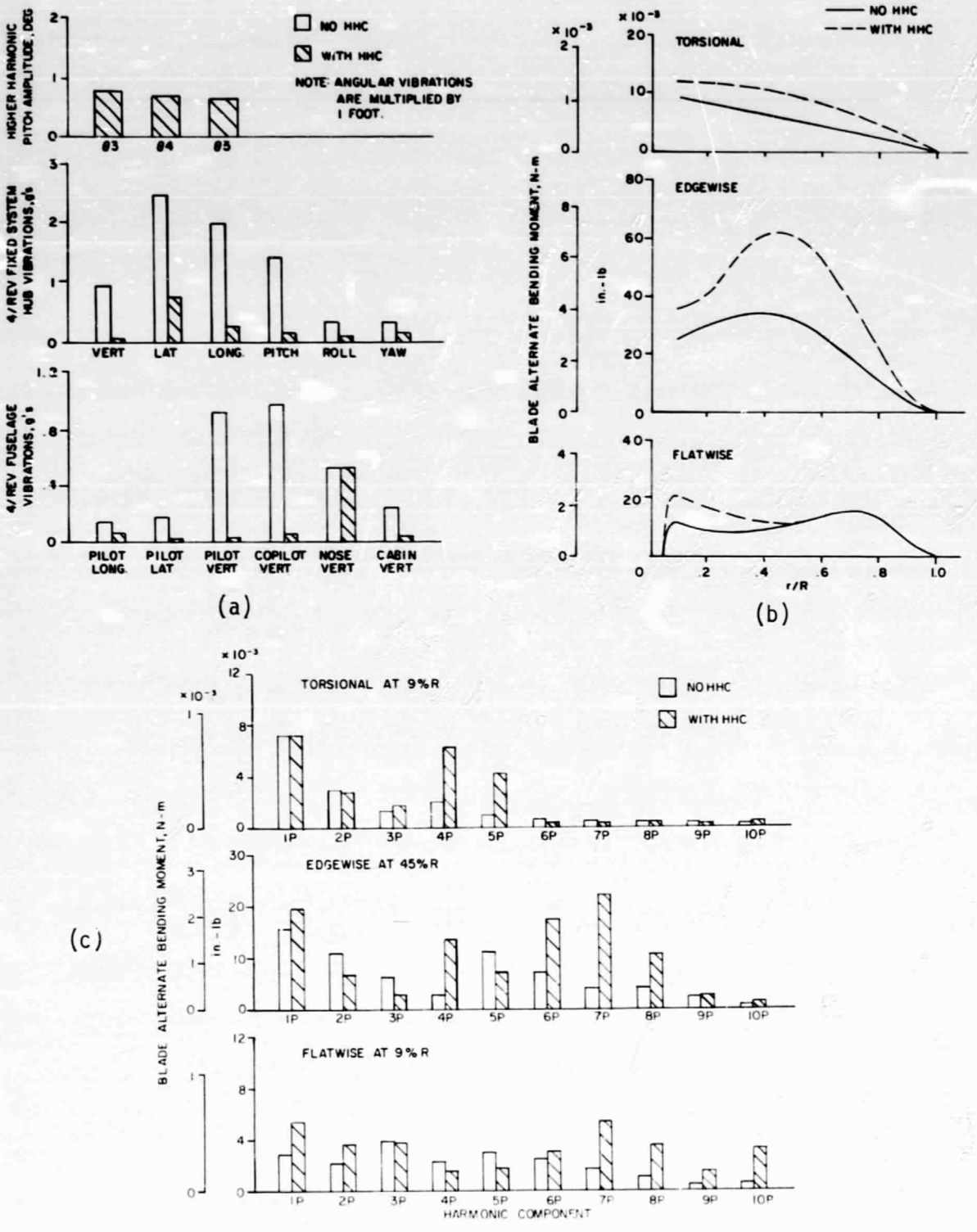

Figure 4.31 Case 7, Min Gross Weight, 150 Kn.

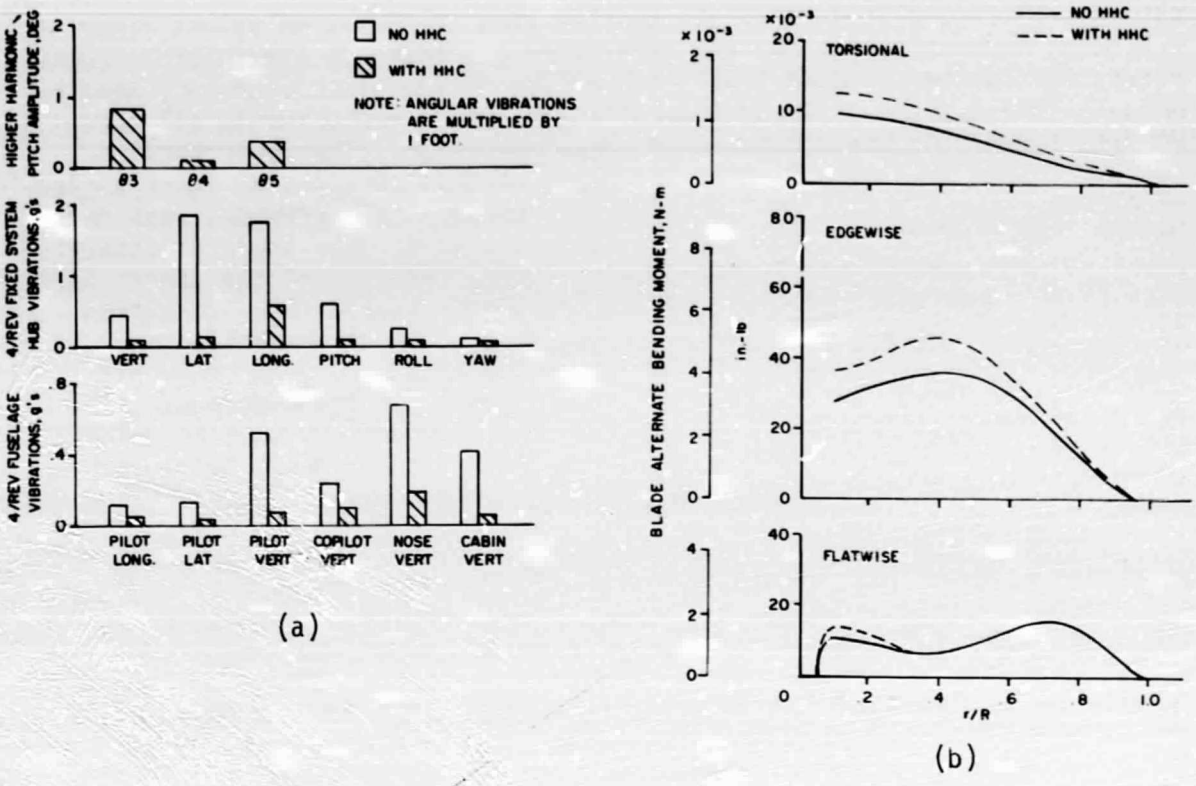

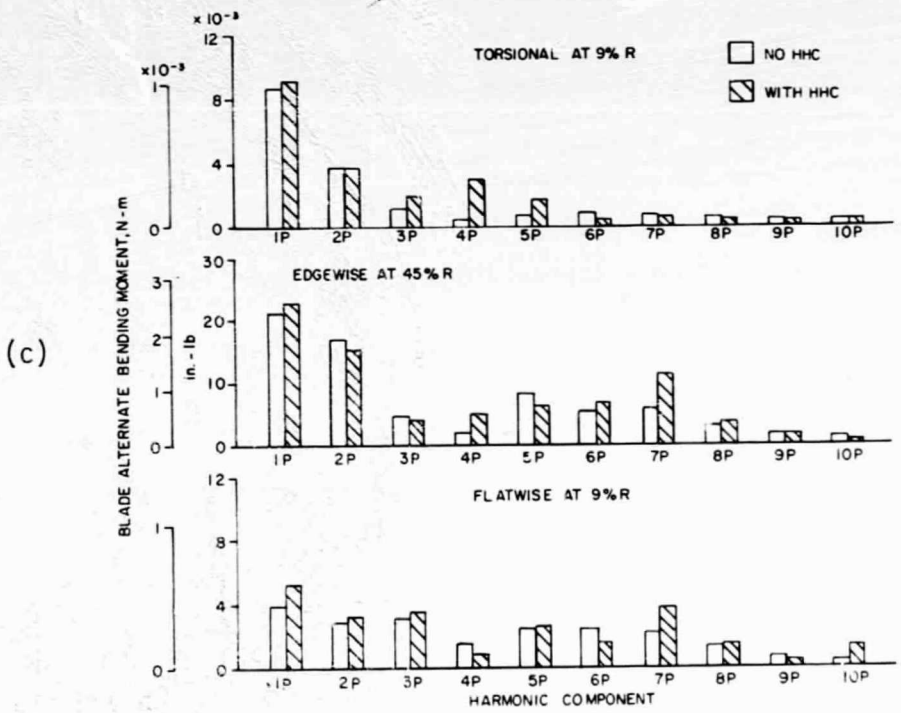

Figure 4.32 Case 8, 110% N_R, 150 Kn.

harmonic pitch amplitudes are all smaller than the baseline values since the vibration magnitudes without the controller are lower to start with. Lower vibrations can be expected from a comparison of the blade vibratory bending moments from Figures 4.13 and 4.32(b) which show a reduction in all three bending moments at the higher rotor speed condition. The lower bending moments result from operation of the blade airfoil sections at lower angles of attack. Since the airfoil section lift curve slope increases with Mach number, the airfoil can generate the same lift at a lower angle of attack resulting in lower higher harmonic blade loads. Activating the controller results in lower blade bending moments for the overspeed rotor condition as is the case for the baseline configuration. From an inspection of Figures 4.14 and 4.32(c), it is found that the 4/rev and 5/rev harmonic components of all three bending moments are lower for the overspeed condition resulting in the overall reduction of the vibratory moments. The effect of the vibration controller on the individual harmonic components of the blade moments is the same at the two rotor speeds.

Effect of Blade Loading - The influence of blade loading is studied by examining the effect of uniformly reducing blade chord by 10%. The hub and fuselage vibration levels and higher harmonic pitch requirements are shown in Figure 4.33(a). As it did for previous cases, the controller effectively reduces weighted fuselage vibration levels. Consistent with results in Section 4.6.1, it is anticipated that a slightly different weighting function could reduce longitudinal vibration further without compromising vertical and lateral levels. Hub vibration levels are only reduced to about 50% of their values without HHC indicating a significant degree of fuselage modal response cancellation is implicit in the vibration solution. This conclusion is substantiated by the relatively low higher harmonic control inputs.

Figure 4.33(b) shows that blade edgewise and flatwise loads are increased substantially by the HHC inputs. Figure 4.33(c) suggest the cause is increases in nearly all harmonic responses. As was discussed for case No. 5, the cancellation of 3/rev and 5/rev rotating hub loads is responsible for lower 4/rev nonrotating hub loads in the face of higher rotating system loads. This case reiterates the need to devise a performance index parameter which will impose blade loads constraints on the vibration solution.

Effect of Blade Radius - To study the effect of disc loading, the rotor blade radius was reduced by 10 percent. The blade natural, uncoupled flatwise, edgewise and torsional frequencies and mode shapes were recalculated and are listed below.

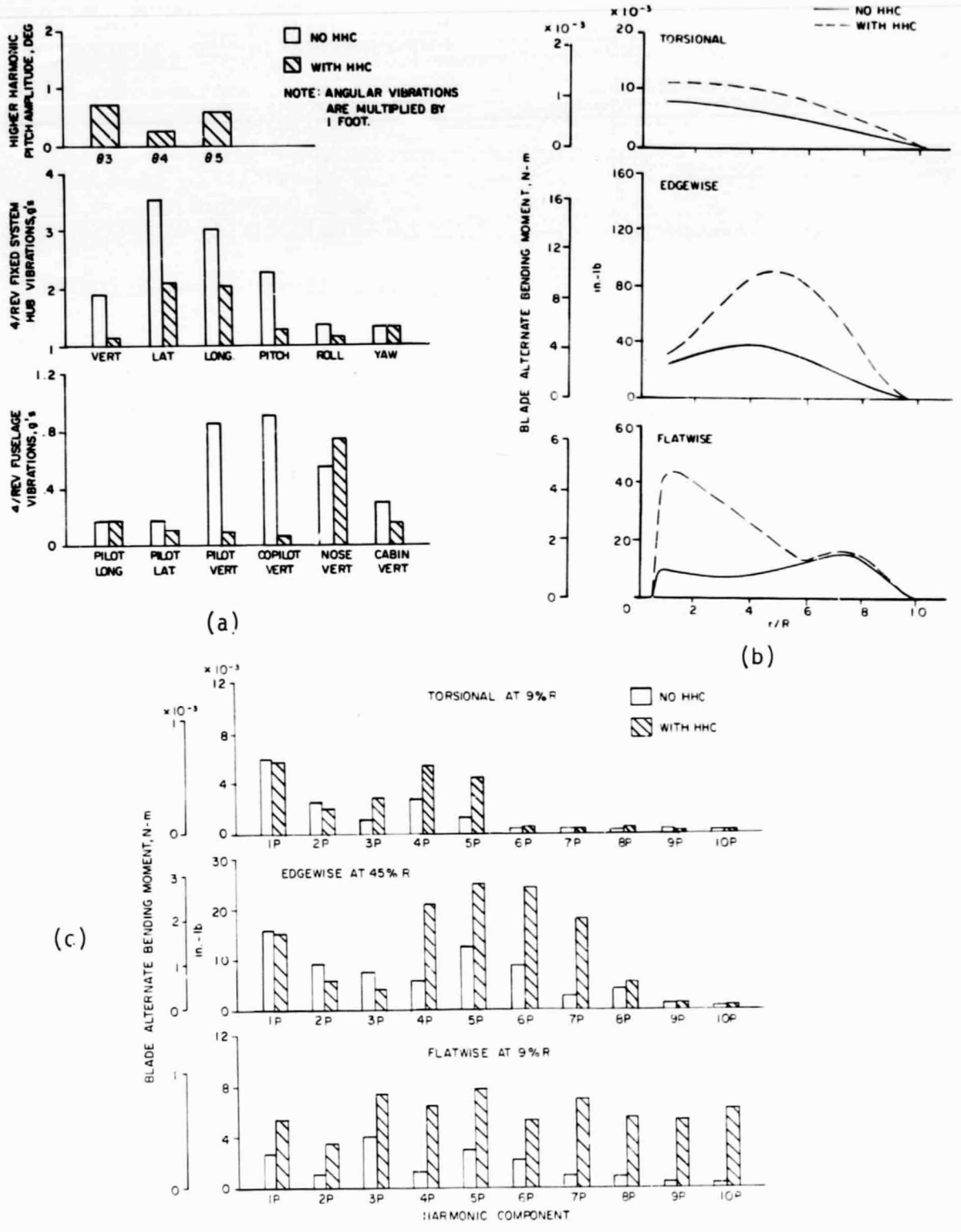

Figure 4.33 Case 9, 90% Chord, 150 Kn.

	Mode	Frequency/Rotor Speed
Flatwise	1	1.01
	2	2.83
	3	5.00
	4	7.74
Edgewise	1	0.28
	2	4.50
Torsional	1	3.86

A comparison with the baseline rotor configuration frequencies, which were discussed in Section 4.5.1, shows that all the blade frequencies are lower for the 90 percent rotor radius configuration.

The vibrations of the hub and fuselage are shown in Figure 4.34(a). Again the controller is very effective in reducing the vibration levels. For this case the reduction in hub vibration is of the same order as that of the fuselage suggesting pure vibratory load reduction as the fuselage vibration reduction mechanism rather that modal response cancellation. Blade loads are shown in Figures 4.34(b) and (c). The increased values of the HHC inputs are reflected by higher blade torsional loads. Edgewise load increases are caused primarily by 7 and 8/rev responses.

Effect of Blade Natural Frequencies - The effect of a different combination of the blade natural frequencies on the performance characteristics of the higher harmonic controller was analyzed. The flatwise mode frequencies were shifted from one side of the dominant excitation frequency to the opposite side in order to change the phase of the modal response by 180 degree. The torsion mode was placed at 3/rev to be in resonance with a major excitation. This case was judged to be a fair test of the adaptive features of the controller with respect to rotor blade dynamics. The second flatwise frequency was increased from 2.85/rev to 3.5/rev and the torsional frequency was lowered from 4.22/rev to 3/rev. The analytical results are presented in Figure 4.35. The controller is quite effective in reducing the vibrations at all the points investigated; the weighted fuselage vibrations are all below .16g. The higher harmonic pitch controls required to minimize the aircraft vibrations are between ½ to 1 degree higher than the corresponding baseline values.

The spanwise and edgewise blade moments are increased by the HHC inputs, Figure 4.35(b). In this case, the principal causes are increased 1 and 2/rev responses resulting from interharmonic coupling and higher 3 and 4/rev responses, Figure 4.35(c).

Effect of Fuselage Frequency - The six flexible fuselage modes discussed in Section 4.5.1 have been used throughout this parametric study. These modes were chosen because their natural frequencies are close to the 4/rev excitation frequency. In this section, the fifth fuselage modal frequency (second vertical) was increased from 15.30 Hz (corresponding to

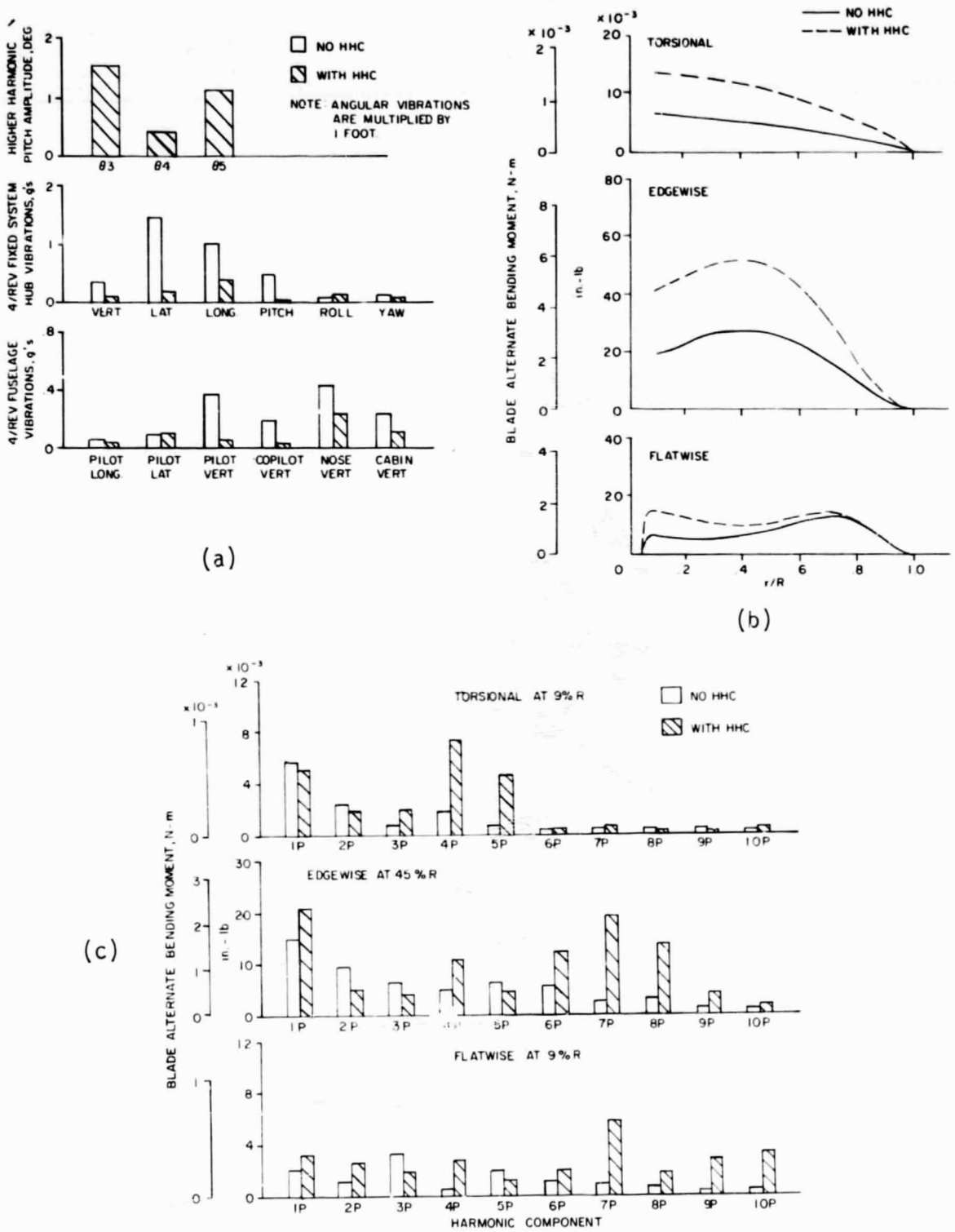

Figure 4.34 Case 10, 90% Radius, 150 Kn·

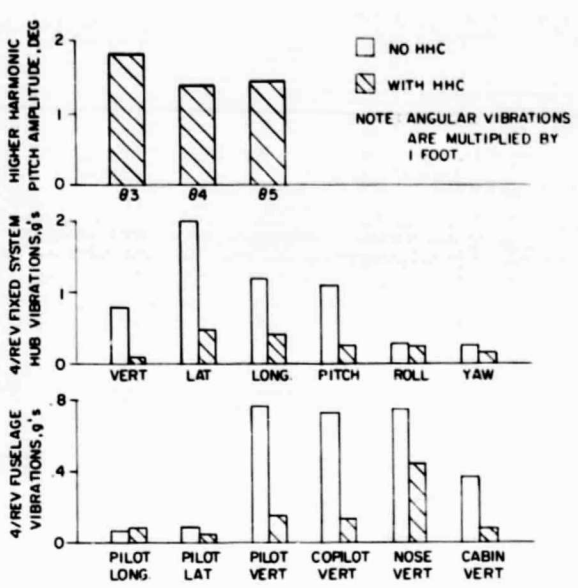

(a)

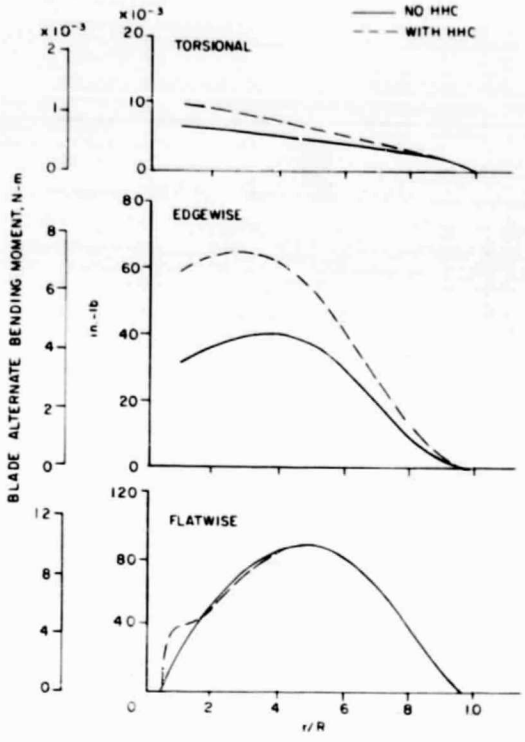

(b)

(c)

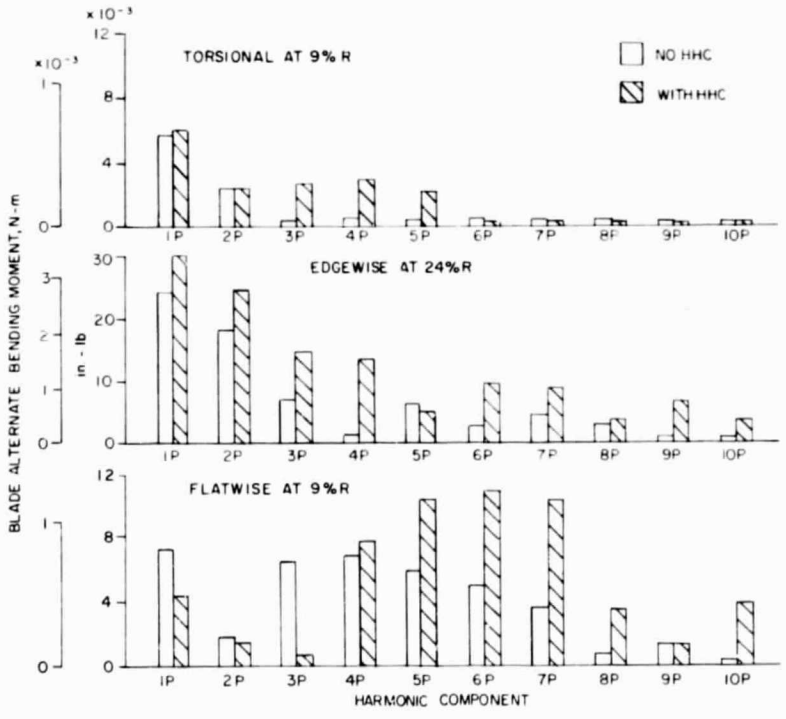

Figure 4.35 Case 11, $\omega_{F2} = 3.5P$, $\omega_{T1} = 3P$.

3.56/rev) to 16.17 Hz (corresponding to 3.76/rev). The increased fuselage frequency results in doubling the amplification factor of that mode for the baseline value. The results are presented in Figure 4.36.

As expected, the vibration levels transmitted to the six fuselage sensor locations are all increased, especially the vertical components (compare Figures 4.7 and 4.36(a)). The hub vibrations show a slight increase in vibration. With the controller activated the fuselage vibrations are reduced by the same order as they have been throughout the parametric studies. Since the hub vibration levels are relative high, considerable fuselage response cancellation is involved in the fuselage vibration solution. The higher harmonic pitch requirements are of the same order as the baseline case.

Again, the blade flatwise and edgewise moments are increased by the controller, Figure 4.36(b), and again the cause is interharmonic coupling, Figure 4.36(c).

Effect of Rotor Type - Up to this point, all the rotor configurations investigated (cases 1 through 12 in Table 4.5) were for an articulated rotor. It was found that in all cases the vibration controller was effective in reducing both rotor hub and fuselage vibrations. Its applicability to an hingeless rotor is investigated in this section.

The soft-inplane hingeless rotor configuration chosen is the same for the gust alleviation controller design discussed in Section 5.1. The important blade first flatwise and edgewise mode frequencies are 1.088/rev and 0.7/rev respectively.

Four flight conditions were analyzed: trimmed level flight at 150, 120 and 30 knots and hover (cases 13 through 16 in Table 4.5). As for the articulated rotor (cases 3 and 4), variable inflow was utilized at 30 knots and in hover for the hingeless rotor (cases 15 and 16). The analytical results are presented in Figures 4.37 through 4.40 and can be compared to the articulated rotor results at the same flight conditions from Figures 4.7, 4.13 and 4.14 at 150 knots and 4.26 through 4.28 at 120 knots, 30 knots and in hover respectively.

The analytical results indicate that the vibration controller can be successfully applied to an hingeless rotor to reduce the rotor hub and fuselage vibrations. It is again pointed out that the transfer matrix between vibrations and higher harmonic cyclic pitch (the T-matrix) originally developed for the baseline configuration (articulated rotor at 150 knots) was used as the initial T-matrix in the evaluation of the vibration controller performance as applied to a hingeless rotor at various forward speeds. This is further substantiation of the ability of the controller to be self adaptive in determining the correct transfer matrix. The vibration reductions for the hingeless rotor over the airspeed range from 0 to 150 kn are comparable to the reductions achieved with the articulated rotor over the same airspeed range; i.e. of the order of 80 to 90%. HHC pitch

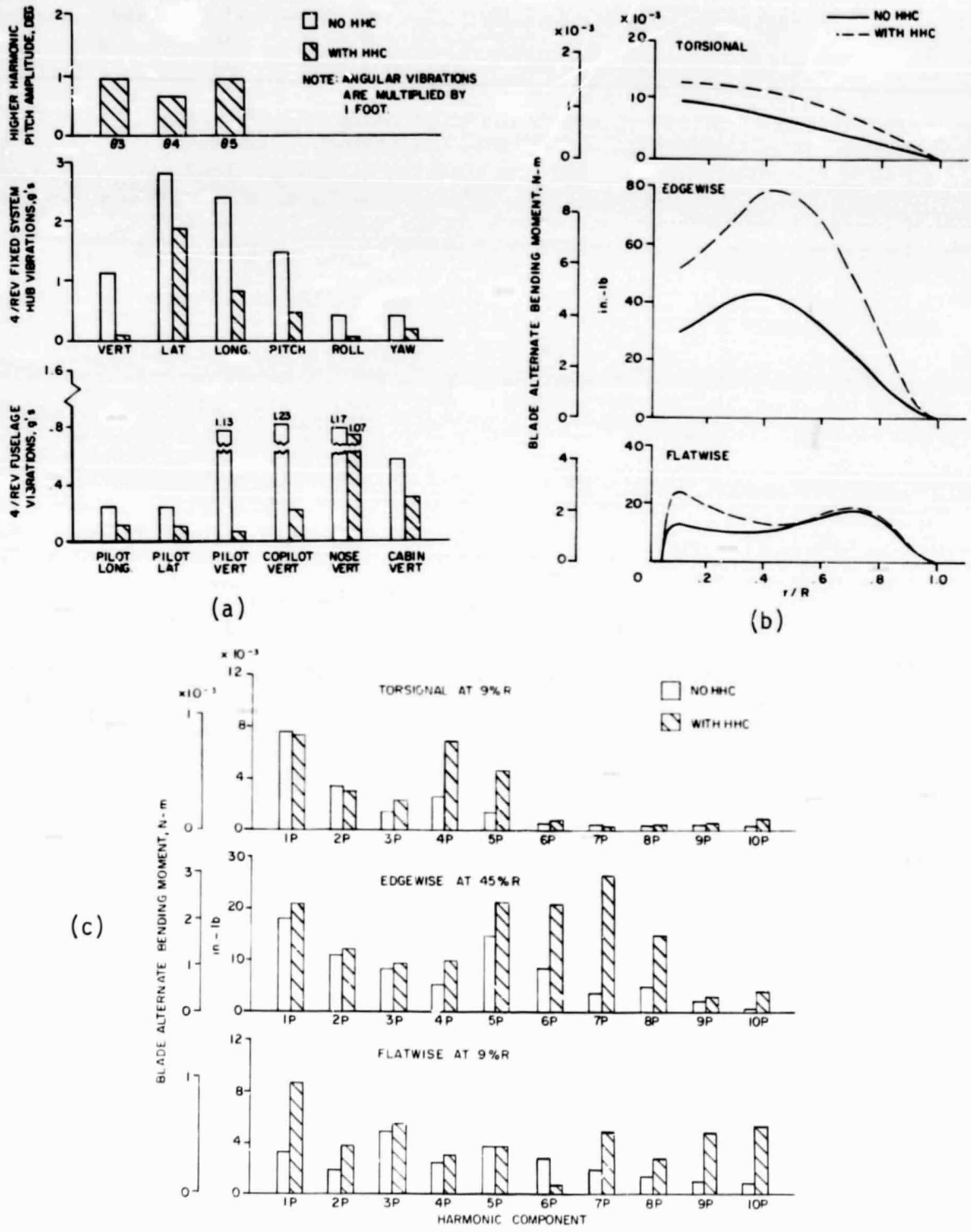

Figure 4.36 Case 12, Double Fuselage Mode Response.

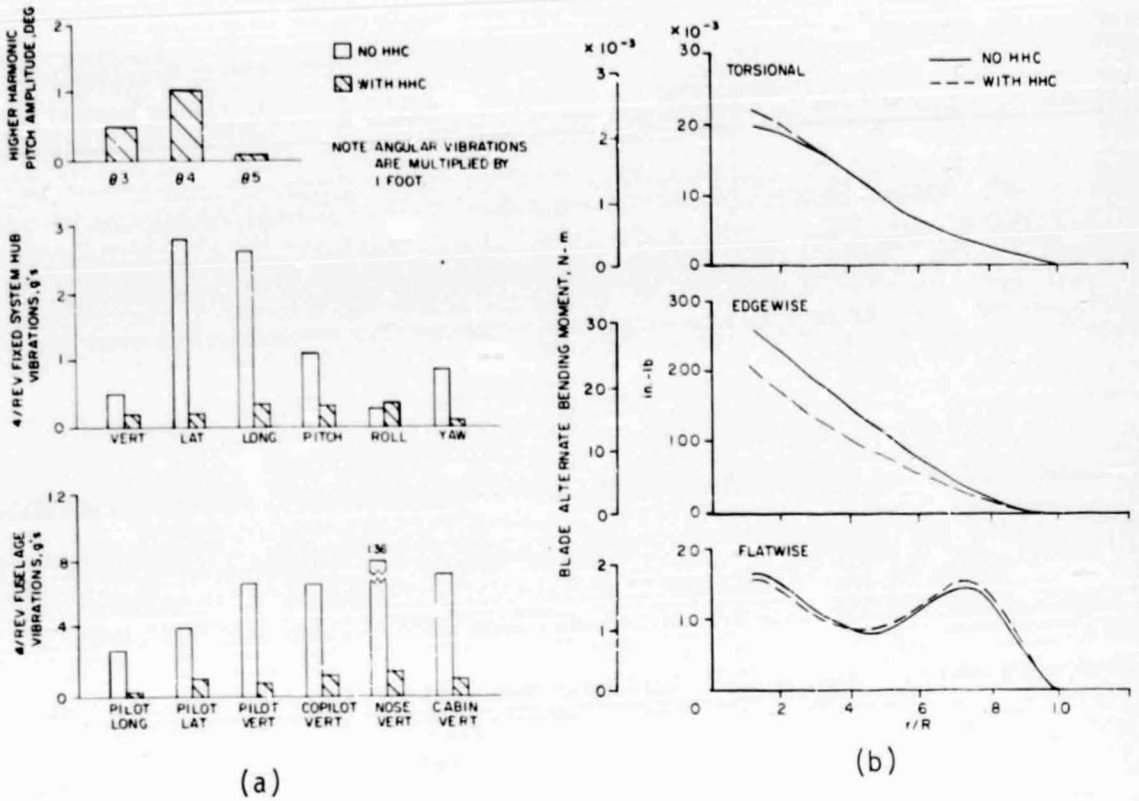

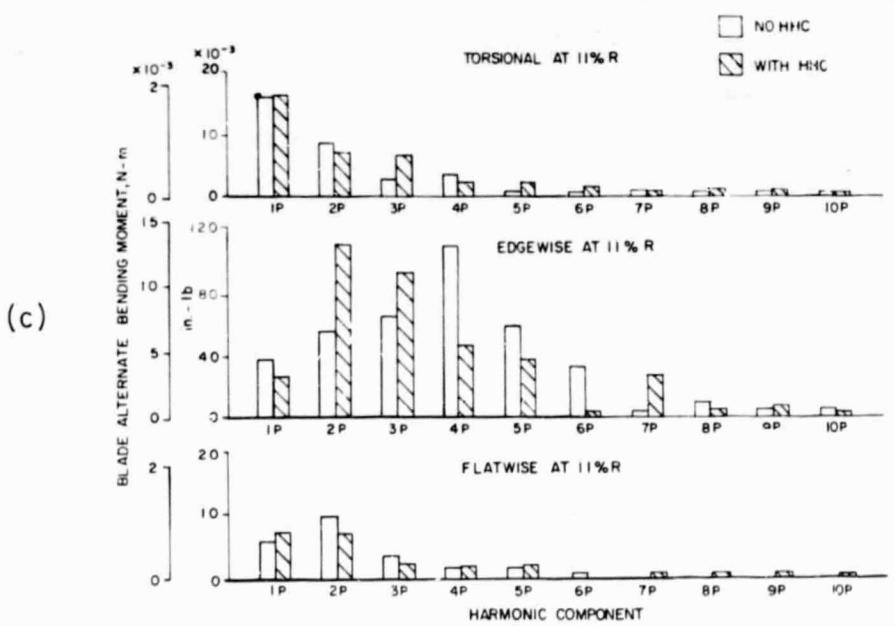

Figure 4.37 Case 13, Hingeless Rotor, 150 Kn.

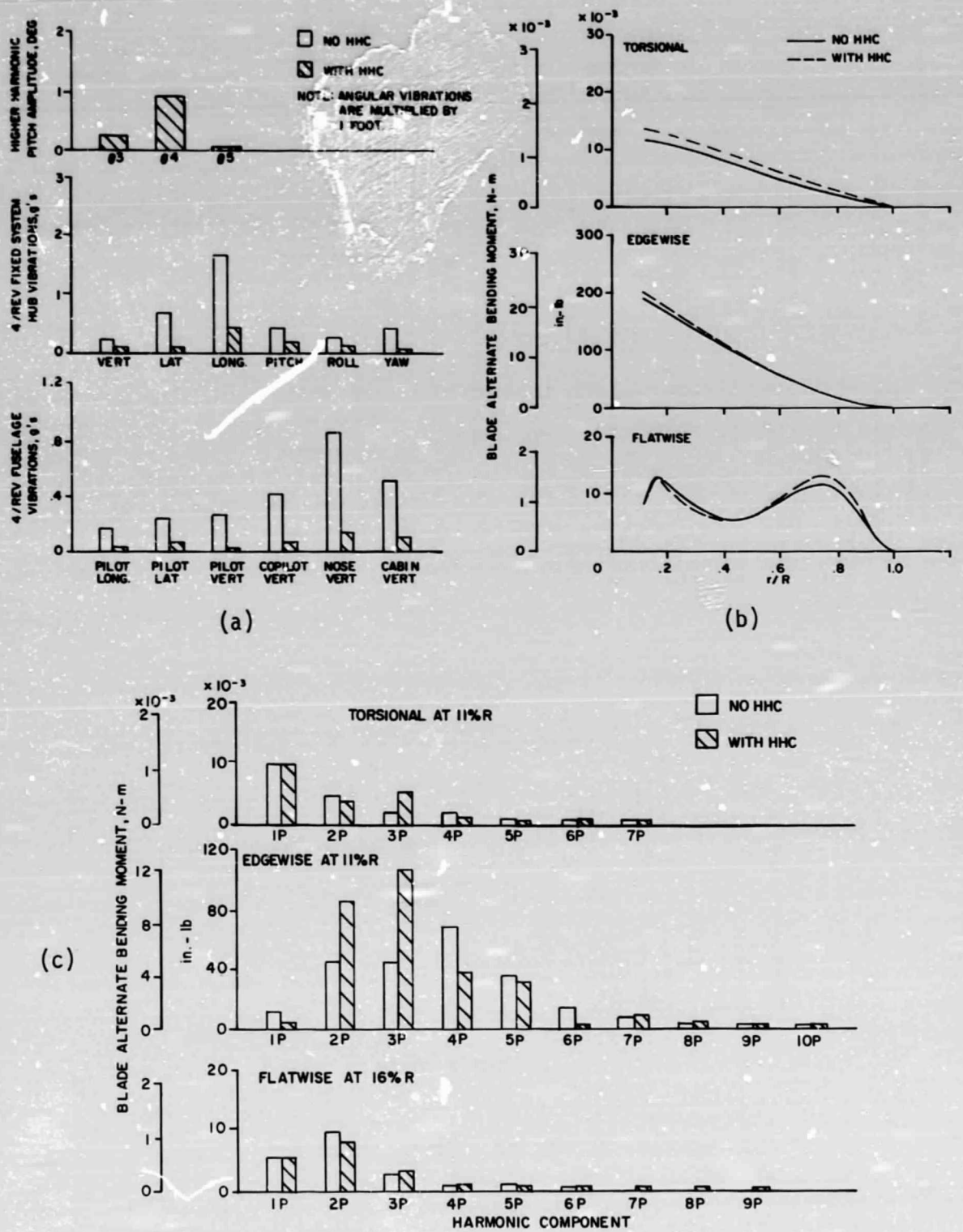

Figure 4.38 Case 14, Hingeless Rotor, 120 Kn.

C-2

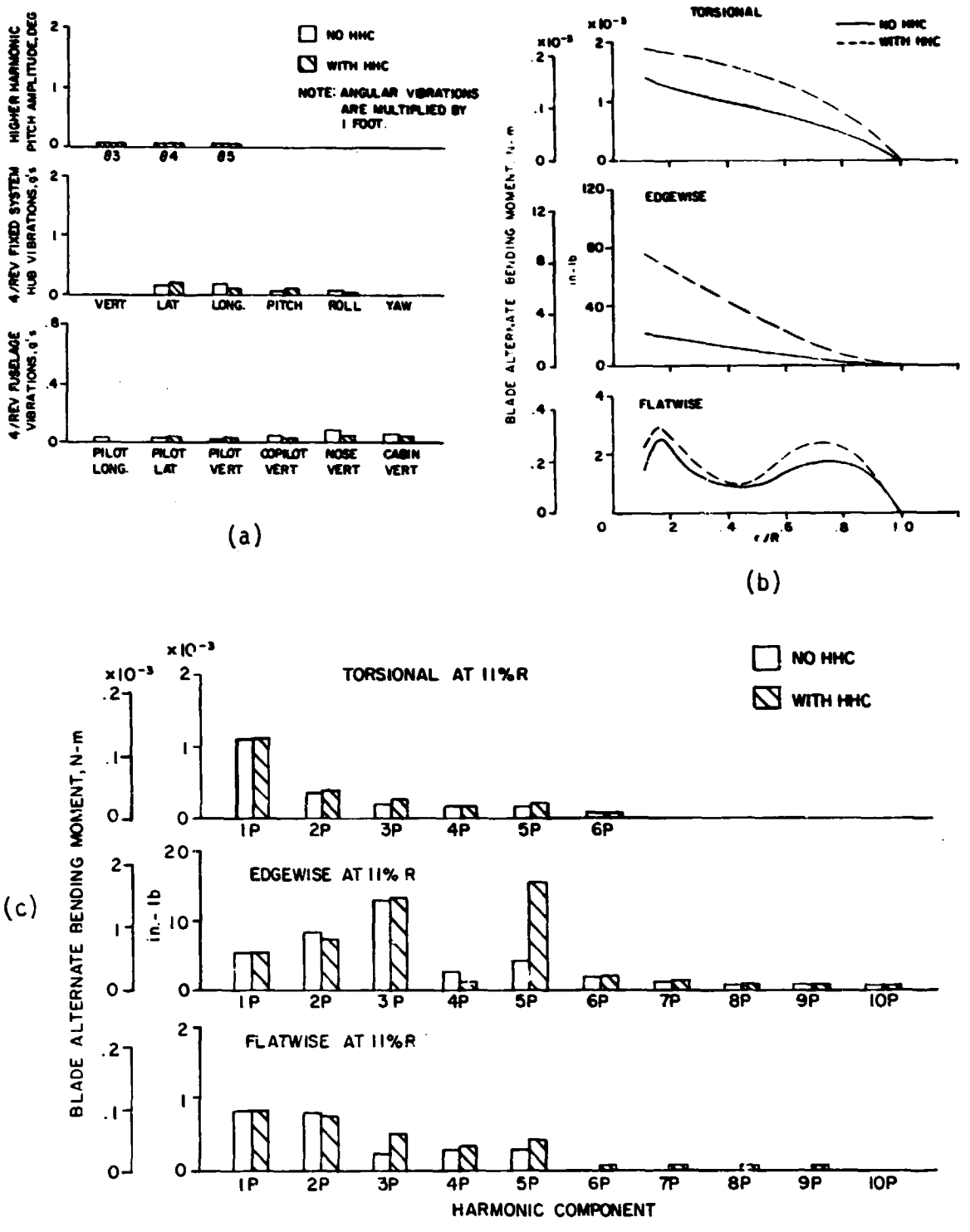

Figure 4.39 Case 15, Hingeless Rotor, 30 Kn.

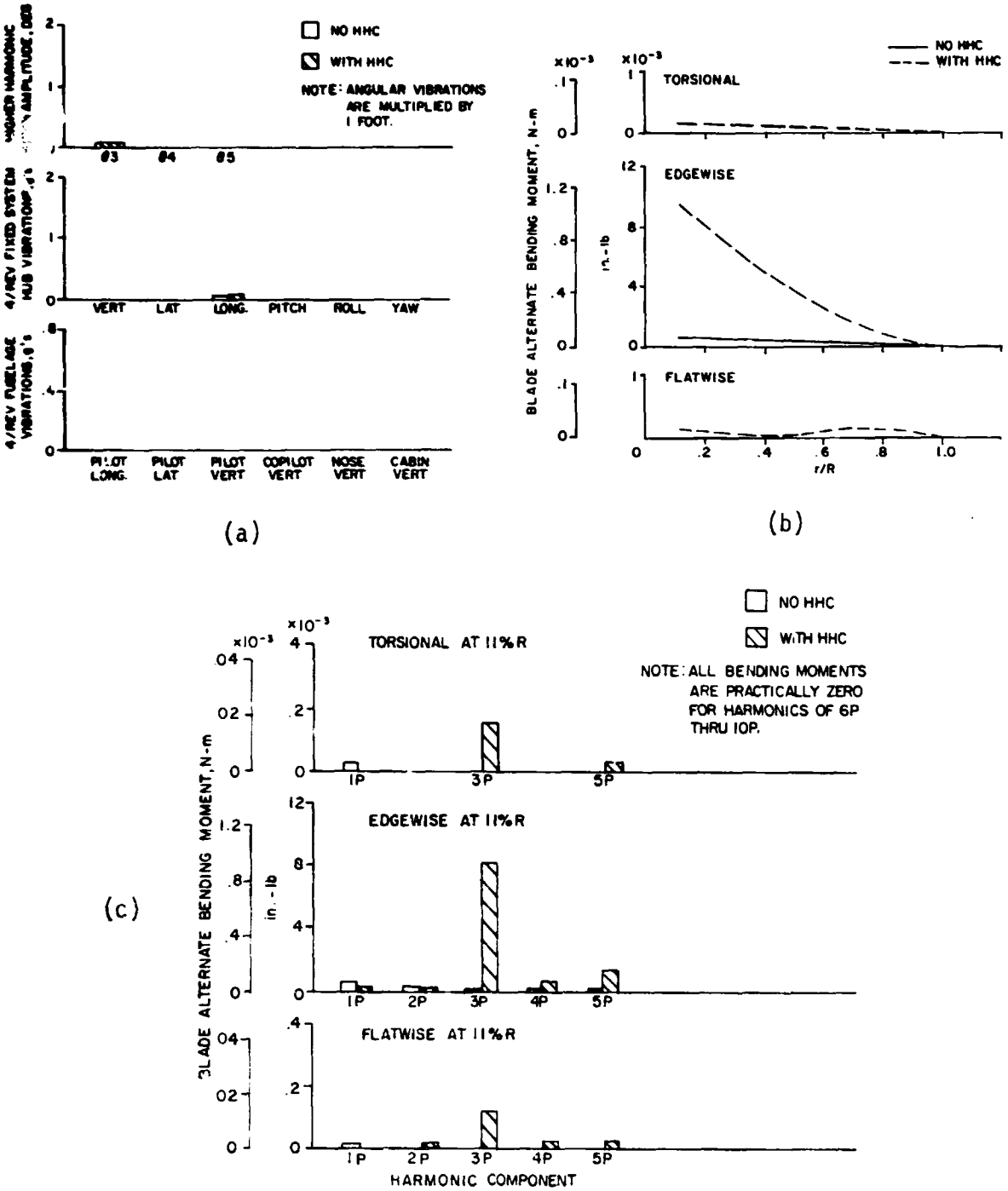

Figure 4.40 Case 16, Hingeless Rotor, Hover.

inputs are also of the same order as for the articulated rotor. Hub vibration levels are reduced substantially indicating that fuselage response cancellation is not the major factor in the vibration solution. Rotor blade loads are not increased significantly; in fact at 150 kn they are actually decreased. This, of course, suggests that harmonic force cancellation from rotating to fixed systems is not significant in the solution. The harmonics of blade loads also show that for this hingeless rotor interharmonic coupling effects are minimal.

Summary of Parametric Studies - From the results of the parametric studies the following conclusions can be drawn relative to the self-adaptive higher harmonic control system. The system is very effective and relatively insensitive to flight condition, rotor loading and rotor configuration. Good to excellent fuselage vibration reductions are achieved for variations in airspeed, rotor speed, disc loading, blade loading, blade frequencies, fuselage frequencies and rotor type. Figure 4.41 summarizes the controller effect over the airspeed range and Figure 4.42 summarizes the controller performance using percent reduction of pilot vertical vibration as an indicator for various parameters studied. Figure 4.42 also show that higher harmonic control input requirements are fairly modest (of the order of one degree at 3, 4 and 5/rev) for all conditions studied.

A possible generalization on relative effectiveness of the controller has emerged. That is, the effectiveness of the controller is improved for all conditions which represent less severe higher harmonic (vibration) loading than the condition at which the controller was optimized. This tendency suggests that a single design condition may suffice for configuring the controller in a helicopter application. Some optimization of the fuselage vibration weighting function will probably be required to achieve a satisfactory overall vibration environment in the three axes.

Fuselage vibration reduction is achieved by two mechanisms. The first mechanism is when all hub vibratory loads are reduced by the HHC inputs resulting in comparable (and linearly dependent) reductions in hub and fuselage vibrations. The second mechanism involves vibration reduction through fuselage response vectoral cancellation. In this case, hub loads are not necessarily reduced by an amount comparable to the fuselage vibrations. Rather the several orthogonal hub loads are adjusted in magnitude and phase by the controller to produce fuselage modal responses which cancel each other to produce low vibration. This condition is manifested by simultaneous low cockpit and cabin vibration and relatively higher hub vibration.

A hub load cancellation mechanism was also revealed by the parametric study. The magnitude and phase of rotating system hub loads at 3/rev and 5/rev are adjusted by the controller to produce lower nonrotating vibratory (4/rev) hub loads. For this case blade loads at 3/rev and 5/rev can be increased. Another mechanism affecting blade loads, which was discussed in Section 4.6.1, and which surfaced repeatedly during the parametric studies

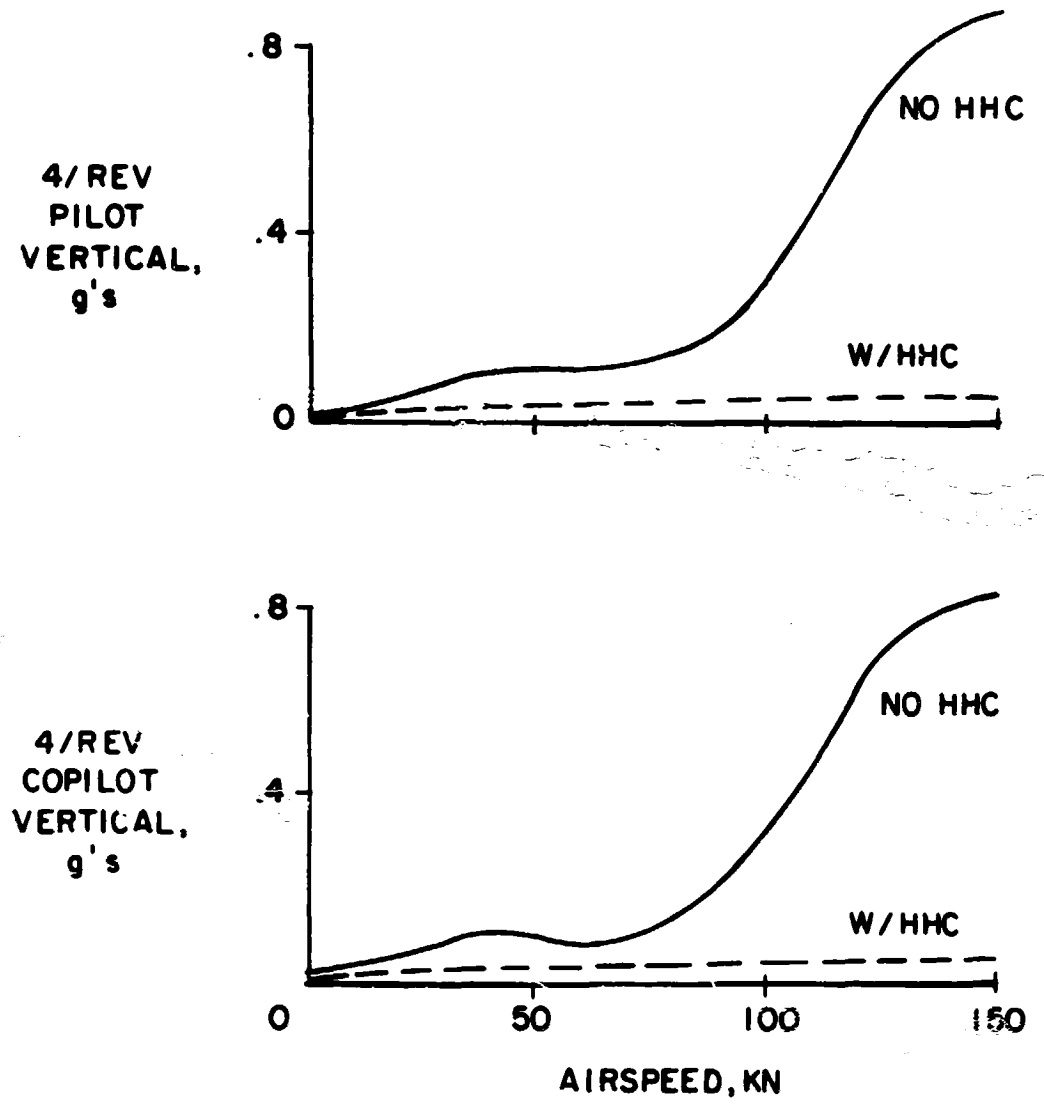

Figure 4.41 Controller Effective Over Airspeed Range.

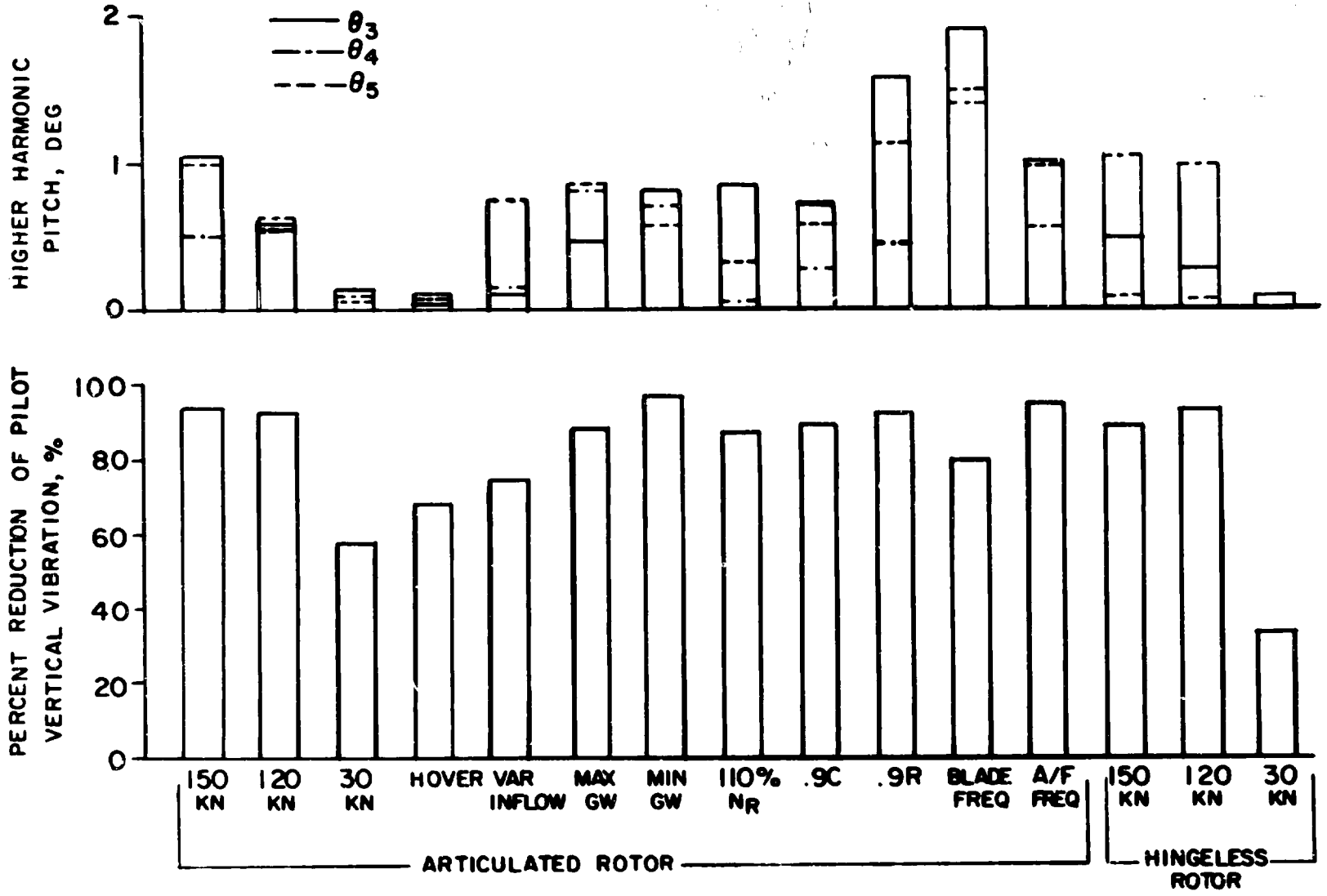

Figure 4.42 Controller Reduces Vibration for Various Aircraft Configurations.

is interharmonic coupling. Interharmonic coupling generates blade responses at frequencies which are $\pm$ 1, 2 and 3/rev separated from the HHC inputs. These blade responses occur because the airload is the product of harmonic velocities at 1, 2 and 3/rev and HHC pitch inputs at 3, 4 and 5/rev. The location of higher rotor blade mode natural frequencies becomes a consideration because the interharmonic coupling causes significant excitations at higher frequencies that are not commonly encountered with a standard helicopter control system. Future work should address the formulation of an appropriate parameter for the performance index which will limit blade load increases due to rotating to stationary system force cancellation and interharmonic coupling.

SECTION 5

GUST ALLEVIATION CONTROL

The helicopter gust alleviation problem offers a challenging control problem because of the complex rotor-fuselage coupling. The ideal controller should make use of rotor measurements to estimate the gust magnitude since the rotor responds to gusts before the fuselage. The gust effects on the fuselage can then be minimized through an optimal feedback mechanism. The optimal formulations for helicopter hover control and gust alleviation that have been investigated in the past have been continuous time controllers, References 19, 23, 30 and 31. This report considers a linear quadratic regulator sampled-data digital controller together with an one-step-ahead predictor. A major advantage of a sampled-data control law is the digital implementation of the large number of multiplications and additions that are required in an optimal formulation.

The linear quadratic regulator (LQR) controller, developed by using a linearized helicopter model, was coupled to the nonlinear simulation, GENHEL, to evaluate its effectiveness in gust alleviation. The controller was then simplified through judicious choice of feedback parameters guided by the experience gained in previous gust alleviation studies, References 18 and 19.

Of the two rotor types, articulated and hingeless, considered in the vibration control study detailed in Section 4, only one is used in the gust alleviation evaluation. The soft-inplane hingeless rotor configuration is chosen because of its high control moment capability consequently it is more sensitive to gust disturbance and more difficult to achieve successful gust alleviation.

5.1 Helicopter and Gust Model

A "hingeless" BLACK HAWK was selected for evaluation of the gust alleviation control design. The rotor configuration was designed to be compatible with the BLACK HAWK stability augmentation system and to be representative of current hingeless rotor systems. The rotor parameters defining the hingeless rotor system are summarized below.

Virtual Hinge Offset, e 9% = .736 m (2.415 ft)

Flapping Spring, K_β 65,250 N-m/rad (50,000 ft-lb/rad)

Lag Spring, K_ζ 505,949 N-m/rad (387,700 ft-lb/rad)

Lag Damping, K_ζ 3,915 N-m/rad/sec (3,000 ft-lb/rad/sec)

Rotating Flap Frequency, ω_β 1.088/rev

Rotating Lag Frequency, ω_ζ .7/rev

SECTION 5

GUST ALLEVIATION CONTROL

The helicopter gust alleviation problem offers a challenging control problem because of the complex rotor-fuselage coupling. The ideal controller should make use of rotor measurements to estimate the gust magnitude since the rotor responds to gusts before the fuselage. The gust effects on the fuselage can then be minimized through an optimal feedback mechanism. The optimal formulations for helicopter hover control and gust alleviation that have been investigated in the past have been continuous time controllers, References 19, 23, 30 and 31. This report considers a linear quadratic regulator sampled-data digital controller together with an one-step-ahead predictor. A major advantage of a sampled-data control law is the digital implementation of the large number of multiplications and additions that are required in an optimal formulation.

The linear quadratic regulator (LQR) controller, developed by using a linearized helicopter model, was coupled to the nonlinear simulation, GENHEL, to evaluate its effectiveness in gust alleviation. The controller was then simplified through judicious choice of feedback parameters guided by the experience gained in previous gust alleviation studies, References 18 and 19.

Of the two rotor types, articulated and hingeless, considered in the vibration control study detailed in Section 4, only one is used in the gust alleviation evaluation. The soft-inplane hingeless rotor configuration is chosen because of its high control moment capability consequently it is more sensitive to gust disturbance and more difficult to achieve successful gust alleviation.

5.1 Helicopter and Gust Model

A "hingeless" BLACK HAWK was selected for evaluation of the gust alleviation control design. The rotor configuration was designed to be compatible with the BLACK HAWK stability augmentation system and to be representative of current hingeless rotor systems. The rotor parameters defining the hingeless rotor system are summarized below.

Virtual Hinge Offset, e 9% = .736 m (2.415 ft)

Flapping Spring, K_β 65,250 N-m/rad (50,000 ft-lb/rad)

Lag Spring, K_ζ 505,949 N-m/rad (387,700 ft-lb/rad)

Lag Damping, K_ζ 3,915 N-m/rad/sec (3,000 ft-lb/rad/sec)

Rotating Flap Frequency, ω_β 1.088/rev

Rotating Lag Frequency, ω_ζ .7/rev

A system identification program was used to generate linear models of the "hingeless" BLACK HAWK at three airspeed: hover, 41 m/s, and 77 m/s (hover, 80 kn, 150 kn). The parameter identification routine analyzes transient data produced by preprogrammed pulse inputs applied to the control system. The program selects a linear model about some trim condition using a forward, stepwise, multiple regression algorithm. The state variables identified are two Euler angles, the six rigid body translational and rotational rates resolved into body axes, the three flapping Fourier variables, three derivatives of these variables, rotor downwash, and the four controls as follows: $\emptyset$, θ, u, v, w, p, q, r, a_{0F}, a_{1F}, b_{1F}, $\dot{a}_{0F}$, $\dot{a}_{1F}$, $\dot{b}_{1F}$, ν, B_{1S}, A_{1S}, θ_0, θ_{TR}.

A linear model, matching the observed response, is determined by the program for each state equation. Coefficients of only those states that are most highly correlated with the response are calculated. These coefficients are calculated using a least squares technique. This stepwise regression method differs from a conventional least squares algorithm in which coefficients would be estimated for all states (including those states that might not be influential in producing the response). The matrixes defining the "hingeless" BLACK HAWK linear models are given in Tables 5.1, 5.2 and 5.3.

The gust model used for the linear helicopter model is an approximation of the Dryden spectrum and consists of three orthogonal first order shaping filters driven by zero mean white noise. The cut off frequency is 1.3 rad/sec and the intensity of the white driving noise is selected to give a 7.62m/s (25 ft/sec) rms gust amplitude in each axis. The three components of gust are shown in Figure 5.1. All three components have peak values of 15.24 m/s (50 ft/sec) and rms values of approximately 7.62 m/s (25 ft/sec). The time correlation of the gust is especially evident in the vertical component, which is nearly totally in the positive direction. This biased condition will be beneficial in illustrating the response improvement that can be achieved when gust estimation and feedback is utilized in the controller. The gust waveforms shown are statistically valid members of the ensemble of gust waveforms. The ensemble average of all waveforms has zero mean. Moreover, due to ergodicity, one would expect any given member of the ensemble to exhibit a time average value of zero, if it is observed for an appropriate length of time. In fact, a thirty-second simulation has shown that the time average value is much closer to zero. The gust model used in the nonlinear GENHEL simulation is essentially the same model used by Briczinski in Reference 19. As shown in Figure 5.2, the three components of the gust model used in the nonlinear simulation is quite similar to those shown in Figure 5.1 for the linear analysis. For the sake of expedience, there was no attempt to make the gust models for the linear and nonlinear analyses the same. In the nonlinear simulation, the gust components are added to the helicopter inertial velocity components in order to calculate the fuselage and rotor angles-of-attack. Following these calculations the gust components are subtracted so that these gust velocities would not become part of the inertial response of the helicopter.

Table 5.1 Linear Model Representation of 'Hingeless' BLACK HAWK at Hover

derivative of state \ state	ϕ	θ	u^*	v^*	w^*	p	q	r	a_{0F}	a_{1F}	b_{1F}	$\dot{a}_{0F}$	$\dot{a}_{1F}$	$\dot{b}_{1F}$	ν^*	B_{1S}	A_{1S}	θ_0	θ_{TR}
$\dot{\phi}_B$ (deg/sec)	0	0	0	0	0	1.0	0	.058	0	0	0	0	0	0	0	0	0	0	0
$\dot{\theta}_B$ (deg/sec)	-.0009	-.002	-.0007	.011	-.0006	-.002	.996	.056	-.005	.002	.034	0	.132	.0004	0	0	.018	0	0
$\dot{u}$ (ft/sec^2)**	-.015	-.553	.042	.037	.020	.012	-.078	-.010	.602	.896	0	-.003	.057	-.011	-.031	-.480	.078	.097	0
$\dot{v}$ (ft/sec^2)**	.556	-.074	-.006	-.015	-.029	.049	.030	.011	0	-.083	-.375	.006	-.017	-.050	.071	.127	-.415	-.222	.210
$\dot{w}$ (ft/sec^2)**	.037	-.039	0	0	-.030	-.021	.005	.025	-10.5	0	-.042	-.026	-.002	.005	0	.059	.078	.398	-.061
$\dot{p}$ (deg/sec^2)	-.166	-3.33	-.849	-.202	-.687	2.03	1.52	.437	2.56	2.10	-116.0	.179	-.703	-1.99	1.54	1.07	-16.6	-8.40	5.50
$\dot{q}$ (deg/sec^2)	.057	-.054	0	-.154	-.122	-.105	.265	-.149	7.86	-13.8	-.397	0	-.264	.071	0	2.56	-.562	-.588	-1.85
$\dot{r}$ (deg/sec^2)	-.086	0	.209	.316	.286	.124	0	-.313	-10.7	0	-5.43	-.882	0	-.115	0	0	0	14.9	-5.28
$\dot{a}_{0F}$ (deg/sec	0	0	0	0	0	0	0	0	0	0	0	1.0	0	0	0	0	0	0	0
$\dot{a}_{1F}$ (deg/sec)	0	0	0	0	0	0	0	0	0	0	0	0	1.0	0	0	0	0	0	0
$\dot{b}_{1F}$ (deg/sec)	0	0	0	0	0	0	0	0	0	0	0	0	0	1.0	0	0	0	0	0
$\ddot{a}_{0F}$ (deg/sec^2)	-.283	.433	-4.96	-.776	66.2	.049	-1.08	-1.38	-896.0	1.13	0	-21.4	0	.068	-65.9	1.13	-.828	674.5	.206
$\ddot{a}_{1F}$ (deg/sec^2)	-.449	7.69	-2.42	21.2	0	63.0	28.3	4.13	0	-128.0	-691.4	0	-26.2	-54.1	-1.63	48.4	-823.7	13.5	-4.57
$\ddot{b}_{1F}$ (deg/sec^2)	.867	4.28	16.8	4.28	3.14	32.5	-63.5	2.22	0	723.6	-221.4	-.580	54.9	-27.5	-4.16	-834.4	-65.8	14.4	3.17
$\dot{\nu}$ (ft/sec^2)**	-.040	.048	-.690	0	9.71	.024	-.222	-.352	2.19	0	.166	-1.46	.012	0	-14.7	0	0	44.1	-.126

* To convert column to m/sec, divide each number in column by .3048
** To convert row to m/sec^2, multiply each number in row by .3048

Table 5.2 Linear Model Representation of 'Hingeless' BLACK HAWK at 41 m/s (80 Knots)

State derivative of state	β	θ	u*	v*	w*	p	q	r	a_{0F}	a_{1F}	b_{1F}	$\dot{a}_{0F}$	$\dot{a}_{1F}$	$\dot{b}_{1F}$	ν^*	B_{1S}	A_{1S}	θ_0	θ_{TR}
$\dot{\beta}_B$ (deg/sec)	0	0	0	0	0	1.0	0	.046	0	0	0	0	0	0	0	0	0	0	0
$\dot{\theta}_B$ (deg/sec)	.001	-.005	.010	.0004	.003	-.002	.999	.005	0	-.006	.014	-.0002	.0004	0	0	.007	-.006	-.006	.004
$\dot{u}$ (ft/sec^2)**	-.020	-.613	0	.018	0	.046	-.137	.028	.773	.783	-.283	0	.017	-.036	.013	-.366	-.358	.151	.013
$\dot{v}$ (ft/sec^2)**	.570	-.016	-.073	-.084	.014	.109	.052	-2.33	-.218	-.323	-.286	-.014	-.034	-.015	-.121	.401	-.236	0	.182
$\dot{w}$ (ft/sec^2)**	.015	-.022	0	-.027	-.107	-.059	2.34	.052	-10.7	.121	-.263	-.027	-.005	0	.041	.120	-.056	.421	.031
$\dot{p}$ (deg/sec^2)	.061	-1.57	-3.54	-.459	-.361	.668	2.03	.997	-4.11	-3.22	-108.5	-.184	-.925	-.808	-1.59	7.90	-7.99	-6.24	6.26
$\dot{q}$ (deg/sec^2)	-.127	.135	.916	.398	-.792	.018	-.834	.059	5.05	-15.2	-2.89	-.083	-.182	.134	.523	3.04	-.623	-1.98	-.266
$\dot{r}$ (deg/sec^2)	-.199	-.278	0	.626	-.997	.144	-.083	-.526	-5.58	-.742	-6.87	-.155	-.179	-.054	3.42	2.87	-2.37	0	-5.38
$\dot{a}_{0F}$ (deg/sec)	0	0	0	0	0	0	0	0	0	0	0	1.0	0	0	0	0	0	0	0
$\dot{a}_{1F}$ (deg/sec)	0	0	0	0	0	0	0	0	0	0	0	0	1.0	0	0	0	0	0	0
$\dot{b}_{1F}$ (deg/sec)	0	0	0	0	0	0	0	0	0	0	0	0	0	1.0	0	0	0	0	0
$\ddot{a}_{0F}$ (deg/sec^2)	-.687	-3.44	-13.3	3.52	70.9	8.28	.854	.884	-922.7	38.6	-31.8	-23.3	-1.21	-6.64	-77.8	-215.0	-65.0	754.1	0
$\ddot{a}_{1F}$ (deg/sec^2)	-8.33	-12.7	0	28.3	23.8	107.9	30.0	11.1	-516.2	106.3	-1110.	-6.62	-23.9	-89.5	-130.0	-289.0	-1332.	361.2	-8.07
$\ddot{b}_{1F}$ (deg/sec^2)	-5.48	4.32	14.8	9.12	0	27.8	-103.7	5.81	280.5	1067.	-24.6	6.40	85.8	-23.9	79.4	-1213.	183.6	268.4	0
$\dot{\nu}$ (ft/sec^2)**	-.140	-.138	-1.78	.209	4.86	.605	-.257	-.110	1.97	4.95	-1.04	-1.37	.188	-.479	-20.6	-17.5	-3.07	46.2	-.091

* To convert column to m/sec, divide each number in column by .3048

** To convert row to m/sec^2, multiply each number in row by .3048

Table 5.3 Linear Model Representation of 'Hingeless' BLACK HAWK at 77 m/s (150 Knots)

State / derivative of state	ϕ	θ	u*	v*	w*	p	q	r	a_{0F}	a_{1F}	b_{1F}	$\dot{a}_{0F}$	$\dot{a}_{1F}$	$\dot{b}_{1F}$	ν *	B_{1S}	A_{1S}	θ_0	θ_{TR}
$\dot{\phi}_B$ (deg/sec)	0	0	0	0	0	1.0	0	-.073	0	0	0	0	0	0	0	0	0	0	0
$\dot{\theta}_B$ (deg/sec)	.018	0	0	-.0004	.002	-.002	1.0	.036	0	-.018	.035	-.0006	.0004	.0002	0	.0095	-.015	-.009	.005
$\dot{u}$ (ft/sec^2) **	0	-.623	-.044	0	.014	.038	.262	.016	.901	.750	-.265	-.012	.020	-.027	.105	-.319	-.289	0	.093
$\dot{v}$ (ft/sec^2) **	.642	-.063	-.022	-.142	0	-.259	.028	-4.37	.476	-.072	-.73	.012	-.026	-.016	0	.262	-.107	-.429	.235
$\dot{w}$ (ft/sec^2) **	.116	.057	-.062	-.090	-.220	.026	4.39	.060	-10.5	-.045	-1.03	-.013	-.008	.0015	-.169	.372	-.220	0	.174
$\dot{p}$ (deg/s^2)	.193	-3.25	-1.10	0	-.816	.961	1.71	1.45	9.33	2.36	-109.7	.140	-.750	-.996	4.92	9.60	-5.02	-18.4	6.42
$\dot{q}$ (deg/sec^2)	.819	0	-.313	-1.32	-1.29	.226	-1.54	.642	4.16	-15.1	-11.2	0	-.179	.078	3.69	3.55	-2.35	-6.39	4.84
$\dot{r}$ (deg/sec^2)	-.179	-.978	.102	1.06	-1.74	.197	-.136	-.587	-7.12	-.567	-8.75	.258	-.121	-.059	18.4	8.19	-3.39	-9.62	-6.89
$\dot{a}_{0F}$ (deg/sec)	0	0	0	0	0	0	0	0	0	0	0	1.0	0	0	0	0	0	0	0
$\dot{a}_{1F}$ (deg/sec)	0	0	0	0	0	0	0	0	0	0	0	0	1.0	0	0	0	0	0	0
$\dot{b}_{1F}$ (deg/sec)	0	0	0	0	0	0	0	0	0	0	0	0	0	1.0	0	0	0	0	0
$\ddot{a}_{0F}$ (deg/sec^2)	2.03	2.04	-2.59	2.75	33.8	6.58	0	2.43	-891.	75.1	-28.6	-12.0	2.28	-5.90	0	-239.5	-38.0	464.0	2.87
$\ddot{a}_{1F}$ (deg/sec^2)	-7.35	0	-7.07	41.15	60.9	130.5	18.4	32.0	-1153.	310.9	-1363.	-18.0	-14.8	-111.2	-404.7	-726.9	-1579.	800.0	24.1
$\ddot{b}_{1F}$ (deg/sec^2)	-5.62	12.8	36.9	-9.98	-19.4	9.15	-124.6	9.17	304.1	1017.	164.1	20.2	103.6	-11.6	434.7	-1074.	419.3	230.4	19.8
$\dot{\nu}$ (ft/sec^2)**	-.059	-.583	-.869	.155	3.06	.507	-.257	.229	.915	6.57	-.965	-.690	.275	-.433	-29.4	-19.9	-1.53	31.7	.159

* To convert column to m/sec, divide each number in column by .3048
** To convert row to m/sec^2, multiply each number in row by .3048

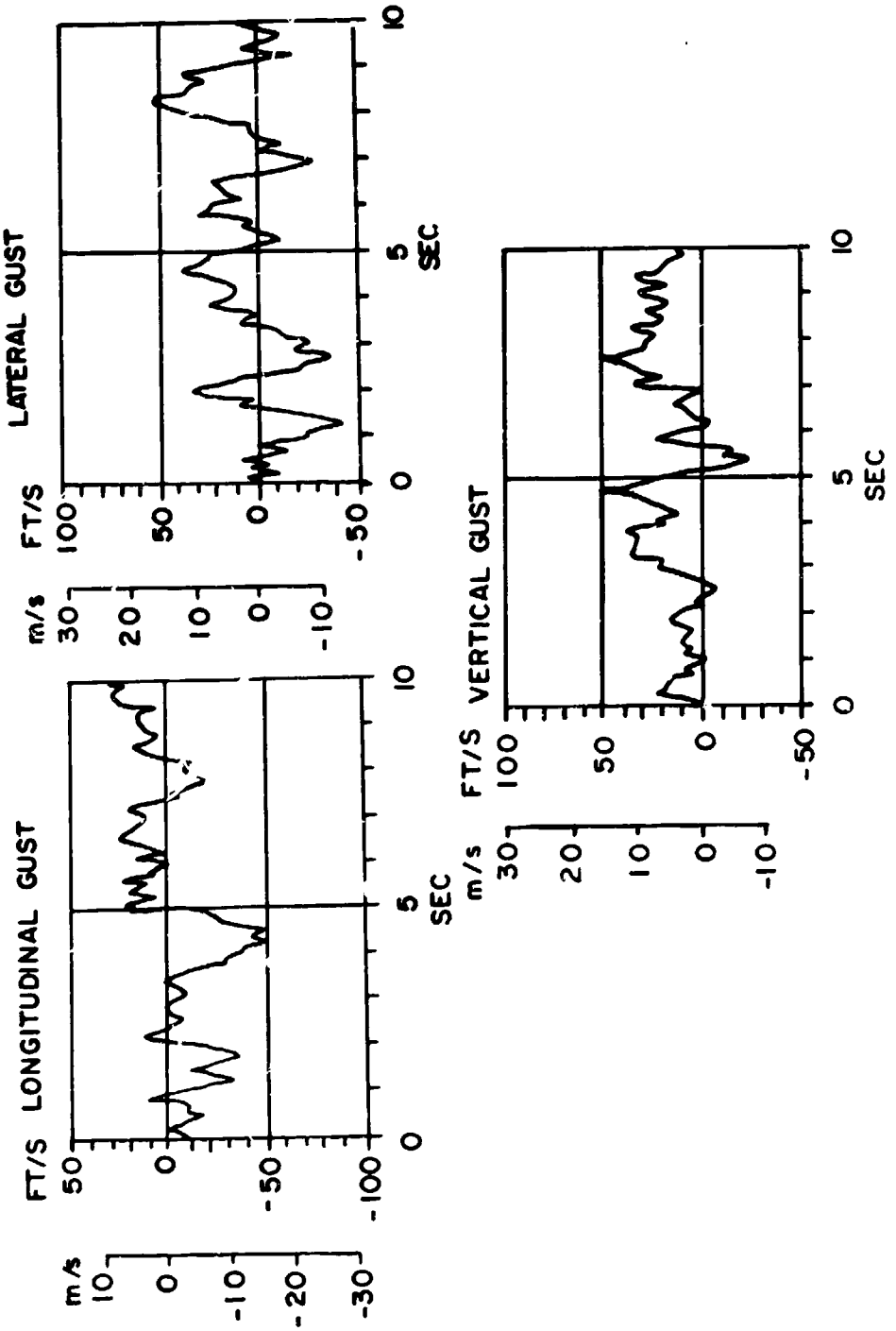

Figure 5.1 Gust Components Used to Disturb the Linearized Helicopter Model.

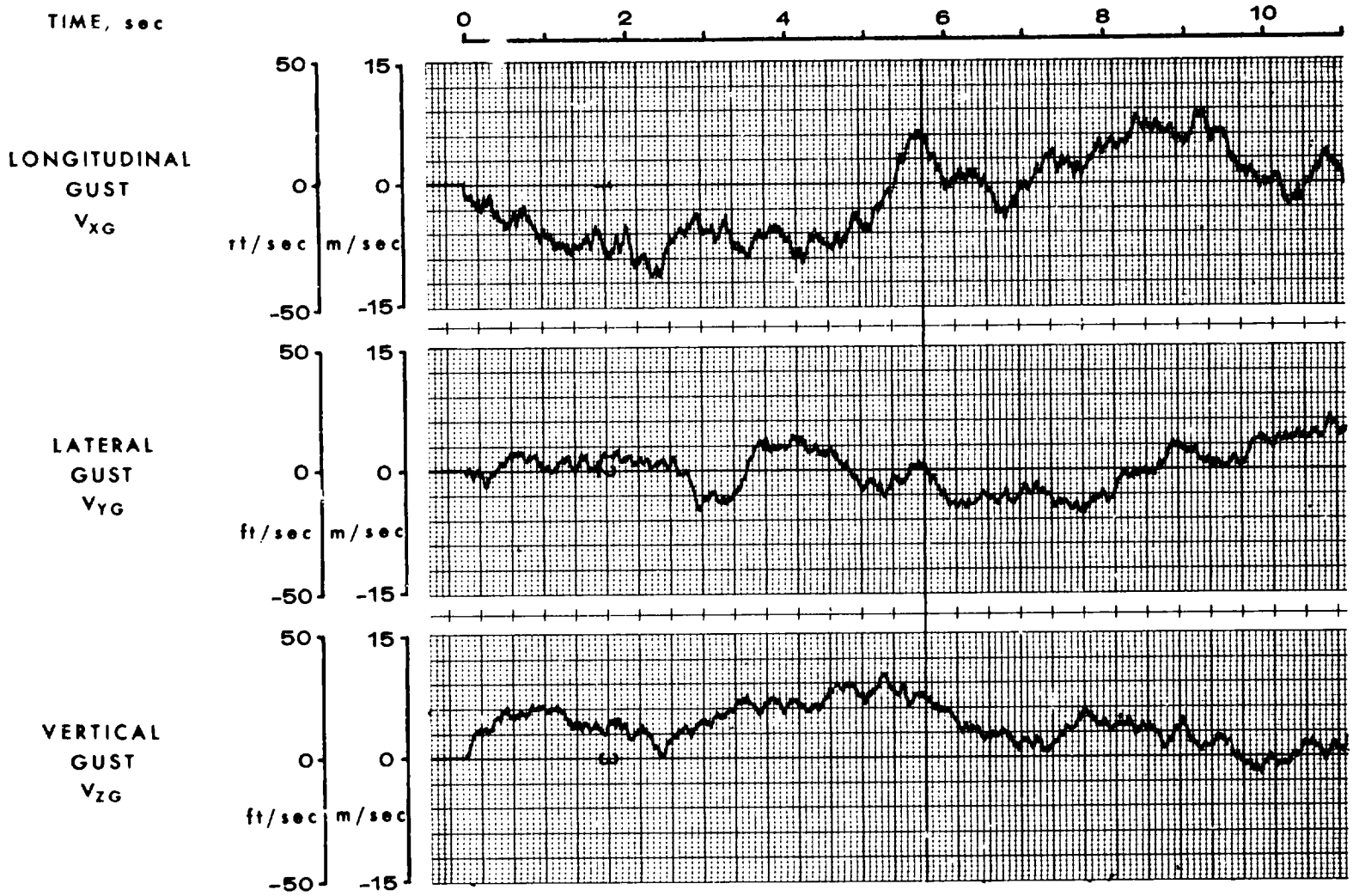

Figure 5.2 Modeled Gust Components Along Body Axis Direction Used to Disturb the BLACK HAWK During the Nonlinear Analysis.

5.2 LQR Controller for Linearized Helicopter Model

Mathematical Formulation - The helicopter and gust dynamical equations are

$$\dot{x} = ax + bu + c\omega \tag{5.1}$$

$$\dot{\omega} = a_g\omega + c_gW \tag{5.2}$$

where

x	=	15x1	helicopter state vector
U	=	4x1	control vector
ω	=	3x1	gust vector
W	=	3x1	independent white driving noise vector
a	=	15x15	helicopter dynamical matrix
b	=	15x4	control coupling matrix
c	=	15x3	gust coupling matrix
a_g	=	3x3	gust dynamical matrix
c_g	=	3x3	driving noise coupling matrix

Defining

$$x = \begin{bmatrix} x \\ \omega \end{bmatrix} \quad A = \begin{bmatrix} a & c \\ o & a_g \end{bmatrix} \quad B = \begin{bmatrix} b \\ o \end{bmatrix} \quad C = \begin{bmatrix} o \\ c_g \end{bmatrix} \tag{5.3}$$

the augmented dynamical system becomes

$$\dot{x} = Ax + Bu + Cw \tag{5.4}$$

X	=	13x1	augmented state vector
A	=	18x18	augmented dynamical matrix
B	=	18x4	augmented control coupling matrix
C	=	18x3	augmented driving noise coupling matrix

The continuous time output regulator problem is to determine

$$u(t) = -F_cX(t) \tag{5.5}$$

which minimizes,

$$J = \lim_{T \to \infty} \int_o^T \left[Y'(t)Q_yY(t) + U'(t)R_cU(t) \right] dt \tag{5.6}$$

where

$$Y = H_yX \tag{5.7}$$

Y	=	1x1	minimized variable vector
H_y	=	1x18	transformation matrix
Q_y	=	3x3	positive semidefinite output weighting matrix
R_c	=	4x4	positive definite control weighting matrix

In this case, the vector to be minimized is the state vector, and H_y is an identity matrix. In general, however, Eq. (5.6) can be transformed into a state regulator problem by defining,

$$Q_c = H'_y Q_y H_y \tag{5.8}$$

the cost function becomes,

$$J = \lim_{T \to \infty} \int_o^T \left[X'(t) Q_c X(t) + U'(t) R_c U(t) \right] dt \tag{5.9}$$

For sampled-data control the continuous time augmented system and cost function given by Eqs. (5.4) and (5.9) are discretized using straight forward integration

$$X\left[(i+1)\Delta\right] = \tilde{A} X(i\Delta) + \tilde{B} U(i\Delta) \quad (X(0) = X_o) \tag{5.10}$$

and

$$J = \lim_{N \to \infty} \left\{ \sum_{i=o}^{N} \left[x'(i\Delta) \tilde{Q} X(i\Delta) + X'(i\Delta) \tilde{S} U(i\Delta) + U'(i\Delta) \tilde{R} U(i\Delta) \right] \right\} \tag{5.11}$$

where

$$\tilde{A} = e^{A\Delta} \qquad \tilde{S} = 2 \int_o^\Delta e^{A'\tau} Q_c G(\tau,o) d\tau$$

$$\tilde{B} = \int_o^\Delta e^{A\tau} d\tau \, B \qquad \tilde{R} = \int_o^\Delta \left[R_c + G'(\tau,o) Q_c G(\tau,o) \right] d\tau \tag{5.12}$$

$$\tilde{Q} = \int_o^\Delta e^{A'\tau} Q_c e^{A\tau} d\tau \qquad G(t,o) = \int_o^t e^{A\tau} d\tau \, B$$

The white driving noise vector is not a factor in the controller design and is therefore omitted in Eq. (5.10).

The cross term in Eq. (5.11) is eliminated by the control variable transformation,

$$U(i\Delta) = -\tilde{F} X(i\Delta) + \tilde{U}(i\Delta) \tag{5.13}$$

with

$$\tilde{F} = \tilde{R}^{-1} \frac{\tilde{S}'}{2} \tag{5.14}$$

The transformed state equation and cost function become,

$$X\left[(i+1)\Delta\right] = \hat{A} X(i\Delta) + \tilde{\tilde{B}} U(i\Delta) \tag{5.15}$$

$$J = \lim_{N \to \infty} \left\{ \sum_{i=o}^{N} \left[X'(i\Delta) \hat{Q} X(i\Delta) + \tilde{U}'(i\Delta) \hat{R} U(i\Delta) \right] \right\} \tag{5.16}$$

where $\hat{A} = \tilde{A} - \tilde{\tilde{B}}F \quad \hat{B} = \tilde{B} \quad \hat{Q} = \tilde{Q} - \frac{\tilde{\tilde{S}}F}{2} \quad \hat{R} = \tilde{R}$ (5.17)

the sampled-data problem is thus reduced to the discrete time regulator problem of minimizing,

$$\lim_{N \to \infty} \sum_{i=o}^{n} \left[X'(i+1)\hat{Q}X(i+1) + \tilde{U}'(i)\hat{R}\tilde{U}(i) \right] \tag{5.18}$$

subject to $X(i+1) = \hat{A}X(i) + \hat{B}\tilde{U}(i) \qquad (X(0) = X_0)$ (5.19)

Where the Δ notation has been omitted for clarity.

The solution is given by

$$\tilde{U}(i) = -\hat{F}X(i) \tag{5.20}$$

From Eqs. (5.14) and (5.20) the total gain is

$$F_C = \tilde{F} + \hat{F} \tag{5.21}$$

A solution for $\hat{F}$ exists if the pair $[\hat{A}, \hat{B}]$ is stabilizable and $[\hat{A}, \hat{D}]$, with $D'D = \hat{Q}$, is detectable. The solution is given by

$$\hat{F} = (\hat{R} + \hat{B}'P\hat{B})^{-1}\hat{B}'P\hat{A} \tag{5.22}$$

$$P = \Phi'P\Phi + \hat{F}'\hat{R}\hat{F} + \hat{Q} \tag{5.23}$$

$$\Phi = \hat{A} - \hat{B}\hat{F} \tag{5.24}$$

The full state vector required in the feedback law of Eq. (5.5) is not directly available. Hence, the state must be estimated from the incomplete, noisy measurement vector. Moreover, due to the accumulated time delays of the numerical computations a state variable predictor must be used.

The discrete time equivalent of Eq. (5.4), including the white driving noise, is

$$X(i+1) = \tilde{A}X(i) + \tilde{B}U(i) + W(i) \tag{5.25}$$

where W is a white noise sequence having a covariance that will produce the same output variance for X(i+1) as the continuous unit variance white noise function W produced on x(t). That is,

$$E\left\{ W(i)W'(i) \right\} = Q_F$$

where $$Q_F = \int_0^{\Delta AT} e \quad C \quad C' \, e^{A'T} \, dT \tag{5.26}$$

The measurement equation is

$$Z(i) = H_Z X(i) + V(i) \tag{5.27}$$

where

$$E\left\{V(i)V'(i)\right\} = R_F \tag{5.28}$$

The optimal predictor minimizes the expected value of the estimation error

$$\lim_{i_o \to -\infty} E\left\{e'(i)\, Ee(i)\right\} \tag{5.29}$$

where

$$e(i) = X(i) - \hat{X}(i) \tag{5.30}$$

and, i_o = initial value of i.

The solution to the optimal predictor exists if $[A', H_Z']$ is stabilizable and $[A', D']$, with $DD' = Q_F$, is detectable. The solution is

$$\hat{X}(i+1) = \tilde{A}\hat{X}(i) + \tilde{B}U(i) + F_F\left[Z(i) - H_Z\hat{X}(i)\right] \tag{5.31}$$

where $\hat{X}$ = 18x1 state estimate vector and the initial condition is

$$\hat{X}(i_o) = E\left\{X(i_o)\right\} \tag{5.32}$$

The gain F_F is found by solving the asymptotic discrete Riccati equation,

$$F_F = \tilde{A}PH'_Z(R_F + H_Z PH'_Z)^{-1} \tag{5.33}$$

$$P = \Phi P \Phi' + F_F R_F F'_F + Q_F \tag{5.34}$$

$$\Phi = \tilde{A} - F_F H_Z \tag{5.35}$$

The matrix $P = P' \geq 0$ represents the steady-state variance matrix of the error e(i).

The separation principle for linear quadratic gaussian systems allows the calculations of feedback gains and predictor gains to be done independently. The complete closed loop stochastic regulator is shown in Figure 5.3.

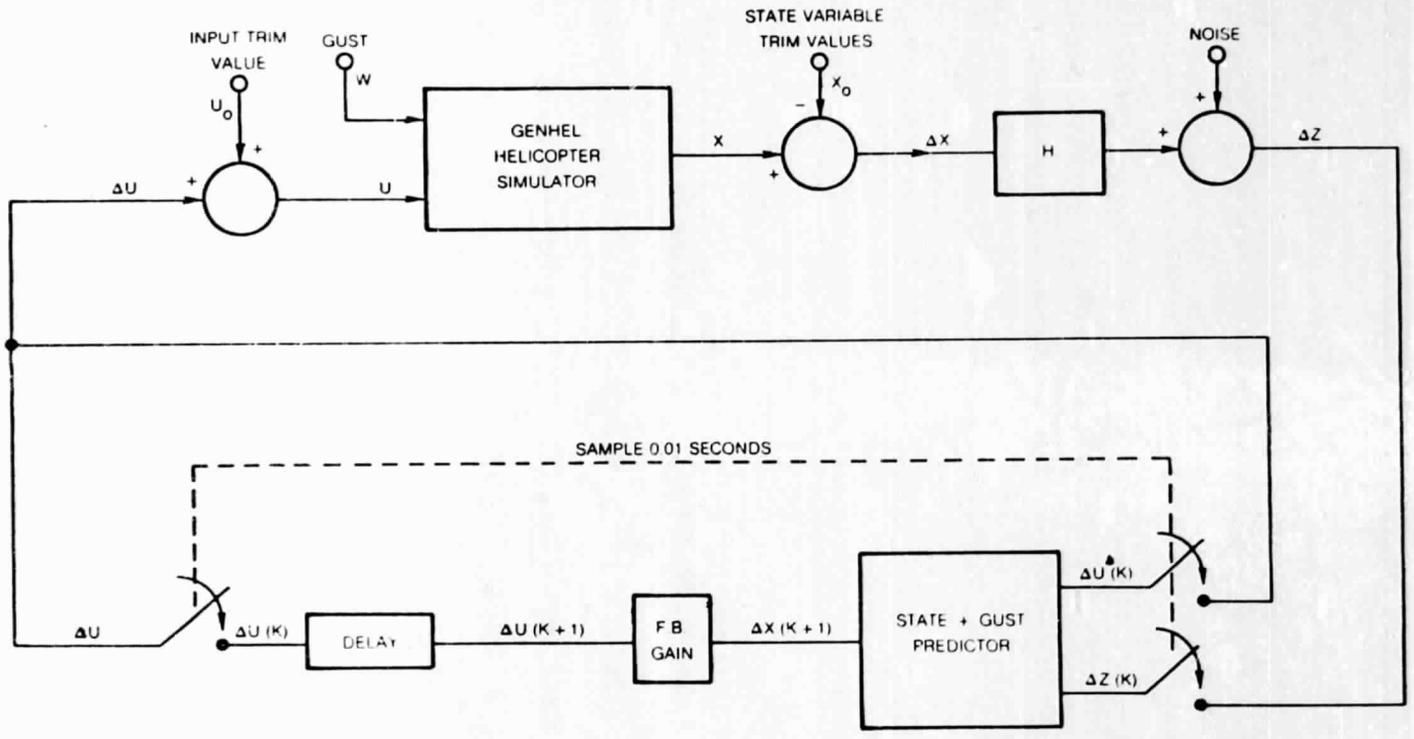

Figure 5.3 Gust Alleviation Controller.

The closed loop system consists of the fifteenth order linearized helicopter dynamics, a .01 second sampler, an 18x7 state variable predictor, a 4x18 state feedback gain matrix and a control input hold. The helicopter dynamics are driven by three orthogonal time correlated gust inputs.

The measurement system consists of noisy measurements of the body attitudes, angular rates, coning angle and coning rate. Measurement errors are 0.2 deg (deg/sec) for body attitudes (rates) and 0.5 deg (deg/sec) for coning angle (rate).

Results - The sample data controller gains and the predictor gains are given in Table 5.4. The discrete time closed loop eigenvalues are listed in Table 5.5. Both the controller eigenvalues and the predictor eigenvalues are within the unit circle, thus indicating stability.

The closed loop system of Figure 5.3 was simulated on the UNIVAC 1110 computer for 1000 samples, giving a total run time of 10 seconds. The full state feedback (including gust feedback) response of the fifteen helicopter state variables for the 150 knot case is shown in Figures 5.4 and 5.5. Good regulation is achieved in all the response modes. Other simulated gust disturbances produced comparable results. Figure 5.6 compares the pitch angle response for the open-loop, no-gust-feedback and full feedback conditions. The rms response is 7^{o}, 2^{o}, and 0.8^{o}, respectively, indicating increasingly improved response. Although the no-gust-feedback controller is an effective regulator, the addition of gust feedback provides an additional 50% reduction in gust sensitivity. A possible disadvantage of gust feedback is the noisier response of the state variables as can be seen in Figure 5.6. Table 5.6 shows that nearly all the body state variables benefit from gust feedback. It is also seen, from Table 5.6, that the rotor state variables are more active when gust feedback is used. This is a direct result of the controller attempting to minimize the gust effects on the helicopter body by varying the rotor pitch.

For this simulation run, the unrestricted rotor control inputs, shown in Figure 5.7 exceed the authority limits of the controller. The rms values of these inputs are approximately 2.5, 1.3, 3.0 and 4.0 degrees respectively for collective, lateral cyclic, longitudinal cyclic and tail rotor pitch. Clamping the inputs at their design limits resulted in increased gust sensitivity on the body state variables as compared to Figure 5.4. Moreover the nonlinear clamping action, although necessary as a last restort, destroys the "optimality" of the controller. The proper method of reducing the control input is to adjust the quadratic weighting matrices in Eq. (5.6). Many choices of weighting matrices were evaluated, and a number of combinations were successful in keeping the input responses within their authority limits. Of course, the penalty for the decreased input was increased gust sensitivity. The original quadratic weights which gave the response shown in Figure 5.4 were judged acceptable, despite the excessive

Table 5.4-A: Feedback Gains

150 Knots

	ϕ	θ	V_x	V_y	V_z	ρ	q	r	a_{0f}	a_{1f}	b_{1f}	$\dot{a}_f$	$\dot{a}_{1f}$	$\dot{b}_{1f}$	λ	W_x	W_y	W_z
B_{1s}	1.2-01	-4.9-01	1.7-01	8.3-01	-9.5-02	2.4-01	-9.7-01	-3.3-01	-1.9-01	9.3-01	-8.9-01	-7.3-03	-4.7-03	-1.3-02	-4.2-01	1.4-02	9.6-02	1.4-01
A_{1s}	1.2-01	1.5-01	-8.2-02	-2.0-01	1.2-02	1.3-01	3.9-01	8.7-01	3.0-01	-5.0-01	-8.6-01	1.6-02	-1.3-02	3.6-03	3.6-01	-3.4-02	-4.9-02	-6.8-02
θ_0	-7.2-02	1.9-01	-1.2-02	-1.6-01	-8.4-01	-7.6-02	3.7-03	8.6-01	1.3-01	-8.4-01	-1.1-01	1.4-02	-7.3-04	8.4-03	8.6-01	-1.5-02	1.2-03	7.3-03
θ_{tr}	2.4-01	1.3+00	-2.2-01	4.3-01	-4.3-02	6.4-02	1.8+00	-6.8-01	3.3-01	-7.7-01	-3.3-01	1.3-02	-4.4-03	7.8-03	-1.6-01	2.2-02	-1.6-01	-7.2-04
	80 Knots																	
B_{1s}	1.1-01	-9.0-01	1.7-01	-1.4-01	-1.1-01	1.5-01	-1.5+00	1.2-01	-5.1-01	1.1+00	-4.5-01	-1.1-02	-2.8-03	-1.8-02	-4.5-02	-1.5-01	-6.3-02	8.2-02
A_{1s}	1.3-01	2.5-01	-1.2-01	-2.0-02	1.2-03	1.5-01	4.0-01	5.5-02	2.9-01	-4.8-01	-8.3-01	6.6-03	-1.3-02	4.1-03	5.1-02	-1.3-02	-1.2-03	-2.9-02
θ_0	-5.5-02	2.9-01	-5.9-02	-9.1-02	-3.1-01	-3.6-02	3.8-01	1.1-01	3.5-01	-3.3-01	-8.2-02	1.1-02	-2.2-03	4.8-03	3.3-02	1.4-02	2.4-02	2.9-02
θ_{tr}	2.9-01	-4.4-02	2.7-02	7.1-01	-7.9-02	1.8-01	-3.1-02	-8.5-01	-1.1-01	-1.3-01	-3.3-01	7.8-03	-4.4-03	-4.0-04	-1.4-01	-2.0-02	-9.9-02	9.8-02
	Hover																	
I_{1s}	3.1-01	-8.4-01	8.3-01	3.1-01	-8.7-02	8.2-01	-1.4+00	2.8-01	-2.0-01	7.6-01	-9.1-01	-1.3-02	-7.1-03	-3.8-02	4.9-02	-1.4-02	2.0-02	-6.9-02
A_{1s}	2.6-01	1.7-01	-1.2-01	1.8-01	5.1-02	1.5-01	5.5-01	-3.4-03	8.9-02	-5.8-01	-8.0-01	4.8-03	-2.4-02	1.9-02	2.8-03	-1.1-02	-4.4-02	1.1-02
θ_0	-1.3-02	2.5-01	-8.9-02	5.8-03	-3.6-01	-1.3-02	3.9-01	1.2-01	2.3-01	-2.1-01	4.8-02	1.0-02	-2.8-03	4.9-03	-2.0-02	-4.9-04	1.4-03	3.8-02
θ_{tr}	1.7-01	-8.4-01	3.0-01	1.6-01	-2.3-01	1.4-01	-9.9-01	-5.3-01	-5.0-01	2.6-01	-4.5-01	7.5-03	-3.3-03	-1.1-02	-3.1-02	-3.1-02	-4.1-02	5.0-02

Table 5.4-B: Predictor Gains

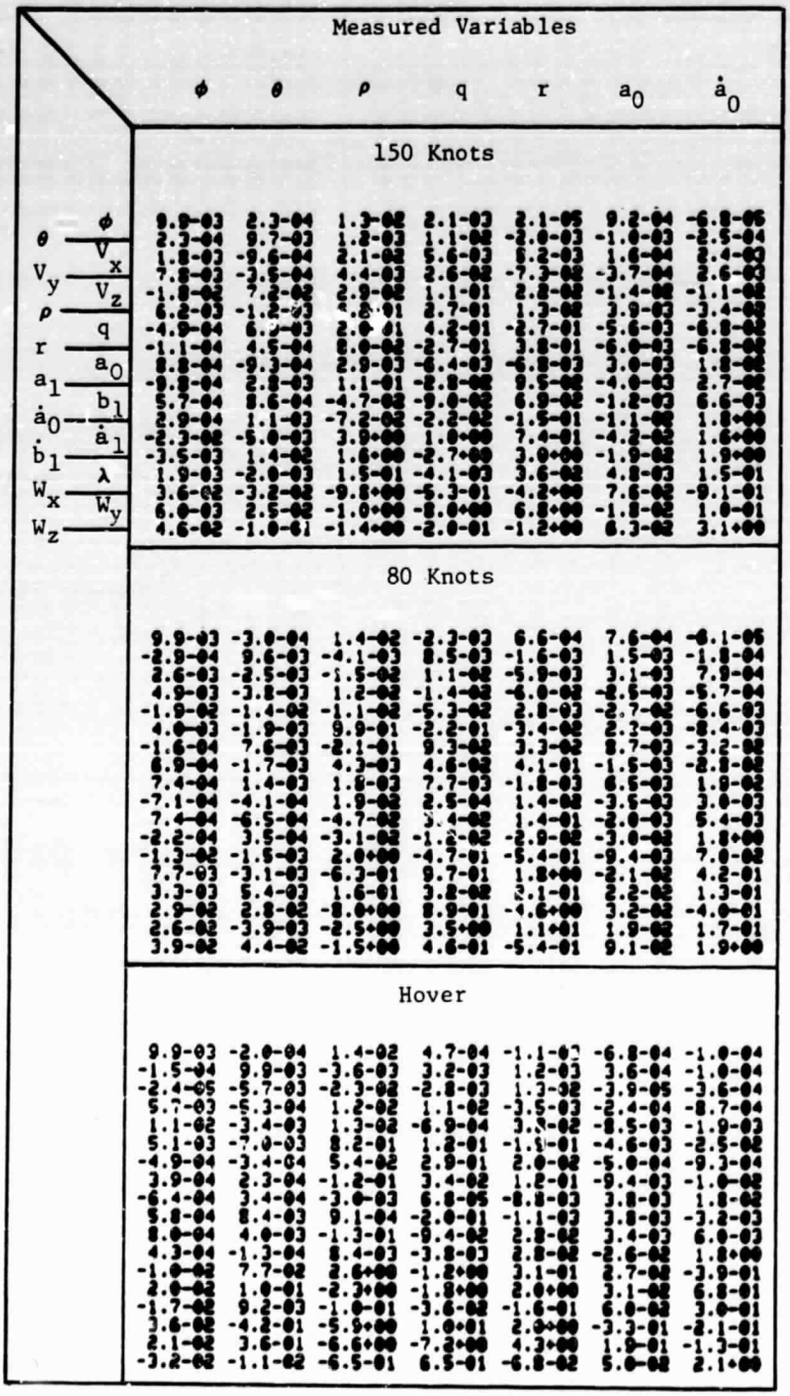

Table 5.5 Closed Loop Discrete Time Eigenvalues

	150 Knots	80 Knots	Hover
Controller Eigenvalues	7.804-01 0.000	7.999-01 0.000	8.256-01 9.054-02
	7.909-01 1.207-01	8.168-01 1.281-01	8.256-01 -9.054-02
	7.909-01 -1.207-01	8.168-01 -1.281-01	8.397-01 0.000
	8.560-01 1.047-01	5.623-01 6.634-01	7.136-01 4.510-01
	8.560-01 -1.047-01	5.623-01 -6.634-01	7.136-01 -4.510-01
	8.788-01 2.510-01	8.703-01 1.107-01	8.780-01 1.033-01
	8.788-01 -2.510-01	8.703-01 -1.107-01	8.780-01 -1.033-01
	4.395-01 8.155-01	8.449-01 2.430-01	8.622-01 2.418-01
	4.395-01 -8.155-01	8.449-01 -2.430-01	8.622-01 -2.418-01
	9.533-01 2.870-02	9.671-01 1.358-02	9.490-01 0.000
	9.533-01 -2.870-02	9.671-01 -1.358-02	9.831-01 0.000
	9.841-01 0.000	9.793-01 0.000	9.872-01 0.000
	9.872-01 0.000	9.872-01 0.000	9.872-01 0.000
	9.872-01 0.000	9.872-01 0.000	9.872-01 0.000
	9.872-01 0.000	9.872-01 0.000	9.935-01 5.029-03
	9.935-01 0.000	9.935-01 0.000	9.935-01 -5.029-03
	9.977-01 2.041-03	9.975-01 2.304-03	9.975-01 2.205-03
	9.977-01 -2.041-03	9.975-01 -2.304-03	9.975-01 -2.205-03
Predictor Eigenvalues	-2.570-02 2.029-01	-1.005-01 3.125-02	-9.447-02 6.251-02
	-2.570-02 -2.029-01	-1.005-01 -3.125-02	-9.447-02 -6.251-02
	6.266-01 2.766-01	4.948-01 3.029-01	6.691-01 2.216-01
	6.266-01 -2.766-01	4.948-01 -3.029-01	6.691-01 -2.216-01
	7.301-01 1.676-01	7.725-01 1.735-01	7.761-01 1.686-02
	7.301-01 -1.676-01	7.725-01 -1.735-01	7.761-01 -1.686-02
	7.613-01 1.134-01	8.583-01 5.492-02	6.963-01 4.854-01
	7.613-01 -1.134-01	8.583-01 -5.492-02	6.963-01 -4.854-01
	9.150-01 0.000	5.871-01 6.721-01	8.794-01 1.404-01
	4.905-01 7.788-01	5.871-01 -6.721-01	8.794-01 -1.404-01
	4.905-01 -7.788-01	9.183-01 0.000	9.519-01 0.000
	9.610-01 2.466-02	9.596-01 1.849-02	9.738-01 2.141-02
	9.610-01 -2.466-02	9.596-01 -1.849-02	9.738-01 -2.141-02
	9.901-01 6.743-05	9.899-01 0.000	9.899-01 0.000
	9.901-01 -6.743-05	9.901-01 0.000	9.903-01 0.000
	1.000+00 0.000	9.998-01 0.000	1.000+00 0.000
	1.000+00 0.000	1.000+00 0.000	1.000+00 0.000
	1.000+00 0.000	1.000+00 0.000	1.000+00 0.000

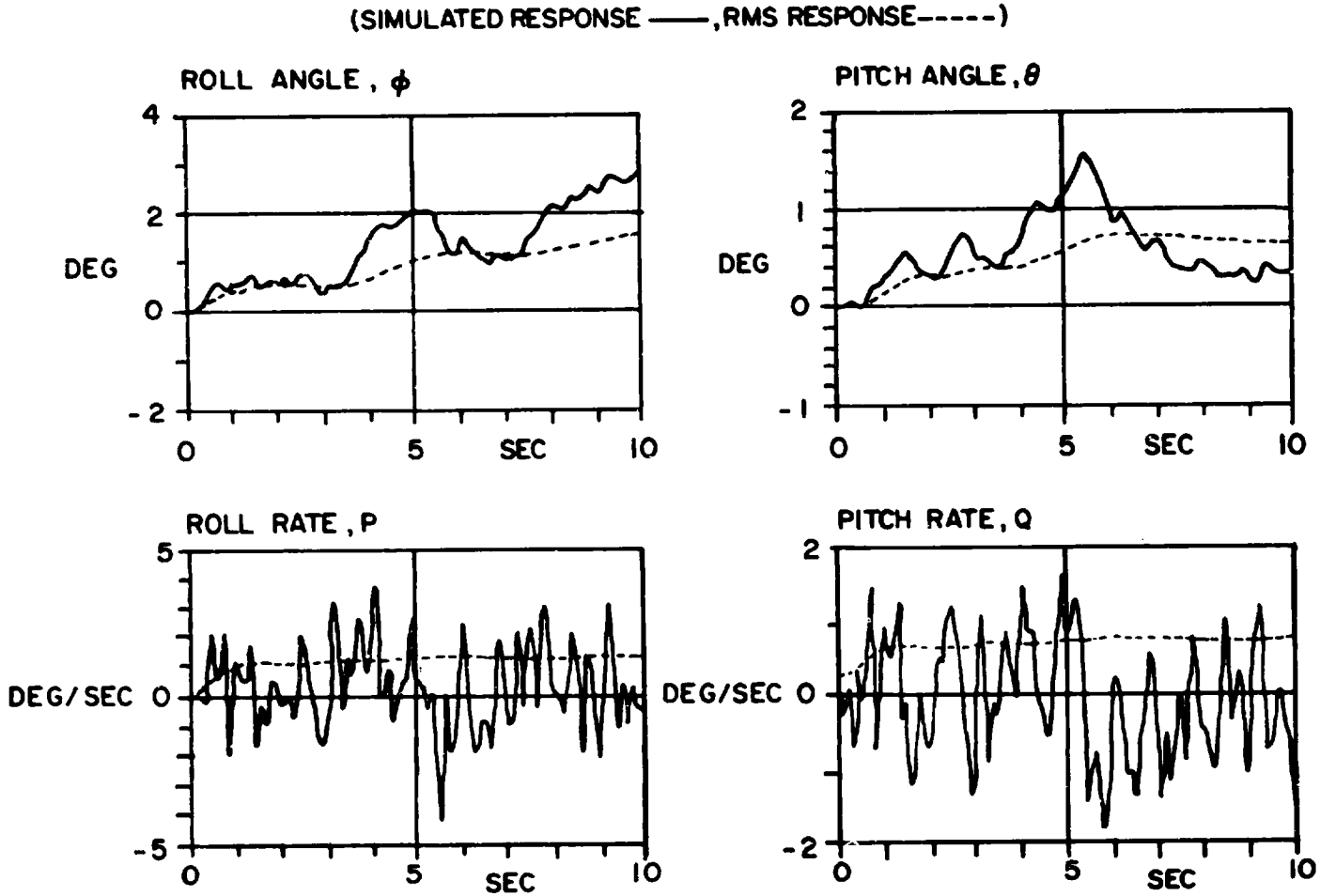

Figure 5.4 Closed Loop Helicopter Response at 150 Knots - Pitch and Roll.

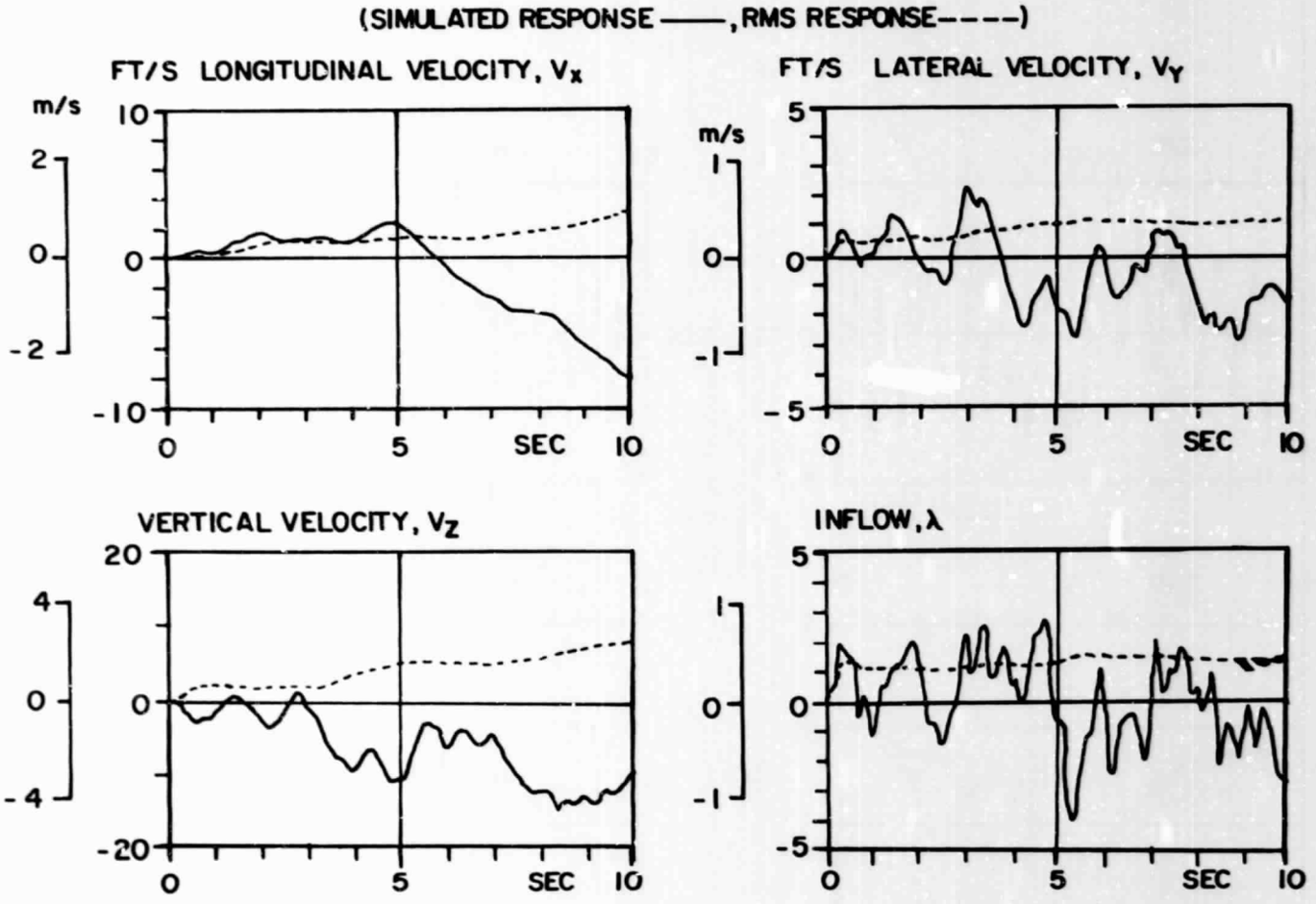

Figure 5.5 Closed Loop Helicopter Response at 150 Knots - Velocities and Inflow.

(SIMULATED RESPONSE ——, RMS RESPONSE - - - -)

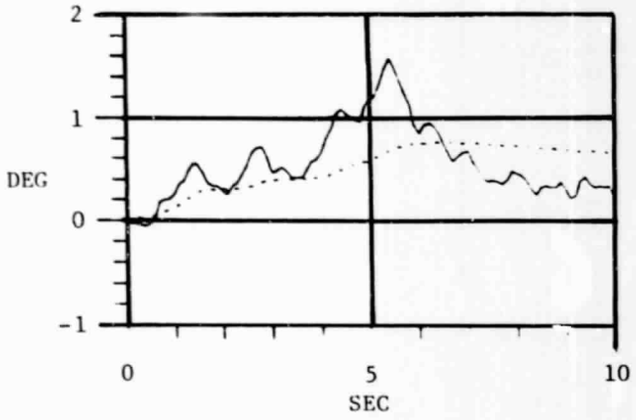

a) FULL STATE FEEDBACK

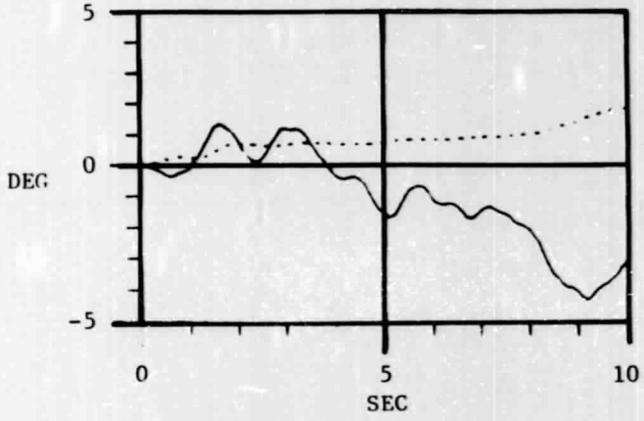

b) NO-GUST FEEDBACK

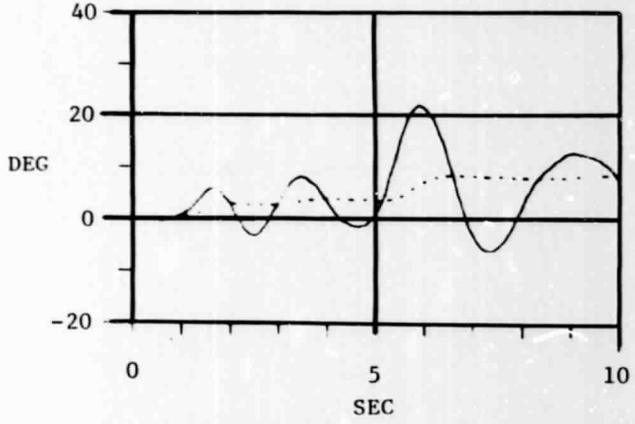

c) OPEN LOOP RESPONSE

Figure 5.6 Pitch Response at Gust With and Without Gust Feedback.

Table 5.6 RMS Gust Sensitivity of Helicopter at 150 Knot With and Without Gust Feedback

(deg, deg/sec, ft/sec)

Body Variable	Full-FB	No-Gust-FB	Open Loop
ϕ	1.2	2.0	13.0
θ	0.7	1.5	8.0
p	1.3	1.5	10.0
q	0.7	1.7	15.0
r	1.0	1.2	20.0
V_x	2.5	1.5	5.0
V_y	1.2	2.5	30.0
V_z	6.0	10.0	25.0
λ	1.5	1.5	2.5
Rotor Variable			
a_{0f}	0.6	0.7	1.0
a_{1f}	2.0	1.3	1.2
b_{1f}	0.4	0.4	0.4
$\dot{a}_{0f}$	8.0	5.0	7.0
$\dot{a}_{1f}$	22.0	10.0	10.0
$\dot{b}_{1f}$	22.0	8.0	8.0

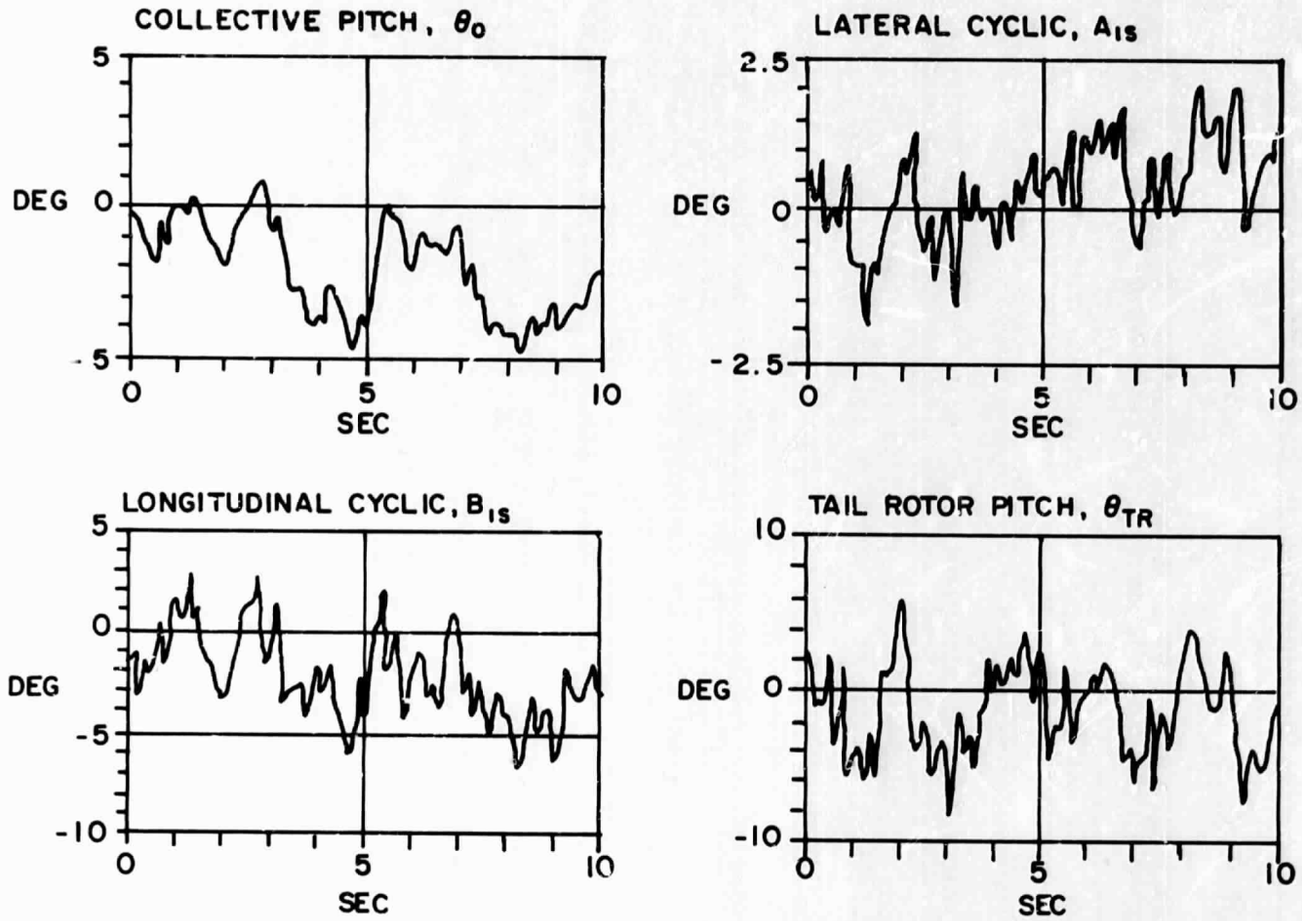

Figure 5.7 Control Input Response at 150 Knots.

inputs, for the following reasons: (1) The 80 knot and hover conditions gave considerably better (smaller) control inputs for the same gust disturbance, as shown in Table 5.7; (2) The simulated gust magnitude is a worst case condition; and (3) The high frequency content of the simulated gust appears to be unduly pronounced, possibly caused by the digital similation of the gust disturbance.

The effectivenss of the one-step-ahead predictor in estimating the gust disturbance is shown in Figure 5.8. The estimation error for all three components has a peak value of about 10 ft/sec or 20% of the peak gust magnitude. It was found that the gust estimation error increased substantially when the coning angle and coning rate measurements were removed.

The 80 knot and hover cases were simulated using their respective feedback and predictor gains. The results, given in Table 5.7, indicate that the sampled data controller is effective in alleviating the effects of gusts on the helicopter body at all three design speeds.

5.3 Gust Controller with Nonlinear Helicopter Model

The purpose of the nonlinear analysis was twofold. First was to evaluate the performance of the optimal LQR feedback scheme discussed in Section 5.2 when interface with the nonlinear GENHEL simulation. Second was to improve and simplify this design.

The Helicopter Flight Dynamics Model, GENHEL, is used to generate the flight characteristics of single rotor helicopters with specified geometric, aerodynamic, and mass properties. Trims and dynamic gust and control response characteristics of the helicopters can be studied in level flight, climb, autorotation, side-flight, rearward flight, and steady state maneuvers. Helicopter stability derivatives can also be generated. The program has been used extensively in the design of Sikorsky helicopters and compound helicopters. The helicopter is represented in this program by a main rotor, tail rotor, fuselage, tail surfaces, control system, and non-linear engine/fuel control simulation, acted on by a simulated gust model. Output forces and moments from each element are summed and used in the general equations of motion to determine the aircraft motion or trim about the standard aircraft axis system. A more detailed discussion of the math model is available in Reference (32).

Nonlinear Analysis - LQR Feedback - The LQR feedback was simulated both without limits and with the standard SAS limits. The addition of the limits had little affect on the system performance.

In general, all of the optimal schemes produced a significant degree of gust alleviation when compared with the basic aircraft with SAS. Figures 5.9, 5.10, and 5.11 compare the transient response of the "hingeless" BLACK HAWK with SAS and with a typical LQR feedback at hover, 41 m/s, and 77 m/s (hover, 80 kn, and 150 kn). In these and following figures

Table 5.7 RMS Gust Sensitivity at 150 Kn, 80 Kn and Hover

(Full-State Feedback)

Body Variable	150 Knot	80 Knot	Hover
ϕ	1.2	0.4	0.3
θ	0.7	0.3	0.5
ρ	1.3	1.0	1.5
q	0.7	0.5	0.3
r	1.0	1.0	1.2
V_x	2.5	0.7	1.0
V_y	1.2	1.0	0.4
V_z	6.0	4.0	2.0
λ	1.5	2.0	10.0
Rotor Variable			
a_{0f}	0.6	1.2	0.3
a_{1f}	2.0	2.0	0.5
b_{1f}	0.4	0.6	0.3
$\dot{a}_{0f}$	8.0	10.0	5.0
$\dot{a}_{1f}$	22.0	25.0	8.0
$\dot{b}_{1f}$	22.0	22.0	8.0

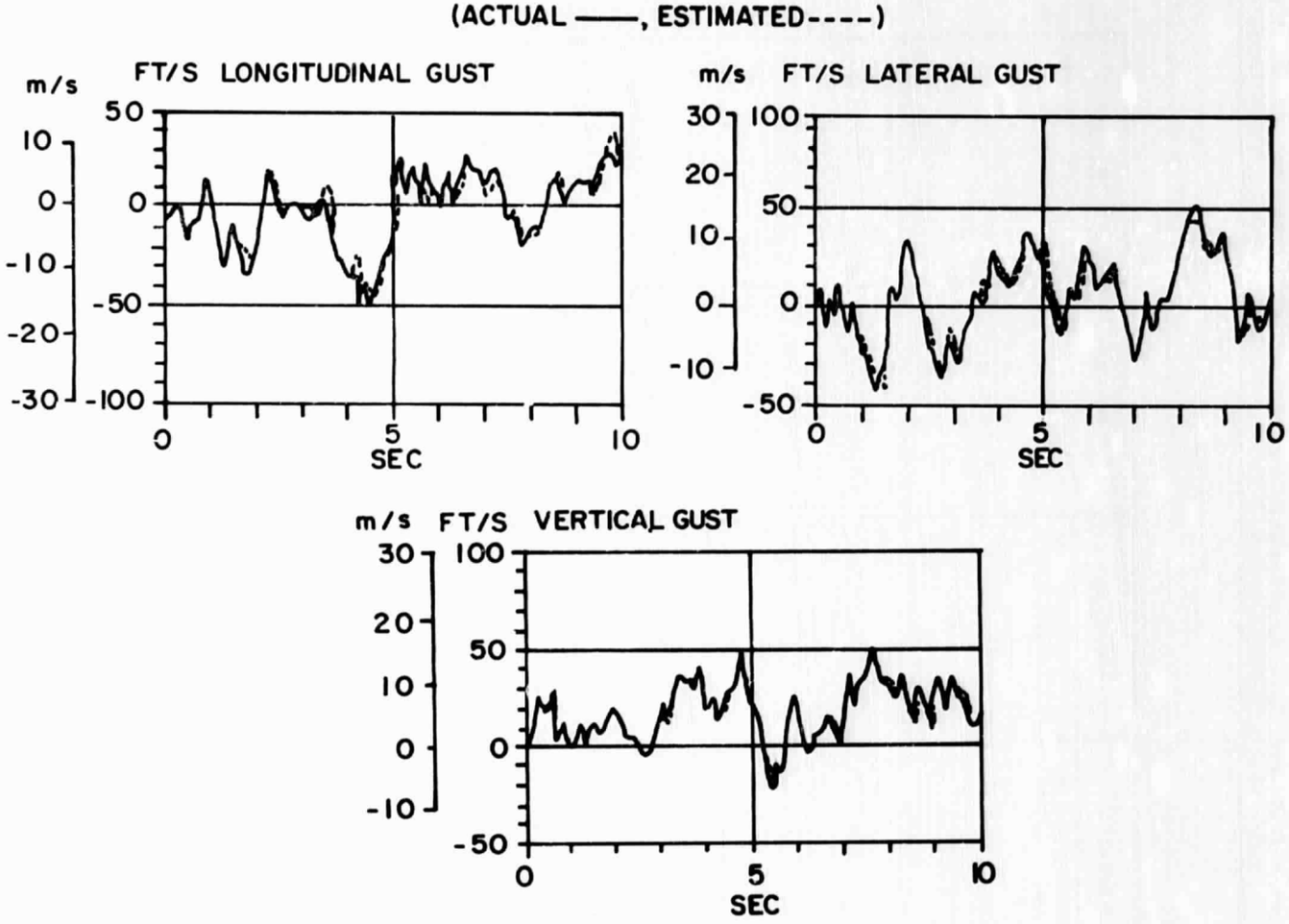

Figure 5.8 Gust Estimation Accuracy.

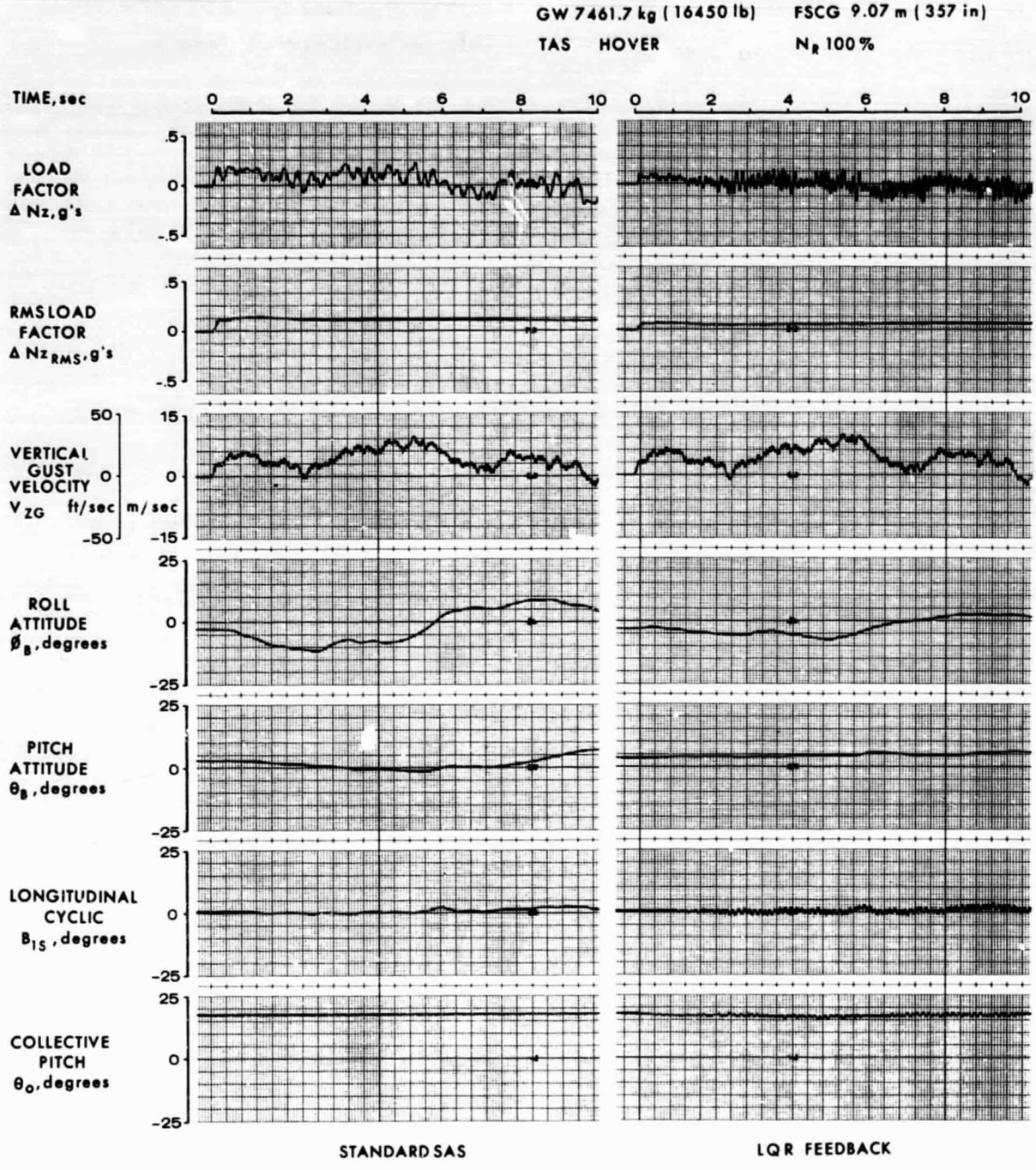

Figure 5.9 Time History Responses of the Simulated 'Hingeless" BLACK HAWK with Standard SAS and LQR Feedback at Hover; Standard Gross Weight, 100% N_R.

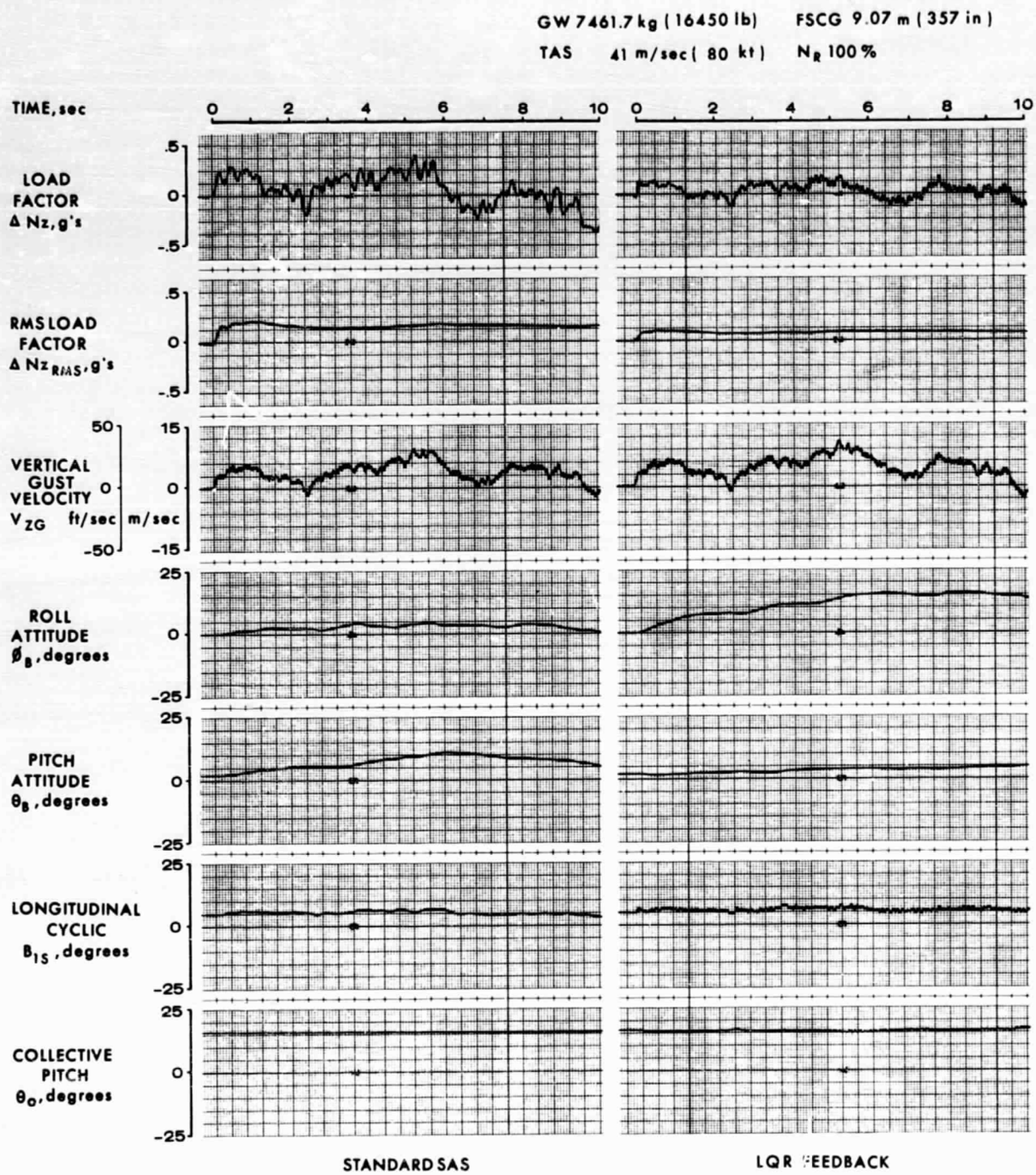

Figure 5.10 Time History Responses of the Simulated 'Hingeless' BLACK HAWK with Standard SAS and LQR Feedback at 41 m/s (80 Knots); Standard Gross Weight, 100% N_R.

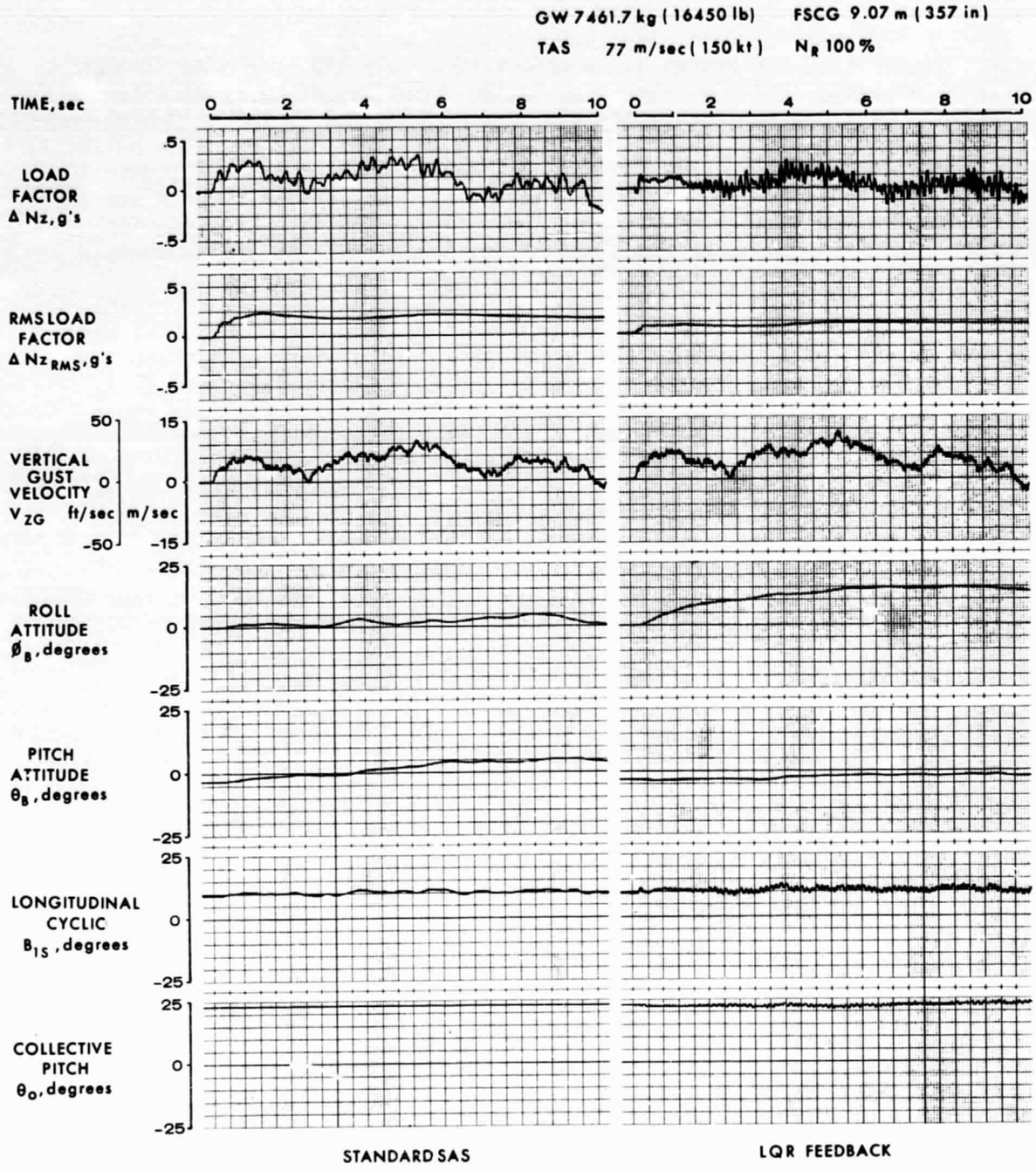

Figure 5.11 Time History Responses of the Simulated 'Hingeless' BLACK HAWK with Standard SAS and LQR Feedback at 77 m/s (150 Knots); Standard Gross Weight, 100% N_R.

showing time history data, ΔN_Z represents the change in aircraft normal load factor from the steady 1.0 g trim value. ΔN_Z RMS is the continuous root-mean-square value of ΔN_Z. V_{ZG} is the component of gust velocity transformed along the helicopter body z-direction and is shown to give some indication of what the gust is doing during the time history. The helicopter roll and pitch attitudes ϕ_B and θ_B are shown as well as the longitudinal cyclic and collective pitch angles B_{1S} and θ_0. All of the figures use the response of the helicopter with the conventional SAS as a baseline for comparison. The transfer functions of the BLACK HAWK SAS are shown in Table 5.8.

At all three airspeeds the reduction in maximum rms load factor was approximately 50%. However, the reduction in the difference between maximum and minimum load factor response was, in general, not nearly as substantial. At both hover and high speed the reduction was only about 20%; at 41 m/s (80 kn) the reduction was 50%. Despite these apparent improvements in gust response, the large peak-to-peak excursions in load factor, small high-frequency oscillations in pitch and roll attitude and load factor, and deviations from trim in roll attitude and heading suggest that further improvement can be made.

Nonlinear Analysis - Suboptimal Controller - In this phase of the nonlinear analysis, a suboptimal controller was developed using the following guidelines:

1) Reduce the complexity of the gust alleviation system.

2) Maintain or improve the good handling qualities of the baseline aircraft.

3) Implement the feedback paths (load factor and angle of attack) which were not available in the linear analysis due to the limitations of the linear model.

4) Restrict the gust controller to operate within the authority and rate limits of the standard SAS.

The complexity of the gust controller was reduced considerably by eliminating those feedback paths that did not produce any noticeable degree of gust alleviation and also any feedback paths that coupled two axes; i.e., pitch attitude into yaw. Briczinski, as reported in Reference 19, spent considerable time with GENHEL evaluating the effects of specific gains on gust alleviation. His results were used to eliminate many of the feedback gains. From the original 72 feedbacks, only 8 were retained and of those, only coning angle and coning rate could not be measured directly by standard aircraft sensors. A Kalman Filter similar to the filter used in the Rotor State Feedback Study (Reference 18) was available in GENHEL to estimate these states from blade flapping data. The other states being fed back (pitch and roll attitude, pitch, roll and yaw rate, and vertical velocity) did not go through a Kalman filter but were used directly from the GENHEL simulation with no filtering.

Table 5.8 BLACK HAWK SAS Transfer Functions

	Rate	Lagged Rate	Washout
$\frac{B_{1S}}{q}$	$= \left[.425 + .150 * \frac{2.04}{2.04\ S + 1} \right]$		$\left[\frac{7\ S}{7S + 1} \right]$
$\frac{A_{1S}}{p}$	$= \left[-.065 - .032 * \frac{.996}{.996\ S + 1} \right]$		
$\frac{\theta_{TR}}{r}$	$= \left[.401 + .641 * \frac{1.05}{1.05\ S + 1} \right]$		$\left[\frac{2\ S}{2\ S + 1} \right]$

An autopilot type of feedback was implemented to stabilize the aircraft about its trim point. Synchronized pitch and roll attitude feedback provided the trim stabilization and pitch, roll and yaw rate feedback provided damping. Synchronized heading feedback was added in the yaw channel to improve the directional stability of the aircraft at and near hover. Vertical velocity into collective increased the vertical damping of the helicopter. The gains selected in pitch, roll and yaw are close to the values used in the BLACK HAWK autopilot system.

The feedback paths added to provide gust alleviation were fuselage angle of attack into pitch and load factor into collective. These new paths, combined with the coning and coning rate feedback paths, and the attitude and angular rate paths, constitute the suboptimal controller. To simulate the authority and rate limits of the standard BLACK HAWK SAS, the controller was limited to $\pm$ 10% authority and $\pm$ 100%/second rate.

Having established the basic form of the suboptimal controller, a large number of transient response runs were made to optimize the gain values of the controller. The gains values were iterated upon until the greatest degree of gust alleviation was achieved at 77 meters/second (150 knots). During the iteration process, gain values were kept within practical limits and their effect on the aircraft handling qualities was minimized. Following the optimization of the controller gains, the performance of the system was checked at 41 m/s (80 knots) and hover. With the exception of the angle of attack gain which was zeroed out in hover, the controller performed very well with fixed gains. The final gains for the suboptimal gust alleviation system are shown in Table 5.9.

Figures 5.12, 5.13 and 5.14 compare the transient response of the "hingeless" BLACK HAWK with SAS and with the suboptimal controller at hover, 41 m/s, and 77 m/s (hover, 80 kn, and 150 kn). The degree of gust alleviation experienced at each airspeed is plotted in Figures 5.15, 5.16, and 5.17. These charts also show the performance of the LQR feedback. At the two higher airspeeds, the gust response alleviation with the suboptimal controller was 70% or greater for either evaluation criterion. At hover the reduction in peak-to-peak load factor response was only about 50%, but the reduction in maximum RMS load factor was still about 70%.

The suboptimal controller was also evaluated for two alternate gross weights and a different rotor rpm, 5216.4 and 9162.7 Kg (11,500 and 20,200 lb) and 105% N_R. The transients in Figures 5.18, 5.19, and 5.20 show that the aircraft sensitivity to gusts changes with gross weight and rpm. However, the degree of gust alleviation is nearly constant, as shown in Figure 5.21.

Since the suboptimal gust controller was simulated with the same limits as the standard SAS, the effect of the system on the aircraft handling qualities should be minimal. The transients in Figure 5.22 show the response of the aircraft to 10%, one second control pulses in pitch, roll, and yaw with the standard SAS and with the suboptimal controller.

Table 5.9 Suboptimal Gust Suppression Feedback Scheme

$$B_{1S} = .60 * \Delta\theta + .30 * q + .50 * \Delta\alpha_f$$

$$A_{1S} = -.095 * \Delta\phi - .093 * p$$

$$\theta_0 = .202 * \Delta V_z + .20 * \Delta a_0 + .005 * \dot{a}_0 - 5.0 * \Delta n_z$$

$$\theta_{TR} = .50 * \Delta\Psi + .593 * r$$

All control are in degrees.

States are in degrees, degrees/second, and feet/second; except n_z in g's.

For ΔV_z in m/sec, gain is .062.

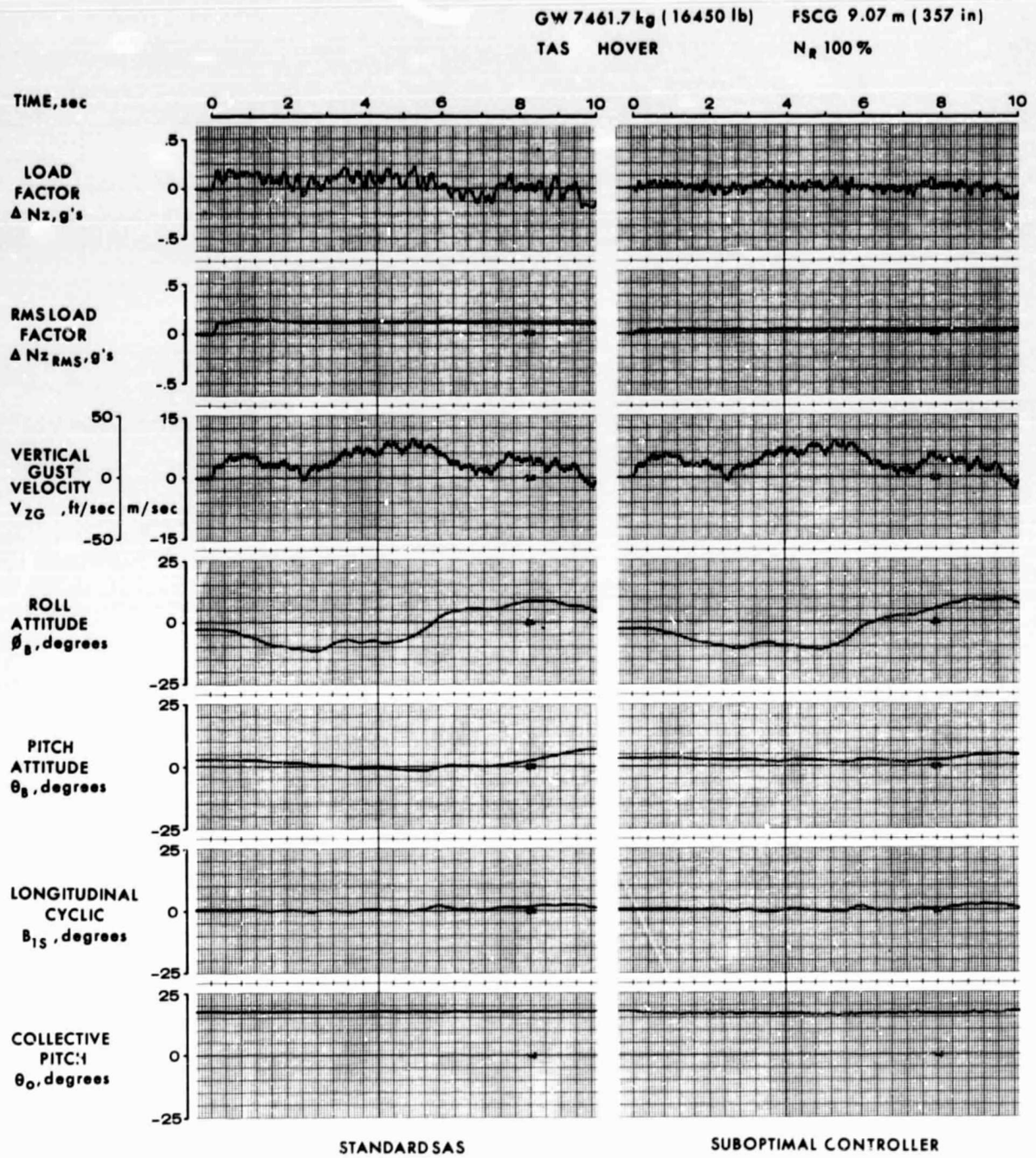

Figure 5.12 Time History Responses of the Simulated 'Hingeless' BLACK HAWK with Standard SAS and Suboptimal Controller at Hover; Standard Gross Weight, 100% N_R.

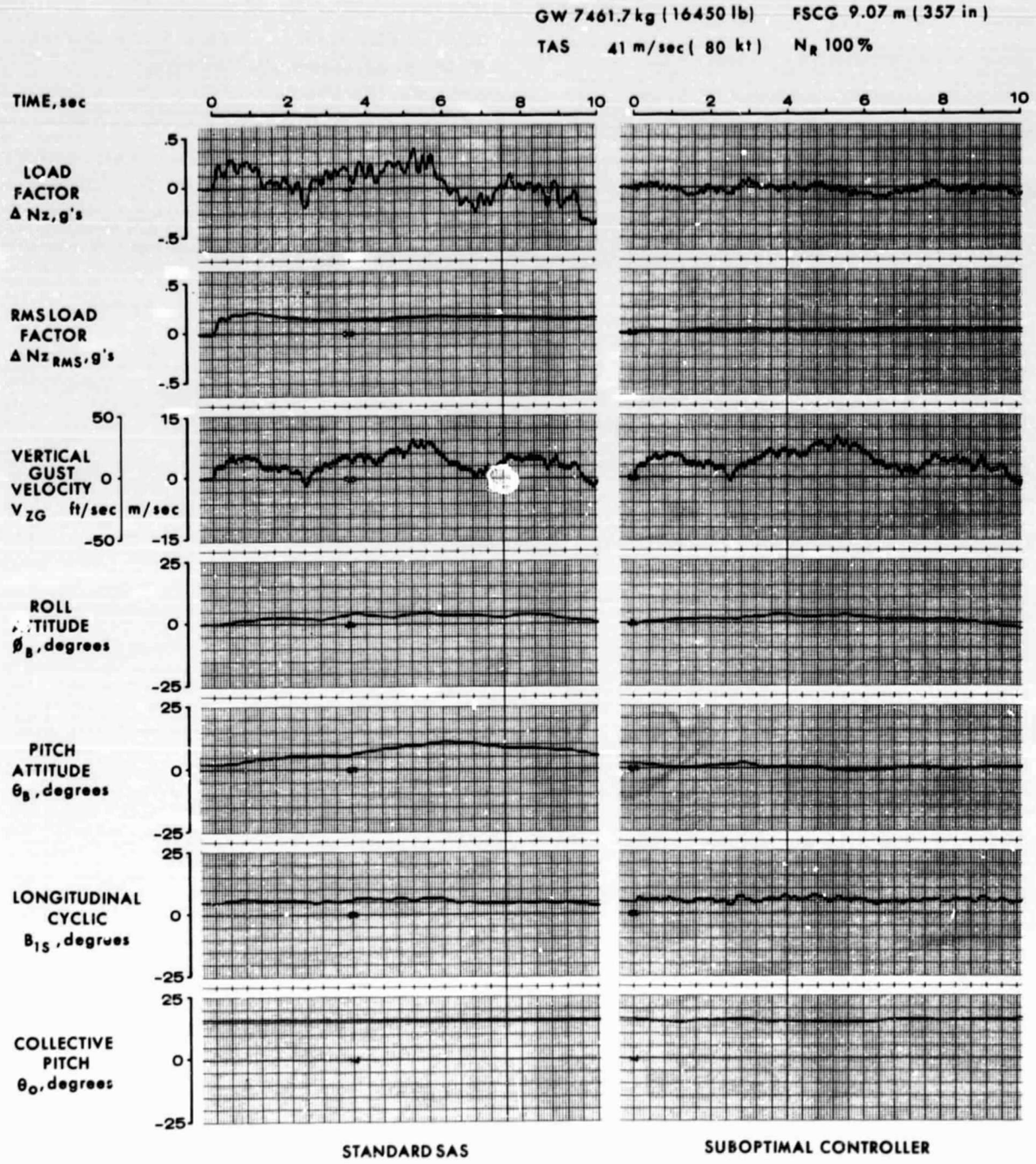

Figure 5.13 Time History Responses of the Simulated 'Hingeless' BLACK HAWK with Standard SAS and Suboptimal Controller at 41 m/s (80 Knots); Standard Gross Weight, 100% N_R.

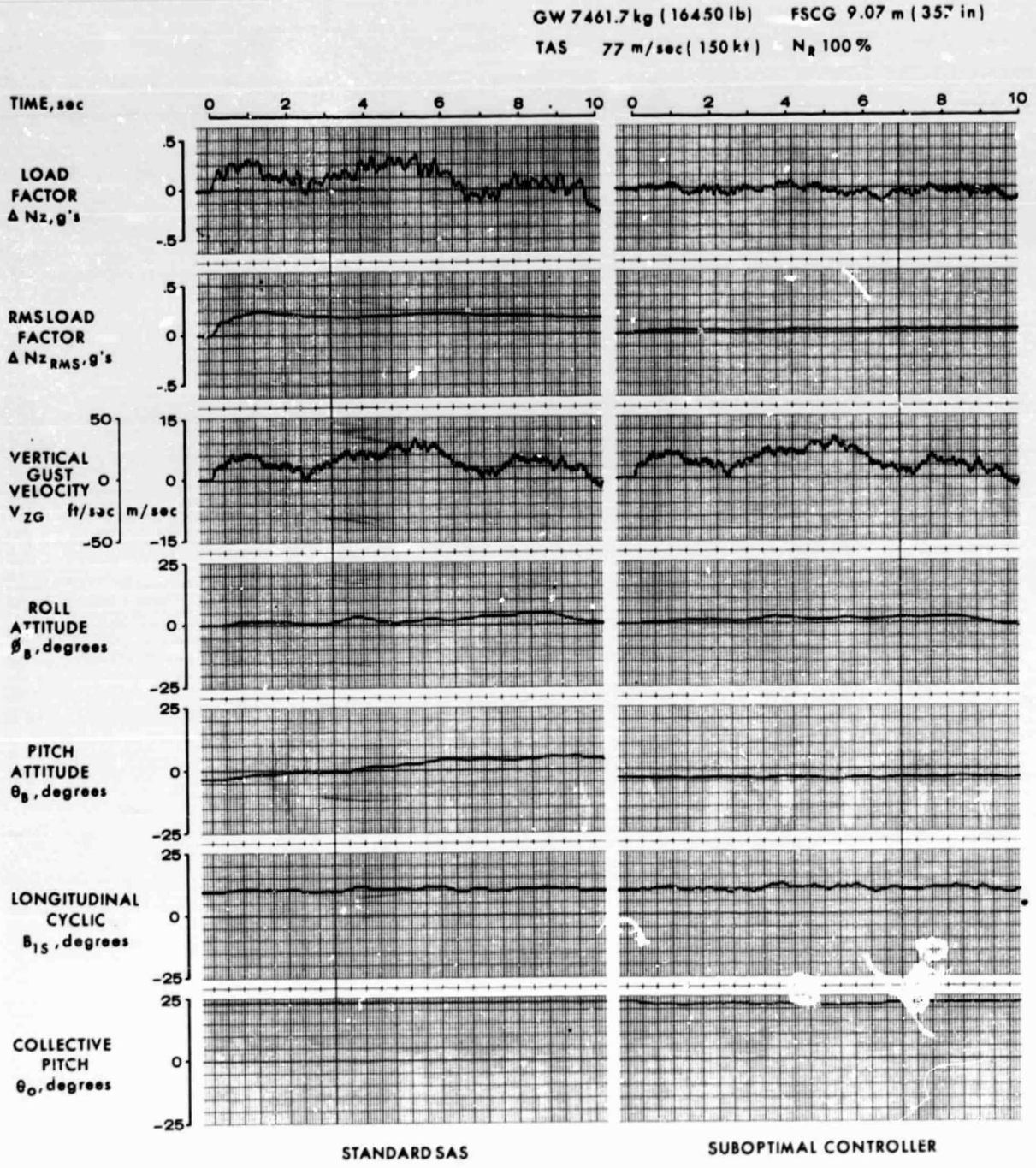

Figure 5.14 Time History Responses of the Simulated 'Hinge[illegible]' BLACK HAWK with Standard SAS and Suboptimal Controller at 77 m/s (150 Knots); Standard Gross Weight, 100% N_R.

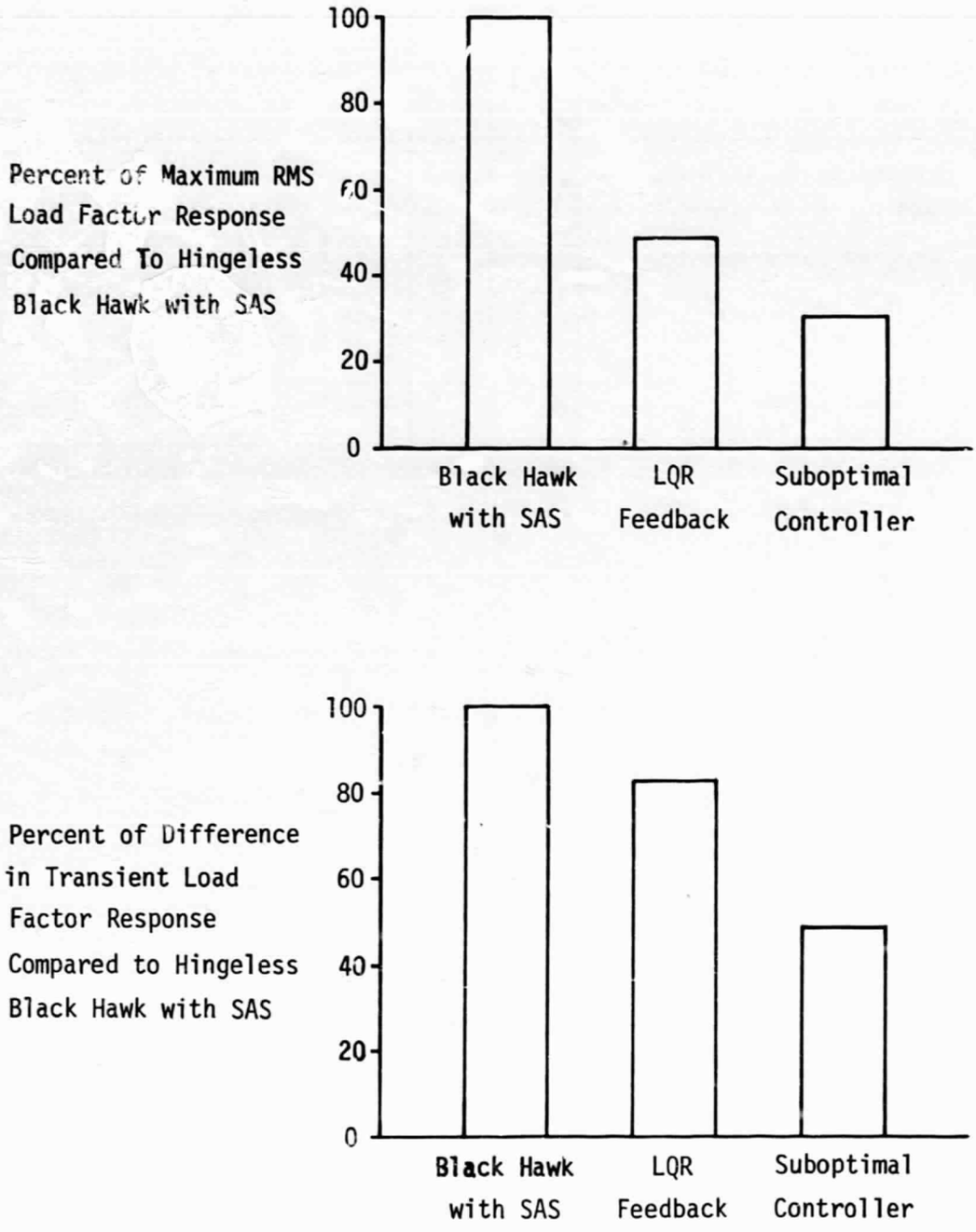

Figure 5.15 Gust Response Alleviation Experienced by Simulated 'Hingeless' BLACK HAWK at Hover.

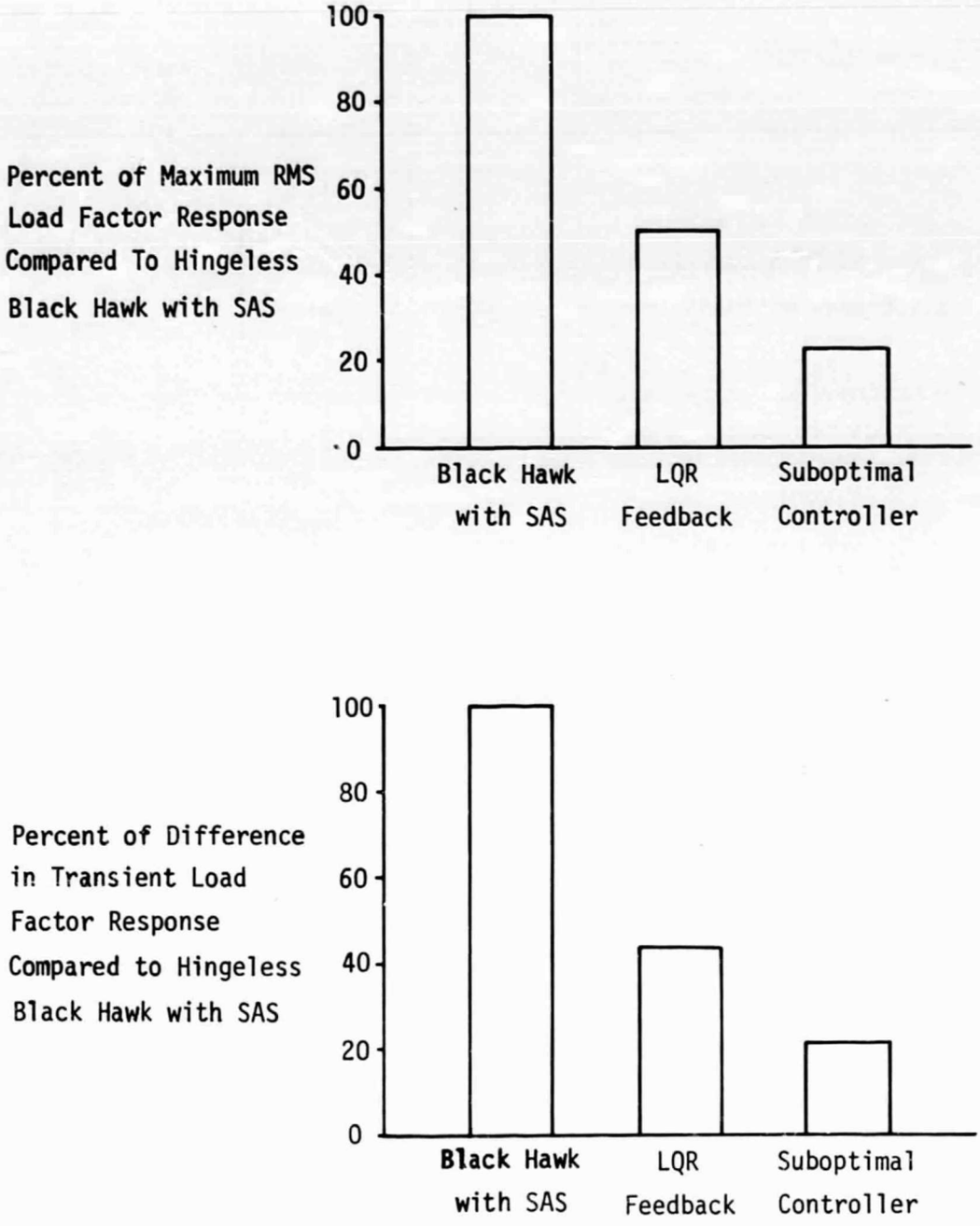

Figure 5.16 Gust Response Alleviation Experienced by Simulated 'Hingeless' BLACK HAWK at 41 m/s (80 Knots).

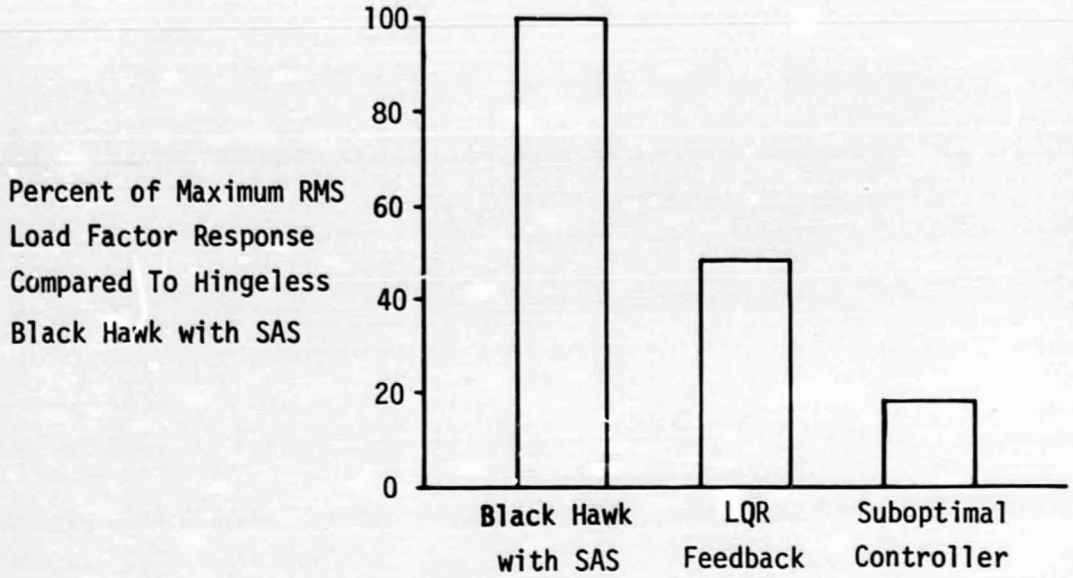

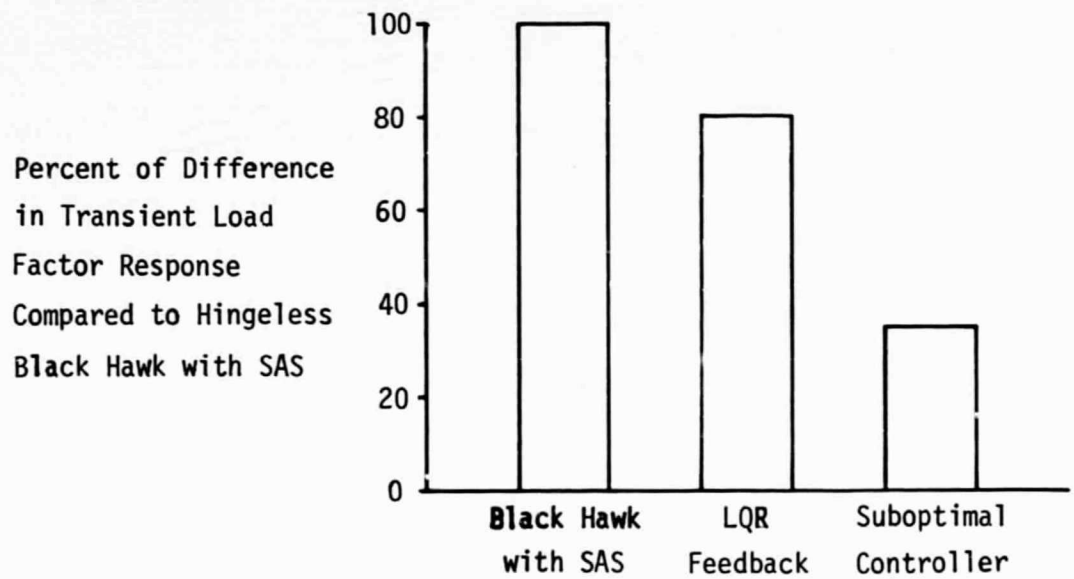

Figure 5.17 Gust Response Alleviation Experienced by Simulated 'Hingeless' BLACK HAWK at 77 m/s (150 Knots).

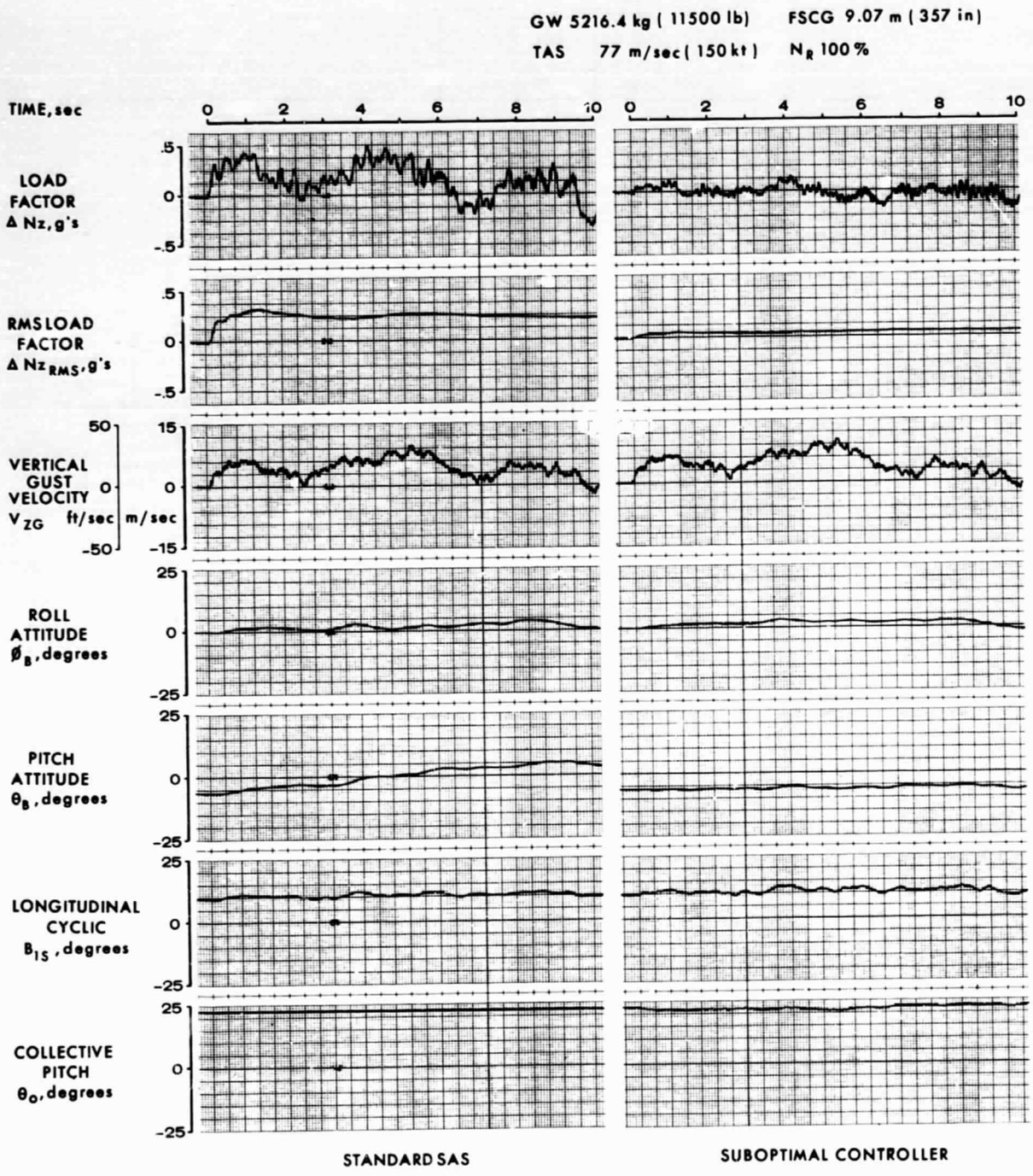

Figure 5.18 Time History Responses of the Simulated 'Hingeless' BLACK HAWK with Standard SAS and Suboptimal Controllers at 77 m/s (150 Knots); Low Gross Weight, 100% N_R.

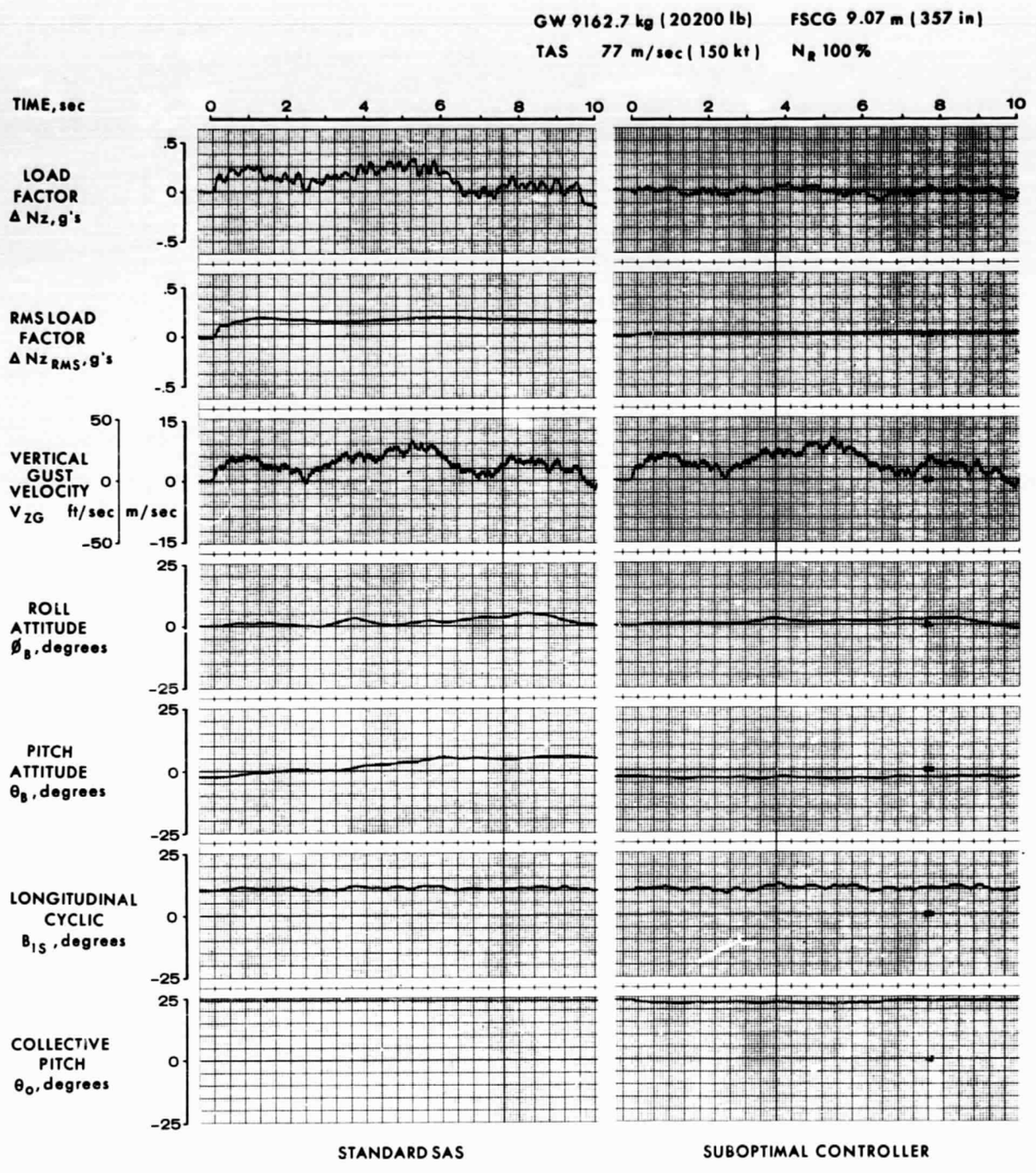

Figure 5.19 Time History Responses of the Simulated 'Hingeless" BLACK HAWK with Standard SAS and Suboptimal Controller at 77 m/s (150 Knots); High Gross Weight, 100% N_R.

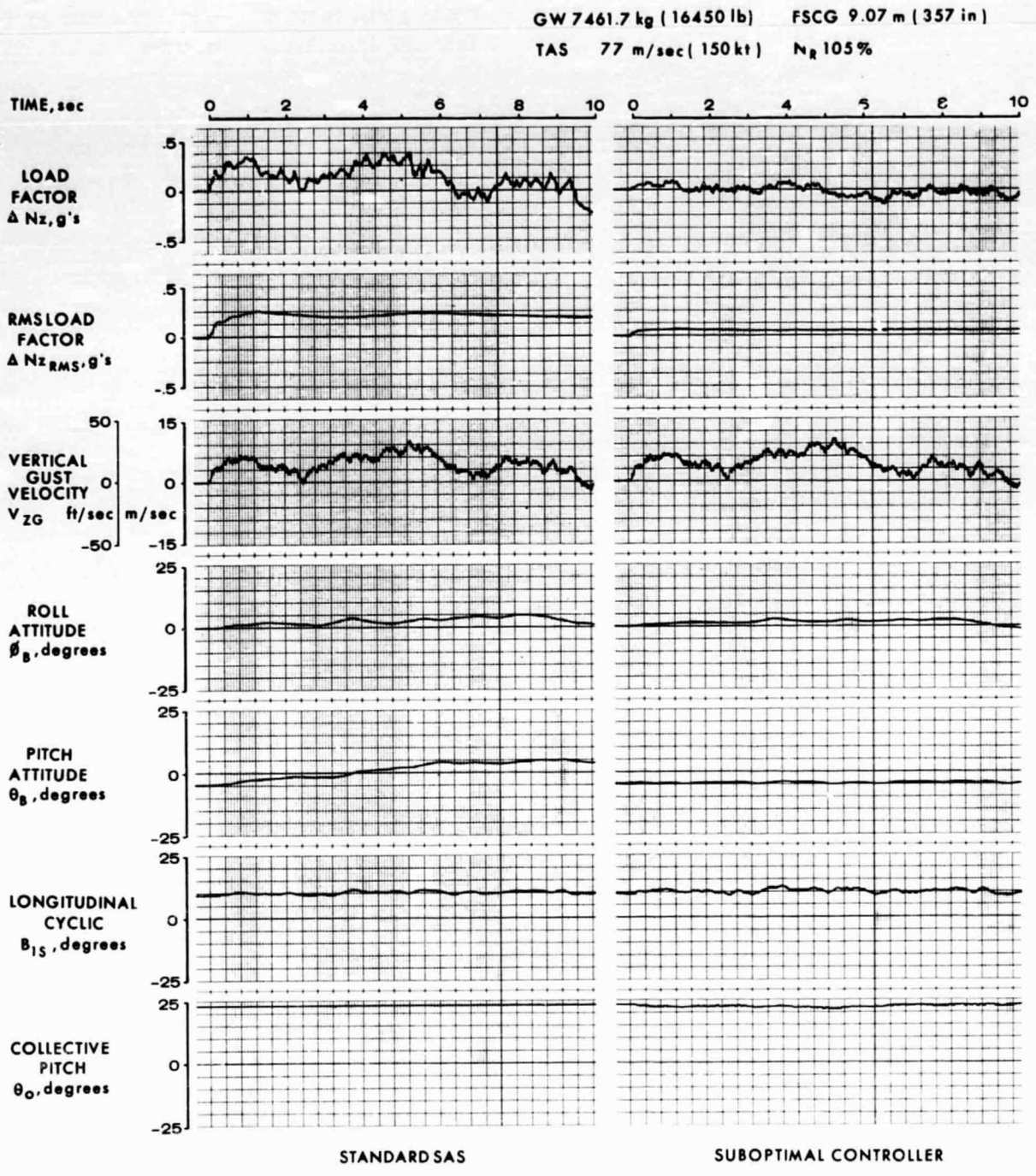

Figure 5.20 Time History Responses of the Simulated 'Hingeless' BLACK HAWK with Standard SAS and Suboptimal Controller at 77 m/s (150 Knots); Standard Gross Weight, 105% N_R.

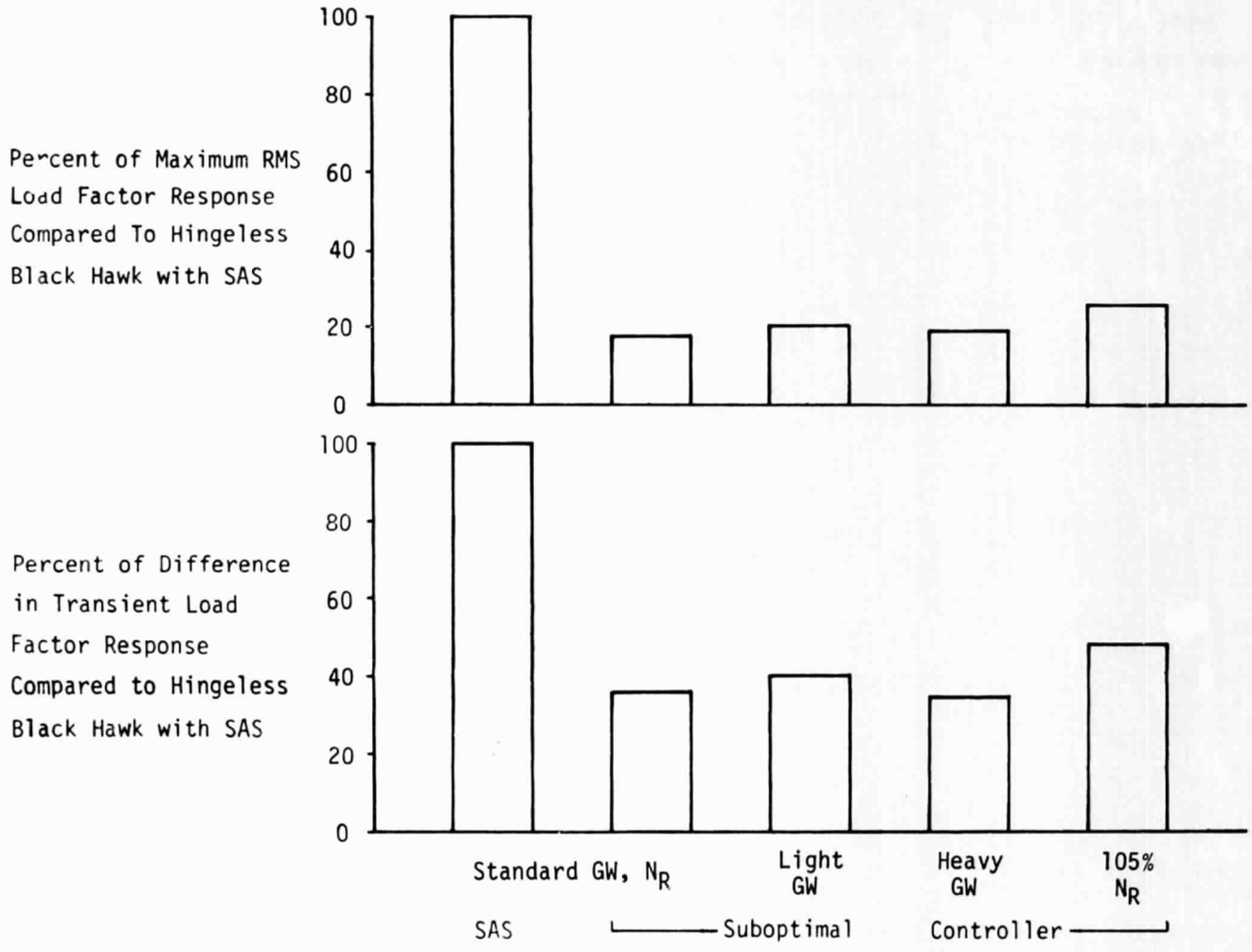

Figure 5.21 Gust Response Alleviation Experienced by Simulated 'Hingeless' BLACK HAWK for Various Off-Design Points at 77 m/s (150 Knots).

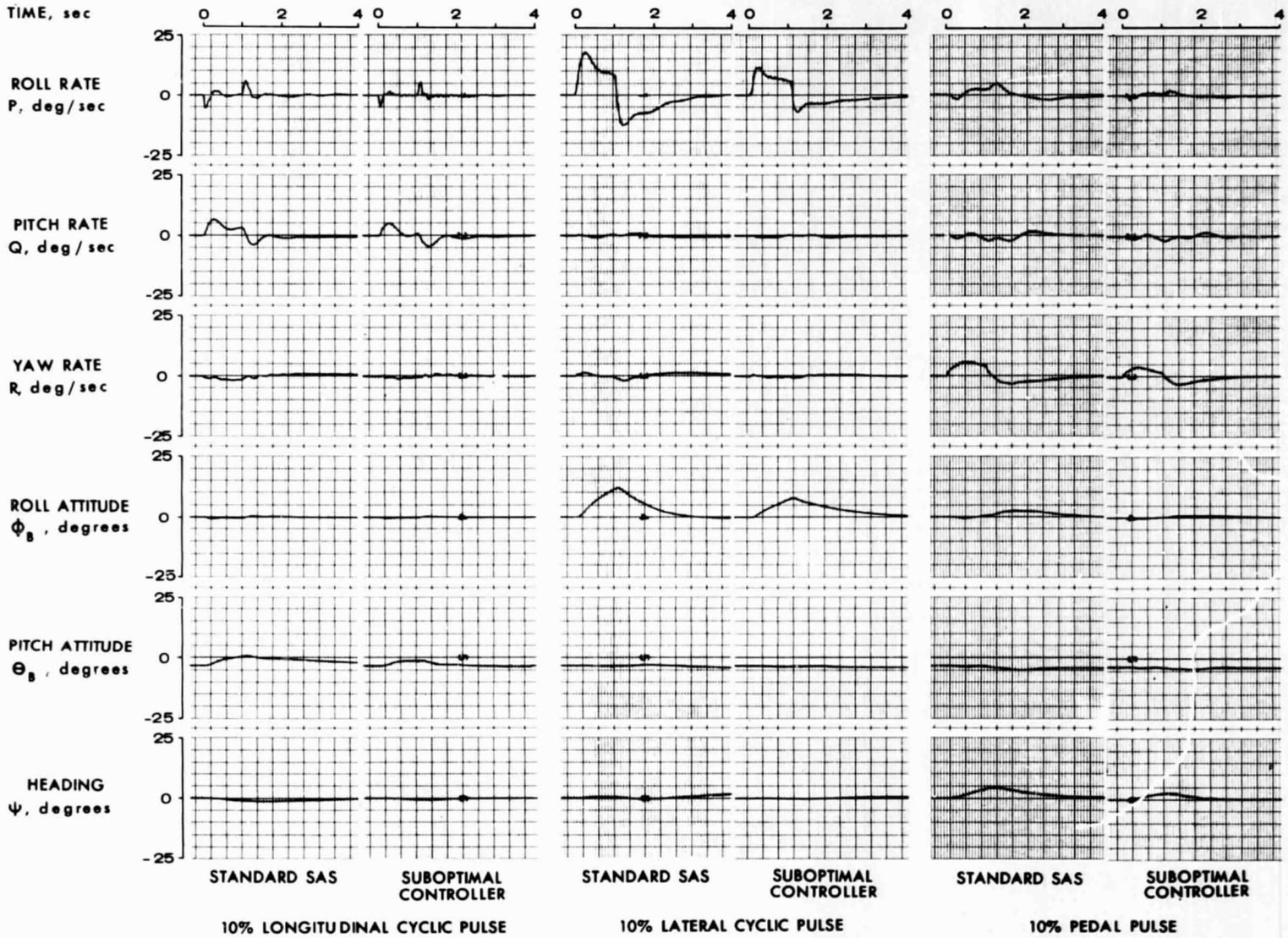

Figure 5.22 Time History Responses of the Simulated 'Hingeless' BLACK HAWK with Standard SAS and Suboptimal Controller to Pitch, Roll and Yaw Control Pulses (10%, 1 sec) at 77 m/s (150 Knots).

These time histories show that the peak angular rate response of the aircraft is only reduced slightly by the higher rate feedback gains of the gust controller. However, the load factor response to a collective pulse is reduced significantly by the controller, as shown in Figure 5.23. Although not simulated, a small amount of collective feed forward could easily compensate for the gust suppression feedback gains.

In summary, the suboptimal controller performed very well at various gross weights, rotor rpm's and airspeeds with only one gain change (no angle of attack feedback in hover). This indicates that the system is adaptable to a wide range of helicopters. Some simulation work would be required, however, to optimize the system gains for a particular aircraft.

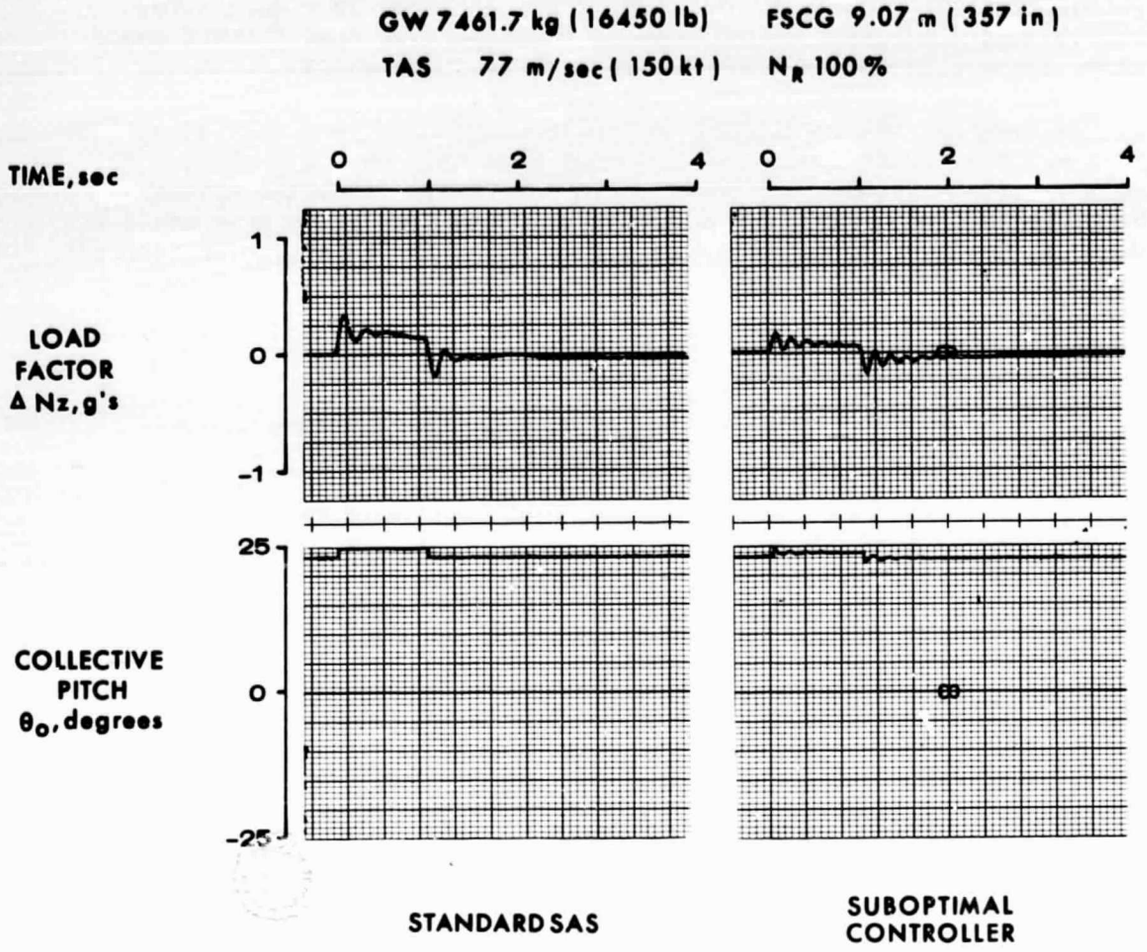

Figure 5.23 Time History Responses of the Simulated 'Hingeless' BLACK HAWK with Standard SAS and Suboptimal Controller to a Collective Pulse (10%, 1 sec).

SECTION 6

IMPLEMENTATION REQUIREMENTS

A preliminary assessment of the hardware implementation requirements of the vibration controller and the gust alleviation system has been made. Due to the rapid change in computer technology and the dependency of the controller system on the total aircraft system, the assessment has been made in terms of the generic design requirements for HHC implementation.

6.1 Vibration Control System

HHC Input Configuration - One of the areas where a significant amount of development work will have to be done is the method used to apply the higher harmonic control commands to the rotor system. During the preliminary hardware assessment, four separate configurations were studied. These are as follows:

1. Apply the HHC inputs to the control system before the primary servos using secondary actuators.

2. Apply the HHC inputs directly to the primary servos by replacing the present mechanical input servo valves with dual (mechanical/electrical) input valves.

3. Apply the HHC inputs to the control system between the primary servos and the stationary swashplate using secondary actuators either in series or in parallel with the primary servos.

4. Apply the HHC inputs directly to each rotor blade by installing a servo between the rotating swashplate and the blade pitch horn.

These configurations are shown schematically in Figure 6.1. Each configuration has its advantages and disadvantages.

The first configuration would be the safest because the basic rotor control system would not be changed except for the frequency response characteristics of the primary servos. Secondary, high frequency actuators could be installed between the mixer and the primary servo input links. Two design issues which must be addressed are the effects of control system flexibility on the high frequency signals and the possibility of the HHC inputs feeding back to the cockpit control sticks.

The second configuration would be the simplest and least costly to implement. The only modifications to the control system would be changes to the primary servos. New dual input servo valves and new hydraulic manifolds would have to be built. The valve assemblies would have one mechanical input valve and two electrical input valves. The outputs of the two electrohydraulic servo valves would be monitored, either electronically or hydraulically to provide a fail-safe operation. This configuration would be

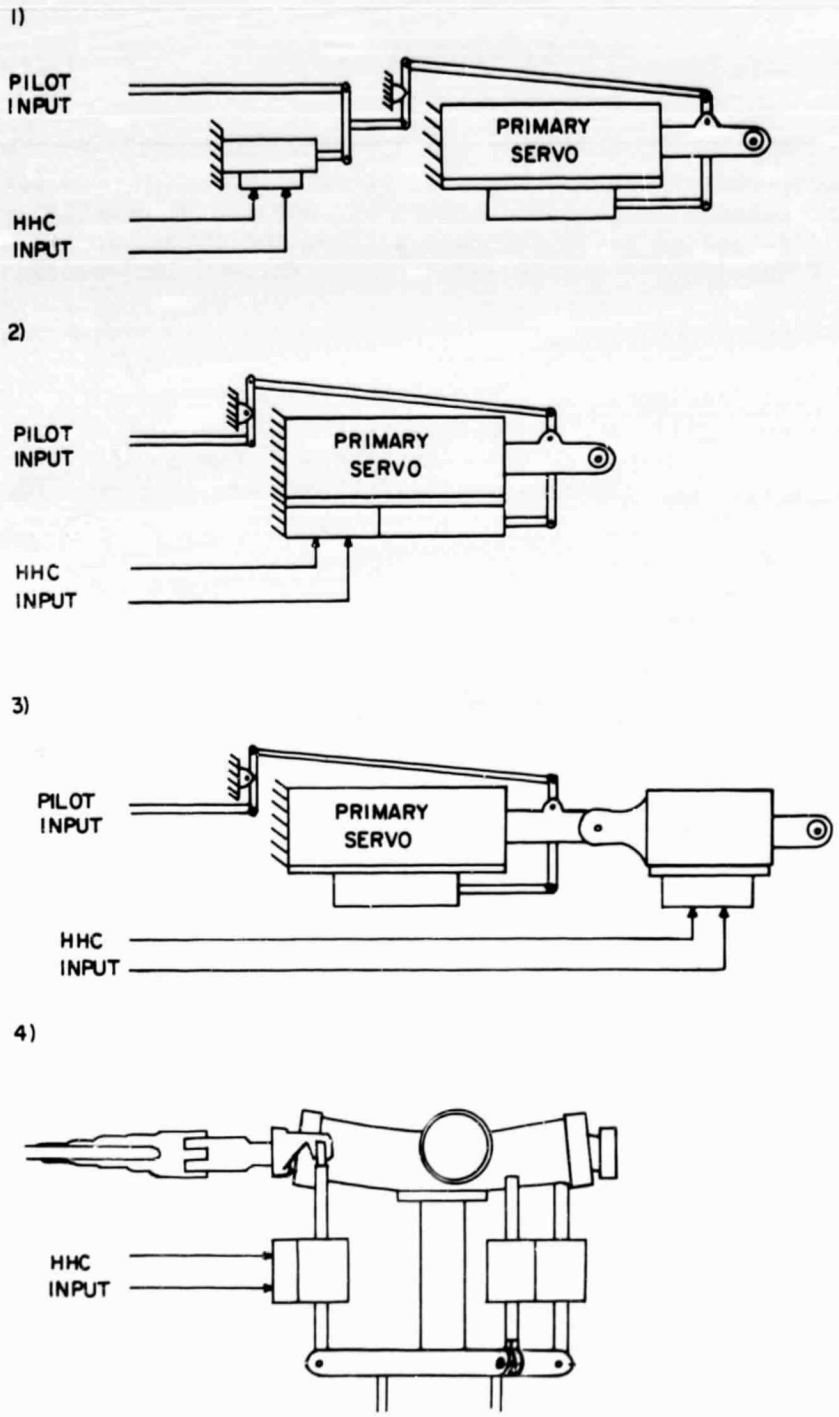

Figure 6.1 HHC Input Configurations.

ideal for most helicopters because the primary servos attach directly to the swashplate. However, in the BLACK HAWK, this is not the case. In fact, one control run from the primary servo output to the stationary swashplate is over three feet long and goes through a walking beam and a bellcrank. A shake test would be required to determine if the mechanical properties of these control runs (flexibility, hysteresis, and deadband) would allow the application of the HHC inputs at or before the primary servos.

The third configuration would be better suited for the BLACK HAWK because the separate HHC actuators could be installed downstream of the primary servos. However, this arrangement would require the development of new high frequency servos which would have to sustain flight loads.

The fourth configuration is the most complex and has the most critical failure mode. With the HHC servos replacing the pushrods between the rotating swashplate and the rotor blades, safety-of-flight considerations are of the utmost importance. The only acceptable failure mode of the servos would be to fail locked-up, in approximately the same position for each actuator. Careful electrical and hydraulic design could provide this characteristic.

Actuator Design Requirements - Detail design of the HHC actuators is a function of input configuration chosen for implementation and the aircraft chosen for installation. With the exception of the second input configuration, a separate actuator must be designed to provide the higher harmonic control inputs. A preliminary assessment of the actuator design requirements has determined that the HHC servos would have the following characteristics:

1. Hydraulically powered
2. Single power piston (flight demo only)
3. Dual electro-hydraulic servo valves
4. Electronic (digital) position feedback
5. Limited authority

Hydraulic power is required for the HHC actuators due to the energy levels involved and the frequency response characteristics desired. In order to apply the higher harmonic control commands to the rotor system, the actuator must have adequate frequency response out to 25-30 Hz. Due to transport lags in the servo, this requirement necessitates the use of a servo valve with adequate response out to at least 40 Hz. At present flight qualified hardware does not exist that meets these requirements, but the technology has been demonstrated experimentally.

Because the HHC actuators need only be fail-safe for a flight test demonstration on an existing aircraft, a single power piston is sufficient. The piston area is a function of input configuration. If the actuators

are upstream of the primaries servos (configuration 1), the loads would be low and only a small piston area would be required. If the HHC actuators are mounted between the primary servos and the stationary swashplate, the power piston must be sized both to sustain normal flight loads and also to overcome the swashplate and blade inertia and rotor airloads for 3P, 4P, and 5P inputs. The control loads associated with the application of HHC have been estimated based on available BLACK HAWK control system frequency response test data and results of the aeroelastic analysis. The maximum increase in vibratory stationary control loads (primary servos) is approximately $\pm$ 13345 N ($\pm$ 3000 lb). This level corresponds to simultaneous one degree inputs in the longitudinal, lateral and collective control axes in the stationary system (1.4 deg of θ_{3P} and θ_{5P}, and 1 deg of θ_{4P} in rotating system). The increase in primary servo piston area necessary to provide this increase in force capability is 8.06 cm^2 (1.25 in^2) with the normal hydraulic supply pressure of 20.7 N/mm^2 (3000 psi). This increase in area is equal to 75% of the area of one primary servo piston in the present BLACK HAWK. If the HHC actuators were mounted in the rotating system, the piston area for HHC inputs could be reduced to about 5.9 cm^2 (.92 square inches). No matter which configuration is employed the primary servos have to generate forces to input HHC in addition to reacting normal flight forces, and performing adequately when these forces are imposed. For a flight demonstration program, the BLACK HAWK primary servo force capacity may be acceptable by limiting the load factor envelope. The maximum servo loads are encountered in high load factor maneuvers. For a new design, resizing of the primary servos will be required.

As discussed previously dual, electrical-input servo valves are used in the HHC actuators. This redundancy allows comparison monitoring to be used to detect electrical or hydraulic malfunctions. Pressures dependent on flow through two valves are applied across a monitor piston. Under normal operating conditions, this piston would only move slightly. However if a failure occurs, the motion would exceed a pre-determined level and a shut off valve would be activated to lock up the servo. A transient fault could be reset, but a hard failure would not allow operation to be continued. Besides monitoring the valves, the HHC actuator output position would also be checked to make sure it agrees with the commanded position.

Although mechanical position feedback would be less expensive, electronic feedback was determined to be superior. Digital implementation of the feedback loops would allow the control system to modify the actuator response as a function of frequency to optimize the high frequency response characteristics needed for higher harmonic control. The digital feedback also simplified the monitoring requirements of the actuator. During the nonlinear analysis of the HHC system an authority limit of $\pm$ 2° was determined to be sufficient to provide good vibration alleviation. For the BLACK HAWK one degree of blade pitch change corresponds to .30 cm (.12 in) linear stroke at the forced swashplate input points when the actuators act collectively or .19 cm (.075 in) when the actuators act differentially.

The hydraulic flow requirement for each HHC actuator is a function of piston area and piston velocity. For the BLACK HAWK, assuming the HHC servo is located between the primary servo and the swashplate, the area is 8.06 cm^2 (1.25 in^2) and the average velocity is about 8.5 inches per second for $\pm$ 1^0 collective motion and about 5.3 inches per second for $\pm$ 1^0 cyclic motion. The greatest hydraulic fluid flow demand for the three actuators in the BLACK HAWK configuration is then approximately 37.8 liters per minute (10.0 gallons per minute). This corresponds to two servo pistons moving at 13.8 in/sec and one piston moving at 3.2 in/sec. At present the BLACK HAWK has two primary hydraulic systems that can each provide 6.2 gpm. Two systems are needed for redundancy, each powering one stage of each primary servo actuator. A third system, powered by the APU, provides back-up. It is apparent that whatever configuration is employed for the HHC servos the flow requirements cannot be met by the present hydraulic system. The most feasible method of providing the needed hydraulic flow would be to add an electrically driven hydraulic pump to supply fluid to the HHC actuators. Power requirements and heat dissipation could be a problem. A possible solution would be the design of a resonant hydraulic driving system. For the flight demonstration on the BLACK HAWK, only one HHC hydraulic system would be needed, since fail-operational capability would not be a requirement. However, if configurations 1 or 2 were employed, the flow requirements would apply to both stages of the primary servos, and two independent additional HHC power systems would be required, each with the capacity described above.

Digital Controller Feasibility - Preliminary analysis has indicated that implementation of the higher harmonic control system in a DEC PDP 11/40 is feasible. Table 4.2 contains the computational requirements of the HHC system. However, this table does not include the update rates required for system stability. In general, the update rate for the actuator control loop must be at least 10 if not 15 or 20 times the highest controlled frequency. For 5/rev commands, this update rate would be of the order of 200 to 400 solutions per second. The HHC actuator positions would have to be sampled at this rate and the new position command would have to be outputted just as quickly. Normally these high I/O rates would severely reduce available CPU time, however the use of direct memory access (DMA) allows the I/O to be performed with virtually no expanditure of CPU time. For the HHC system, the PDP 11/40 would need two DMA controllers, one for input and one for output. The CH-53E Dual Digital AFCS uses DMA to provide update rates as high as 160 solutions per second. While the actuator control loops are being solved at 200-400 Hz, the parameter identification and minimum variance gain calculations would be performed at much lower rates, 10-20 Hz.

The combination of the high rate control loop computation and the lower rate identification and minimum variance computations will severely tax the capabilities of the PDP 11/40 computer. A more practicable solution is a hybrid system which separates the control loop from the other computations. The actuator controller would be analog electronics which would generate the HHC commands from amplitude/phase signals updated periodically (5 Hz) by the digital system. Block diagrams of the two HHC systems are shown in Figure 6.2.

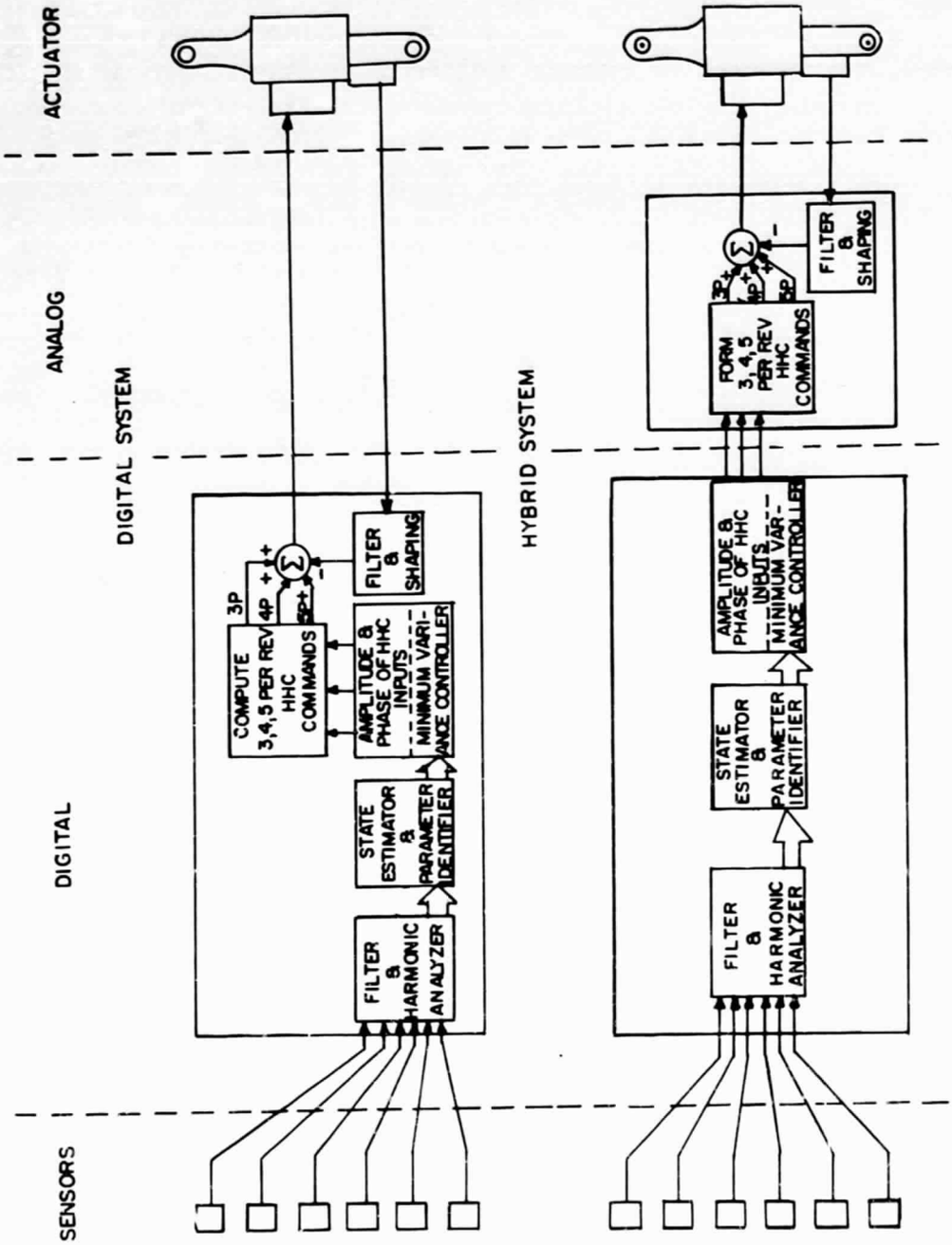

Figure 6.2 HHC System Block Diagrams.

Regardless of which mechanization is selected during preliminary design, a single computer would be adequate for wind tunnel testing of the HHC system. For flight demonstration hardware the electronics would have to be a dual, comparison monitored system to provide fail-safe operation. A new aircraft designed with higher harmonic control as part of the basic aircraft would require a fail-operational system. This requirement can be met with three computers and tandem servos. Table 6.1 provides an estimate of the component weights of the HHC system for various installations.

To summarize, higher harmonic control is feasible with present or near term technology. Hybrid implementation of the HHC algorithms would allow the use of a commercially available digital computer without severely burdening the processor. The most cost effective input configuration is to modify the aircraft primary servos to accept both mechanical and electrical commands. This arrangement is suitable for most helicopters because the primary servos attach directly to the stationary swashplate. The only problem area is the large hydraulic flow requirements dictated by the high frequency inputs into the rotor. Unconventional designs using resonant actuator systems might reduce these requirements.

6.2 Gust Alleviation System

The non-linear analysis of the gust alleviation system demonstrated that the system could provide good performance within the limitations of the existing Stability Augmentation System (SAS). Implementation of the gust controller in the BLACK HAWK would require the addition of a limited authority SAS-type actuator in the collective control axis. This collective servo has been developed for the SH-60B. The BLACK HAWK SAS is redundant and would interface easily with the dual gust controller.

The computational requirements of the optimal controller are provided in Table 6.2. For the suboptimal system these requirements are reduced by an order of magnitude. The only portion of the suboptimal system that would use significant computational time would be the tip-path-plane (Kalman) resolver. During the rotor/vehicle state feedback investigation, Reference 18, the sampling rate of the blade flapping measurements was 24 per revolution. This rate would be about 100 samples per blade per second for the BLACK HAWK and was used during the non-linear analysis. The most cost effective approach would be to incorporate the gust controller software into the PDP 11/40 higher harmonic control system computers. However, without actually programming one of the computers it is difficult to determine whether both programs could be executed simultaneously.

More development work will have to be done to develop some of the sensors needed by the gust alleviation system. In the past blade flapping has been measured by potentiometers mounted on the rotor blade flapping hinges. This worked fine on the older technology rotor heads having a well defined mechanical flapping hinge. However, with the advent of elastomeric bearings and/or hingeless rotor systems potentiometers are useless. Another method must be found to sense blade flapping. Possibilities include the use of fiber optic and laser technology.

Table 6.1 HHC System Component Weights

COMPONENTS	WIND TUNNEL TEST kg (lb)	BLACK HAWK RETROFIT kg (lb)	RSRA RETROFIT kg (lb)	NEW AIRCRAFT DESIGN	
				SEPARATE HHC SYSTEM Kg (lb)	INTEGRATED HHC SYSTEM kg (lb)
HHC ACTUATORS	12.25 (27) (3 @ 9)	12.25 (27) (3 @ 9)	2.27 (5) (Modify primary)	20.41 (45) (Tandem HHC servos 3 @ 15)	1.81 (4)
HHC COMPUTERS	22.68 (50) (PDP 11/40 1 @ 50)	45.36 (100) (PDP 11/40 2 @ 50)	45.36 (100) (PDP 11/40 2 @ 50)	23.13 (51) (New computers 3 @ 17)	2.72 (6)
HYDRAULIC PUMPS	13.61 (30) (1 @ 30)	13.61 (30) (1 @ 30)	13.61 (30) (1 @ 30)	27.22 (60) (2 @ 30)	20.41 (45)
TOTAL	48.53 (107)	71.21 (157)	61.23 (135)	70.76 (156)	14.95 (55)

TABLE 6.2 Computational Requirements for Gust Alleviation Controller

Z (15 × 1)

SUBROUTINE	NUMBER OF ADDITIONS	NUMBER OF MULTIPLICATIONS	COMPUTATION TIME* (msec)	
			ADDITIONS	MULTIPLICATIONS
ESTIMATOR	648	666	1.73	7.03
CONTROL	68	72	.18	0.76
LIMITER	8	4	.02	0.04
TOTAL	724	742	1.93	7.83

SAMPLE TIME -- 50 msec

TOTAL COMPUTATION TIME -- 9.8 msec

* DEC PDP 11/40 PROCESSOR

TIME INCLUDES SOURCE ADDRESS TIME, DESTINATION ADDRESS TIME, EXECUTE/FETCH TIME

The other sensor which may have to be improved is the angle-of-attack sensor. At present, fuselage angle-of-attack is measured by a boom-mounted vane attached to a potentiometer. This arrangement works fine for flight test instrumentation. Whether or not the performance of this sensor is adequate for feedback purposes will have to be determined. An alternative might be to develop a servo-driven sensor to measure angle of attack. This new sensor would measure the local angle of attack using a symmetrical airfoil and pressure sensors. The airfoil would be positioned by a servo to equalize the pressure on its upper and lower surfaces.

SECTION 7

CONCLUSIONS

The most important conclusion that can be drawn for the analytical results presented is that significant reductions can be made in helicopter vibration and gust response alleviation with the use of active feedback control. Fuselage vibration reductions on the order of 80-90 percent and gust response reductions on the order of 50 percent were achieved with active control. A major portion of these reductions is attributed directly to the specific separate control system designs for vibration and for gusts. This suggests the need to tailor a control system for a specific requirement. The results demonstrate that both the vibration and gust control systems contain the specific ingredients required for maximum effectiveness. Both of these control systems should serve as the building blocks for the first generation of hardware. Specific conclusions concerning the vibration and gust control systems follow.

1. The marriage of higher harmonic control with the real time self-adaptive (RTSA) controller is a very effective control system design approach for vibration reduction. The reason for the demonstrated success of the RTSA is that it combines the best of the transfer matrix approach, which takes advantage of the periodic nature of helicopter vibration, with a real time tracking, identification, and minimum variance computation scheme capable of implementing higher harmonic control every rotor revolution. An update capability on the order of once per 1 or 2 revs is required for effective vibration control over the total helicopter flight envelope.

2. Implementing higher harmonic control through oscillation of the standard swashplate configuration is adequate to achieve the 80-90 percent level of vibration reduction. This approach permits oscillating the swashplate at N/rev for control of N/rev fuselage vibrations for an N-bladed rotor helicopter.

3. The amplitude of higher harmonic control angles at 3, 4 and 5/rev required to reduce vibrations is on the order of 1 degree. This result agrees with other published theoretical and experimental results.

4. The studies reported herein have shown that rotor blade loads may or may not be increased significantly by HHC inputs. The potential for control inputs that do not increase blade loads has clearly been demonstrated.

5. Rotor blade loads can be increased by higher harmonic control inputs as follows. Torsional load increases are, in general, directly proportional to the magnitude of HHC inputs and occur at HHC input frequencies. Blade flatwise and edgewise responses can be increased by two mechanisms: rotating to fixed system hub load vectoral cancellation and interharmonic coupling. Blade loads can be increased by vectoral cancellation whenever stationary system 4/rev loads are decreased by proper

phasing of rotating system 3/rev and 5/rev loads rather than by reducing their amplitudes. Interharmonic coupling can increase blade loads at harmonic frequencies which are $\pm$ 1, 2 and 3/rev separated from the HHC input frequencies. Airloads at these frequencies are generated by the product of HHC input frequencies (3, 4 and 5/rev) and 1, 2 and 3/rev rotor blade velocities.

6. Two methods of controlling blade loads exist. The first is to devise a performance index comprised of appropriate hub vibration measurements which eliminates the potential for hub load vectoral cancellation. The second is to include a blade load measurement in the performance index either directly or indirectly through a state estimator.

7. Rotor performance is not significantly affected by optimum higher harmonic control for vibration. A five percent loss was noted for the 150 kn case. Although this loss is within the accuracy of the performance analysis, the potential exists to use an indicator of rotor performance such as steady torque in the controller computations as another weighted variable so that rotor performance would be unaffected (or even minimized).

8. The use of local sensors provides more effective local vibration reduction than the use of remote sensors near the rotor hub, indicative of significant modal vectoral cancellations occurring in the fuselage as a result of higher harmonic control. Therefore it is expected that active vibration control with local sensors would be equally effective for minimizing vibration from many sources (empennage response, canopy pressures, etc) in addition to the main rotor by inducing favorable fuselage modal vectoral cancellation.

9. Vibration reduction with the active controller is sensitive to the weightings used for each vibration sensor. The reason for this is related to the fundamental characteristic of the fuselage modes used.

10. The results show the need for a real time identifier and tracking capability of a vibration controller, not only because of time-varying changes during transients and maneuvers, but also because the relationship between vibration and higher harmonic control is nonlinear. The real time identifier and tracker must work in close harmony with the $\Delta\theta$ limiter and the time allotted between updates in order to minimize the nonlinear effects as well as the transient vibratory response to control inputs. This provides an accurately updated transfer matrix for optimum control angle calculations at each update. A good combination was a $\Delta\theta$ limiter of 0.1 degree coupled with a 1 rev time between updates.

11. The vibration controller is tolerant of noisy measurement signals. Noise levels up to 15 percent noise-to-signal ratio had no discernable effect on controller performance.

12. The vibration controller provides good vibration reduction for all flight conditions. It also functions satisfactorily for a variety of disc

loading, blade loading, blade frequencies, fuselage frequency combinations and rotor types.

13. The generality of the vibration controller is further enhanced by its adaptability. The closed loop analysis was excercised using the T-matrix that corresponds to the 150 kn high speed level flight condition as the initial T-matrix for all other parametric variations. For all the cases studied, the controller was able to identify and update the T-matrix satisfactorily and command a set of higher harmonic control inputs that minimize vibrations.

14. A nonlinear analysis using a sophisticated helicopter simulation and a gust model is necessary for the analytical design of a gust suppression controller because the linear analysis does not sufficiently represent the "real" aircraft, e.g., the authority and rate limits.

15. It was found to be quite difficult to design an optimal controller using a complex linear model and LQR theory which functions satisfactorily with a sophisticated nonlinear model.

16. Significant reductions in gust response can be produced with angle-of-attack feedback into pitch and load factor feedback into collective pitch.

17. Based on a preliminary assessment of the hardware implementation requirements for the vibration controller, the higher harmonic control is considered feasible with present or near term technology. Hybrid implementation of the HHC algorithms would allow the use of a commercially available digital computer without severely burdening the processor. The most cost effective input configuration is to modify the aircraft primary servos to accept both mechanical and electrical commands. This arrangement is suitable for most helicopters because the primary servos attach directly to the stationary swashplate.

18. The key design issues that need to be resolved for successful hardware implementation are: primary servos, hysteresis, swashplate stiffness, blade strength, blade mode frequencies, hydraulic supply, power required for hydraulics, computer and weight.

SECTION 8

RECOMMENDATIONS

Based upon the results presented, the following recommendations are made. For the vibration portion of the contract, there are four definite areas requiring additional attention to further understand and refine active vibration control.

1. The HHC analysis and controller developed herein should be applied to and correlated with available data acquired in wind tunnel tests of model rotors employing HHC.

2. Refinements and additional study of the vibration controller is recommended to advance the vibration controller configuration towards a full scale hardware design. Recommended refinements would include increased number of vibration sensors, optimization of weighting function, inclusion of a measurement filter, blade stresses and rotor torque and inclusion of control system swashplate dynamics. No major refinements are deemed necessary. The areas of additional study would include evaluation of controller performance with these refinements and also analytical simulation of transient and maneuvers (pullups, turns, descents, flares) to provide a rigorous evaluation of the RTSA vibration controller.

3. After evaluation of the controller with these refinements, a first generation flightworthy controller hardware design and development is recommended for full scale wind tunnel test evaluation. Hands-on evaluation and the capability to parametrically change controller characteristics for set wind tunnel conditions is the next logical step in the controller development and is an obvious milestone to be achieved in the maturity of active vibration control. Also, only hardware design aiming at flightworthiness will surface the real design problems.

4. Significant questions were uncovered during the analytical study to warrant further investigations into the fundamentals of higher harmonic control. Most of the questions are directed towards the open loop application of higher harmonic control and are therefore somewhat divorced from the active controller concept. However these questions impact not only controller performance but the very concept of higher harmonic control. Therefore there is a definite need for more study in these areas. The most pressing questions are: a) How non-linear is the vibration-higher harmonic control relation and what is the source and extent of the nonlinearity? Is it airspeed, thrust or control amplitude related? System nonlinearity generally implies possible local solutions. It this possible for higher harmonic control? b) What is the mechanism by which rotor performance is affected by 3, 4 and 5 per rev higher harmonic control. Can the mechanism be used to advantage to imporve rotor performance? c) What happens to harmonic blade motions with optimum higher harmonic control? Do the blades

seek a modal vectoral cancellation of shears and moments at the blade root or is there an overall reduction in modal excitations? d) For optimum higher harmonic control what are the characteristics of the blade spanwise harmonic airloads compared to the airloads with no active control?

As for the gust suppression, the following tasks are desirable to further the advancement of the state-of-the-art.

1. Further analytical studies of gust suppression algorithms would be desirable with a pilot in the loop. This would be best accomplished using the NASA Ames motion simulator.

2. Flight test a gust suppression controller on the NASA CH-53 or RSRA.

REFERENCES

1. Wood, E. R., Powers, R. W., and Hammond, C. E., On Methods for Application of Harmonic Control, Fourth European Rotorcraft and Powered-Lift Aircraft Forum, September 1978.

2. McHugh, Frank J., and Shaw, John, Helicopter Vibration Reduction with Higher Harmonic Blade Pitch, Third European Rotorcraft and Powered-Lift Aircraft Forum, September 1977.

3. Kretz, Marcel, Relaxation of Rotor Limitations by Feedback Control, Proceedings of the 33rd Forum of AHS, May 1977.

4. McHugh, Frank J., and Shaw, John, Benefits of Higher Harmonic Blade Pitch: Vibration Reduction, Blade Load Reduction, and Performance Improvement, Proceedings of the American Helicopter Society Mideast Region Symposium on Rotor Technology, August 1976.

5. Sissingh, G. J., and Donham, Robert E., Hingeless Rotor Theory and Experiment on Vibration Reduction by Periodic Variation of Conventional Controls, NASA SP352, February 1974.

6. Balcerak, John C., and Erickson, John C. Jr., Suppression of Transmitted Harmonic Vertical and Inplane Rotor Loads by Blade Pitch Control, Cornell Aeronautical Laboratories; USAAMRDL TR69-39, July 1969.

7. Daughaday, Hamilton, Suppression of Transmitted Harmonic Rotor Loads by Blade Pitch Control, Cornell Aeronautical Laboratories; TR67-14, November 1967.

8. An Experimental Investigation of a Second Harmonic Feathering Device on the UH-1A Helicopter, Bell Helicopter Company, USAAMRDL TR62-109, June 1963.

9. Arcidiacono, P. J., Theoretical Performance of Helicopters Having Second and Higher Harmonic Feathering Control, JL AHS, 1961.

10. Howes, H., Perley, R., and Weisbrich, A., Design Study of a Feedback Control System for the Multicycle Flap System Rotor (MFS), NASA CR-151960, January 1977.

11. McCloud, John L., III, An Analytical Study of a Multicycle Controllable Twist Rotor, Proceedings of the 31st Forum AHS, May 1975.

12. Kretz, Marcel, Research in Multicyclic and Active Control of Rotary Wings, Proceedings of the 1st European Rotorcraft Forum, September 1975.

13. McCloud, John L., III, and Kretz, Marcel, Mutlicycle Jet-Flap Control for Alleviation of Helicopter Blade Stresses and Fuselage Vibration, NASA SP352, February 1974.

14. Kretz, Marcel, Aubrun, Jean-Noel, and Larche, Marc, March 1971 Wind Tunnel Tests of the Dorand DH 2011 Jet Flap Rotor, NASA CR-114693 and CR-114694, June 1973.

15. McCloud, John L., III, Wind Tunnel Test Results of a Full Scale Multicyclic Controllable Twist Rotor, Proceedings of the 34th Forum of AHS, May 1978.

16. McCloud, John L, III, Studies of a Large Scale Jet Flap Rotor in the 40-by-80-Foot Wind Tunnel, Presented at Mideast Region Symposium AHS, Status of Testing and Modeling Techniques for V/STOL Aircraft, Philadelphia, Pa., October 1972.

17. Lemnios, A. Z., and Smith, A. F., An Analytical Evaluation of the Controllable Twist Rotor Performance and Dynamic Behavior, USAAMRDL TR72-16, May 1972.

18. Briczinski, S. J. and Cooper, D. E., Flight Investigation of Rotor/Vehicle State Feedback, NASA CR-132546.

19. Briczinski, Stanley J., Analytical Investigation of Gust Suppression Techniques for the CH-53 Helicopter, NASA CR-145013.

20. Kuczynski, W. A., and Sissingh, G. J., Characteristics of Hingeless Rotors with Hub Moment Feedback Controls Including Experimental Rotor Frequency Response, NASA CR 114427 and 114428, January 1972.

21. Bergquist, R. R., Helicopter Gust Response Including Unsteady Aerodynamic Stall Effects, USAAVLABS TR 72-68, May 1973.

22. Johnson, R. L. and Hohenemser, K. H., On the Dynamics of Lifting Rotors with Thrust or Tilting Moment Feedback Controls, JL AHS, January 1970.

23. Johnson, Wayne, Optimal Control Alleviation of Tilting Proprotor Gust Response, Journal of Aircraft, March 1977.

24. Farrar, F. A. and Michael, G. J., Nonlinear Stochastic Control Design for Gas Turbine Engines, ONR Report CR215-247-2F, June 1978.

25. Farrar, F. A. and Michael, G. J., Large-Signal Estimation for Stochastic Nonlinear Multivariable Dynamic Systems, ONR Report CR215-247-1, March 1977.

26. Biggers, James C., and McCloud, John L, III, A Note on Multicyclic Control By Swashplate Oscillation, NASA TM-78475.

27. Bryson, A. E. Jr. and Ho, Y.C., Applied Optimal Control, Blaisdell Publishing Co., Walthum, Mass., 1969.

28. Singleton, R. C., On Computing the Fast Fourier Transforms, Comm. ACM 10(10) 1967, pp 647-654.

29. Bielawa, R. L., Aeroelastic Analysis for Helicopter Rotor Blades with Time-Variable, Nonlinear Structural Twist and Multiple Structural Redundancy - Mathematical Derivation and User's Manual, NASA CR-2638, October 1976.

30. Murphy, R. D. and Narendra, K. S., Design of Helicopter Stabilization Systems Using Optimal Control Theory, Journal of Aircraft, Vol. 6, No. 2, Mr-Ap 1969.

31. Hall, W. E., Jr. and Bryson, A. E., Jr., Inclusion of Rotor Dynamics in Controller Design for Helicopters, J. Aircraft, Vol. 10, No. 1, April 1973.

32. Hansen, K. C. and Mulcahy, G., The Role of Flight Dynamic Modeling in Helicopter Certification, Technical Paper No. 780515, Society of Automotive Engineers, May 1978.